University of Southampton

Faculty of Biological Sciences

School of Biological Sciences

Investigating the mechanisms of tau secretion across neuronal networks in health and disease

by

Dianne Marquez Lopez

Thesis for the degree of PhD

May 2023

University of Southampton

Abstract

Faculty of Biological Sciences

School of Environmental and Life Sciences

Doctor of Philosophy,

Investigating the mechanisms of tau secretion across neuronal networks in health and disease

by

Dianne Marquez Lopez

The accumulation of insoluble neurofibrillary tangles, composed of hyperphosphorylated tau, is one of the main pathological hallmarks of tauopathies. Growing evidence indicates that the release and re-uptake of pathogenic tau seeds mediates the spread of tau pathology along living and intact neuronal networks via 'prion-like' mechanisms. Moreover, there is evidence showing that neuronal activity can regulate tau secretion and accelerate cell-to-cell propagation of tau pathology *in vitro* and *in vivo.* What molecular mechanisms drive and mediate activity-dependent secretion of physiological and pathological tau remains to be investigated.

Sensitive biosensors that are able to monitor the release and re-uptake of tau in connected neuronal networks under different conditions are currently limited. Split nanoluciferase (NLuc) complementation reporters, which are composed of two subunits, a large bit (LgBiT; 17.6kDa) and a smaller bit (HiBiT; 11 amino acid) is a highly-sensitive bioluminescent biosensor that can be used to monitor cell-to-cell transfer of tau in different conditions. Structural complementation of the split HiBiT and LgBiT reporters re-constitutes the NLuc enzyme, which generates a bright luminescent signal. Tagging tau with these reporters will allow the mechanisms of tau release and re-uptake to be closely dissected, under pathological and physiological conditions. A greater understanding of the mechanism involved in the spread of tau pathology will help in the development of effective treatments in the future.

Table of Contents

Table of Tables

Table of Tables

Table of Figures

Table of Figures

Table of Figures

Research Thesis: Declaration of Authorship

Print name:

Title of thesis:

I declare that this thesis and the work presented in it are my own and has been generated by me as the result of my own original research.

I confirm that:

1. This work was done wholly or mainly while in candidature for a research degree at this University;
2. Where any part of this thesis has previously been submitted for a degree or any other qualification at this University or any other institution, this has been clearly stated;
3. Where I have consulted the published work of others, this is always clearly attributed;
4. Where I have quoted from the work of others, the source is always given. With the exception of such quotations, this thesis is entirely my own work;
5. I have acknowledged all main sources of help;
6. Where the thesis is based on work done by myself jointly with others, I have made clear exactly what was done by others and what I have contributed myself;
7. None of this work has been published before submission

Signature: ..... Date:.....

Acknowledgements

I would like to acknowledge a lot of people but I will only mention a few here.

Firstly, I would like to express my gratitude to Gerald Kerkut and IFLS for funding my research and for the generous financial support they provided to get me through my PhD.

Secondly, I would like to express my deep and sincere gratitude to Dr. Katrin Deinhardt who has been a kind and supportive supervisor. Thank you so much for helping me get through the last 4 years and for always giving the best advice and the fastest feedback in B85. I would also like to say thanks to Dr Mark Coldwell and Dr Jonathan West for their guidance and support at the early stages of my PhD.

I would also like to acknowledge and give thanks to Dr Mariana Vargas-Caballero and Hannah Warming for their input on my project especially the work on electrophysiology. With that, I would like to give thanks to the members of the lab past (Connor and Aleks) and present for the big and little things that helped me along the way. I would make special mentions to Lauren and Hannah for being the best friends anyone could ask for. Thank you for all your emotional and lab support. I could not have gone through this whole process without them.

I would like to say thanks to my mum, dad, sister and brother for always giving me unconditional love and support. Thank you for believing in me always. Of course, I would also like to say thanks to my wonderful therapist, cook, hype-man, best-friend and adventure partner, Eric, who has been an absolute legend.

Finally, I would like to express my gratitude and dedicate my work to a very special person in my life, Inang Sinyang. You have been a constant inspiration of why I wanted to finish this PhD. I love you grandma.

Publications

- **Lopez D** , Maltby C, Warming H, Vargas-Caballero M, Divecha N, Vargas-Caballero M, Coldwell M, Deinhardt K. “A luminesence-based reporter to sudy tau secretion reveals overlapping mechanisms for the release of healthy and pathological tau. *Frontiers of Neuroscience*. Mar 2023.”– In submission

- Hallinan G, **Lopez D,** Vargas-Caballero M, West J, Deinhardt K. “Co-culture of Murine Neurons Using a Microfluidic Device for The Study of Tau Misfolding Propagation”. *Bio-protocol*. Aug 20 (2020); 10(16)

Definitions and Abbreviations

AAV.....Adeno-associated virus

Aβ.....Amyloid Beta

α-synuclein.....Alpha synuclein

ACSF .....Artificial Cerebral Spinal Fluid

AD.....Alzheimer's disease

AGD .....Argyrophilic Grain Disease

AIS .....Axon initial segment

AMPA .....α-amino-3-hydroxy-5-methyl-4-isoxazolepropionic acid

APF .....Annular photo fibrils

APOE .....Apolipoprotein E

APP .....Amyloid precursor protein

ALP .....Autophagy-lysosomal pathway

bp .....Base pair

BSA .....Bovine Serum Albumin

Ca2+ .....Calcium

CBD.....Corticobasal Degeneration

CHO .....Chinese Hamster Ovary

CNS.....central nervous system

CPS .....Conventional protein secretion

CSF.....Cerebral Spinal fluid

CREB.....AMP response element-binding protein

CMV.....Cytomegalovirus

CFP .....Cyan Fluorescent Protein

Cryo-EM .....Cryo-electron microscopy

DIV.....Days in vitro

DMEM .....Dulbecco's Modified Eagle Medium

Definitions and Abbreviations

DNA..... Deoxyribonucleic acid

dNTP ..... Deoxyribonucleotide Triphosphate

EC ..... Entorhinal cortex

ECII ..... Entorhinal cortex layer II

ER ..... Endoplasmic reticulum

ELISA ..... Enzyme-linked immunosorbent assay

ESCRT ..... endosomal sorting complex required for transport

EVs ..... Extracellular vesicles

FRET ..... Fluorescence resonance energy transfer

FTD ..... Frontotemporal Dementia

FTDP-17..... Frontotemporal dementia with Parkinsonism linked with chromosome 17

GAGs ..... Glycosaminoglycans

GAPDH ..... Glyceraldehyde 3-phosphate dehydrogenase

GFP..... Green Fluorescent Protein

GZ..... Gabazine

GH ..... GFP-HiBiT

GOF ..... Gain of function

GWAS..... Genome Wide Association Studies

GZ..... Gabazine

HEK..... Human embryonic kidney

NanoBiT ..... Nano Luciferase Binary Technology

HSC..... Heat Shock Cognate

HSP..... Heat Shock Protein

HSPG ..... Surface heparan sulphate proteoglycans

HSV/TK..... Herpes simplex virus thymidine kinase type 1 gene

IDP..... Intrinsically disordered protein

iPSCs..... Induced pluripotent stem cells

ISF.....Interstitial spinal fluid

KCl .....Potassium chloride

KDL .....Kinase, Ligase and DpnL

LCS.....Live cell substrate

LDLRs.....Low-density lipoprotein receptors

LE.....Late-endosomes

LOAD .....Late-onset AD

LOF .....Loss of function

LRP1.....Low-density lipoprotein 1

MAP.....Microtubule Associated Protein

MAPT.....Microtubule Associated Protein Tau

MTBD .....Microtubule-binding domain

MVBs .....Multi-vesicular bodies

Ms .....Seed-competent monomer

Mi .....Inert monomer

NBM .....Neurobasal medium

NEB.....New England Biolabs

NFT .....Neurofibrillary Tangles

NLuc .....Nanoluciferase

NMDA.....N-methyl-d-aspartate

NPF .....Narrow picks filament

PBS .....Phosphate Buffered Saline

PCR .....Polymerase Chain Reaction

PDL .....Poly-D-lysine

PET .....Positron Emission Tomography

PFF.....Pre-formed fibrils

PHF .....Paired Helical Filaments

PHP.....Phosphomimetic

PI(4,5)P2, ... phosphatidyl inositol 4,5 phosphate

PiD..... Pick's disease

PNS..... Peripheral nervous system

PrP..... Pathogenic prion protein

PSP ..... Progressive Supranuclear Palsy

RE ..... Restriction endonucleases or Restriction enzymes

RFP ..... Red Fluorescent Protein

RLU..... Relative light units

RPM ..... Rotations per minute

RMP ..... Resting membrane potential

rSAP..... shrimp alkaline phosphatase

RT ..... Room temperature

secNLuc..... Secretory Nanoluciferase

SEM..... Standard Error of Mean

SF ..... Straight Filaments

SDS-PAGE..... Sodium docecyl sulphate-polyacrylamide gel electrophoresis

TAE..... Tris base, acetic acid and EDTA

TBS ..... Tris Buffered Saline

TBS-T..... Tris Buffered Saline with tween

TC..... Tissue culture

TD..... Tangle-only dementia

TFEB1 ..... transcription factor E

TNT..... Tunnelling nanotubes

TTX..... Tetrodotoxin

TRPML1..... lysosomal calcium channel mucolipin TRP channel 1

VSCC..... Voltage-sensitive calcium channels

UPS..... Unconventional protein secretion

WPF..... Wide pick's filament

WT.....Wild Type

YFP.....Yellow Fluorescent Protein

Chapter 1 Insight to the spread of tau pathology

1.1 Neurodegenerative Diseases

The human brain has a complex structure and is made up of 100 billion neurons which all come together to form functional neuronal networks. Through their highly extensive dendritic and axonal structures, neurons are able to form numerous synaptic connections. This allow them to gather and transmit short- to long-range electrochemical signals. This allows efficient communication between different areas of the brain and the rest of the nervous system. It is this complex formation of functional neuronal networks that drive cognition, learning, memory and behaviour (Ahmed et al., 2016). When these neuronal connections breakdown as a result of neurodegeneration, manifestation of 'dementia' symptoms can occur. This includes a decline in cognitive ability, memory deficits and impairment in language and behaviour(Robinson et al., 2015).

Neurodegeneration is a term used to describe a group of chronic disorders that occurs as a result of progressive neuronal death either in the central nervous system (CNS) or in the peripheral nervous system (PNS). Degeneration of neurons in the brain leads to debilitating brain disorders, such as Alzheimer's Disease (AD) which is the most prevalent cause of late-onset dementia. Familial AD, such as frontotemporal dementia (FTD), also exists and leads to earlier manifestation of the disease (Robinson et al., 2015). The key hallmarks of these neurodegenerative diseases are the accumulation of protein inclusions.

Understanding the neuropathological mechanisms involved in the development of neurodegenerative disease the number of people diagnosed is predicted to increase by 204% by 2050 (Alzheimer's Society, 2017), primarily due to the changing population demographics and increases in life expectancy. This is likely going to put a huge socio-economic pressure in the current healthcare system. Importantly, as there are currently no disease-modifying treatments for neurodegenerative diseases there is an urgent need to find effective therapeutic interventions to treat early and/or delay the onset of these disorders.

1.1.1 Tauopathies

Tau pathology is a term used to characterise the abnormal accumulation of tau aggregates or neurofibrillary tangles (NFTs) in the brain. Tau pathology is particularly prevalent in tauopathies. It has been shown that the abnormal phosphorylation of tau proteins, leads to the production of highly pathogenic tau that oligomerise and fibrilise to form NFTs which therefore contributes to the development of cognitive impairment in AD (see review by Kametani and Hasegawa, 2018).

Tauopathies are a class of neurodegenerative diseases characterised by the accumulation of insoluble intracellular tau aggregates in the brain. Different types of tauopathies are characterised by the tau aggregates that accumulate in neurons and/or glial cells. It is often found in the brains of people with neurodegenerative diseases, including but not limited to AD, PiD, Argyrophilic Grain Disease (AGD), Progressive Supranuclear Palsy (PSP), and Corticobasal Degeneration (CBD) as well as Tangle-only Dementia including FTD and Parkinsonism linked with chromosome 17 (FTDP-17) (Clavaguera et al., 2013)(Figure 1). A diverse morphology of protein aggregates can be observed in the human brains in these different types of tauopathies (Figure 1). Although these diseases share a common feature, in that tau-positive aggregates are central to brain pathology, different tauopathies have distinct clinical and neuropathological presentations (see review by Kametani and Hasegawa, 2018). This is influenced by a wide range of factors such as: environmental influence, other co-morbidities (such as the presence of other protein aggregates), cellular and regional presentations (further discussed in 1.4.2).

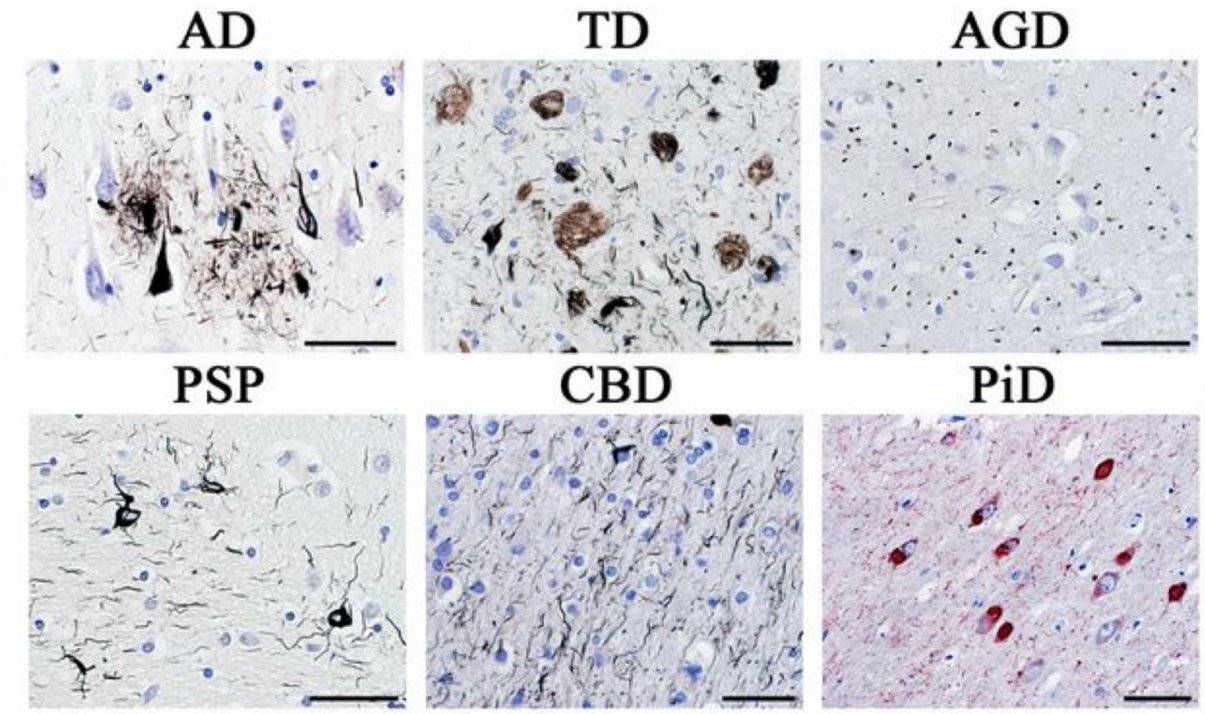

Figure 1. Tau pathology observed in different sporadic human tauopathies.
Different sporadic human tauopathies including, Alzheimer's Diseases (AD) Pick Disease (PiD), Argyrophilic Grain Disease (AGD), Progressive Supranuclear Palsy (PSP), and Corticobasal Degeneration (CBD) as well as tangle-only dementia (TD) form distinct protein inclusions with diverse morphology in the human brain. Gallyas-Braak silver-positive and AT100 immunostaining were used to observe different tau protein inclusions. (Scale bars, 50 µm). Adapted from Clavaguera et al., 2013.

1.1.2 Primary and secondary tauopathies

Distinct tau protein aggregates accumulate in different tauopathies. In AD, senile beta-(β)-amyloid (Aβ) plaques and intracellular NFTs are found in the brains of patients; pick bodies are often found in patients with Picks Disease (PiD), whereas Lewy bodies are hallmarks of Lewy body dementia (LBD) to name a few examples (Morris *et al.*, 2011; Tudorică *et al.*, 2017).

Tauopathies can be further separated into two categories: primary and secondary tauopathies. PiD, AGD, PSP, FTDP-17 and CBD are examples of primary tauopathies, as these diseases have abnormal tau as the main cause of the pathology, whereas secondary tauopathies, such as AD and Down Syndrome, are diseases that have tau and other co-proteins contributing to the overall neurodegeneration process.

Below, I will discuss only two primary and secondary tauopathies that are relevant to my project: 1) AD, which is considered the most common secondary tauopathy (as major defects in Aβ

processing also fuels the disease pathogenesis), and 2) FTD, which is a primary tauopathy as tau plays a major role in the disease progression (Irwin, 2016).

1.1.2.1 Alzheimer's Disease

Patients with AD manifest with progressive cognitive impairment as pathology initially affects the hippocampus and entorhinal cortex (EC). This is then followed by behavioural and emotional changes at the later stages of the disease as the pathology progresses in other cortical regions, including the frontal lobe and limbic regions (Robinson et al., 2015). AD is now known to have an extensive prodromal stage (10-20 years), with the earliest clinical diagnosis occurring decades after extensive physiological changes, including severe neuronal loss and brain atrophy. Due to the lack of therapeutic interventions, there is a great need to learn more about the exact neuropathological mechanisms of the AD particularly in the early stages of the diseases.

There is now a substantial amount of evidence highlighting the role of Aβ plaques and NFTs in the pathogenesis of AD (see review by Kametani and Hasegawa, 2018). The presence of extracellular senile Aβ plaques, made up of oligomeric Aβ, and NFTs (which consist of hyperphosphorylated tau proteins) has been implicated in neuronal degeneration and cognitive disfunction in AD (Hanger *et al*., 2009; Reitz, 2012). Both proteins have important physiological roles in the human brain, particularly in the maintenance of neuronal functioning and survival, but these proteins can become pathological in disease. Despite what is already known about these aggregates it is still highly debated which pathological protein(s), tau and/or Aβ, has the central role in the neuropathogenesis of AD (Kametani and Hasegawa, 2018). However, It has been repeatedly shown that progression of tau pathology in the brain strongly correlate to neuronal degeneration and cognitive impairment in AD patients than Aβ pathology (see review by Nelson *et al.*, 2012).

1.1.2.2 Frontotemporal dementias

FTDs are a group of primary tauopathies which are clinically characterised by behaviour disturbances, cognitive impairments and motor dysfunctions, are caused by the degeneration of neurons in the frontal and temporal lobes in conjunction with subcortical brain areas (Goedert et al., 2012). Different mutations in the tau gene can either result in an altered amino acid sequence or altered pattern of tau isoform expression. One rare disorder that arises as a consequence of a missense mutation in the tau gene is FTD and Parkinsonism linked to chromosome 17 (FTDP-17). This is an autosomal dominant neurodegenerative disorder and is characterised by personality changes, cognitive impairments, and motor symptoms. Missense mutation of the codon at position 301 in the tau open reading frame results in the production of a leucine (L) or serine (S)

instead of proline (P). These tau mutations give rise to tau-positive inclusions in the brain of patients (see review by Goedert et al., 2012). Tau mutations are further discussed in section 1.2.3.

1.1.3 Pattern of tau pathology is distinct in different tauopathies

The build-up of tau aggregates follows an anatomically predicted and defined pathway in the brain that is characteristic of the type of tauopathy and the clinical progression. This stereotypical pattern of spreading varies between different tauopathies. This is well characterised in AD, and has been the basis of Braak staging (Braak and Braak, 1991). In the earlier stages of AD, the accumulation of NFTs initially begins in a small population of projection neurons in layer II of the entorhinal cortex (EC), an area that is highly connected to memory related neural systems (Figure 2) (Braak et al., 2011). As the disease progresses, accumulation of tau aggregates then spread to connected brain regions such as the hippocampus, including the dentate gyrus and cingulate cortex, and eventually to the rest of the neocortex (Braak and Braak, 1991). This pattern of spread was shown to strongly correlate to the severity of patient clinical outcomes (e.g., memory and cognitive impairments) (Schwarz et al., 2016). In contrast, abnormal accumulation of tau initially begins in the frontal and temporal lobes in FTD.

Although the mechanisms of this stereotypical spread of tau pathology still remains unclear, there are a lot of evidence showing that tau pathology spreads intercellularly along anatomically connected pathways. This has been shown in human tissue, animal models and imaging studies (Duyckaerts et al., 1997; Lewis and Dickson, 2016; Schöll et al., 2016; Vogels et al., 2020). *In vitro* and *in vivo* studies that indicate the propagation of tau pathology are further discussed in 1.5. Interestingly, In AD the area in the brain that more likely to succumb to tau pathology are brain areas that are highly connected through the Braak pathway. The development of positron emission tomography (PET) tracers, such as ^{18}F-AV-1451, has been pivotal to our understanding of the different pathogenesis of tauopathies. This PET tracer selectively binds to the NFTs and not to other types of aggregates in the brain. This allows tau pathology to be mapped, quantified and examined in relation to cognitive performance in AD and/or non-AD living human brains and in post-mortem tissues (Chien et al., 2013; Schöll et al., 2016; Xia et al., 2013). Some of these studies show that ^{18}F-AV-145 binding patterns correlate with the neuropathological staging of tau which increase in proportion to the degree of cognitive impairment and dementia severity. They also showed that spatial patterns of tau tracer binding were in close parallel with patterns of neurodegeneration in the brain. Moreover, these PET studies have shown that tau burden may be influenced by connectivity(Lowe et al., 2018). In many neurodegenerative diseases, those that presented the greatest neuropathology and atrophy where areas in the brain that had the greatest functional and structural brain connectivity. These areas of the brain maybe more

vulnerable because of higher metabolic demands. This therefore may explain why these densely connected regions are likely to succumb to the propagation of tau pathology via 'prion-like' mechanisms (discussed in further in 1.4.1 and 1.5).

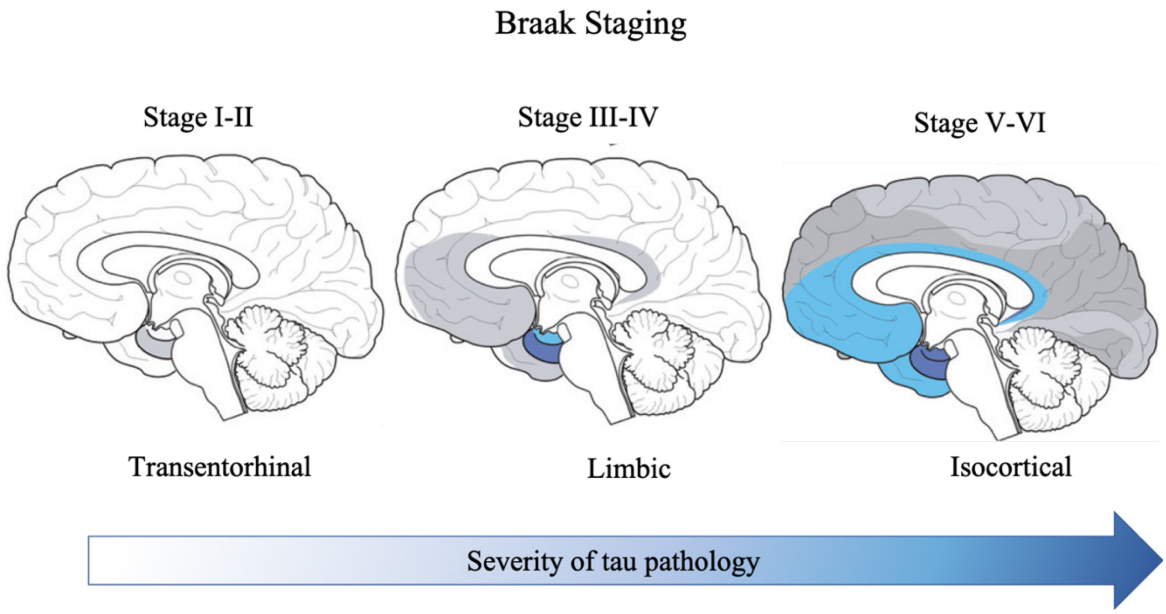

Figure 2. Tau pathology has a distinct anatomical pattern of spread in AD.
Tau pathology and the pattern of spread varies between different tauopathies. In the prodromal stage of AD, this initially begins in the trans-entorhinal regions, which involves the entorhinal cortex (Stage I-II). Using the perforant pathway, tau pathology then spreads to connected regions such as the hippocampus and the limbic areas, including the dentate gyrus and cingulate cortex (Stage III-IV). Once tau pathology spreads to the isocortical areas (Stage V-VI) at the later stages of the disease, patients begin to show clinical symptoms of AD. Adapted from Rüb *et al.*, 2017.

1.2 MAPT tau

1.2.1 MAPT gene structure and tau isoforms

Tau is a microtubule-associated protein (MAP) encoded by the *MAPT* gene. It is located in the human chromosome 17, at position 17q2, and consists of 16 coding exons (as shown in Figure 3A). The encoded tau protein can be subdivided in four main parts: 1) an amino-terminal (N-terminal) region which is encoded by exon 1-5; 2) a proline-rich region which is encoded by exon 7 and 9; 3) a microtubule-binding domain (MTBD), encoded by exon 9-12, and 4) a carboxyl-terminal region (C-terminal) (Figure 3A) (Glenner and Wong, 1984). The MTBD consist of four repeat domains R1, R2, R3 and R4, which will be referred to as microtubule-binding repeats.

Alternative splicing of the tau primary transcript, particularly exons 2, 3 and 10 (Figure 3B), generates six main tau isoforms in the CNS. The amino acid length of these tau isoforms range between 352 to 441 with molecular weights of 45 to 65 kDa (Goedert *et al.*, 1989). The six different tau variants can be distinguished by the presence of three (3R) or four (4R) repeated-regions of exon 10 in the C-terminal part, and the absence (0N) and presence of one (1N) or two (2N) inserts encoded by exon 2 and 3 in the N-terminal domain (Goedert *et al.*, 1989; Andreadis, Brown and Kosik, 1992). Alternative splicing in these exons results in six tau isoforms that can be characterised by six nomenclatures: 2N4R, 1N4R, 2N3R, 0N4R, 1N3R and 0N3R. A higher molecular weight tau isoform (110kDa) also exist in the adult PNS; this is known as 'Big Tau' and is caused by the addition of a larger exon termed 4a in the tau transcript (see review by Fischer and Baas, 2020).

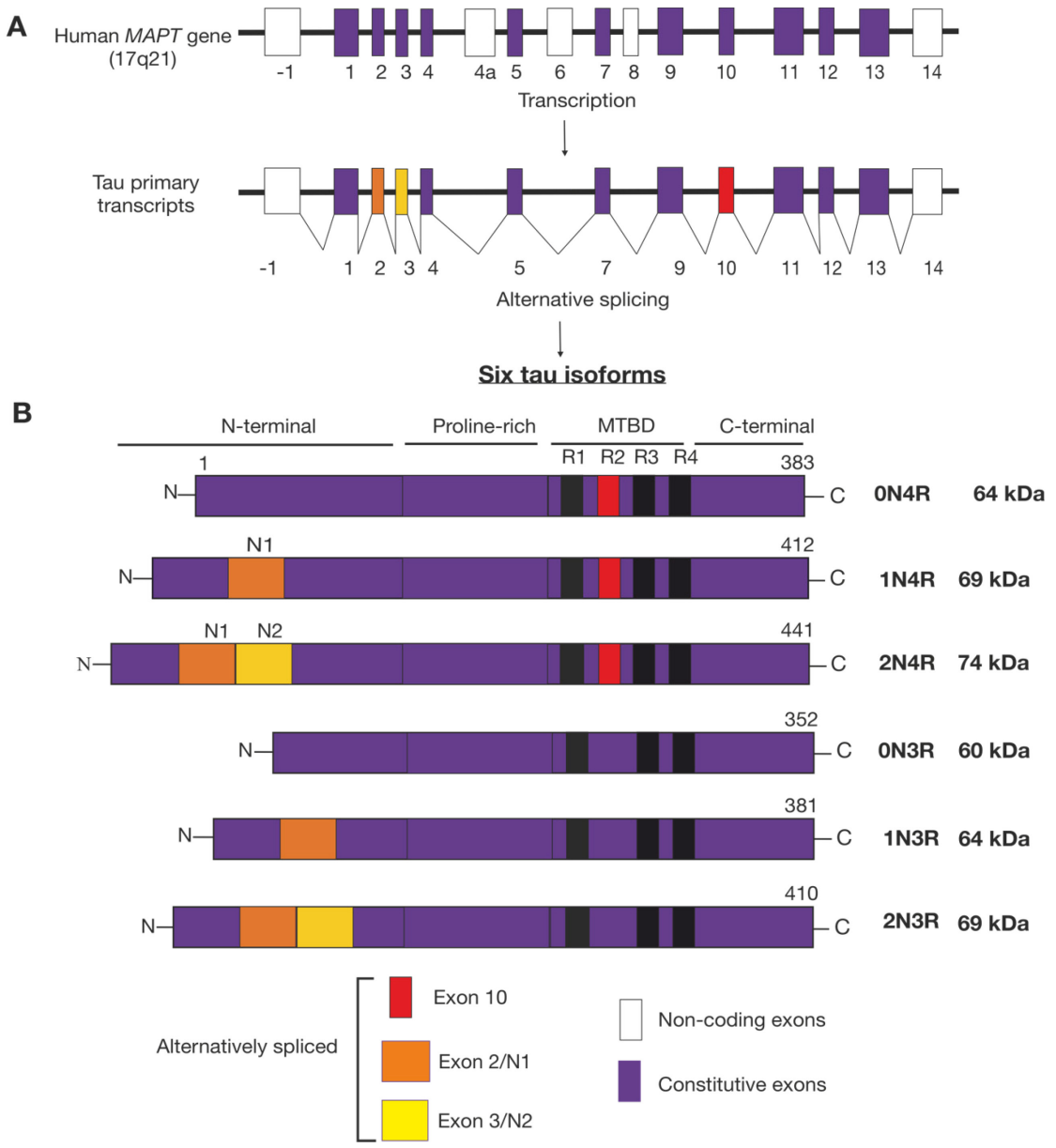

Figure 3. Schematic representation of the splice variation of the human tau gene.

A) MAPT gene encoding human tau protein is located in chromosome 17 at position 17q21 (upper panel). It contains 16 exons but the primary transcript only contains 13 exons (lower panel). Exon 1,4,5,7,9,11,12 and 13 are constitutive, while exon 2, 3 and 10 are alternatively spliced which gives rise to six different mRNA transcripts leading to the production of six tau isoforms. The N- and C-terminal regions of the proteins are subdivided by four different domains: N-terminal domain, proline-rich domain, microtubule binding domain (MTBD) and the C-terminal domain. The presence of 4 (4R, top 3 isoforms) or 3 (3R, bottom 3 isoforms) repeats of the MTBD and the inclusion of either 0 (3R0N/4R1N) or 2 (3R3N/4R/2N) N-terminal inserts produces six different splices isoforms of tau. Adapted from Morris et al., 2011.

Different tau isoforms are preferentially expressed at different stages of neuronal development. In early stages of development, 0N3R tau is the only isoform expressed. However, all six tau isoforms become expressed in a developed adult human brain (Andreadis et al., 1992) and exist in an equal 1:1 4R:3R ratio (Goedert and Spillantini, 2017). This balanced ratio between different 4R and 3R become altered in neurodegenerative diseases like AD; the equal 4R:3R ratio changes to 2:1, with the 4R tau isoform mainly found in aggregates often found in the brains of AD patients (Ginsberg *et al.*, 2006 ; Iqbal et al., 2016). Tau isoforms indicated differences in aggregation potencies and cellular accumulation which may drive tau isoform specific differences that exists between tauopathies. This is further discussed in 1.4.2.

In addition, tau expression in different cellular compartments and populations differ. While tau is highly expressed in the axon of neurons, with a selective preference towards the synapse, there is only a small amount of tau in the somatodendritic compartment (Mandell and Banker, 1996; Morris et al., 2011). Although tau is highly abundant in neuronal cell, it can also be found in glial cells but in limited amounts (e.g., oligodendrocytes) (see review by Morris *et al.*, 2011).

1.2.2 Physiological functions of tau

Tau belongs to a family of microtubule-associated proteins (MAP). Tau is predominantly located in the CNS and highly abundant in neurons, but exists in lower amounts in oligodendrocytes (see review by Buée et al., 2000). The role of intracellular tau is well established as a regulator of microtubule assembly and axonal transport dynamics (Figure 4). Tau is able to bind directly to microtubules through its MTBD region (specially through the 3R and 4R regions). This tau-microtubule interaction is highly regulated by kinases and phosphatases. In the normal human brain, tau is mainly located in the axonal compartment, but is also located in smaller amounts in the somatodendritic compartments, including, the nucleus and plasma membrane, and synapses (Buée et al., 2000). It's physiological roles in the dendritic compartments are currently unknown but some have shown that it could have a role in synaptic plasticity (Chen et al., 2012).

Besides microtubules, tau also has a wide-range of intracellular and extracellular molecular partners including but not limited to DNA or RNA (Sultan et al., 2011), plasma membrane proteins (e.g., muscarinic receptors, sulphated proteoglycans) (Gómez-Ramos et al., 2009; Holmes et al., 2013), and synaptic proteins such as synaptogyrin, Fyn kinase and PSD-95 (Ittner et al., 2010; McInnes et al., 2018; Pooler et al., 2012a; Sultan et al., 2011). Because of this, tau may also have novel function such as a neuronal signalling molecule, neuronal polarity, DNA protection, and synaptic regulation.

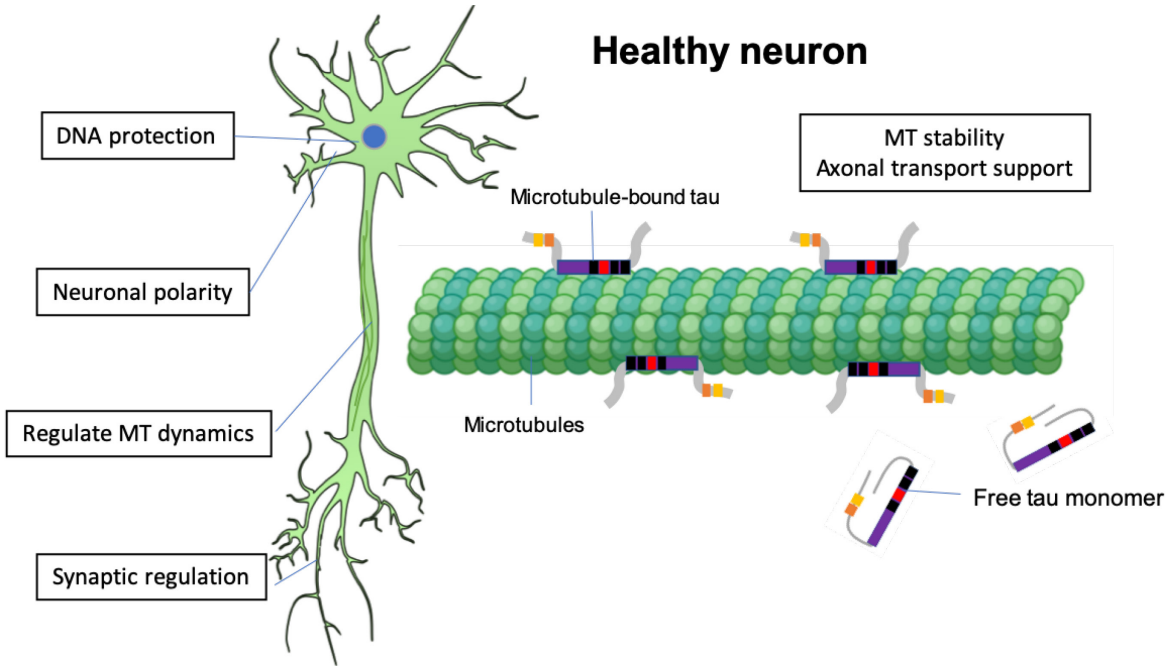

Figure 4. Illustration of the physiological functions of tau.

1.2.3 Tau mutations

At least 53 mutations in the *MAPT* genes have been identified, most of which are located in the MTBD (Ghetti et al., 2015). The majority of these mutations are found in patients diagnosed with FTDP-17 (see section 1.1.2.2 for FTDs). The most characterised missense mutations are those located in exon 10, which correspond to the R2 domain. Missense mutations can occur in exon 10 located at codon 301 of *MAPT* tau leading to amino acid change from a proline to leucine (P→L) or proline to serine (P→S), which can be denoted as P301L or P301S, respectively (Hasegawa et al., 1998; Bugiani *et al.*, 1999). As this region has direct contact with the microtubule network, mutations in this region have been closely associated with impaired microtubule dynamics and assembly (Hasegawa et al., 1998). There are multiple studies that have looked into these mutations (Fischer et al., 2007; von Bergen et al., 2001). These studies have shown that P301L mutation has higher propensity to become hyperphosphorylated and more efficient at forming β-sheets during aggregation when compared to wild-type (WT) tau. This occurs because of the change from P→L residue which therefore leads to stronger β-sheet formation in this specific region (Fischer et al., 2007; von Bergen et al., 2001). Mutations within exon 10 (P301L, P301S) can only exist in 4R-tau because this amino acid is located in the second repeat of the MTBD (Morris et al., 2011). Other missense mutations locating outside exon 10, but within the MTBD, also affect tau and microtubule interaction. Furthermore, other types of mutations, such as intronic mutations in the splicing region following exon 10 can also shift the 3R/4R balance (Morris et al., 2011).

1.2.4 Post-translational modifications of tau

Various spectroscopic studies have shown that tau is naturally an intrinsically disordered protein (IDP), which means that it is natively unfolded as well as lacking a well-defined and stable, three-dimensional structure (Jeganathan et al., 2006; Jeganathan et al., 2008). In normal conditions, the structure of tau in solution is best described as a random-coil, much like a 'paperclip', with the C- and N- terminal domain folded over the repeated regions of the MTBD domain in solution (Jeganathan et al., 2006). Tau can shift between a microtubule-bound state to an unbound, highly soluble random coil as a consequence of various post-translational modification (PTMs).

PTMs such as phosphorylation, acetylation, crosslinking by transglutaminase, glycation, isomerisation, nitration, sumoylation, oxidation and ubiquitination, play roles in the regulation of tau function and structure (Andreadis et al., 1992). However, phosphorylation is the most common PTMs and has been closely associated with neuropathogenesis of tauopathies (Hanger et al., 2009). Full-length tau (4N2R) is known to be phosphorylated in 85 sites; 45 occur at serine (S) residues, 35 in threonine (T) and 5 at tyrosine (Y) residues. About 40 phosphorylation sites have been identified to be AD-related (Figure 5) (Hanger et al., 2009). Phosphorylation of tau is tightly regulated by kinases and phosphatases. Under physiological conditions, the rate of phosphorylation and dephosphorylation are at a dynamic equilibrium (Martin et al., 2013). When this balance is disturbed, either through impaired kinase and phosphatase activity or other PTMs, tau can undergo pathological structural and functional changes, causing a misfolding event. This eventually leads to the accumulation of intracellular tau aggregates which have detrimental effects on neuronal functioning and survival (Hanger et al., 2009).

Supporting evidence suggest that hyperactivity of kinases such as extracellular regulated kinase 1 and 2, glycogen synthase 3, cyclin-dependent protein kinase 5 and reduced activity of phosphatases such as, protein phosphatase 1 and 2A work in combination to induce abnormal hyperphosphorylation and therefore tau pathology (see review by Buee *et al.*, 2000; Hanger et al., 2009). This highlights the importance of regulating homeostatic balance in cellular processes and that in AD this is perturbed.

In AD, as a consequence of hyperphosphorylation, tau can misfold to gain secondary structure, and can transition from a natively unfolded protein into a pathogenic misfolded and insoluble entity, rich in β-sheet conformations (von Bergen et al., 2001; Von Bergen et al., 2005). Abnormal phosphorylation can cause a cascade of events (as outlined Figure 7 and Figure 6): 1) it will induce tau to detach from microtubules and 2) the random-coil structure of soluble tau could unravel, causing the N-terminal and C-terminal region to move away from the microtubule-binding repeats regions, causing it to be exposed to further phosphorylation. This situation can initiate the

interaction of 'sticky' microtubule-binding repeats regions causing the formation of filaments and tangles, rich in β-sheets. Aggregation of tau under pathological condition is further discussed in section 1.4.

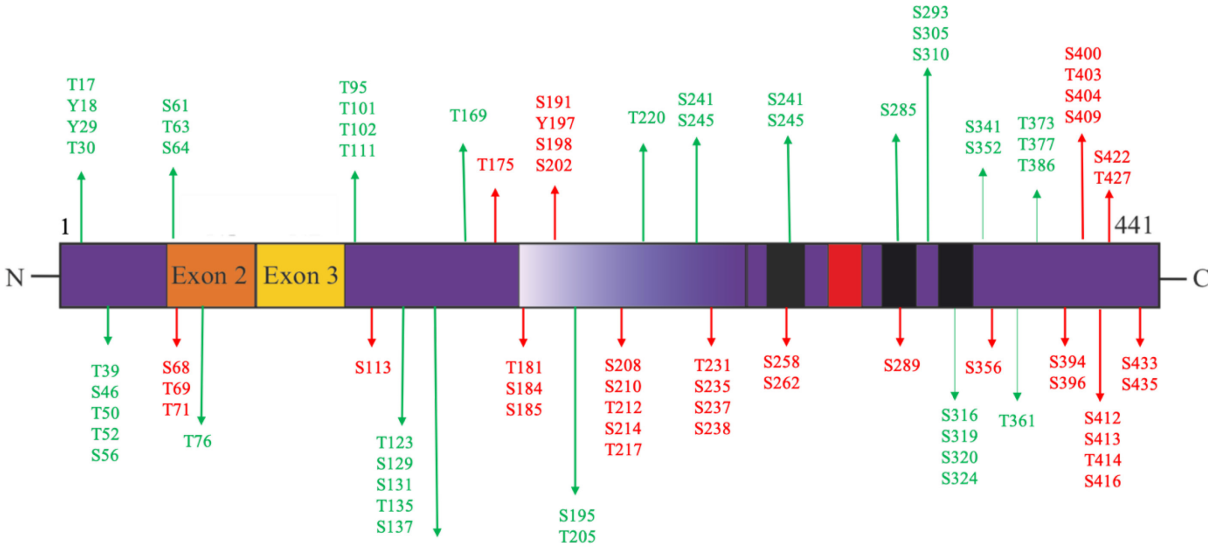

Figure 5. Phosphorylation sites of full-length tau (4N2R).
Physiological phosphorylation sites (green) and disease-associated phosphorylation sites (red) which have been identified in literature (adapted from Hanger et al., 2009).

1.3 Tau dysfunction

1.3.1 Loss-of-function vs gain-of-toxic function

One of the ongoing debates for the role of tau in neurodegenerative diseases is whether tau pathology is caused by the loss-of-function (LOF) of tau or through its gain-of -toxic function (GOF) (see review by Mudher et al., 2017)(Figure 6). While phosphorylation of tau protein is part of normal cell function, abnormal hyperphosphorylation of tau proteins can lead to structural changes that causes them to detach from microtubules, and eventually lead to the formation of NFTs. This cascade of event eventually leads to LOF and GOF mechanisms.

Firstly, increased detachment of tau from microtubules leads to impairments in microtubule dynamics and stability. As a consequence of being sequestered in NFTs, there is generally reduced quantities of native tau able to maintain the cells normal biological functions (Figure 4). Hyperphosphorylation-mediated loss of tau function can lead to axonal transport and synaptic deficits, as well as the mis-sorting and mislocalisation of nuclear and synaptic proteins (Eftekharzadeh et al., 2018; Hoover et al., 2010; McInnes et al., 2018; Wu et al., 2021)(Figure 6). Although the loss of tau function can induce some neuronal deficits, complete ablation of tau protein expression is not enough to affect the viability and fertility of animals (Dawson et al., 2001; Harada et al., 1994); however, homozygous knockouts mice models of the MAPT gene (*MAPT-/-*) did start developing motor and behavioural deficits at a later age. Harada et al., (1994), who was the first to develop the tau knockout mice, showed that another MAP protein can perform similar functions to tau (Harada et al., 1994). In these MAPT-/- knock out mice, *MAP 1A* gene expression increased 2-fold in response to the lack of tau in young mice (Harada et al., 1994). This suggests that other compensatory mechanisms or proteins could support the functionality of the cell without tau. Interestingly, in double-knockouts of *MAPT* and *MAP1A*, mice developed severe phenotypes including, impairments in axonal elongation, neuronal migration, and disrupted the maturation of primary neurons, when compared to single-knockouts of these mice (Takei et al., 2000). This shows that the cellular machinery is equipped to deal with the lack of tau function. As the roles of tau is emerging, it is likely that we will learn more modes of toxicity via LOF mechanisms.

There are increasing amount of evidence indicating that tau pathology is driven by the GOF. Different pathogenic forms of tau, including, but not limited to misfolded soluble oligomers and tau with abnormal PTMs, can deteriorate synaptic and neuronal functioning, particularly early in disease (see review by Tracy and Gan, 2018). Aberrant hyperphosphorylated tau has been shown to impair axonal transport and trafficking. This has been clearly shown in the work by Hallinan and

colleagues who demonstrated that misfolded tau can impair lysosomal trafficking, thus reducing number of available lysosomes in the distal axon of primary hippocampal neurons (Hallinan et al., 2019). Interestingly, misfolded tau was not acutely toxic as neurons remained viable and electrically competent (Hallinan et al., 2019). However, misfolded tau was able to propagate misfolding and aggregation efficiently in a connected neuronal network. This showed that tau-induced toxicity may be due the spread of misfolded tau early in the disease process. Indeed, one of the strongest evidence for the tau GOF is the formation of ordered tau assembly from misfolded and aberrant tau proteins, and their ability for propagate along connected neuronal networks before overt neurodegeneration (see review by Goedert and Spillantini, 2017). As a consequence of the accumulation of pathogenic misfolded tau protein aggregates, the eventual formation of NFT could result in space-occupying GOF. However, toxicity of this is debated as there is evidence showing that neurodegeneration and dysfunction can be rescued even with the presence of NFTs (SantaCruz, 2005).

Pathogenic tau oligomers have also been shown to disrupt cytoskeleton integrity, causing impairment in anterograde and retrograde trafficking along the microtubules (Mietelska-Porowska et al., 2014). Moreoever, pathogenic tau can exert GOF by instigating mitochondrial damage (Shafiei et al., 2017). Tau oligomers, in particular, have been closely associated with damage to mitochondrial membrane components causing the activation of pro-apoptotic pathways (Shafiei et al., 2017). Furthermore, tau has also been shown to be mislocalised in the somatodendritic compartment (Tracy and Gan, 2018). Here, mislocalised tau disrupted synaptic plasticity and memory of mice expressing human tau (hTau) with mutations that mimic aberrant acetylation (Tracy and Gan, 2018). Likewise, a transgenic mice model of tauopathy, which expresses regulated P301L human mutant tau ($hTau^{P301L}$), showed that pathogenic tau mislocalises to the dendrites and dendritic spines, causing detrimental effects in long-term potentiation which is important in learning and memory function (Hoover et al., 2010). In the same study, when cultured hippocampal neurons were expressed with tau mutant that mimics hyperphosphorylation, mis-localised tau reduced α-amino-3-hydroxy-5-methyl-4-isoxazolepropionic acid (AMPA) and N-methyl-d-aspartate (NMDA) receptors at the dendritic synapses, which in turn impaired synaptic transmission (Hoover et al., 2010). Taking all of these studies together, it is likely that pathological changes in tau may lead both LOF and GOF mechanisms. In the early stages of disease, the LOF of tau could eventually convert to GOF.

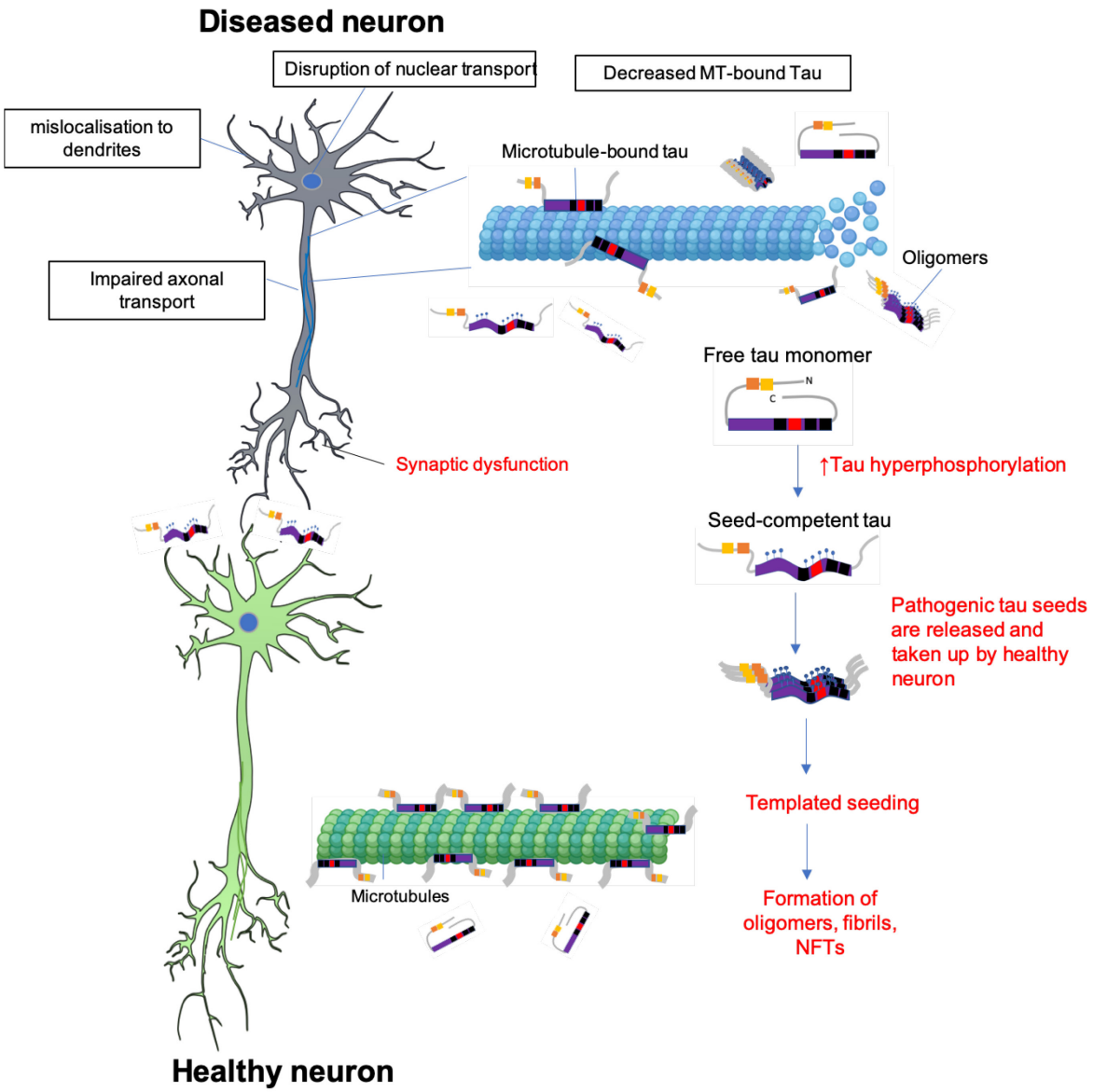

Figure 6. Illustration of the loss of function and gain of toxic function of tau.

In normal conditions, tau is associated with microtubules, via the microtubule binding repeat domains (e.g., R1, R2, R3, R4), where it regulates microtubule structure and dynamics. The transition of free tau monomer and microtubule-associated tau is tightly regulated by post-translational modifications. In diseased conditions, tau may become hyperphosphorylated which causes increased detachment from microtubules. This reduces natively folded tau availability to support microtubule dynamics and further leads to axonal transport deficits and tau mislocalisation to dendritic compartment. Tau can also disrupt mitochondria and nuclear transport. In solution, free tau monomers in solution folds in a random coil manner. When tau is hyperphosphorylated, the protein can open up exposing the protein to further misfolding, which subsequently leads to seed-competent tau. This catalyses the formation of large tau assemblies such as insoluble fibrils, rich in β-

sheet structures and eventually neurofibrillary tangles (NFTs). These toxic tau seeds can be released and be taken up by healthy neurons and initiate templated seeding. As toxic tau seeds are able to induce their misfolded conformation to naïve tau monomers, this process leads to the propagation of tau pathology in connected neuronal network. The formation of oligomers leads to synaptic dysfunction.

1.3.2 Which tau protein species causes toxicity?

Different tau species have been proposed to mediate the neuronal toxicity observed in tauopathies. Although NFTs are hallmarks of tauopathies, there is evidence showing that smaller molecular species of tau induce the most toxicity, rather than large insoluble aggregates (Michel et al., 2014; Mirbaha et al., 2015; Tian et al., 2013). When tau production was suppressed in a transgenic mouse model expressing regulatable 0N4R tau P301L (also known as the rTg4510 model), behavioural deficits were rescued even after the formation of NFTs (SantaCruz, 2005). Interestingly, NFT formation still increased despite ablation of tau expression showing that it is not essential for neuronal loss.

There is still ongoing debate about which tau species (e.g., monomers, dimers, oligomers and small fibrils) is the most potent in spreading tau misfolding and aggregation, thus more neurotoxic. In a recent study, tau oligomers showed to be the most potent in inducing tau aggregation when applied to tau monomers than tau fibrils (Ghag et al., 2018). However, tau oligomers are quite hard to define as they come in different sizes. There is also evidence showing that smaller species of tau (e.g., monomers, dimers, trimers) can induce neurotoxicity (Michel et al., 2014; Mirbaha et al., 2015; Tian et al., 2013).Trimers containing three molecules of misfolded tau were most neurotoxic when applied to SH-SY5Y cells (Tian et al., 2013). More studies are needed to determine which tau species is more neurotoxic.

1.4 Tau aggregation

In order to understand the mechanisms of tau aggregation, it is important that definitions and terminologies are clarified as they are highly inconsistent in literature. Tau aggregation is defined as the process in which tau molecules self-assemble into a highly ordered tau structures or aggregates, that are rich in β-sheet structure (Goedert and Spillantini, 2017). These include oligomers, fibrils, filaments and NFTs. Similar β-rich protein structures can be seen in other disease-associated proteins such as α-synuclein, huntingtin and Aβ. These are often described as amyloidogenic proteins because they have well-defined cross β-sheet structures. Tau aggregates can be identified by using β-sheet sensitive dyes (e.g., Thioflavin T, Congo Red) and are usually highly insoluble (see review by Mudher *et al.*, 2017), however some smaller oligomers and fibrils can be soluble too. Tau accumulation can be loosely used to describe the build-up of tau aggregates (of variable sizes) in the cell. Further discussed in this chapter is the initiating process that leads to tau misfolding and consequently to the formation of different filaments that define different diseases.

1.4.1 Defining 'prion-like' mechanisms

The propagation of tau pathology in connected brain areas are often described as 'prion-like'. In order to understand what this means and why 'prion-like' is use, it is first important to understand what prions are.

Prions are self-replicating protein aggregates that are found in transmissible, genetic and sporadic degenerative diseases that affect the brains of mammals (Prusiner, 1982). Prion diseases includes but are not limited to Creutzfeldt-Jakob disease, Gerstmann-Sträussler-Scheinker syndrome chronic wasting disease in deer and elk; scrapie in sheep; and bovine spongiform encephalopathy. The ability to self-replicate arises due to the multiple existence of different prion protein (PrP) isoform conformations: PrP^{C}, is the natively folded cellular isoform of prion protein, and the PrP^{SC}, is the highly-infectious misfolded protein found in the prion diseases. The replication that occurs in prion diseases commences when the PrP^{SC} induces a conformational transformation on the PrP^{C} via a templated-directed manner, causing misfolding and the formation of more infectious and transmissible aggregates (Prusiner, 1982). Similarly, this aggregate spreading phenomena has also been observed in proteins associated with various neurodegenerative diseases such as tau, Aβ and α-synuclein in many tauopathies (i.e. AD, PD, ALS) (Fraser, 2014; Frost and Diamond, 2010). The term 'prion-like' is used when describing these proteins as they do not fully encompass all of the characteristics that define prion proteins, although prion-like proteins are able to self-propagate, they are not transmissible from person to person (Fraser, 2014). However, like prions,

they would be able to keep the same biological properties and generate the same pathological lesions even after many passages.

There is accumulating evidence to suggest that tau pathology can spread across neuronally connected circuits in the brain of patients with tauopathies, via 'prion-like' mechanisms (De Calignon et al., 2012; Liu et al., 2012; Mudher et al., 2017) (Figure 7A-C). This occurs when a pathogenically misfolded tau protein, often referred to as a tau 'seed', is released and taken up by a connected neuron, where then it induces conformational misfolding of healthy natively folded tau (Goedert and Spillantini, 2017; Lewis and Dickson, 2016). This phenomenon is termed, 'templated seeding' (Figure 7C). Further recruitment of natively folded tau monomers via a nucleated-manner results in more misfolding and the formation of toxic tau assemblies (Figure 7C). This eventually forms larger aggregates and insoluble NFTs inside cells. Therefore, these misfolded tau seeds can act as a catalyst in a reaction that leads to the 'prion-like' spreading of tau pathology (Goedert and Spillantini, 2017; Lewis and Dickson, 2016). Pathogenic tau 'seeds' that exists in different tauopathies have distinct structures and dictates clinical progression of the disease.

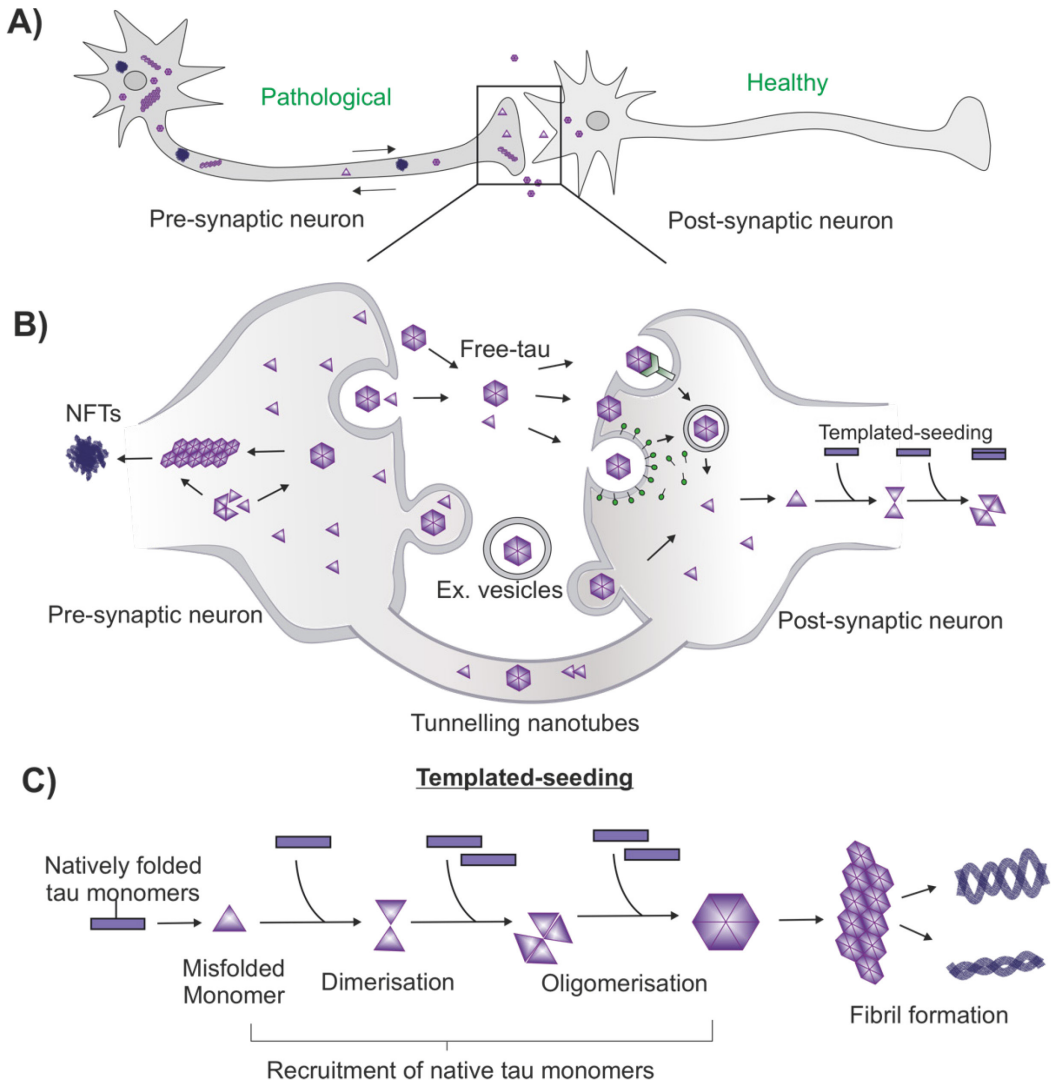

Figure 7. Schematic diagram of tau aggregation and propagation across connected neuronal networks.

A-B) Illustration of the potential mechanisms of prion-like propagation of pathogenic tau species in a connected neuronal network. Pathogenic tau seeds can be secreted as a membrane free protein, released inside extracellular vesicles such as exosomes and ectosomes, or be transported via tunnelling nanotubes. These pathogenic tau seeds are taken up by healthy neurons. Once in the cytosol of the recipient post-synaptic cell, pathogenic seed-competent tau templates its misfolded conformation to healthy native tau, which subsequently produces downstream aggregation. C) Mechanisms of templated-seeding. Pathogenic tau with seeding properties recruits natively folded tau monomers and templates its misfolded conformation causing further misfolding. This leads to fibril formation and eventually larger aggregates. The minimum unit for a pathological tau seed is currently unknown, but this acts as a building block to recruit more tau proteins to form larger fibrils and NFTs. Image is adapted from Goedert and Spillantini, 2017.

1.4.2 Tau misfolding and seeding

1.4.2.1 Tau self-assembly in AD

Prior to the assembly of tangles, an initial misfolding event must first occur, however, this process is poorly understood. It is thought the aberrant PTMs may initiate tau self-assembly. Aberrant PTMs, such as phosphorylation of disease-specific residues or truncation may result in the detachment of tau from the microtubules which initiates a cascade of events that eventually lead to abnormal folding of tau (Figure 6). In solution, the normal 'paper clip' conformation becomes unfolded (Jeganathan et al., 2008); the N- and C-terminus move away from the MTBD, exposing it to further PTMs. This exposes the fragments of tau containing the MTBD that promote tau self-aggregation. Hyperphosphorylation of tau is the most common PTM associated with increased tau misfolding. There are at least 40 phosphorylation sites, primarily located in the proline-rich region and C-terminal domains of tau, that has been closely associated with AD (Figure 5) (Hanger et al., 2009).

Many studies have tried to recapitulate tau self-assembly *in vitro*. Due to its hydrophilic nature full-length tau has very low tendency to aggregated *in vitro*. However, it has been shown that the addition of polyionic factors such as heparin, nucleic acid or arachidonic acid, has been shown to induce efficient aggregation of tau (reviewd by Kuret *et al.*, 2005; Goedert and Spillantini, 2017). It has been found that tau's ability to self-aggregate is encoded in its own sequence. von Bergen and colleagues showed that the presence of two hexapeptide motifs in the R2 and R3 repeats of the MTBD, ^{275}VQIINK^{280} (PHF6) and ^{306}VQIVYK^{311} (PHF6*), located in the N-terminal region, are the crucial sequences that determine ability of tau to self-aggregate (von Bergen *et al.*, 2000). When these motifs are exposed, tau is able to undergo seeded aggregation. This event is believe to initiate the formation of the ordered self- assembly of tau (Jeganathan *et al.*, 2008; see review by Avila *et al.*, 2016).

1.4.2.2 Distinct forms of tau monomers encode strains

Although tau monomers are relatively unstructured and does not spontaneously self-assemble, in certain conditions, tau can conform to states that enable them to become seed-competent and form larger tau assemblies. Kaufman et al., (2016) initially found that inoculation of 18 distinct disease-associated tau strains in the brain of WT mice led to a large variability in tau pathology pattern, rate of disease progression and fibril formation (Kaufman et al., 2016). This observation supported the idea that the existence of certain tau strains, with defined protein structure, may give rise to different tauopathies. In contrast, there is evidence showing that different forms of monomeric tau can encode strains information (this can also be referred to as a conformer and is

described in 1.4.3.1), rather than larger tau entities, which in turn dictate the diversity of tau aggregate structures that are often observed in tauopathies (Mirbaha et al., 2018; Sharma et al., 2018). Mirbaha et al., (2018) also demonstrated that monomeric tau can adopt two different conformational state: an inert tau monomer (M_i) that does not spontaneously self-assemble, and a tau monomer which has the ability to self-aggregate and have high seeding capabilities (M_s). It has been proposed that inability of M_i to self-assemble may be owing to the fact that the PHF6 and PHF6* motifs may be hidden in tau hairpin structures and therefore inaccessible, as previously discussed (Mirbaha et al., 2018). On the other hand, M_s for has been shown to have the ability to propagate from cell-to cell, and spread its misfolded structure to other tau monomers (Mirbaha et al., 2018). M_s is proposed to be the building block of seeded-aggregation. Moreover, It was also established that M_s derived from a single strain can give rise to different sub-strains that has different structures (Sharma et al., 2018). Whether M_S precedes or follows the formation of large tau aggregates still remains to be elucidated.

1.4.2.3 Which tau seeds cause propagation?

It is currently debated which species of tau are released and taken up by cells, as well as initiate a new round of fibrilisation and templated seeding of native tau. It has been shown that tau monomers are the minimum unit required for tau propagation (Michel et al., 2014). Marc Diamond's lab suggested that tau trimers are the most pathogenic of other tau units as they are capable of triggering spontaneous tau seeding and propagation in cultured cells (Mirbaha et al., 2015). On the other hand, there is a substantial evidence indicating oligomers, larger units of tau, as the toxic tau seed responsible for tau propagation and synaptic dysfunction (Shafiei et al., 2017). For instance, the levels of tau oligomers have been shown to correlate well with the clinical symptoms of AD and PSP patients (Lasagna-Reeves *et al.*, 2012a). Furthermore, synaptic and mitochondrial dysfunction can be observed when oligomers, endogenously derived from AD-brains, are injected into the brain of wild-type mice, whereas tau monomers or fibrils do not elicit any severe pathologies (Lasagna-Reeves et al., 2011). It has also been independently shown that oligomeric tau is also capable of inducing endogenous tau to misfold and propagate in a 'prion-like' manner from healthy brain regions in mice (Lasagna-Reeves *et al.*, 2012; Wu *et al.*, 2013).

1.4.3 Tau conformers define different tauopathies

1.4.3.1 Definition of a tau conformer

The observation that tau filament morphologies differs between tauopathies has led to the idea that tau can fold and aggregate in many ways giving rise to different molecular conformers or 'strains' (Crowther and Goedert, 2000). A *bona fide* conformer or strains can be defined by structural and biochemical features, and/or their ability to resist proteolytic enzymes (Falcon et al., 2018; Fitzpatrick et al., 2017; Goedert et al., 1989). In this review, a seed-competent conformer is defined as a self-assembled proteinaceous molecule or aggregates that has a protease-resistant core. The core units of a seed-competent conformer, made up of aberrant or misfolded tau, must be capable of propagating its conformation properties to naïve and soluble version of itself and be able to recapitulate similar neuropathological characteristics *in vivo* (Goedert and Spillantini, 2017; Kaufman et al., 2016; Sanders et al., 2014).

1.4.3.2 Structural differences between disease-associated conformers

Studies have shown that tau filaments have a central core composing of highly ordered β-sheet structures, that is embedded in an unstructured fuzzy coat (Berriman et al., 2003; Barghorn et al., 2004). And more recently, cryo-electron microscopy (cryo-EM) has reveal that diseases-associated tau filament core has been shown to adopt a combined cross-β/β-helix, and that there are differences in filament cores between tauopathies (Falcon et al., 2018; Fitzpatrick et al., 2017). Using cryo-EM, structural differences between tau filament conformers were found in AD and PiD (Falcon et al., 2018; Fitzpatrick et al., 2017). The core of these filaments are structurally distinct between different tauopathies as demonstrated by PiD and AD (Falcon et al., 2018; Fitzpatrick et al., 2017).

AD cores are composed from two individual protofilaments containing residues 306-378, which coincides with the hexapeptide motifs of the repeat regions in the MTBD. They also found that different ultrastructural polymorphs exist in AD and PiD tau filaments; In AD, these filaments can be categorised by two different types: paired helical filaments (PHF) and straight filaments (SF). Although the overall 3D structure is different, the two core protofilaments of PHFs and SFs have the same C-shaped sub-units that are arranged slightly differently when packed together (Figure 8, right) (Fitzpatrick et al., 2017). Similarly, different types of filaments have also been isolated in PiD, including narrow pick filament (NPF) and wide picks filament (WPF) (Figure 8). In contrast to AD, filaments taken from PiD patients organise themselves differently; the core tau sub-units adopt J-shaped form (Figure 8, left) (Falcon et al., 2018). The tau conformer that result in the development of chronic traumatic encephalopathy has also since been discovered (Falcon et al.,

2019). These tau conformers are proposed to have an effect in the way tau interacts with other factors, tissue components, sites of aggregation, and levels of cytotoxicity which could explain the variable neuropathological and clinical manifestation of each tauopathies (Goedert and Spillantini, 2017).

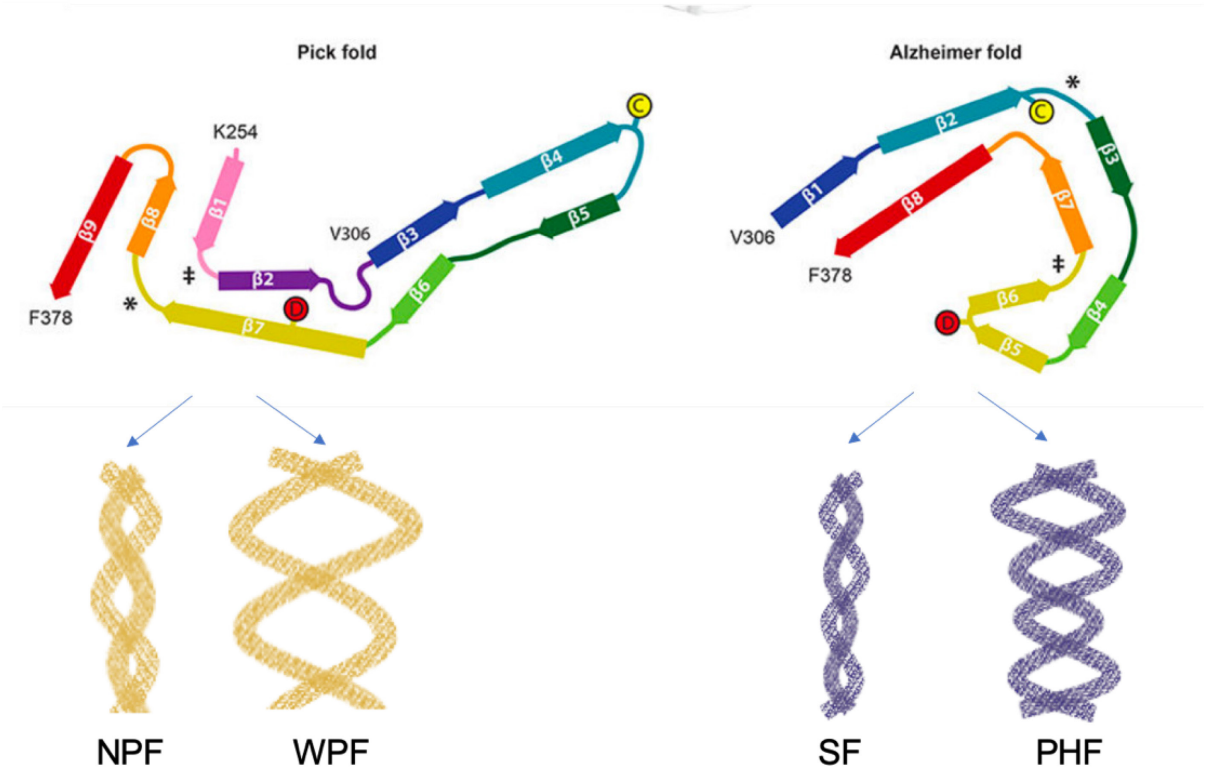

Figure 8. Comparison in core filament structures between different tauopathies. PiD adopts a J-shaped form, whereas AD assumes a C-shaped form. Different variations of filaments may also exist for each PiD and AD. For PiD, narrow pick filament (NPF) and wide picks filament (WPF) has been identified. For AD, straight filaments (SF) and paired helical filaments (PHF) were identified. Image adapted from Falcon et al., 2018 and Goedert and Spillantini, 2017.

1.4.3.3 How tau isoforms affect tau conformers and aggregation

Besides displaying distinct morphological structures, different tau conformers in tauopathies accumulates in specific cells and in certain brain regions, as well as vary in isoform composition (e.g., 3R +4R, 3R, 4R) (see review by Clavaguera et al., 2015). For instance, in AD, intracellular inclusions are mainly made out of PHFs composing of all six isoforms (e.g., 3R and 4R) that are restricted to neurons. In PiD, tau deposits aggregates into Pick's bodies inside neurons and glia, mainly composing of 3R tau. In comparison, mainly 4R tau are observed in tau-positive aggregates in patients with CBD and PSP; these are found in both neurons and glial cells (e.g., oligodendrocytes and astrocytes) (Clavaguera et al., 2015). Furthermore, differential toxicity and seeding potential may exists within different isoforms. Rate of aggregation has been reported to be faster in 4R isoforms over 3R(Goedert and Jakes, 1990). Moreover, it has been reported that expression of 4R tau isoforms in *Drosophil*a leads to greater neurodegeneration and impairments in learning and memory, whereas expression of 3R tau lead to axonal transport defects and locomotor impairments (Sealey et al., 2017). These two isoforms also displayed distinct phosphorylation patterns. These differences in pathological potencies are not because of differential expression levels of these isoforms, but rather a consequence driven by isoform-specific structural biology (Sealey et al., 2017). This may explain why certain isoforms of 3R and/or 4R exists in different types of tauopathies.

1.4.3.4 Tau conformers dictates heterogeneity of disease

Tauopathies demonstrate high heterogeneity in its clinical presentation; the pattern of neuropathology, the appearance of NFT in the brain, rate of progression, and cellular and regional involvement is unique in different diseases (see review by Goedert and Spillantini, 2017). It has been suggested that the presence of distinct tau conformers that exist within different tauopathies gives rise to this variability (Kaufman et al., 2016; Sanders et al., 2014). Interestingly, recent evidence suggests that that different conformers may also exist within the same tauopathy (Dujardin et al., 2020). Dujardin et al., 2020 found that there are different tau conformers demonstrating distinct biochemical and biophysical characteristics exist with within AD. This may explain why different individuals with the same disease diagnosis presents distinctive clinical course. It is unclear what molecular drivers causes this diversity within a common phenotype, but this study emphasises the need for personalised medicine for threating tauopathies.

1.5 Propagation of tau pathology

1.5.1 Evidence of cell-to-cell tau transmission

The pathogenic tau species responsible for the propagation of tau pathology along the anatomically connected pathway via prion-like mechanisms, are still debated (Walsh and Selkoe, 2016). Various *in vitro* and *in vivo* studies have been able to recapitulate this prion-like behaviour by demonstrating that misfolded and pathogenic tau seeds can be released from an affected cell, be taken up by connected cells (via synaptic and non-synaptic routes), where they can then template the misfolded conformation on to naïve soluble tau, and ultimately initiate a cascade of events in generating larger tau aggregates (Frost et al., 2009; Pickett et al., 2017; Wang et al., 2017; Wu et al., 2013)(Figure 7).

Firstly, tau has been shown to escape cells via multiple routes under both pathological and physiological conditions in neuronal and non-neuronal cell model systems (Chai et al., 2012; Karch et al., 2012; Pooler et al., 2013; Saman et al., 2012; Simón et al., 2012b; Yamada et al., 2014). There are studies showing tau can be released during normal synaptic activity (Pooler et al., 2013; Yamada et al., 2014). This raises the possibility that tau could have a role in the extracellular space. Mechanisms of tau secretion are further discussed in 1.7. Secondly, it has been shown that pathogenic tau can be taken-up by non-neuronal and neuronal cells in culture. *In vitro*, misfolded tau can be taken-up and induce templated seeding in recipient cells. Frost et al., (2009) showed that misfolded tau can be transferred between co-cultured human embryonic kidney cells (HEK293) and neuronal precursor (C17.2) cells (Frost et al., 2009). Direct application of synthetic pre-formed fibrils (PFF) into the extracellular medium of C17.2 cells, resulted in the new formation of tau aggregates in the recipient cells. These results have since been replicated in vitro using HEK293 biosensor cell lines, HeLa and primary neurons (Kfoury et al., 2012; Wu et al., 2013) . These studies collectively showed that a 'donor' cell is capable of releasing pathogenic tau proteins into the extracellular space. Recipient cells take-up these seed-competent tau proteins. Once inside, the conversion of soluble naïve tau commences and templated seeding causes the formation of new aggregates.

Transgenic mice models have been pivotal in understanding transmission and spreading of tauopathy in the brain. One of the earliest studies that clearly demonstrated the ability of tau to recruit and seed aggregation *in vivo* was done by Michel Goedert's lab in 2009. Firstly, PFFs were isolated from a transgenic mouse expressing a human mutant tau (hTau) containing a point mutation at position 301, often seen in patients with FTDP (P301S)-termed Tau^{P301S} from now on (Clavaguera et al., 2009). PFF extracted from the Tau^{P301S} mice were then inoculated to the brains

of healthy mice (also known as ALZ17 line), expressing wild-type (WT) tau. This caused WT hTau to assemble into filaments. These filaments were first observed in the injection site but later progressed into anatomically connected brain regions. Moreover, inoculation of AD-derived patient brain extracts in to the brains of ALZ17 mice also demonstrated similar findings (Clavaguera et al., 2013; Lasagna-Reeves et al., 2012b). These studies suggest that a connectome-dependent transmission of misfolded and pathogenic tau aggregates could explain the anatomical pattern of spread often seen in different tauopathies.

One of the earliest evidence of tau seeding of endogenous tau *in vivo* was reported by De Calignon and colleagues, who generated a transgenic mouse model (e.g. rTgTauEC) that selectively overexpressed $hTau^{P301L}$ in neurons located in the layer II of EC (De Calignon et al., 2012). The group then monitored the aggregate formation in connected neuronal circuit and brain regions. Accumulation of tau aggregates was initially observed in neurons from EC II, where the human tau transgene is selectively expressed, but with time this was found to eventually spread to connected brain areas, first in the dentate gyrus, hippocampus and then to rest of the cingulate cortex. The EC layer II consists of neurons that that regulate communications in the brain; it provides direct input and output to the hippocampus and the rest of the cortex. Interestingly, $hTau^{P301L}$ proteins were detected in neurons that did not express mutant $hTau^{P301L}$ transgene mRNA and are distant to the EC (De Calignon et al., 2012). Furthermore, co-localisation of endogenous mouse tau with NFTs that consisted of mutant $hTau^{P301L}$was observed, thus concluding that misfolded tau must have the ability to recruit and template healthy and native tau into aggregates. Another independent *in vivo* study also supports the concept that tau pathology progresses in a circuit- based manner (Liu et al., 2012). A mouse model was generated to restricted expression of mutant $hTau^{P301L}$ in the EC (using a neuropsin promoter). In this mouse, tau pathology was seen in the EC initially (Liu et al., 2012). This then spread to synaptically connected brain regions that radiate from the EC. The spread of tau pathology in these mice followed the monosynaptic and trans-synaptic cortico-hippocampal and cortico-cortico connections. Collectively these suggest that tau propagates via a synaptically connected neuronal circuit in the brain.

1.5.2 Synaptic-mediated transmission of tau pathology

Although various research groups also reported the ability of cells to pass misfolded tau from one cell to another in connected brain regions it was still unclear whether tau aggregates move from one cell to another as a consequence of cell damage, cell proximity or via synapse-mediated mechanisms (Holmes et al., 2014; Kfoury et al., 2012; Takeda et al., 2015). There are accumulating evidence showing that the propagation of tau pathology may occur in synaptic-mediated

mechanisms. In a study using co-cultured systems and an artificial neuronal network in microfluidic devices, the role of synaptic connectivity in the transmission of tau pathology are highlighted in primary hippocampal neurons (Calafate et al., 2015). In this study, the use of microfluidic devices allowed the compartmentalisation hippocampal neurons harbouring either seed-competent tau aggregates and physiological tau. These artificial networks allowed Calafate and colleagues to elucidate whether the presence of synaptic contacts between neurons facilitates the cell-to-cell transfer of pathological tau. They found that removing the expression of important synaptic adhesion molecules, such as neuroligin 1, neuroligin 2 and neuroligin 3, which determine synaptic contacts in neurons were able to significantly reduce pre- and post-synaptic connectivity. As a consequence of the reduced expression of these synaptic adhesion molecules, tau propagation in the artificial neuronal networks were attenuated. On the other hand, when they increased synaptic connectivity, tau propagation was enhanced. Interestingly, inhibition of neuronal activity also led to significant reductions in tau aggregation and propagation. These evidence strongly suggest that synaptic connectivity and neuronal activity are capable of modulating cell-to-cell transfer of tau aggregates *in vitro* (Calafate et al., 2015).

Furthermore, analysis of post-mortem AD brains at different Braak stages, have shown that tau seeding is enriched in synapses that are located in the early Braak Pathway, that are devoid of any tau pathology (DeVos et al., 2018). They found that instead of being released by degenerated neurons, efficient tau aggregation and propagation occur via synaptic mechanisms and can be spread in a healthy intact connected neuronal network (DeVos et al., 2018; Goedert and Spillantini, 2017).

One of the important questions of tau propagation studies is the origin of the initiating tau aggregates that 'kick-starts' the cascade of events that results in the spreading of tau pathology. It is proposed that those released or able to traverse from cell-to-cell must be seed-competent tau to induce aggregation of soluble tau (Guo and Lee, 2011). However, other studies have also shown that under physiological conditions, neuronal stimulation can modulate the release of tau from pre-synaptic neurons, which suggest that normal physiological tau may have a role extracellularly (Pooler et al., 2013; Yamada et al., 2011). However, it is still unclear whether physiological tau can also be transferred cell-to-cell. This topic is highly debated in literature, and the nature of tau propagation under physiological and pathological conditions are still to be elucidated.

1.5.2.1 Selective vulnerability

One of the salient characteristics of many neurogenerative diseases, particularly tauopathies, is the selective vulnerability of different cell population and regions of the brain that are likely to

succumb to tau pathology. It is thought that this selective vulnerability is why tau pathology begin in selective and variable regions of the brain depending on the tauopathy. For example, in AD, tau pathology initially begins in the EC, whereas the frontal temporal lobe is affected first in FTD.

It is still unclear why some proteins, which show widespread expression, accumulate aberrantly in one subset of cells while other neighbouring cells, which are seemingly similar to the affected ones, remain unaffected. This idea that certain cellular populations are more prone to the build-up of pathology-associated proteins is what is referred to as selective vulnerability (Braak et al., 2011; Nelson et al., 2012).

The neuronal populations that seem to demonstrate the earliest deleterious effects of tau aggregation are large pyramidal neurons in ECII, the subiculum, the CA1 region of the hippocampus, cholinergic neurons in the basal forebrain, and noradrenergic neurons in the locus coeruleus (see review by Fu, Hardy and Duff, 2018). On the other hand inhibitory neurons that express calcium-binding partners, for example, parvalbumin, somatostatin, calbindin-D28k, and calretinin are reported to be less affected by pathogenic tau aggregates (Fu, Hardy and Duff, 2018). In a recent study, using AD-derived induced pluripotent stem cells (iPSCs) from patients with APP mutations, rostral neurons composing of a mixture of inhibitory and excitatory neurons, demonstrated greater susceptibility to AD-related phenotypes (i.e., generation of Aβ and the responsiveness of tau to Aβ) than those located in the caudal neurons (mainly composing of inhibitory neurons). It is still unclear why this happens but it is suggested that genetic profiles expressed by different neuronal populations could play a role. This may result in the selective vulnerability of cells located in the Braak pathway, leading to morphological, electrophysiological and biochemical properties that are not able to cope with environmental stressors (Fu et al., 2018).

1.5.3 Non-synaptic transmission of tau pathology

1.5.3.1 Glia-mediated spread of tau pathology

There is an increasing amount of evidence indicating a glial-mediated spread of tau pathology. In this regard roles of astrocytes and microglia in spreading tau pathology seem particularly important (see review Leyns and Holtzman, 2017). Microglial and astrocytes could be contributing to the spread of misfolded tau along synaptically connected neuronal circuits by taking up extracellular tau and re-secreting it back out. For example, microglial cells have been shown to be internalise soluble and insoluble forms of tau, as well as release it into the extracellular space via exosomes (Asai et al., 2015; Saman et al., 2012). Asai and colleagues found that the reactive microglial cells accelerated tau propagation and that depletion of microglial activity can

significantly decrease tau propagation *in vivo* (Asai et al., 2015). This is further corroborated by other studies showing that microglial cells can actively phagocytose phosphorylated tau from the extracellular space in vitro and in vivo (Bolós et al., 2016). Similar findings are observed in astrocyte, which have been reported to also internalise pathogenic tau aggregates and cause further spreading by releasing them back into the extracellular space.

1.6 Role of neuronal activity in the propagation of tau pathology

1.6.1 Evidence of physiological tau release

It was previously believed that this is due to the release of intracellular tau from degenerated cells because the accumulation of tau in the CSF correlated with neuronal cell death and the progression of AD (Hampel et al., 2010). However, the fact that tau can be found in the CSF of animals (Yamada et al., 2011), human AD patients and controls suggest that neurons can secrete it into the extracellular space in both physiological and pathological conditions (Hampel et al., 2010). Indeed, there are evidence showing that tau can be secreted from cells without overt neurodegeneration. Tau has been shown to be present in the culture medium of cell lines overexpressing tau (Chai et al., 2012), primary neurons (Bright et al., 2015; Karch et al., 2012; Pooler et al., 2013), ISF and CSF of mice (Yamada et al., 2011; Yamada et al., 2014) and humans (Hampel et al., 2010; Magnoni et al., 2012).

It has been shown that under physiological conditions, neuronal activity can stimulate the release of endogenous tau from healthy and rat cortical neurons *in vitro*, without overt neurodegeneration (Pooler et al., 2013). They showed that endogenous tau can be released when neurons are stimulated using different depolarising agents such as potassium chloride (KCl), glutamate or AMPA receptor agonist. Interestingly, tau release can be induced by the stimulation of specific receptors that can be physiologically regulated (Pooler et al., 2013). For instance, AMPA-receptor mediated tau release was inhibited when tetrodotoxin (TTX) was applied to cells. TTX, which is a voltage-gated sodium ion channel blocker, was efficient in inhibiting neuronal activation. Tau release was also inhibited when they used a specific AMPA-receptor antagonist. In contrast, stimulation of NMDA receptors did not induce tau release. They also found that treatment with tetanus toxin which cleaves synaptobrevin, inhibited AMPA-induced tau release thus suggesting the partial role of pre-synaptic vesicle release mechanism. This group and others further show evidence that intracellular calcium may be regulating tau release (Croft et al., 2017; Pooler et al., 2013). Similar findings have been found *in vivo*. Yamada and colleagues developed a microdialysis technique to harvest endogenous interstitial fluid (ISF) within the hippocampus of awake, freely moving mice (Yamada et al., 2011). They found that stimulating neuronal activity by application of picrotoxin, a $GABA_A$ receptor antagonist, in the hippocampus by reverse microdialysis, was able to enhance tau released in the ISF. Interestingly, application of TTX, which inhibits neuronal activity by blocking voltage-gated sodium channels, was able not able to reduce tau ISF levels below baseline. Others have also reported that tau can be released in extracellular vesicles, called ectosomes, in physiological conditions(Dujardin et al., 2014). Collectively, these

studies provide evidence that tau release is an active physiological process that is regulated by neuronal activity.

The role of tau in the extracellular space once released by cells remains to be unknown. Indeed, application of extracellular tau into medium of iPSC-derived or primary cortical neurons has been shown to modulate electrical activity (Bright et al., 2015). Extracellular tau could also act as a signalling molecule by binding to cell surface receptors. For example, work by Gomez-Ramos and colleagues has shown that extracellular tau can bind to M1 and M3 receptors of SH-SY5Y cells, and primary cultured neurons which can alter calcium signalling (Gómez-Ramos et al., 2006; Gómez-Ramos et al., 2008). Understanding its role in the extracellular space may provide a better understand of release of tau in physiological and pathological conditions.

1.6.2 Activity-dependence of tau pathology

An accumulating amount of evidence has shown that neuronal activity may be involved in promoting tau secretion and re-uptake, as well as the spreading of tau pathology in connected neuronal networks (Schultz et al., 2018; Wu et al., 2016; Yamada et al., 2014). Wu et al (2016) proposed that tau is released by activity-dependent mechanisms (Wu et al., 2016). They tested this hypothesis by stimulating cultured primary neurons (using picrotoxin) and by assessing the rate of internalisation of tau. In vitro, they found that stimulating neuronal activity increased the rate of tau internalisation when compared to unstimulated cells (Wu et al., 2016). *In vivo,* optogenetic stimulation of the hippocampal cell layer resulted in greater accumulation of mutant tau in cell bodies when compared to unstimulated conditions (Wu et al., 2016). Overall these results showed that stimulating neuronal activity not only increased tau released into the extracellular space but it also exacerbated tau pathology. However, it remains unclear whether neuronal stimulation is the primary driver of a tau seeding event.

The link between neuronal activity and the progression of tau pathology still remains unexplored. However, it has been reported that neurons in the AD brain could be hyperexcitable (Kazim et al., 2021). Recent research has headed towards the idea that neuronal activity may be involved in a feedback mechanism where in neuronal activity could increase tau pathology, which could then alter synaptic neurotransmission and subsequently enhance tau aggregation and propagation. Increase in extracellular tau could then further enhances neuronal activity and catalyses other neurodegenerative processes such as the accumulation of Aβ. In support of this, Aβ plaques have been shown to clusters around hyperexcitable neurons in animal models of AD (Busche et al., 2008). Both tau and Aβ could have a dual effect on the progression of tau pathology by modulation of excitability. There are some studies that have showed that Aβ induced

hyperexcitability can enhance the progression of tau pathology (Rodriguez et al., 2020). Equally, tau has been shown to be capable of regulating Aβ production by neuronal hyperactivity (Bright et al., 2015). Bright et al.,(2015) reported that application of extracellular tau in iPSC-derived cortical neurons and primary cortical neurons can increase activity, which in turn further exacerbated tau secretion and caused an increase in Aβ production (Bright et al., 2015). Furthermore, they found that neutralising extracellular tau resulted in reduced neuronal hyperexcitability which in turn lowered Aβ production *In vitro* and *in vivo*. Recently, it has been shown that human pathogenic tau and Aβ have very different effects in the brain in vivo (Busche et al., 2019); they revealed that tau suppressed and silenced neuronal activity, whereas Aβ caused enhanced neuronal hyperexcitability. Two-photon calcium imaging in a mouse model that had dual expression tau and Aβ showed that tau-dependent suppression of activity dominated Aβ-dependent hyperexcitability. These studies therefore suggest that tau and Aβ may be part of a neuronal activity regulated feed forward loop that results in protein aggregation and impaired cell signalling.

1.6.3 Role of phosphorylation, truncation and mutation in tau release

As tau is a target for various PTMs, many speculate what state tau is preferentially secreted in physiological and pathological conditions. This may give information of its origins and mechanism of release. Hyperphosphorylation has been proposed as the main driver of disease progression in tauopathies, with 40 phosphorylated sites observed in AD and only 9 in control patients (Hanger et al., 2009). Several groups have shown that phosphorylation may promote the recruitment of tau to the PM (Pooler et al., 2012b) as well as encourage the secretion of tau in the extracellular space (Katsinelos et al., 2018; Plouffe et al., 2012).

While there are reports that hyperphosphorylated tau is secreted into the extracellular space, the majority of it is mainly secreted as monomeric and/or non-phosphorylated form (Croft et al., 2017; Kim et al., 2010; Pooler et al., 2013). Furthermore, there are studies showing that decreases in phosphorylation may be associated with AD progression (Hampel et al., 2010). Indeed, the phosphorylation of threonine 181 (pT181) is widely used to detect tau in the CSF of AD (Hampel et al., 2010). It is still controversial whether phosphorylation sites such as S199, S202, T205, S396 and S404 take part in pathogenic or physiological tau secretion (see review by Pérez et al., 2018). This led to the question whether site-specific phosphorylation drives tau secretion.

Various truncated tau variants have also been shown to be secreted into the extracellular space. It is possible that before tau is processed for tau secretion, it must first undergo site-specific phosphorylation and/or truncation. Indeed, abnormal tau cleavage has been closely associated with AD progression because they have been found in NFTs. Truncation at the C-terminus, at aspartate D421 (D421) has been shown to increase the rate of tau secretion (Plouffe et al., 2012). Others propose that different tau variants lacking a proline-region or truncated in the N-terminus are selectively secreted in a distinctive manner to full-length tau or not secreted at all (Kim et al., 2010; Plouffe et al., 2012) . When Dujardin et al., (2014) evaluated vesicular forms of tau secreted in the ISF of transgenic mice of sporadic tauopathy and in stable cell line expressing human 1N4R tau (N1E115-h1N4R), they concluded that under physiological conditions, full-length tau are the species mainly secreted, whereas truncated species (at the C-terminus) are preferentially secreted in an overexpression system.

Mutations in tau can also facilitates the rate of tau secretion. Karch et al., (2012) demonstrated the FTD-associated tau mutations significantly reduced the amount of tau secreted into the extracellular space when compared to WT. Interestingly, level of 4R and 3R isoforms secreted also varied (Karch et al., 2012). Further investigation is necessary for to elucidate the role of mutations in tau secretion. In summary, tau secretion could be facilitated by different factors such as phosphorylation, truncation or by the presence of aggregated intracellular tau.

Since both phosphorylated, non-phosphorylated, full-length and truncated forms have been found in the extracellular space, it is still inconclusive whether phosphorylation and/or truncation can mediate the secretion of tau. it is possible that different tau conformers could take different routes of tau secretion. Various mechanisms by which tau is secreted are further discussed in this chapters.

1.7 Mechanisms of tau release

1.7.1 Conventional and Unconventional Protein Secretion

Cellular protein secretion is classified into two categories: classical and unconventional protein secretion (Figure 9). The classical protein secretion (CPS) is a highly regulated process that is important for delivering proteins and cargoes to the plasma membrane and to the extracellular space. In this pathway, proteins can either undergo constitutive or regulated protein release. Firstly, proteins containing signal peptides are targeted towards the endoplasmic reticulum (ER) then to the trans-Golgi network, where they are processed and packaged and stored into secretory vesicles prior their exit after plasma membrane fusion (Kim et al., 2018). Secretory vesicles only fuse to the plasma membrane in response to an external stimulus. This is known as the regulated secretory pathway and only exists in selective specialised cells such as primary neurons. In contrast, the constitutive secretory pathway is far more common and exists in all cells. This involves the continuous delivery of proteins into the PM from the Golgi, without the need for external stimuli.

Leaderless proteins like tau that lack a signal peptide sequence, are likely secreted by unconventional protein secretion (UPS) (Kim et al., 2018). UPS allows proteins to by-pass the ER-Golgi network and is classified in four different types (Figure 9). Firstly, pore formation and ABC transporters allow leaderless cytosolic proteins to be secreted via non-vesicular routes. Examples of cytosolic proteins that are secreted through these pathways are fibroblast growth factor (FGF2) and Tec kinase (Kim et al., 2018) (yellow circles in Figure 9). Other UPS-secretory route can be mediated by autophagy-associated vesicles (e.g., lysosomes, late endosomes) (orange circles Figure 9). Finally, transmembrane proteins, such as integrins, can also be translocated to the plasma membrane by GRASP-dependent pathway, which allows the Golgi to be by-passed (red circles Figure 9).

Several lines of evidence have shown that tau can be released by neurons into the extracellular space by by-passing the ER-Golgi network via unconventional secretory pathways. Two types of extracellular tau are detected: the majority exist as membrane-free and a small proportion are found in vesicles (Dujardin et al., 2014; Pooler et al., 2013; Rodriguez et al., 2017; Saman et al., 2012). Various non-vesicular and vesicular mechanisms have been proposed to mediate the trans-cellular transfer of tau (Figure 10). However, whether tau follow separate and/or overlapping secretory and re-uptake mechanisms in physiological and pathological conditions still remains to be investigated.

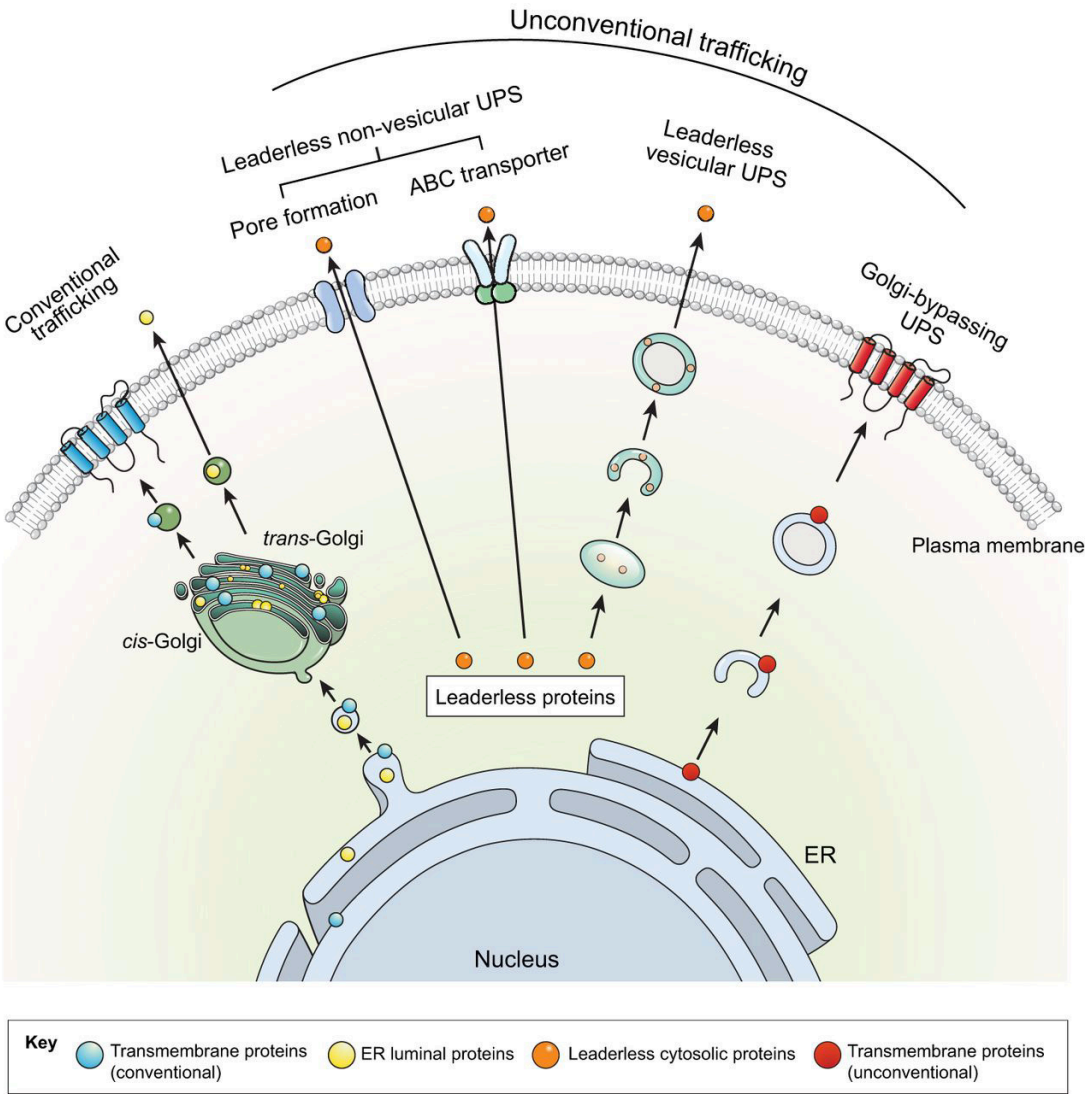

Figure 9. Differences between conventional and unconventional protein secretion pathways. Conventional protein secretion involved the ER-Golgi network, whereas, unconventional protein secretion involves the trafficking of leaderless proteins and by-passing of the ER-Golgi network. (Taken from Kim et al., 2018).

1.7.2 Relevance of tau immunotherapy

One of the ongoing debates in current literature is whether tau is secreted as a membrane-free protein or if it is encapsulated in extracellular vehicles (EVs). The most convincing evidence that supports the secretion of tau as a membrane-free protein comes from tau immunotherapy studies. With the understanding that extracellular tau, which is secreted by cells into the extracellular space, could be the driving force for the cell-to-cell propagation of tau pathology in the brain, passive tau immunisation has been proposed to reduce extracellular levels and therefore provide a way to halt the progression of tau pathology. It has been reported that immunodepleting specific pathogenic tau species and conformation/s are capable of blocking neuronal uptake and cell-to-cell propagation *in vitro* and *in vivo* (Albert et al., 2019; Courade et al., 2018; Nobuhara et al., 2017; Vandermeeren et al., 2018). In order for anti-tau antibodies be successful at immunodepleting pathogenic tau species in the extracellular space, the majority of tau must be released as a membrane-free protein to be accessible for the antibody.

Interestingly, comparative studies have been valuable in comparing the efficacy of different anti-tau antibodies that target different tau epitopes and conformation's (Courade et al., 2018; Nobuhara et al., 2017). Passive immunisation of transgenic mouse (rTG4510) overexpressing $hTau^{P301L}$, with antibodies targeting the N-terminal domain of tau, efficiently removed extracellular tau by 72-85% (Nobuhara et al., 2017). In contrast, others reported that antibodies targeting the C-terminal epitopes of tau was more efficient in reducing human AD-tau *in vivo* and *in vitro* (Albert et al., 2019; Courade et al., 2018). Why different anti-tau antibodies are more effective than others are currently unknown. However, as there is increasing evidence to suggest that distinct tau conformers exist in different tauopathies and in same disease phenotype, a mixture of anti-tau antibodies may be required to halt the progression of tau propagation in the brain.

1.7.3 Membrane-free tau

Multiple unconventional secretory mechanisms have been proposed to mediate the secretion of membrane-free tau into the extracellular space. This include the following processes: 1) direct translocation through the plasma membrane, 2) modulation of plasma membrane, and 3) membrane organelle mediated secretion (Figure 10). This section highlights key papers that strongly support the membrane-free tau secretion (Table 1-1).

1.7.3.1 Direct translocation across the plasma membrane

There is an increasing body of evidence to suggest that membrane-free tau can be released to the extracellular space via direct translocation across the plasma membrane. Two recent studies concluded that tau can escape cells by direct translocation using the following process (Katsinelos et al., 2018; Merezhko et al., 2018): 1) tau modification leads to the microtubule detachment (e.g., hyperphosphorylation) and mis-localisation, 2) recruitment to the cytosolic plasma membrane using specific lipids(e.g. phosphatidyl inositol 4,5 phosphate ($PI(4,5)P_2$), cholesterol, sphingolipids) , and 3) binding to a transmembrane protein that will facilitate extracellular release such as heparan sulphate proteoglycans (HSPG) (Figure 10). These two independent studies demonstrated that phosphorylation plays an important in modulating microtubule-tau association and therefore secretion. A phosphomimic tau (e.g., Tau^{E14}) was overexpressed in neuroblastoma (SH-SY5Y) and Chinese Hamster Ovary (CHO) cell lines (Katsinelos et al., 2018). In the Tau^{E14} mutant, 14 serine/threonine residues are mutated into glutamate to mimic a hyperphosphorylated tau protein; the substitution of glutamate adds a negative charge to the protein that mimics the addition of a phosphate group on proteins. The overexpression of the Tau^{E14} mutant induced higher tau secretion propensities, in comparison to other tau variants, including WT tau (Tau^{WT}) and unphosphorylated tau (Tau^{AP}). Similar findings were seen in N2a cells (Merezhko et al., 2018). When the culture medium was assessed in these cells, tau was mainly found independent of EVs and ATP in N2a cells; ~99% of secreted tau in the culture media was devoid of membranes, with the majority of secreted tau being dimers, trimers and tetramers. Furthermore, application of calcium ionophore ionomycin, reduced tau secretion which excluded the involvement of the classical secretion pathway. Collectively, tau was mainly found as a free protein and its secretion is likely affected by phosphorylation state of tau (Katsinelos et al., 2018; Merezhko et al., 2018).

Interestingly, both studies reported that hyperphosphorylated tau was capable of interacting with the components, such as cholesterol and sphingomyelin and $PI(4,5)P_2$, of the inner cytosolic leaflets of the plasma membrane (Katsinelos et al., 2018; Merezhko et al., 2018). To determine whether this tau-plasma membrane interaction could be mediating secretion they disrupted cholesterol and sphingomyelin levels in N2A cells and primary neurons, which are important lipid species that maintain plasma membrane rigidity and ordered structure. This caused tau secretion to be reduced. Importantly, this recruitment to the plasma membrane is accompanied by alterations in membrane integrity. Application of docosahexaenoic acid, a polyunsaturated fatty acid which encourages membrane fluidity, tau secretion was significantly upregulated (Katsinelos et al., 2018). Collectively, this shows that tau interacts with plasma membrane components and is required to initiate the tau secretion process.

Interestingly, tau also follows the same secretory pathway as other proteins such as FGF2. Upon binding to PI(4,5)P_2, FGF2 has been shown to translocated across the plasma membrane, and is followed by the binding to HSPGs (Zehe et al., 2006). As tau also lacks signal peptide like FGF2, it is speculated whether this mechanistic plasma membrane translocation process of FGF2 can be full extrapolated and be used to predict the secretion of tau. Indeed like FGF2, glycosaminoglycans (GAGs) have been implicated in tau secretion by aiding PI(4,5)P_2 to complete the translocation process (Katsinelos et al., 2018; Merezhko et al., 2018). HSPGs are highly abundant in the plasma membrane and have previously been implicated in the cellular re-uptake of aggregated tau (Holmes et al., 2013). To identify the role of HSPGs in tau secretion, sodium chlorate, a compound used to inhibit the biosynthesis of sulphated GAGs, and/or heparinase, an enzyme which breaks down heparin, was applied to neuronal cell lines (e.g., SH-SY5Y and N2a) overexpressing tau^{E14} variant, and in primary hippocampal and cortical neurons (Katsinelos et al., 2018; Merezhko et al., 2018). In all cells, sodium chlorate resulted in a dose-dependent decrease of tau secretion, without affecting intracellular tau levels. Importantly, the finding that reduced secretion of endogenous tau in primary neurons strongly suggested that HSPGs might be involved in physiological tau secretion and that the mechanisms of secretion may follow the same pathway as pathologically overexpressed tau (Katsinelos et al., 2018). The role of other sulphated GAGs (e.g., chondroitin and dermatan) in the secretion of tau was excluded, as application of chondroitinase ABC had no effect in the tau media levels. However, application of heparinase I and heparinase III, which are inhibitors specific for HSPGs, led to a decrease in both intra- and extracellular tau. This suggest that HGSPs are specifically involved in tau secretion (Merezhko et al., 2018). Interestingly, disrupted tau secretion in Tau^{E14}-overexpressing CHO_{745} cells, which are deficient in sulphated GAGs in the cell surface because they lack xylosyl transferase, an important enzyme for proteoglycan biosynthesis, was rescued when co-cultured with WT-CHO cells with normal sulphated GAG biosynthesis. This suggest that even HSPGs in neighbouring cells are capable of facilitating UPS of tau. Collectively, HSPGs may play an important role in the secretion of tau.

1.7.3.2 Modulation of the plasma membrane

Another scenario in which could contribute to membrane-free tau in the extracellular milieu is by modulating plasma membrane structures to facilitate escape (Figure 10). In this regard, tau has been shown to cause plasma membrane deformation *in vitro* (Ait-Bouziad et al., 2017; Elbaum-Garfinkle et al., 2010). It is widely known that tau can aggregate in the presence of negatively charged nucleators (e.g., heparin, RNA, arachidonic acid)(Kuret et al., 2005). As anionic phospholipids, which maintains membrane electrostatics by providing negative charges, are enriched in the plasma membrane (Platre and Jaillais, 2017), these can modify the intrinsically disordered proteins, thus, can act as nucleator that recruit and promote tau fibrillisation (Ait-

Bouziad et al., 2017). This is plausible as there are 20% anionic lipids in the inner leaflet of plasma membrane. Furthermore, as a natively unfolded protein, tau has been shown to take an α-helical conformation when it binds to membranes of primary hippocampal neurons *in vitro* (Ait-Bouziad et al., 2017). The R2 and R3 of the MTBD, which contains the two hexapeptide motifs (PHF6* and PH6) essential for the formation of PHFs, are known to undergo folding upon plasma membrane interaction, resulting in the production of amphipathic α-helices; these are proteins that contains both hydrophobic and hydrophilic properties (Ait-Bouziad et al., 2017). The amphipathic α-helices are suggested to disrupts plasma membrane functionality by acting as 'molecular tweezers' that can extract and re-arrange phospholipids in plasma membrane. This leads to the formation of highly stable tau/phospholipid complexes. Although no biological consequences (e.g., cell death) have been seen upon tau-plasma membrane interaction, these tau/phospholipid complexes could play an important role in tau trafficking, toxicity and/or cell-to-cell propagation (Ait-Bouziad et al., 2017).

In addition, tau has also been reported to disrupt the membrane by forming pores-like structures in the plasma membrane (Lasagna-Reeves et al., 2014; Patel et al., 2015). Using high-resolution atomic force microscopy, Patel et al., (2015) showed that tau monomers and predominantly globular oligomers are found irreversibly associated with in these pore-like structures within the lipid bilayer. These tau 'ion' channels were capable of modulating conductivity (Patel et al., 2015). Similarly, tau has also been shown to form annular photo fibrils (APF) which has the tendency to form spherical pore-like structures in membranes (Lasagna-Reeves et al., 2014). APFs are formed from tau oligomers, and are reported to be capable of penetrating the plasma membrane of cells derived from post-mortem the brain tissue of patients with PSP and DLB, as well as in the brain and spinal cord of transgenic P301L mice model (i.e., JPNL3). At a cellular level, tau APF-mediated pores are found in both the plasma and organelle membranes, as well as show cell-type specificity in different brain regions and type of neurodegenerative diseases. Although these studies lack evidence showing the direct penetration of tau during the secretion process, it highlights the PTMs and pathogenic mutations may have a large impact in the ability of tau to generate these pore-like structures in vitro and in vivo. Interestingly, other amyloidogenic proteins associated with other neurogenerative disease, such as Aβ, α-synuclein, are also capable of forming APF (Lasagna-Reeves et al., 2014) which suggest that these pore-like structures could facilitate the pathogenic secretion of several misfolded aggregating proteins, leading to cell-to-cell propagation. Importantly, the formation of these pores could also provide a mechanism in which tau can escape vesicles in the extracellular space (if it is secreted this way) or after cellular re-uptake in the post-synapse.

1.7.3.3 Membrane-organelle mediated release

An Increasing body of evidence suggest that autophagosomes, late endosomes (LE) and lysosomes could have a role in the unconventional secretion of membrane-free tau in the extracellular space in both physiological and pathological conditions (reviewed by Malik et al., 2019) (Figure 10).

Late-endosomes (LE) contain highly acidic lysosomal enzymes and are important for protein clearance and degradation. These organelles are capable of fusing with the plasma membrane to release their intracellular cargo into the extracellular space; this depend on intracellular calcium signalling. Rodriguez et al., (2017) suggested that membrane-free tau secretion could be mediated by GTPase Rab7A, which is associated with late endo-lysosomal trafficking (e.g., LE). In primary cortical neurons and HeLa cells, tau and Rab7A showed partial co-localisation (Rodriguez et al., 2017). Upon deletion of Rab7A expression using small interfering RNA application, there was significant reduction (by ~50%) of secreted tau in the extracellular medium in HeLa cells, whereas increased Rab7A expression significantly increased tau secretion. This all occurs in living and viable cells. Direct and/or indirect contribution of Rab7A in tau secretion and intracellular protein expression in primary cortical neurons and HeLa cells were also assessed. They wanted to see if tau secretion was linked to intracellular protein levels between different model systems. In both system, suppression of Rab7A reduced level of tau secreted in the extracellular space. However, Rab7A suppression didn't affect intracellular tau levels in primary neurons. In contrast, this was reduced in HeLa cells. In this system, Rab7A suppression encouraged tau degradation. This discrepancy highlights the differences in secretory pathways involved between model systems. As inhibition of Rab7A expression did not fully block tau secretion, other secretory pathways could also be involved in tau secretion. Interestingly, Rab7A expression has been shown to be upregulated in vulnerable brain areas (e.g., basal forebrain, hippocampus and frontal cortex) as well as in the CSF of AD patients and those with mild-cognitive impairment, when compared to controls (Armstrong et al., 2014; Ginsberg et al., 2010). Furthermore, the mutant huntingtin, a misfolded protein associated with Huntington's disease, has also been reported to be secreted using LE and/or lysosomes in N2A cells. Thus, one can speculate whether LE and Rab7A could be important in the secretion of misfolded proteins.

Other GTPase proteins such as Rab1A, have also been recently implicated in the regulation of tau secretion (Mohamed et al., 2017). In comparison to Rab7A, which is mainly associated with LE, Rab1A is a Rab GTPase that regulates vesicular protein trafficking from ER to the Golgi, then to the plasma membrane. Firstly, Mohammed and colleagues propose that an increase in neuronal hyperexcitability can lead to an increase in vesicular-free tau secretion in primary cortical

neurons, which is in accordance to previous findings *in vitro* and *in vivo* (Pooler et al., 2013; Yamada et al., 2014). By analysing the presence of GM130, a protein marker found in the cis-Golgi, they observed an increase in Golgi fragmentation in response to neuronal hyperexcitability. It was noted that the increase in Golgi fragmentation was also associated with an upregulation of dephosphorylated and C-terminally truncated tau in the cell culture media. Moreover, suppression of Rab1A expression increased Golgi fragmentation and tau secretion in both cortical neurons and HeLa cells (Mohamed et al., 2017). Based on the data, it is still unclear what mechanisms are involved in Rab1a-mediated Golgi fragmentation and tau release.

As tau can also be found in endo-lysosomes, it has been speculated whether endo-lysosomes can directly fuse to the plasma membrane to release tau into the extracellular space (Xu et al., 2018). This can be done in multiple pathways. Firstly, the misfolding-associated pathway can be activated when misfolded proteins accumulate excessively (Xu et al., 2018). Activated misfolding-associated pathway results in the capture of misfolded proteins, such as ta and α-synuclein, using chaperone ubiquitin carboxyl-terminal hydrolase 19 (UPS19) located at the ER. Misfolded tau can then be sorted and transported into the lumen endo-lysosomes where it is targeted for secretion. This was reported to be mediated by co-chaperone system, including Heath Shock Cognate 70 kDa (Hsc70/Hsp70) and DNAJC5 (Fontaine et al., 2016). They show that tau is secreted as a free-protein via a SNAP23-dependent pathway. SNAP23 is a SNARE protein mediates the fusion of intracellular vesicles with the plasma membrane, thus allowing exocytosis. Other SNARE proteins that has been implicated in unconventional protein secretion of tau include VAMP8. This is a R-SNARE has been shown to mediate a decrease in intracellular tau accumulation by enhancing tau secretion in N2a cells (Pilliod et al., 2020).

The role of lysosomes has also been implicated in transneuronal propagation of tau. In a recent paper, transcription factor E (TFEB), which is an essential regulator of lysosomal biogenesis, have been shown to participate in the clearance of truncated human mutant tau, in cultured primary neurons and in a transgenic mice model of AD (e.g., PS19) (Xu et al., 2020). This lysosomal exocytosis is said to be dependent on TFEB and lysosomal calcium channel mucolipin TRP channel 1 (TRPML1) signalling. Inhibiting the expression of TFEB in mouse and cultured neurons resulted in the reduced release of human mutant tau in the extracellular space. It also enhanced intracellular accumulation of misfolded and aggregated tau, and augmented tau pathology. Thus, this study proposes that aberrant intracellular tau can activate specifically TFEB-TRML1- mediated lysosomal exocytosis (Xu et al., 2020). In addition, it was found that an increase in TFEB expression in astrocytes was sufficient in reducing hippocampal tau pathology in transgenic P301S mice (Martini-Stoica et al., 2018) . They show that astroglial TFEB is capable of modulating the uptake and clearance of extracellular tau, thereby reducing tau spreading. Based on these studies, TFEB

could therefore present an active mechanism pathway that can promote tau clearance that can be therapeutically targeted in the future.

Protein homeostatic levels of cytosolic proteins are tightly regulated by the autophagy-lysosomal pathway (ALP) and the ubiquitin-proteasomal system. And recently, impairment of the ALP has been implicated in the spreading of tau pathology in the tauopathy brains of humans and mice (Chen et al., 2020). It is reported that impaired p300/CBP acetyltransferase activity, best known as a transcriptional cofactor, can promote the secretion of pathogenic tau fibrils and cell-to-cell propagation in cell lines, primary neurons and human IPSC-induced neurones. Inhibition of p300/CBP enhanced autophagic flux not only reduce tau secretion but also was sufficient in reducing tau accumulation and the cell-to-cell spreading of tau fibrils *in vivo*.

The secretion of tau via these mechanisms could be activated during high stress loads. It could be a co-ordinated protein quality control mechanism which allows cells to avoid the intracellular accumulation of misfolded protein.

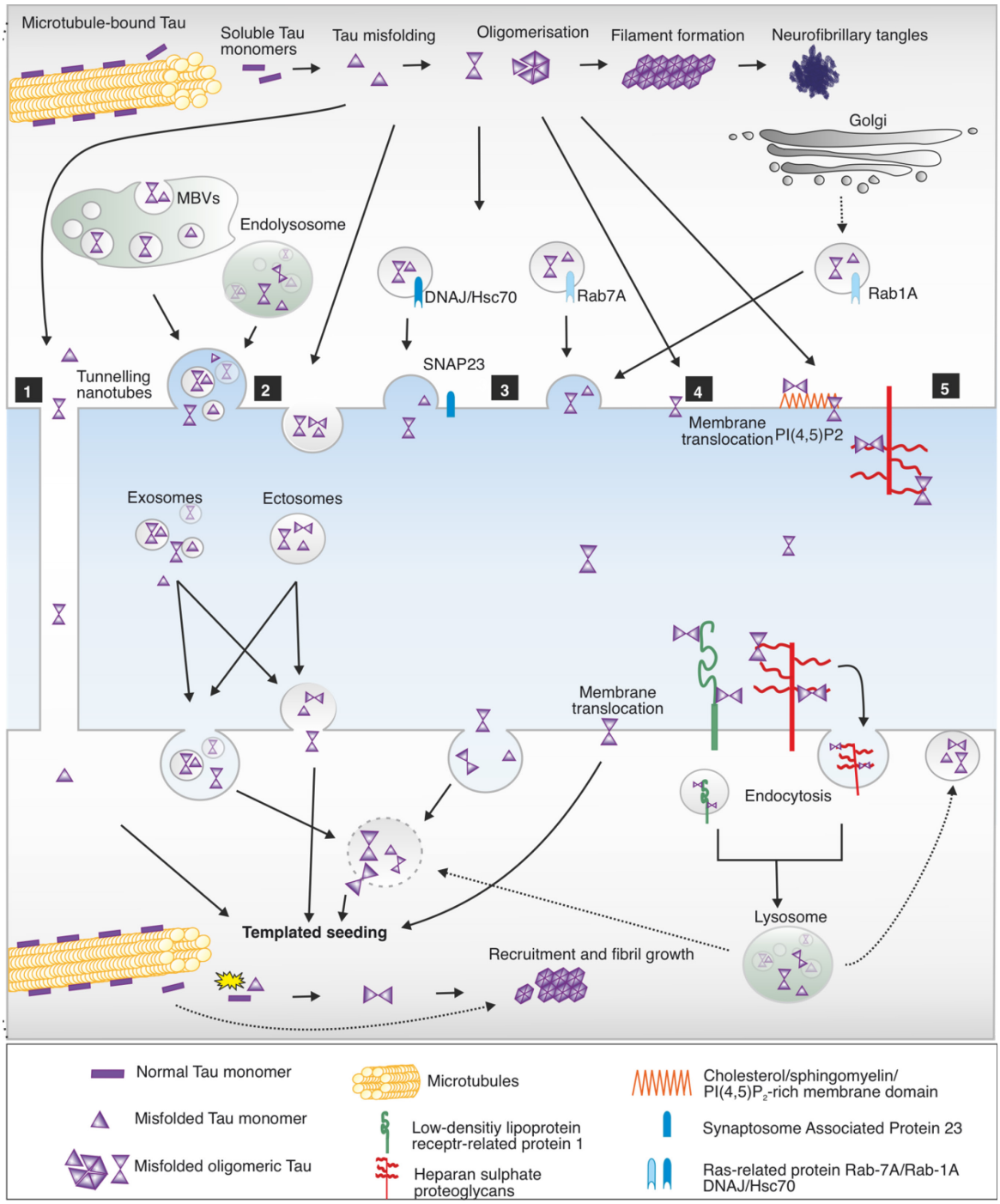

Figure 10. Mechanisms of tau release and re-uptake.

Tau conformers can be transferred from one cell to other via multiple secretory pathways. (1) Tau seeds can be transferred through tunnelling nanotubes which directly connects two neighbouring cells in close proximity. (2) Tau can be packaged inside membrane organelles such as late endosomes and multi-vesicular bodies and direct fusing to the plasma membrane results in the release of extracellular vesicles such as ectosomes and exosomes. (3) Tau packaged inside synaptic vesicles (derived from late-endosomes, lysosomes) can be released into the extracellular space by fusing with the plasma membrane. (4) Modulation of plasma membrane structures

such as pore-formation, allow the secretion of membrane-free tau. (5) Direct translocation across the plasma membrane can be mediated by tau-phospholipid and heparan sulphated proteoglycan (HSPG) interaction. Tau can be internalised by different mechanisms such as receptor-mediated endocytosis and macropinocytosis. Regardless of secretion, pathogenic tau seeds eventually reach the cytosol. Tau seeds that arrive as membrane-free are able to initiate templated misfolding of healthy tau into pathogenic misfolded conformation to occur. On the other hand, for that do not arrive membrane-free in the cytosol, for templated misfolding be initiated tau seeds must facilitate endo-lysosome escape.

1.7.4 Vesicular tau

Several lines of evidence have shown that tau can be released by neurons into the extracellular space as vesicle-bound proteins in both physiological and pathological conditions. These key findings are summarised in (Table 1-2). There are two main types of vesicles found in the extracellular space: ectosomes and exosomes. Exosomes, which tend to be smaller (40-100 nm) than ectosomes (50–1000 nm), are produced by the inward budding of late endosomes/MVBs, to produce intraluminal vesicles. These MVBs are then trafficked into the plasma membrane where it is released as exosomes. In contrast, ectosomes are produced directly from the shedding of the cell membrane (Sebastián-Serrano et al., 2018).

Exosomes have been shown to play a critical role in the transmission and propagation of tau (Saman et al., 2012; Simón et al., 2012b). Saman et al., (2012) showed that exosome-mediated secretion of phosphorylated tau occurs when overexpressed in MC1 cells (human neuroblastoma-derived immortal cell line) (Saman et al., 2012). The authors also demonstrated the first evidence correlating increased exosome-mediated tau secretion with elevated phosphorylation in the CSF, which is often found in early AD (Friedhoff *et al.*, 1998 or see review by Hampel *et al.*, 2010). Furthermore, Simon et al., (2012) also suggested that exosome-mediated exit of tau from non-neuronal cells occurs as a cellular compensatory mechanism to eliminate the excessive accumulation of intracellular tau proteins. This mechanism of release could potentially explain why tau is detected, not only in AD patients, but at lower levels in the CSF of healthy humans and animals (Hampel et al., 2010).

In support of these findings, Wang and colleagues recently demonstrated that exosomes can mediate trans-neuronal transfer of tau species, including monomers, oligomers and aggregates, using microfluidic devices cultured with primary neurons (Wang et al., 2017). In contrast to previous findings which describe tau secretion via non-exosomal pathways (Pooler et al., 2013), increased neuronal stimulation resulted in upregulated exosome-mediated tau release in these cells. Tau was also released via exosomes in neuroblastoma cell lines (N2a). Furthermore, when N2a cultured cells, expressing repeat domain of tau ($Tau^{RD\Delta K}$) were incubated with exosomes isolated from the CSF of AD patients, seeded aggregation was observed. To do this they employed split-luciferase fragment complementation technique (Wang et al., 2017). Similar findings were seen in mice models of tauopathy (Polanco et al., 2016). Tau-exosomes derived from the brains of rTg4510 mice (which expressed $hTau^{P301L}$ mutation), are capable of seeding tau aggregation in a threshold-dependent manner in tau biosensor HEK293 cell lines (see section 1.9.1.). This means is that, in order for efficiently induce misfolding and aggregation in native tau in recipients' cells, tau seed levels within these exosomes needs to meet a certain threshold. This group reports that

exosomes mediate a slow-seeding effect in neurons, which could be mimicking the slow progression of AD. However, it is noted that the origins of the exosomes analysed are unknown; it could be from a mix of pool originating from neuron or glia, (e.g., microglial).

Furthermore, exosome-dependent tau release has also been reported in microglia (Asai et al., 2015; Wang et al., 2017). Asai et al., (2015) suggested that microglia are capable of phagocytosing tau-containing neurons and release tau in exosomes. Neuronal activity increased tau release via exosome in microglia. They also show robust findings of significantly reduced tau propagation after the inhibition of exosome synthesis (Asai et al., 2015). Other groups has also associated EVs-mediated tau release with microglia (Crotti et al., 2019).

Tau pre-synaptic release by ectosomes has also been suggested as another potential route for cell-to-cell transfer (Dujardin et al., 2014). By harvesting the vesicles released in the ISF of rats, Dujardin and colleagues demonstrated that under physiological conditions, the cell-to-cell transmission of endogenous WT tau could be mediated by ectosomes. This might suggest that vesicular tau has a role in cell-to-cell communication. However, they noticed that this mode of transport seemed to vary depending on the model system; when they over-expressed human WT tau in vitro and in vivo (using lentiviral expression), they found that tau is mainly associated to ectosomes (23%), but also exosomes (2%), whereas in physiological conditions, tau is only detected in ectosomes. It is possible that initially, endogenous tau is a preferentially secreted via ectosomes. However, intracellular tau accumulation could trigger a stress-induced compensatory mechanism that leads it the activation of exosome-mediated tau release. This group admits that the major form of secreted tau is in the free form (Dujardin et al., 2014). These EVs could be important mediators of intercellular communication under physiological conditions, but also be involved in the transmission of tau pathology when the process becomes deregulated.

Another question is whether tau is packaged inside the vesicles or if it associates with these vesicles externally. If so, how does it do this? Dujardin et al., (2004) found that tau was packaged inside the EVs rather than being bound in the outer surface of the vesicle membrane. However, they could not conclude whether it was anchored via intracellular transmembrane proteins or not (Dujardin et al., 2014).

Table 1-1 Summary of studies for the secretion of membrane-free tau

Mode of secretion	**Mechanism**	**Model system (cell lines and primary neurons)**	**Tau expression**		**Characterisation of extracellular tau**	**References**
			Endogenous tau	Overexpressed tau		
Direct plasma membrane translocation	HSPGS/PI(4,5)P2	- SH-SY5Y - CHO - Hippocampal neurons	Mice	WT/E14/AP	Hyperphosphorylated E14-expressed cells secreted soluble and FL-tau (E14>WT and AP)	Katsinelos et al., 2018
	HSPGS/PI(4,5)P2	- N2a - Cortical neurons	Rat	WT (0N4R)	Hyperphosphorylated, oligomeric (e.g., dimers/trimers or tetramers B-sheet aggregates)	Merezhko *et al.*, 2018
Membrane organelle -based secretion	SNAP23 DNAJ/Hsc70	- HEK293T - M17 Mouse - WT or Transgenic mice (e.g., Cspa-/- and Cspa - Organotypic slice from WT mice	Mouse (CSP-/- and CSP-/+)	WT, P301L and R406W		Fontaine et al., 2016
	DNAJ/Hsc70/USP-19/ late endosomes	- WT or Transgenic mice (e.g., USP19-/-) - HEK293 - COS7	Mice		Unidentified	Xu et al., 2018
	Late endosomes /Rab7A	- Rat cortical neurons - HeLa cells	Rat	WT (0N4R)	Hypo-phosphorylated tau	Rodriguez et al., 2017
	Late endosomes VAMP8	- N2a cells - Mice hippocampal slices	Mice	P301L and R406W > WT	Hypo-phosphorylated and truncated at C-terminal	Pilliod et al., 2020

Autophagy-lysosomal pathway	- HEK293T cell - Rat cortical neurons - Human iPSC-derived neurons - Human CSF - WT and Transgenic mice	Mice	Truncated, and FL-tau Phosphorylated and unphosphorylated tau	Chen et al., 2020
Golgi/Rab1A	- Hela - Rat cortical neurons	Rat	Unphosphorylated tau	Mohamed et al., 2017

Table 1-2 Summary of studies for the secretion vesicle-bound tau

Mode of secretion	Mechanism	Model system (cell lines and primary neurons	Tau expression		Characterisation of extracellular tau	References
			Endogenous tau	Overexpressed tau		
Vesicle-bound	Exosomes	- COS-7 - HEK293		2N4R	FL-truncated tau	(Simón et al., 2012b)
	Exosomes	- M1C - Human CSF		0N4R	C-terminal truncated tau. Phosphorylated at T181, S202/T205, T212/S214 and T23/S235	Saman et al., 2012
	Exosomes	- Rat cortical/ neurons - Rat hippocampal organotypic slices - N2A - Human brain/CSF	Rat	2N4R ΔK280	Vesicular: Monomeric and oligomeric tau phosphorylated and unphosphorylated at S262/S356 and S396/S404	(Wang et al., 2017)
	Exosomes	- PS19 mice - Microglia		2N4R P301S (1N4R)	Aggregated, oligomeric phosphorylated at S96/S404	(Asai et al., 2015)
	Exosomes	- WT and Transgenic mice (e.g., rTG4510) - HEK293 cells	Mice	WT and P301L	P301L>WT Phosphorylated at T181, S262 and S422	(Polanco et al., 2016)

Ectosomes and exosomes	Rat cortical neurons NIE-115 Rodent ISF	Rat	1N4R	Primary neurons: Ectosomes - Dephosphorylated, FL-tau. C- and N-terminally truncated ISF: ectosomes – FL-tau and fragments Cell line: C-terminal fragment	(Dujardin et al., 2014)

1.7.5 Tunnelling Nanotubes

Beside UPS, the role of tunnelling nanotubes (TNTs) has gained a lot of attention in recent years, primarily in the propagation of misfolded proteins as has been associated with the spreading of prions and even prion-like proteins (e.g., huntingtin and α-synuclein) (Victoria and Zurzolo, 2017). TNT can also be hijacked by pathogens such as bacteria, viruses and can exist in cancer cells *in vivo* and *in vitro* (Matejka and Reindl, 2019).

TNTs, which are long membranous structures, have been shown to bridge the cytosol of different types of cells (Figure 7C and Figure 10); the cytoskeleton of TNTs have been reported to be composed of tau, actin and microtubules (Austefjord et al., 2014; Tardivel *et al.*, 2016). These highly dynamic structures can stretch up to 100 µm in length, with a diameter of 50- 80 nm, which allow them to play their part in intercellular transfer of cellular materials, varying from cytoplasmic molecules, plasma membrane components, vesicles and organelles, in adjacent neurons. They also have a proposed role in neuronal communication. However, it is unclear how these TNTs form and support the spreading of tau pathology in connected neuronal networks. The data on this subject are very limited. There only two studies directly addressing TNT and its role in tau propagation. HeLa and catecholaminergic murine cells, which has been previously used to model TNTs in culture, were shown to efficiently internalise exogenous and fluorescently-labelled human fibrillar tau (Abounit et al., 2016). Interestingly, when these cells were exposed to exogenous tau fibrils, TNT formation was upregulated. This indicated that tau fibrils were able to enter cells and induce the production of TNTs to facilitate its spreading to other cells in close proximity. Findings in catecholaminergic murine cells were further corroborated in an independent study (Tardivel et al., 2016).

Moreover, the increase production of TNTs upon application of extracellular human tau (1N4R) (monomer and fibrils) were also reported in rat primary cortical cultures (Tardivel et al., 2016). But only fibrillar tau was seen to be transferred through TNTs. The presence of TNTs was assessed by specific tubulin-negative and actin-myosin-10-positive staining. But it's not known whether tau is transported as a free protein or within membranes/vesicles. Also, TNT's are not very well defined in primary neurons, more studies are required to characterise the different tubular bridges that exist between different cells.

It is still unclear what exactly causes the cells to increase TNT production. One possibility could be that the intracellular accumulation of tau fibrils could induce stress; after all, lysosomal damage, formation of reactive oxygen species, and viral infection have been reported to trigger TNT formation (Victoria and Zurzolo, 2017). As a consequence of stress, it may induce the cell to

produce these TNTs, which in turn favour the transfer of tau, further contributing to the spreading of tau fibrils (Abounit et al., 2016). However, it is not elucidated what type of tau species are transferred through TNTs. It would be interesting to see if these TNTs can facilitate the spread of pathogenic tau species/conformers *in vivo*. Indeed, the presence of TNTs *in vivo* was been identified in MHC class II+ cells mouse corneal stromas (Chinnery et al., 2008) and cancer cells (Matejka and Reindl, 2019).

Despite robust findings supporting UPS of tau, either through EVs or free secretion, some researchers propose that multiple active routes and mechanisms were equally involved in tau propagation (Simón et al., 2012b). It is possible that when a disease threshold of tau accumulation is reached, and the cells reach a certain level of stress, the UPS pathway is stimulated and cells may compensate for excessive tau expression by secreting tau in multiple pathways. This is particularly useful because when cells are no longer capable of pumping tau out of the cell, other release mechanisms may be useful. However, how this would relate into the spread of pathogenic tau seen in connected neuronal circuits still remains to be elucidated.

1.8 Tau internalisation

Following secretion in the extracellular space, pathological tau (monomers, oligomers, fibrils, or aggregates) can be taken up by recipient healthy cells. The mechanism involved in this is still unclear under different conditions, but it will likely depend on whether tau is released as a membrane free protein or within membrane vesicles (Figure 7C). After cellular re-uptake, pathogenic tau will either be re-secreted, processed for degradation, or commence the templated misfolding of healthy recipient tau.

1.8.1 Mechanisms of tau internalisation

The exact mechanisms of tau entry into cells under physiological and pathological conditions is still poorly understood. Endocytosis has been proposed as one of the major routes in which tau is taken-up from the extracellular space (Figure 10). Endocytosis is a cellular process that allows the internalisation of substances outside of the cell membrane. The plasma membrane buds off to form intracellular vesicles containing extracellular cargo. There are three main types of endocytosis: phagocytosis, pinocytosis and receptor-mediated endocytosis. There is evidence that pinocytosis and receptor-mediated endocytosis could be a possible route for cell-to-cell propagation.

Firstly, bulk-endocytosis or macropinocytosis, is a type of pinocytosis, that involves the ruffling of the cell membrane, allowing the internalisation of extracellular fluids, and the formation of large intracellular vacuoles, also referred to as macropinosomes, in the recipient cells. Once internalised, these macropinosomes can be transported into the endo-lysosomal pathway. Wu et al., (2012) showed that tau oligomers can be internalised this way. Others also showed that pathogenic tau fibrils can be taken up by bulk endocytosis, both in vivo and in vitro (Holmes et al., 2013). In this study, truncated and full-length tau fibrils are shown to be capable of directly stimulating micropinocytosis to induce cellular re-uptake. These tau fibrils were contained within actin-dependent macropinosomes rather than endocytic vesicles. This was confirmed by application of macropinosome inhibitors which markedly reduced the cellular uptake; this include cytochalasin D and latrunculin (which inhibit actin polymerisation), as well as 5-N-ethyl-Nisopropyl-amiloride and rottlerin (which inhibit sodium-proton exchanger and protein kinase C, respectively). Furthermore, to be internalised, they showed that tau fibrils bind to HSPGs, which promotes tau endocytosis, in primary hippocampal neurons and C17.2 cells (Holmes et al., 2013). Interestingly, application of heparin mimetics, which act as a competitive inhibitor to tau binding site on HSPG, lead to a blockade in HSPG-tau interaction. This blocked tau uptake, seeded aggregation and transcellular propagation of tau aggregation (Holmes et al., 2013). Others have

also shown this tau-heparan sulphate interaction in iPSC-derived neurons and mouse brain slice culture (Rauch et al., 2018). Using CRISPR interference technology, this group screened for tau re-uptake modulators and found hits in genes involved in HSPG biosynthesis and endocytosis. They found that modulation of 6-O-sulfation, using HSPG enzymes, strongly influenced tau re-uptake in CNS cell lines, iPSC-derived neurons, and mouse brain slice culture. Knockdown of these enzymes lead to the increased tau-HSPG binding and re-uptake. Conclusively, these suggest that HSPG-mediated internalisation of tau is regulated by 6-O-sulfation patterns of HSPGs.

Furthermore, Rauch et al., (2020) recently showed other cell surface receptors that may also facilitate the internalisation of tau. Low-density lipoprotein receptors (LDLR), are a family of cell-surface receptor proteins that are highly expressed in the post-synaptic neurons of many cells, and play an important role in the endocytosis of extracellular molecules. This group showed that low-density lipoprotein 1 (LRP1), one of several LDLRs, could be involved in the internalisation of toxic tau seeds and the subsequent spreading of tau pathology to connected brain regions (Rauch et al., 2020). By genetically silencing the expression of LRP1 in H4 neuroglioma cell lines and iPSC-derived neurons, using CRISPR interference technology, this group showed that it can fully block the uptake of soluble monomeric tau of different isoforms (0N3R, 0N4R, 1N3R, 1N4R and 2N3R), oligomers, and diseases-associated mutant tau (e.g., K18 and K19 tau fragments); it also partially blocked the up-take of tau fibrils. This suggests that LRP1 could facilitate the physiological and pathological re-uptake of tau in the brain. Interestingly, application of receptor-associated protein, a small chaperone protein known to bind specifically to LRP1, in the cell culture medium resulted in concentration-dependent blockade of tau re-uptake in WT H4 cells and iPSC-derived neurons. This group was also able to map out specific ectodomains in LRP1 that mediates tau-LRP-1 interaction and internalisation. In this respect, lysine residues located in tau, in high proportions, may be critical. They also find that other LRP1-binding partners that targets these sites, such as lipid transporter ApoE, are capable of competing for uptake in HEK293T cells (Rauch et al., 2020).

In addition, they showed that LRP1 is critical in the spreading of both pathogenic and physiological tau in the brain using an adeno-associated virus (AAV) mice model of tau spread that was recently developed (Wegmann et al., 2019). This model allows the AAV-transduced donor expressing $hTau^{P301L}$ and recipient neurons to de distinguished, allowing tau spread to be visualised using immunofluorescence labelling. The AAV encodes for a fluorescent GFP protein and $hTau^{P301L}$, connected with a P2A peptide that self cleaves during translation (GFP-P2A-$hTau^{P301L}$). Transduction of AAV- GFP-P2A-$hTau^{P301L}$ in donor cells, results in the production of separate GFP and $hTau^{P301L}$ proteins (Wegmann et al., 2019). The receiving neurons which will take up $hTau^{P301L}$, can therefore be identified by the absence of GFP and the presence of $hTau^{P301L}$. Using this mouse

model of tau spreading, Rauch and colleagues injected AAV-GFP-P2A- hTau^{P301L} and an AAV carrying a short hairpin RNA that downregulates the expression of LRP1 into the hippocampus (Rauch et al., 2020). Ablation of LRP1 expression in these mice, led to a complete reduction of tau spread in connected recipient neurons *in vivo* (Rauch et al., 2020). In contrast, control mice with normal LRP1 expression had increased tau re-uptake and tau spreading. Collectively, this group strongly show evidence that LRP1 could determine tau propagation in the brain. But it is likely that other receptor-mediated mechanisms are also at play. LRP1 could act along with HSPG's to facilitate the internalisation of tau. How exactly they do this is still subject to future investigation.

1.8.2 Tau species internalised

There is currently conflicting evidence showing varying results in what tau species are preferentially internalised under physiological and pathological conditions, as well as what causes subsequent tau propagation in neuronal networks. Some suggest that small monomeric and oligomeric species are likely the propagating and internalised tau species, whereas others suggest that only larger oligomers and/or fibrils are selectively internalised. In contrast, Rauch et al., (2020) showed that physiological tau monomers and pathogenetic tau oligomers and fibrils can be taken up by cells. While this study showed that re-uptake mechanisms of both physiological and pathological tau species may overlap, it might also be possible that different tau species could use different routes of re-uptake mechanisms. Lower MW tau species or aggregates (e.g., monomers, trimers and oligomers) have been proposed to use HSPG-dependent micropinocytosis. In contrast, larger aggregates have been proposed to prefer the dynamin-dependent bulk-endocytosis. The discrepancies seen in these studies may be due to the differences in cell culture systems and the source of tau protein to induce re-uptake. More studies will be needed delineate the differences between tau species under different conditions.

1.8.3 Endo-lysosomal escape of tau

Once internalised, pathogenic tau seeds will need to be free from intracellular membrane vesicles/organelles in order to template on to naïve healthy tau in a recipient cell (Figure 10). If tau is indeed secreted as a free protein into the extracellular space, and internalised by endocytosis, it will be trapped within intracellular endo-lysosomal-vesicles. It is still unknown how exactly tau escapes the endosomal membrane. As previously mentioned in section 1.7.4, there is evidence that tau can disrupt membrane integrity, properties, and cause membrane deformation to facilitate direct plasma membrane translocation and/or endosomal escape (Ait-Bouziad et al., 2017; Lasagna-Reeves et al., 2014; Patel et al., 2015).

It has been suggested that tau aggregates can cause endocytic vesicles to rupture in SH-SY5Y and primary cell cultures (Calafate et al., 2016; Flavin et al., 2017). Using a galectin-3-binding assay, which involves the application of galectin-3, a lectin that binds to β-galactosidase that is present on the intracellular lumen of endocytic vesicles, endo-lysosomal vesicle damage was detected after application of tau aggregates (Calafate et al., 2016). This is consistent to the findings that cell penetrating peptides produced by bacterial and viral pathogens are capable of hijacking endosomes in order to be released into the cytosol of the recipient cells (Varkouhi et al., 2011) . The ability to induce vesicle rupture could also be a conserved mechanism of cellular invasion by other disease-associated amyloidogenic proteins such as α-synuclein and huntingtin (Flavin et al., 2017). Importantly, different strains of tau may also dictate the potency of vesicle rupture and therefore, seeding and propagation efficiency; full-length 1N4R tau fibrils showed significantly stronger endocytic rupturing when compared to tau fibrils made from 1N3R isoform. Although these data complemented earlier findings that tau is internalised via an endocytic pathway (Holmes et al., 2013; Wu et al., 2013), the mechanism involved is still unclear and needs further investigation. It would also be interesting to know if the same process can occur under physiological conditions, whether WT tau can also escape endo-lysosomes *in vivo*.

In addition, recent evidence suggests that impairment of the endosomal sorting complex required for transport (ESCRT) pathway could be mediating endo-lysosomal escapes of tau seeds into the cytosol, promoting prion-like propagation of tau pathology (Chen et al., 2019). In accordance to previous findings, this group found that exogenous application of tau seeds (fibrils derived from AD brain extracts) were endocytosed and cause aggregation. Knockdown of important genes that areas involved in ESCRT-III machinery, such as *CHMP6* and *CHMP2A* with *CHMP2B*, lead to the destabilisation of the endo-lysosomal membrane and the dysfunction of endo-lysosomal repair mechanisms. This caused seed-competent tau to be leaked into the cytoplasm at a faster rate, which subsequently accelerated tau seeding in the biosensor HEK293T cell-based model of tau aggregation and propagation (Kfoury et al., 2012). In contrast to previous findings, tau fibrils did not directly rupture the endosomal membrane. But this could be due to the ability of different tau seeds to induce variable toxicity in different cell types.

Collectively, it's likely that seed-competent tau escapes these endocytic vesicles into the cytoplasm to induce tau misfolding in naïve endogenous tau in recipient cells; but how exactly this happen still remains to be elucidated.

1.9 Biosensors for studying aggregation and the propagation of tau pathology *in vitro*

1.9.1 Florescence-based assays

The development of biosensors has been pivotal in understanding the mechanisms of tau aggregation and the spread of tau pathology. Marc Diamond and colleagues previously developed a fluorescence resonance energy transfer (FRET) and cell-based tau aggregation assay that allows the detection of proteinaceous tau seeding *in vitro* (Holmes et al., 2014; Kfoury et al., 2012). FRET involves measuring the transfer of energy from a donor fluorophore to an acceptor fluorophore. The Diamond lab engineered a HEK293 cell line expressing tau repeated domains, containing disease-associated hTau^{P301S} mutation, that is fused with either CFP (donor) or YFP (acceptor). They then monitored the difference in FRET signal during the co-expression of the tau constructs only, and after the addition of tau fibrillar seed. With a much higher sensitivity than previous methods, the FRET signals in this biosensor system showed significant tau seeding after the addition of a small amount of tau PFF. Using this method, they were able to provide robust evidence showing the prion-like templating of tau in their system. With this biosensor system, others also found that tau seeds don't just occur in the brain regions that have already developed tau pathology, but are also present in other regions that are connected to a Braak pathway that has not developed overt tau pathology yet (DeVos et al., 2018; Kaufman et al., 2016). This was particularly highlighted in the more recent study which demonstrated detectable tau seeding in frontal white matter tracts and the optic nerve. The fact that these regions contain axons with limited to no neuronal cell bodies suggested that tau aggregates can transcellularly transverse along connected circuits (DeVos et al., 2018).

Other fluorescence-based assays, which utilised self-assembling split green fluorescent protein (GFP), have also been explored in studying tau aggregation *in situ* (Chun et al., 2010). The split-GFP complementation assay is composed of two spontaneously associating fragments, a smaller GFP fragment (GFP11) and a larger GFP fragment (GFP1-10), form the full-length fluorescent fluorophore when co-expressed in cells. Although it is a valuable tool for measuring tau aggregation, the biggest disadvantages of fluorescent-based assays are limited by the time lag of GFP chromophore formation after assembly and the irreversibility of the process, which could potentially hinder analysis. There is also the problem of potential false positives due to auto-fluorescent compounds (see review by Ohmuro-Matsuyama and Ueda, 2019). There is therefore a greater need for more robust and effective assays for tau aggregation and propagation analysis.

1.9.1.1 Recapitulating the propagation of tau pathology *in vitro*

Neuronal networks in the brain are highly organised structures with multiple connections and specific spatial organisation, which are very difficult to mimic *in vitro.* In order to effectively study the exact mechanism of tau propagation across neuronal networks *in vitro*, researchers had to venture into using existing microfluidic devices, mainly because it provided an effective platform in which neuronal connectivity can be spatially organised and compartmentalised.

The first microfluidic device was first developed to isolate axonal growths from the somatodendritic parts of cultured cells (Taylor et al., 2003). The device consisted of two separate cell culture channels which are only connected through small microgrooves or microchannels that are small enough to allow fluidic isolation of axons (<450µm), and exclude the soma and the dendrites of neurons. This method allowed others to develop a unidirectional neuronal circuit where growing neurons plated from the first chamber is able to selectively project and extend its axons in one direction towards the adjacent chamber (via microgrooves) to form connections on post-synaptic dendrites and soma of the cultured cells in the second chamber(Taylor et al., 2003). The advantage of using microfluidic devices in propagation studies is that compartments can be fluidically isolated, preventing any molecular cross-talk, and therefore different cell populations can be cultured and investigated under different environments. As this method provide the spatial organisation that might happen *in vivo,* particularly the highly organised network in the brain that mass cultures cannot recapitulate, a variety of molecular processes can be investigated such as the propagation of tau aggregates in along neuronal networks in diseased brains (Dinh et al., 2014; Taylor et al., 2003). This method allows researchers to visualise neurons at a single-cell resolution and therefore a really useful method for studying tau propagation *in vitro.*

Previous microfluidic compartmentalised devices were re-designed by my group (the Deinhardt and West lab), so that the devices isolated the axonal terminals from the somatodendritic regions, and allowed neurite outgrowth in one direction which would therefore recapitulate the highly organised neuronal networks *in vivo* (Holloway et al., 2019). By transfecting disease-related tau plasmids to primary hippocampal neurons that are cultured in these devices, my lab group was able to create an *in vitro* system to study the transfer of pathogenic tau between connected neuronal cells (Hallinan et al., 2019). To visualise the aggregated tau, this system utilises different fluorescent proteins tagged to tau plasmids including green and red fluorescent proteins (e.g. GFP-Tau^{E14} and RFP-Tau^{WT}) (Figure 11B-C). In this system, Hallinan et al., (2019) showed that when cultured in the devices alone, cells expressing mutant GFP-Tau^{E14} are capable of misfolding and aggregating efficiently and robustly in the distal axons, when compared to cells overexpressing full-length RFP-Tau^{WT} (Figure 11D). Misfolded tau was detected using a highly

specific antibody, MC1, which is capable of detecting conformational change by binding to an amino acid sequence of tau (epitope $_{313}$VDLSKVTSKC$_{322}$) in the third repeat of the MTBD when it becomes misfolded; tau aggregates was demonstrated by the differential distribution in fluorescence along the axon. With this, Hallinan et al., (2019) was able to identify the formation of tau aggregates in the affected 'donor' cells expressing GFP-Tau^{E14} and its ability to seed its misfolded conformation to healthy RFP-Tau^{WT} in 'acceptor' cells. When GFP-Tau^{E14} 'donor' cells are co-cultured with 'acceptor' cells expressing RFP-Tau^{WT} in the compartmentalised microfluidic devices, the number of cells positive for aggregation in RFP-Tau^{WT} cells significantly increased over time to the same extent as the 'donor' GFP-Tau^{E14} cell (Figure 11D). Overall, these data demonstrate that tau aggregates efficiently spread and propagates anterogradely from donor distal axons to the acceptor cytosol and that GFP-Tau^{E14} is capable of triggering the misfolding of RFP-Tau^{WT} (Hallinan et al., 2019).

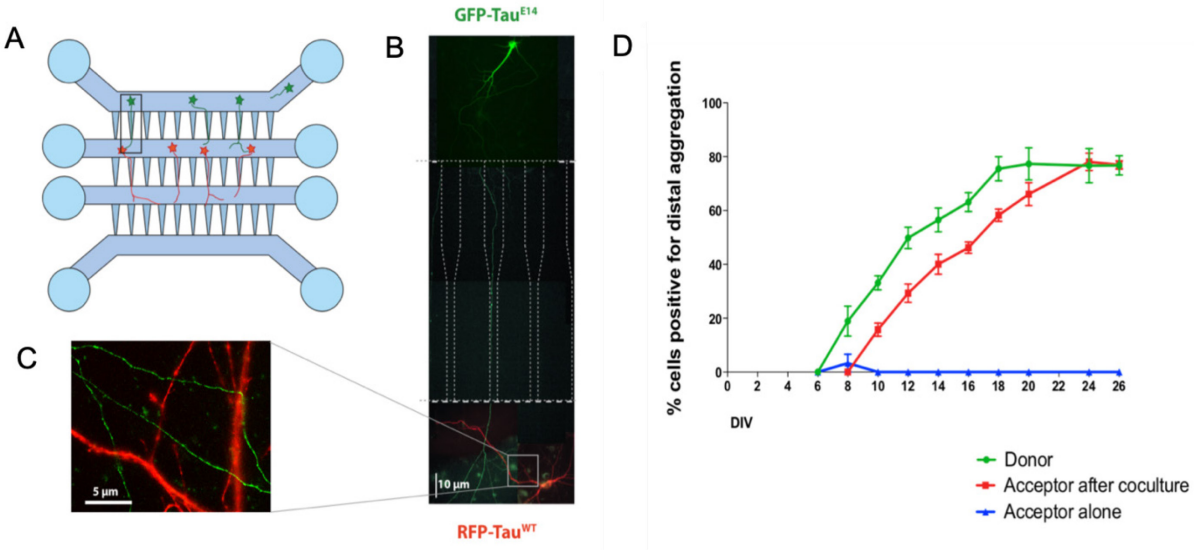

Figure 11. Pathogenic tau misfolds and aggregate efficiently, and propagate to connected cells. A) Schematic diagram of the set-up in compartmentalised microfluidic device. B) GFP-Tau^{E14} expressing donor cells (green) connected to RFP-Tau^{WT} acceptor cells (red). C) Axons from GFP-Tau^{E14} cells intersects with the dendrites of RFP-Tau^{WT}. D) Neurons were transfected at DIV1 and the fluorescent distribution along the distal axons of the donor and acceptor cells were analysed for 26 days for aggregation. Donor GFP-Tau^{E14} cells efficiently aggregated, whereas acceptor RFP-Tau^{WT} cells did not when cultured alone, however, when co-cultured together RFP-Tau^{WT} cells begins to demonstrate similar rates of aggregation as the donor. But there is a 3.7 day delay in the first appearance of aggregates in acceptor cells from donor cells (taken from (Hallinan et al., 2019).

In this system, before aggregation is detectable in donor cells, misfolded tau (which is observed via MC1 staining) can already be detected in both donor and acceptor neurons (Figure 12). The fact that misfolded tau can be detected in acceptor cells way before the appearance of aggregates in donor cell strongly suggest that tau misfolding and trans-neuronal transfer of smaller and lower molecular weight tau species occurs upstream of aggregate formation. In order to seed aggregation in recipient neurons, misfolded tau proteins must have been released by donor cells and taken up by acceptor cells. Collectively, this suggest that this assay is a late read out for tau aggregation. This assay was not able to monitor the release and re-uptake of misfolded tau species in the connected neuronal network. Furthermore, as there are increasing evidence that tau release can occur under physiological tau conditions, measuring the movement of Tau^{WT} in the existing *in vitro* assay is currently not possible. The assay relies on the appearance of misfolded and aggregated tau in the acceptor cells to indicate that release and re-uptake has taken place. As far as we know, there is currently no sensitive and effective *in vitro* system that can directly detect the release of tau as it propagates across a connected neuronal network under both physiological and pathological conditions. Although this *in vitro* system is robust and reproducible, there is a need to improve the resolution of the assay in order to get a better mechanistic insight to the release and re-uptake of misfolded tau.

This therefore still leaves unanswered questions including: 1) whether tau release occur under both physiological and pathological conditions, 2) what overlapping and/or differential molecular mechanisms are involved in tau release, 3) once it is in the extracellular space how does tau enter the post-synaptic neuron?

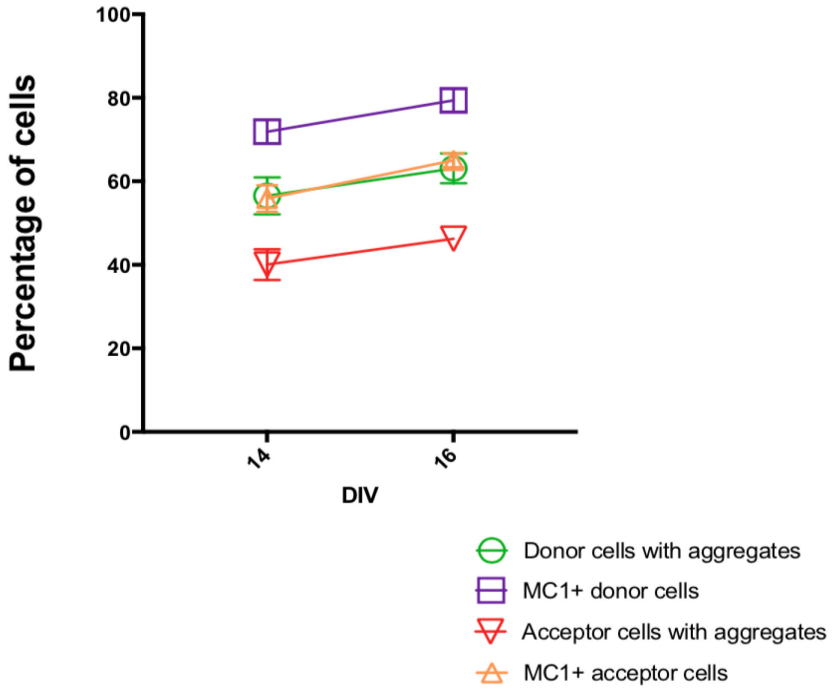

Figure 12. Misfolded tau occur before the appearance of tau accumulates in both donor and acceptor cells in the distal axons of cells at DIV 16 (taken from Grace Hallinan's thesis).

1.9.2 Bioluminescent-based assays

Other biosensors that have garnered a lot of attention recently are the use of novel bioluminescent luciferases which have been used in numerous biomedical applications (England et al., 2016). The production of bioluminescence is an enzymatic process involving the interaction of an enzyme (e.g. luciferase) and its substrate (e.g. luciferin). The resulting signal can be observed visually using a bioluminescent camera or measured quantitively using a luminometer. One of the newest luciferases that has been recently been developed is Nanoluciferase (NLuc). This luciferase enzyme was first isolated from the chemicals spewed by the deep-sea shrimp *Oplophoris gracillirostris*, which are secreted as a protective mechanism from predators (England et al., 2016). The reaction between ATP-independent NLuc and the optimised substrate, called furimazine (an analogue of coelenterazine), in the presence of oxygen, yields a chemical called furimamide and the generation of a high-intensity glow-type luminescent signal (Hall et al., 2012).

NLuc offers more advantages to traditional luciferases such as those from *Renilla reniformis* (sea pansy) or *Photinus pyralis firefly*; it is smaller (19 kDa) in size therefore it is likely to have less interference to native protein expression; the bioluminescent signal generated is highly stable (in the culture medium or inside cells); the light intensity is >100 fold brighter, with a maximum

emission spectrum of 460 nm, and well sustained compared to traditional luciferases and so would accommodate for a low expression level.

Using NLuc, the Nano Luciferase Binary technology (NanoBiT), a novel structural split-bioluminescent complementation reporter, was recently developed to allow sensitive quantitative investigation of protein interactions (Figure 13). The original NanoBiT consists of two subunits, the large N-terminal portion (LgBiT; 18kDa) and a small C-terminal section (SmBiT; 11 AA fragment), which can both be fused to proteins of interest at the C- or N-terminus (Figure 13A) (Dixon et al., 2016). When proteins of interest that are fused with LgBiT and SmBiT interact with each other, the two NLuc subunits also come together to form an active enzyme, and in the presence of furimazine will generate a strong bioluminescent signal. Alternatively, this NanoBiT complementation assay was further improved for different applications. It was reconstructed by optimising the complementation of the low affinity SmBiT (K_D > 100 μM) to the LgBiT (Figure 13). After trying various peptides with different affinities to LgBiT, the 11 amino acid HiBiT peptide (1.3 kDa), was found to have the highest affinity (K_D > 700 μM) to LgBiT. The replacement of the five amino acids from SmBiT (VTGYRLFEEIL) to achieve high affinity HiBiT (VSGWRLFKKIS) allows the spontaneous complementation of the HiBiT and LgBiT without the aid of fusion partners (Figure 13)(Dixon et al., 2016).

This NanoBiT complementation assay has both advantages and disadvantages. Due to its small size (so less interference with protein partners), exceptionally high affinity to LgBiT and ease of use, the HiBiT peptide tag has been shown to be valuable in many areas of biological science research. It has been used to investigate protein expression to study signalling pathways (Oh-hashi et al., 2017; Schwinn et al., 2018), monitor protein degradation in cells, allow quantification surface receptor and internalisation (Rouault et al., 2017) and finally it has also been used to for monitoring viral infection and release (Sasaki et al., 2018). The use of the HiBiT-tag also has lots of advantages over traditional detection methods. Due to its enhanced brightness, live cell imaging using luminescence microscopy is therefore more feasible. Furthermore, the availability of a recombinant LgBiT (untagged by proteins) and also both a cell-permeable and impermeable version of the substrate, furimazine, allows this system to be a highly versatile and powerful tool to interrogate molecular function in different experimental conditions (Johanna Lee, 2019).

In addition, there are others that have also used similar split-luciferase complementation systems which would serve as a valuable source for understanding in designing a sensitive and effective *in vitro* system for the studying tau propagation (Wegmann et al., 2016). In a recent study by Wegmann et al., (2016), a split *Gaussian* luciferase, were fused with either the N- or C-terminal part of tau. This was used to monitor the formation, release and internalisation of stable tau

aggregates in both immortal and neuronal cell cultures. This sensitive assay provided evidence that oligomeric tau is: i) freely secreted and not membrane-bound, ii) is stable, iii) can be internalised by connected neighbouring cells, and iv) that the dimerization of tau does not necessarily lead to pathogenic tau aggregation (Wegmann et al., 2016). Split-bioluminescent complementation reporters could therefore offer a valuable and versatile tool for monitoring tau secretion and re-uptake across neuronal networks.

To do this, I am developing our existing *in vitro* system and taking advantage of the available split-NanoBiT complementation reporters. The availability of the membrane impermeable recombinant LgBiT and furimazine, which can be directly applied to the extracellular space, will allow the detection of free-membrane secreted HiBiT-tagged tau upon the generation of a strong bioluminescent signal. Similarly, a LgBiT protein can be transfected in acceptor cells to detect the internalisation of HiBiT-tagged tau and will also monitor the exact moment mutant tau seeds to healthy tau prior to formation of aggregation.

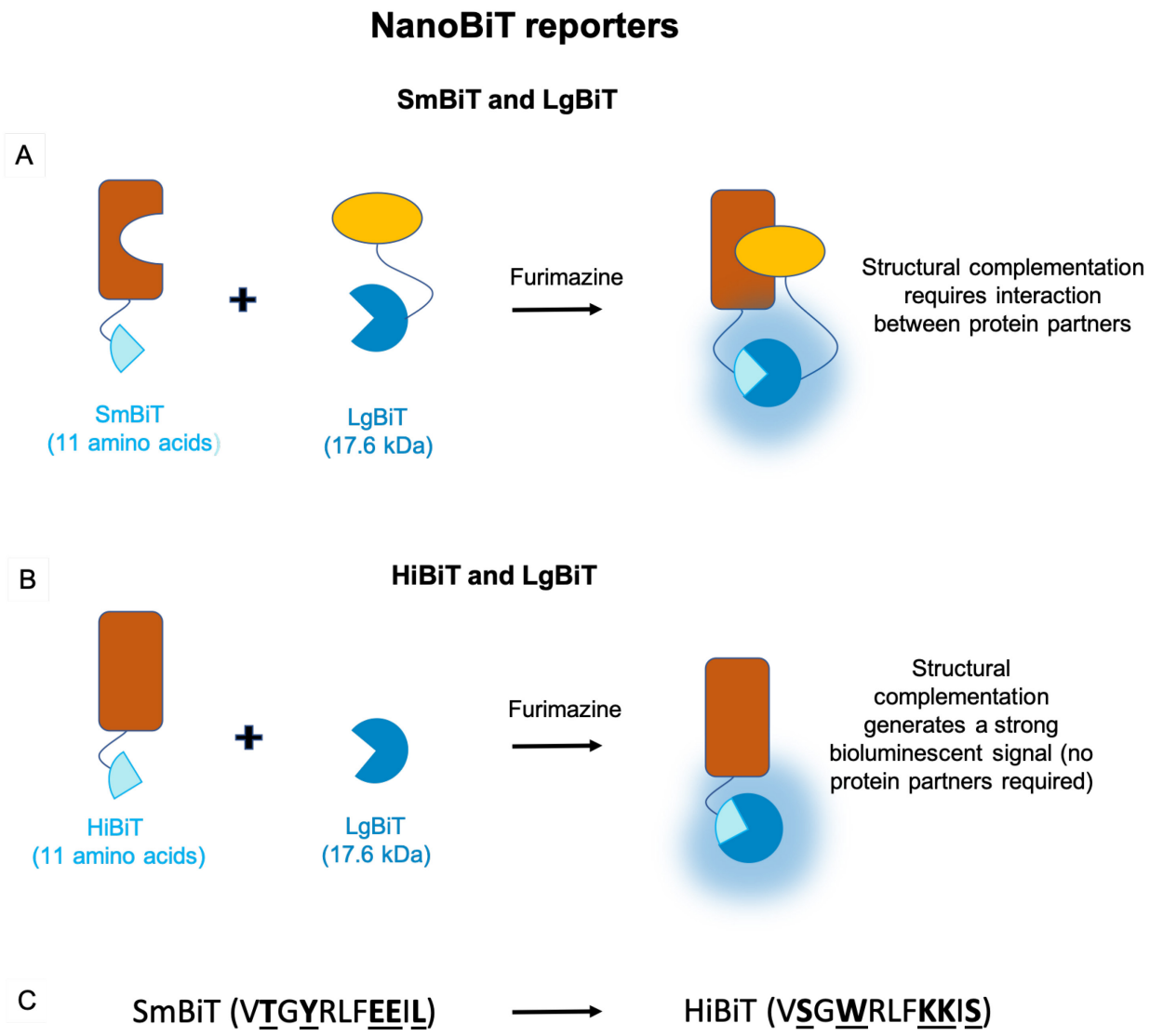

Figure 13 The components of the different types of Nano Luciferase Binary Technology (NanoBiT).

A) Initial version of the split-NanoBiT reporters composing of SmBiT and LgBiT. This requires the interaction of fusion proteins in order to form complementing split-NLuc enzyme. B) Due to the strong affinity of HiBiT and LgBiT, interactions of protein partners are not required. Upon close interaction of HiBiT and LgBiT a strong bioluminescent signal is generated. Yellow and brown shapes = proteins partners. C) Five amino acid changes from SmBiT results in a sequence that leads higher binding affinity of HiBiT to LgBiT. Changes in SmBiT include: threonine (T) changed to a Serine (S), a tyrosine (Y) changed to a tryptophan (W), two glutamate (E) residues changed to two lysine (K) residues and a leucine (L) changed to a S (adapted from Promega, 2019).

1.10 Project Hypothesis and Objectives

As a leaderless protein, I hypothesise that both wild-type and mutant tau are released into the extracellular space via unconventional protein secretion as a membrane-free protein under both physiological and pathological conditions. Based on current research, tau secretion can be modulated by neuronal activity in physiological (Pooler et al., 2013; Yamada et al., 2014) and pathological conditions (Wu et al., 2016). In disease conditions, cells could attempt to minimise the intracellularly accumulation of pathogenic tau by secreting these aberrant misfolded proteins at a faster rate than under physiological conditions. As a consequence of this process, pathogenic tau seeds released in the extracellular space are subsequently taken up by healthy adjacent cells, causing downstream templated misfolding and propagation along a connected neuronal network.

Multiple UPS mechanisms have been proposed to mediate pathological and physiological secretion and re-uptake. However, the differential secretion of different tau variants during neuronal activity remains to be explored. As different tauopathies have distinct pattern of tau spreading, it is likely that tau conformers may also have distinct secretory pathways and that it may be influenced by neuronal activity. Recent evidence suggests that tau can be released and be taken up by direct translocation across the plasma membrane via sulphated proteoglycans (Holmes et al., 2013; Katsinelos et al., 2018; Merezhko et al., 2018; Rauch et al., 2018). However, the exact role of sulphated proteoglycans in the activity-dependent secretion of different tau variants remains to be elucidated.

In this project, I developed a sensitive *in vitro* biosensor assay to monitor the differential secretion and re-uptake of tau variants in the context of neuronal activity in both physiological and pathological conditions. It will also give an insight to the state of tau when it is released into the extracellular space. Is tau released as membrane-free protein or are they packaged in extracellular vesicles? Furthermore, the role of sulphated proteoglycans in mediating activity-dependent tau secretion will also be investigated. These findings will shed light in the molecular mechanisms involved in the cell-to-cell transmission of different tau variants, which will hopefully aid the development of therapeutic interventions for specific tauopathies. Due to time-constraints, this project will focus on tau secretion.

Main objectives:

1. To develop and validate a sensitive NanoBiT-Tau biosensor to monitor tau secretion and re- uptake *in vitro*

- To generate NanoBiT-Tau biosensor that will allow tau secretion and re-uptake to be monitored in primary hippocampal neurons . Molecular biological techniques will be used to incorporate the split NanoBiT reporters (e.g., LgBiT and HiBiT) into existing tau expression vectors (e.g. , GFP-Tau^{WT}, GFP-Tau^{E14}, GFP-Tau^{P301L}) and to generate new NanoBiT-tau constructs.

- NanoBiT-tau reporters will be validated using a wide range of functional assays to ensure that the addition of the NanoBiT-tau reported on the tau expression vectors are not altered. The fluorescence, bioluminescence, aggregation propensity and expression of each NanoBiT-Tau construct were assessed.

- Assay sensitivity will be assessed to ensure that tau secretion and re-uptake can be detected above assay background.

2. To investigate differential secretion of tau variants in primary hippocampal neurons

- The NanoBiT-tau biosensor will be used to detect differential tau secretion between wild-type and mutant tau in primary hippocampal neurons.

- To investigate the state in which wildtype and mutant tau variants are released into the extracellular space (i.e., membrane-free tau or vesicular tau).

3. To establish the molecular mechanisms mediating activity-dependent secretion of wild-type and mutant tau

- Using electrophysiological recordings and the NanoBiT-tau biosensor, activity-dependent secretion between wild-type and mutant tau will be investigated. To do this, pharmacological agents that either enhance or inhibit neuronal activity will be used and the secretion of tau in these conditions will be monitored.

- To investigate whether sulphated proteoglycans, a highly abundant protein structure in the plasma membrane, may mediate the direct translocation of tau across the plasma membrane. The presence or absence of neuronal stimulation in primary hippocampal neurons will establish whether sulphate proteoglycans have a mechanistic role in activity-dependent secretion of wild-type and mutant tau

Chapter 2 Materials and Methods

2.1 Materials

All chemicals and reagents used for the molecular biology were supplied from New England Biolabs and Promega, unless otherwise stated. All cell culture media and plastics were obtained from Gibco ThermoFisher Scientific and Greiner Bio-One, respectively. Other reagents for biochemical techniques and electrophysiological recordings were obtained from Sigma and ThermoFisher Scientific, unless otherwise stated.

2.1.1 DNA plasmids

All information regarding original plasmid constructs that were used in the project are listed in Table 2-1.

Table 2-1. Original plasmids used in the project

Name	Vector backbone	Encodes	Length (bp)	Resistance	Source
eGFP	pEGFP-C3	Green Fluorescence Protein	4700	Kanamycin	Clontech
GFP-Tau^{WT}	pRK5	0N4R tau	6519	Ampicillin	Addgene, plasmid # 46904 (Hoover et al., 2010)
GFP-Tau^{E14}	pRK5	0N4R tau, with 14 serine/threonine sites mutated to glutamate (mimicking hyperphosphorylation)	6519	Ampicillin	Addgene, plasmid # 46907 (Hoover et al., 2010)
GFP-Tau^{P301L}	pRK5	0N4R tau, with single point mutation at position 301 resulting in	6519	Ampicillin	Addgene, plasmid # 46908

		change from a proline to leucine			(Hoover et al., 2010)
GFP-HiBiT-Tau^{WT}	pRK5	0N4R tau, with HiBiT in N-terminus	6591	Ampicillin	Cloned Section 2.13.1.3
GFP-HiBiT-Tau^{E14}	pRK5	0N4R tau, with HiBiT in N-terminus	6591	Ampicillin	Cloned Section 2.13.1.2
GFP-HiBiT-Tau^{P301L}	pRK5	0N4R tau, with HiBiT in N-terminus	6591	Ampicillin	Cloned Section 2.13.1.3
secNLuc	SV40	Secretory Nanoluciferase	3621	Ampicillin	Promega N198A
GFP-HiBiT	pRK5	GFP-HiBiT with stop codon in C-terminus	5145	Ampicillin	Cloned Section 2.13.2.1
IL6-GFP-HiBiT	pRK5	IL6 secretory signal added upstream of GFP-HiBiT	5229	Ampicillin	Cloned Section 2.13.2.2
LgBiT	pBiT1.1-N	LgBiT protein under weak expression vector (HSV-TK)	3858	Ampicillin	Promega Section 3.2.1
HaloTag-LgBiT	CMV	HaloTag-LgBiT in CMV promoter	N/A	Kanamycin	A gift from Promega Section 3.2.1
LV- GFP-HiBiT-Tau^{WT}	pLV-EL1a-SV40-Puro	0N4R tau, with HiBiT in EF1a-SV40 expression vector	10391	Ampicillin Puromycin	Cloned Section 2.15
LV- GFP-HiBiT-Tau^{E14}	pLV-EL1a-SV40-Puro	0N4R tau, with HiBiT in EF1a-SV40 expression vector	10391	Ampicillin Puromycin	Cloned Section 2.15
LV- GFP-HiBiT-Tau^{P301L}	pLV-EL1a-SV40-Puro	0N4R tau, with HiBiT in EF1a-SV40 expression vector	10391	Ampicillin Puromycin	Cloned Section 2.15
LV- GFP-HiBiT Δ	pLV-EL1a-SV40-Puro	IL6-GFP-HiBiT in EF1a-SV40 expression vector	9233	Ampicillin Puromycin	Cloned Section 2.15

LV- IL6-GFP-HiBiT Δ	pLV-EL1a-SV40-Puro	GFP-HiBiT in EF1a-SV40 expression vector	9317	Ampicillin Puromycin	Cloned Section 2.15
VSV-G	pCMV	Lentivirus envelope protein	8454	Ampicillin	A gift from Divecha lab
Gag-Pol	psPAX2	Lentivirus packaging plasmid	12260	Ampicillin	A gift from Divecha lab
LV-GFP	P156RRL-sinPPT-CMV-GFP-PRE-NheI	Lentivirus GFP	7889	Ampicillin	A gift from Divecha lab
E60	pLV-EF1a-SV40-Puro	Lentivirus envelope protein	8498	Ampicillin	A gift from Divecha lab

2.2 Molecular cloning techniques

2.2.1 Routine PCR

Forward and reverse primers were used to produce and amplify DNA inserts. For each PCR reaction, a master mix recipe was made up on ice. The annealing temperature was adjusted according to each primer pair, and final extension time varied depending on the amplicon size; the thermocycling conditions for routine PCR amplification are outlined in Table 2-3, unless stated otherwise. To confirm the correct amplification required for down-stream processing, PCR products were ran on an agarose gel electrophoresis, described section 2.2.2, followed by PCR/gel clean-up, as outlined in section 2.2.3.

Table 2-2. Routine PCR amplification master mix recipe

	Volume (µl)	**Final concentration**
5 x Q5 Reaction Buffer	10	1x
10 mM dNTPs	1	200 µM
10 µM Forward primer	2.5	0.5 µM
10 µM Reverse Primer	2.5	0.5 µM
Template DNA	variable	<1,000 ng
Q5 High-Fidelity DNA polymerase	0.5	0.02 µg/µl
5X Q5 High GC Enhancer	10	(1x)
filtered-distilled water (filtered-dH_2O)	to 50 µl	

Table 2-3. Thermocycling conditions for routine PCR amplification

Step	Temperature (°C)	Time (seconds)
Initial denaturing	98	30
25-35 cycles of:		
Denaturing	98	10
Primer Annealing	60-72	10-30
Extension	72	20-30 seconds/Kb*
Final Extension	72	120*
Hold	4-10	∞

*The optimal settings were variable for different sets of primers and reaction described in Table 2-4.

Table 2-4. List of primers used for the generation of constructs in the project.

Yellow = restriction sites; Red = linker sequence; Blue= full or partial HiBiT/LgBiT sequences; Underlined = stop codon; bp=base pairs; SDM=site-directed mutagenesis

Primer No.	Primer orientation	Primer sequence (5'→3')	Length (bp)	Expected amplicon size (bp)	Primer use
1	For	TTTTTGATCCTCCGGCGGCGGCGGCTCCGTGTCCGGCTGGCGGCTGTTCAAGAAGATCTCCTCCGGCGGCGGCTCCA	77	78	PCR- to generate HiBiT insert
2	Rev	TTTTTGATCTGGAGCCGCCGCCGGAGGAGATCTTCTTGAACAGCCGCCAGCCGGACACGGAGCCGCCGCCGCCGGAG	77	78	PCR -to generate HiBiT insert
3	For	TTTTTATCGATGGTCGCCACCATGGTGAGCAA	32	811	PCR – to isolate GFP-HiBiT insert, with BamHI restriction site
4	Rev	TTTTTGGATCCGGAGCCGCCGCCGGAGGAGATCTTCTTGAACAGCCGCCAGCCGGACACGGAGCCGCCGCCGCCGGAGGAACCCTTGTACAGCTCGTCCATGCCGA	106	811	PCR- to isolate GFP-HiBiT insert, with BamHI restriction site
5	For	TTTTTATCGATGGTCGCCACCATGG	25	811	PCR- SDM restriction site in GFP-HiBiT, with ClaI restriction site
6	Rev	TTTTTGGATCCGGAGCCGCCGCCGGAG	27	811	PCR- SDM restriction site in GFP-HiBiT, with BamHI restriction site
7	For	TTTTTTGAGTCGACCTGCAGAAG	23	547	SDM – to generate a stop codon after GFP-HiBiT

8	Rev	TTTTTGCCGCCGGAGCTAATCTT	23	547	SDM – to generate a stop codon after GFP-HiBiT
9	For	TTTTTCTGGGCCTGCTCCTGGTGTTGCCTGCTGCCTTCCCTGCCCCAGTGAGCAAGGGCGAGGAG	70	9317	SDM PCR- addition of IL6 signal to GFP-HiBiT
10	Rev	GGAGAAGGCAACTGGACCGAAGGCGCTTGTGGAGAAGGAGTTCATGGTGGCGACCATCGAT	66	9317	SDM PCR PCR-addition of IL6 signal to GFP-HiBiT
11	For	TTTTTATCGATGCCACCATGGTCTTCACACTCGAAGAT	38	543	PCR- amplification of LgBiT, with ClaI restriction site
12	Rev	TTTTTGGATCCTCCACCGCTCGAGCCTCCACC	32	543	PCR- amplification of LgBiT, with BamHI restriction site
13	For	TTTTTATCGATGGTCGCCACCATGGTGA	29	1969	PCR – amplification of GFP-HiBiT-Tau^{WT}, GFP-HiBiT-Tau^{E14} and GFP-HiBiT-Tau^{P301L} with ClaI restriction site
14	Rev	TTTTTTCTAGATCACAAACCCTGCTTGGCCA	31	1969	PCR – amplification of GFP-HiBiT-Tau^{WT}, GFP-HiBiT-Tau^{E14} and GFP-HiBiT-Tau^{P301L} with XbaI restriction site
15	For	TTTTTATCGATGGTCGCCACCATGAACTCCTT	32	892	PCR – amplification of secGFP-HiBiT, with ClaI restriction site
16	Rev	TTTTTTCTAGATCAGCCGCCGGAGCTAATCT	31	892	PCR – amplification of secGFP-HiBiT, with XbaI restriction site
17	For	TTTTTATCGATGGTCGCCACCATGGTGA	28	811	PCR – amplification of GFP-HiBiT, with ClaI restriction site
18	Rev	TTTTTTCTAGATCAGCCGCCGGAGCTAATCT	31	811	PCR – amplification of GFP-HiBiT, with XbaI restriction site

2.2.2 Agarose Gel Electrophoresis

Agarose gel electrophoresis was used to identify the correct molecular weight of DNA fragments, following processes such as, restriction digest and PCR. Most agarose gels made were at 1 %, unless otherwise stated. Agarose gels were made by fully by dissolving agarose power (Thermo Fisher Scientific) in 100 ml of 1 x TAE buffer (40mM Tris acetate and 1mM EDTA) and by heating the solution in a microwave at 70% power for 3 minutes mainly used, unless stated otherwise. After being cooled at room temperature (RT), 4µl of 10,000 x Gel red (Biotium) was added to the agarose solution to allow visualisation of the DNA bands under UV light. The gel was poured into a secured cassette, with the appropriate comb added, and was allowed to solidify prior to use. The gel was placed in an electrophoresis tank containing 1 x TAE buffer and was run at 120 volts (V) for ~45-70 minutes after sample loading. The DNA ladder was prepared by adding 1 µl GeneRuler DNA Mix (Fisher) 2 µl quick loading dye and 9 µl of 0.22 µm sterilized filtered-dH_2O (nuclease-free). Samples were prepared by the addition of a quick loading dye. DNA bands were visualised using G:BOX (Syngene) imager.

2.2.3 PCR/Gel Clean-up

Following gel electrophoresis and/or PCR reactions, DNA fragments were purified in accordance to the manufacturer's guidelines provided in the Macherey Nagel Nucleospin Gel and PCR clean-up kits.

2.2.4 Restriction digest of plasmid backbone and inserts

Plasmid vector and DNA inserts were linearized using specific restriction enzymes that produce complementary cohesive 'sticky' ends. Treatment with restriction enzymes (10 units, *U,* were used to digest one µg of DNA) generates linearized vector and digested inserts with complementary cohesive ends. A typical restriction digestion reaction mixture used throughout the project is outlined in Table 2-5. All reaction mixtures were incubated at 37 ^{o}C for 1-4 hours. To prevent the re-annealing of the linearized vector, 5'-phosphates were removed by the addition of 1 unit of shrimp alkaline phosphatase (rSAP, NEB) for every 1 pmol of DNA ends. The mixture was incubated at 37^{o}C for 30 minutes. To stop the reaction, samples were heat inactivated at 65^{o}C for 5 minutes. Restriction digestion reactions were loaded on an agarose gel and all desired DNA fragments were then isolated using a UV illuminator and scalpel, and subsequently cleaned-up using the Macherey Nagel Nucleospin Gel and PCR clean-up kit (as outline in 2.2.2). The purified products were used for downstream processes (i.e. ligation).

Table 2-5. A "typical" double restriction digestion for different RE's

Component	Volume (Promega)	Volume (NEB)
DNA (µg/µl)	1	1
Restriction enzyme 1 (*U*/µg DNA)	10	10
Restriction enzyme 2 ((U/µg DNA)	10	10
10x RE Buffer (µl)	2	1
BSA (µl)	0.2	N/A
Filtered-dH_2O (µl)	Up to 20	Up to 10

2.2.5 Ligation of vector and insert

Linearized vector and inserts were ligated using T4 DNA ligase. Different molar ratio between vector and inserts (i.e. 1:0, 1:1, 1:3 and 1:5) were calculated using the formula in Figure 14. Ligation reaction required for different vector:insert molar ratio is indicated in Table 2-6. T4 DNA ligase buffer was thawed and resuspended at RT. Each reaction was mixed by pipetting up and down, and then microcentrifuge briefly to collect samples, followed by incubation either at 16 °C overnight or at RT for 15 minutes.

How to calculate molar ratio of Vector : Insert

$$\frac{\text{kb of insert}}{\text{kb of vector}} \text{ X ng of vector} = \text{ng of insert needed for a 1:1}$$

Figure 14. Formula for calculating the mass of insert required at 1:1 molar insert:vector ratio in the range needed for a typical ligation reaction.

(kb = kilobases; ng = nanogram)

Table 2-6. Example of a set up for a 1:0 and 1:3 ligation reaction mixture of a vector and insert DNA.

Reagent	1:0	1:3
T4 DNA Ligase Buffer (10X)	2	2
Vector DNA (4 kb)	60 ng	60 ng
Vector (1 kb)	0 ng	37.5 ng
Nuclease-free water	to 20 µl	to 20 µl
T4 DNA Ligase (3 U/µl)	1 µl	1µl

2.2.6 Determination of DNA concentrations

DNA concentrations were determined by a spectrophotometer (Thermo Fisher NanoDrop 2000c UV-Vis), which measures based in the absorbance at 260/280 nm.

2.2.7 Agar plate preparation

Solid agar was melted using a microwave and supplemented with 0.1 % 100 mg/ml ampicillin antibiotic to make a final concentration of 100 µg/ml next to an open Bunsen flame. Subsequently, the agar mixture was poured into 10 cm sterile petri dishes and was allowed to set. The plates were wrapped in cling film then stored at 4^0C until further used for up to 2-4 weeks.

2.2.8 Bacterial transformation

Chemically competent *E.coli* cells derived from DH5α (C2988; NEB) or HB101 (Stbl3; C7373303; ThermoFisher) were thawed slowly on ice for 15 minutes. On ice, 5 µl ligation reaction and 50µl of thawed competent cells were added in an Eppendorf tube and was mixed by swirling of the pipette tip. The cell-ligation mixture was placed on ice for 30 minutes, and was subsequently heat shocked at 42 ^{o}C in a hot water bath for 30-45 seconds. The mixture was immediately cooled and placed on ice for 2 minutes. Near an open Bunsen flame, pre-warmed 150 µl SOC outgrowth media (NEB; 2 % vegetable petone, 0.5 % yeast extract, 10 mM NaCl, 2.5 mM KCl, 10 mM $MgCl_2$, 10 mM $MgSO_4$, 20 mM Glucose) was added to the cell-ligation mixture and was then placed in a shaking incubator for 1 hour at 37 ^{o}C. The cell-ligation mixture was then plated into pre-warmed agar plates (components described in section A.4.2) were incubated overnight at 37 ^{o}C.

2.2.9 Plasmid mini-prep

Following bacterial transformation in section 2.2.8, single colonies of transformants were picked from the agar plates using sterile pipette tips and cultured in 50ml falcon tubes containing 3ml LB media (1 % (w/v/ bacto-tryptone, 0.5 % (w/v) bacto-yeast extract and 1 % (w/v) NaCl dissolved in 1L deionised water) supplemented with 100 mg/ml ampicillin, under a Bunsen flame. Falcon tubes were incubated overnight at 37 ^{o}C with shaking. Falcon tubes were centrifuged at 4,000 *x g* for 10 minutes at 4 ^{o}C and the supernatant was discarded appropriately. The pellet was used plasmid purification as indicated by the manufacturer's instructions from the Machereley Nagel NucleoSpin Plasmid DNA kits that was used for the mini-prep.

2.2.10 Q5 site directed mutagenesis

Q5 Hot Start High Fidelity DNA polymerase and custom-made primer pairs were used to amplify the desired sequence via PCR. Firstly, all PCR components, indicated in Table 2-7, were added into a PCR tube. The mixture was then vortexed and briefly spun on a microcentrifuge to collect all liquid into the bottom of the tube, before being placed on a thermocycler at specific cycling conditions (as an example, PCR cycling conditions to generate CMV-GFP-HiBiT are described in Table 2-8). Each Q5 SDM PCR setting may vary depending on specific forward and reverse primers. After the PCR, the reaction mixture was subjected to a kinase, DpnI and ligase (KDL) treatment for 5 minutes at RT, by adding all the reagents shown in Table 2-9 into an Eppendorf tube. Incubation with KDL mixture led to the phosphorylation and ligation of single-stranded DNA to form circularised plasmids. This treatment also causes the removal of template DNA and isolation of desired PCR product. After KDL treatment, the reaction mixture was transformed into high efficiency DH5α competent cells and purified (as outlined in in 2.2.8 and 2.2.9. All purified plasmids were run on a 1% agarose gel as outlined in section 2.2.2. The desired plasmid sequence was checked by sequencing.

Table 2-7. Components of Q5 SDM reaction PCR reaction mixture

	Volume (µl)	Final concentration
Q5 Hot Start High Fidelity 2x Master Mix	12.5	1X
10 µM Forward Primer	1.25 µl	0.5 µM
10 µM Reverse Primer	1.25 µl	0.5 µM
Template DNA (1-25 ng/µl)	1 µl	1-25 ng
Nuclease-free water	Up to 25	Up to 25

Table 2-8. PCR cycling conditions specific for Q5 SDM of CMV-GFP-HiBiT

Step	Temperature (°C)	Time (seconds)
Initial denaturing	98	30
30 cycles of:		
Denaturing	98	30
Primer Annealing	64*	30
Extension	72	240 *
Final Extension	72	240*
Hold	4	∞

*Varies depending on different plasmid constructs

Table 2-9. KDL reaction mixture

	Volume (µl)	Final concentration
PCR product	1	
2X KDL Reaction Buffer	1.25	1X
10X KDL Enzyme Mix	1.25	1X
Nuclease-free water	Up to 10	

2.2.11 pGEM-T easy vector system

The pGEM-T easy vector system was used as an alternative to clone generated PCR products (as described in Figure 15). The pGEM-T easy vectors provided are linearized vectors with thymidine (T)- overhangs in each of the 3'-end to ensure efficient ligations and to prevent re-annealing of the vector. To ensure successful ligation to the linearized vector, all PCR products were A-tailed, using GoTaq DNA polymerase, which adds adenosine (A)-overhangs to the 3'-ends of the DNA fragments. All reagents for A-tailing PCR products (given in Table 2-10) were mixed in a tube. The mixture was spun briefly in a microcentrifuge and subsequently incubated at 70 ^{o}C for 30 minutes. After, the A-tailed PCR product was then ligated into the pGEM-T easy vector; the ligation reaction was set up as described in Table 2-11 in another Eppendorf tube. Reactions were mixed by pipetting and were incubated for 1 hour at RT. The ligation products were transformed into high efficiency JM109 competent cells and purified as outlined in 2.2.8 and 2.2.9.

The correct insertion of the PCR product into the multiple cloning region of the vector leads to the interruption of the Lac Z gene, which encodes for β-galactosidase, an enzyme that catalyses the hydrolysis of β-galactosides (such as X-gal or 5-bromo-4-chloro-3-indolyl-β-D-galactopyranoside) into its monosaccharides and galactose. This reaction results in the appearance of a blue precipitate. This therefore allows the correct recombinant clones to be isolated using blue/white screening on indicator plates. Successfully cloned plasmids appear as white colonies, as this indicated the impaired β-galactosidase expression, whereas blue colonies represent original re-circularised vector plasmids that does not containing PCR inserts. To make the selection plates, 100 µl of 100 mM isopropyl β-D-1thiogalatopyranoside (also known as IPTG) and 20 µl of 50 mg/ml X-Gal, were spread over agar plates (section 2.2.7) prior to transformation. After, white colonies were picked and was purified (section 2.2.9).

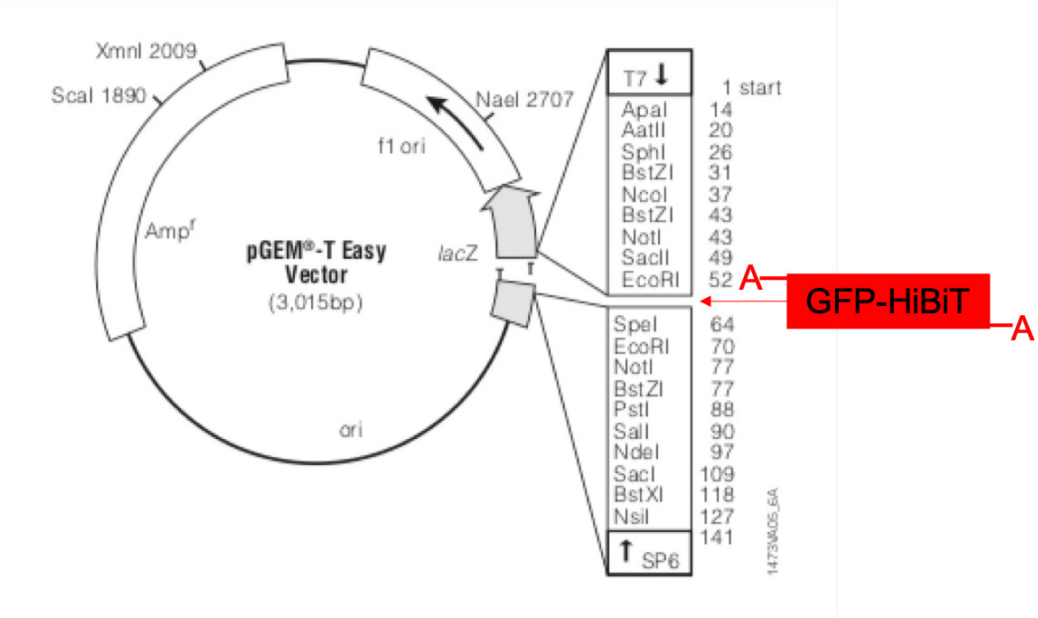

Figure 15. Plasmid map of the pGEM-T Easy Vector from Promega.

The linearized plasmid contains "T" overhangs which allows compatibility to the "A" overhangs of GFP-HiBiT insert. As cloning site is located in the middle of the lacZ gene, disruption in the expression of the β-galactosidase enzyme allows blue/white screening for successful cloning of GFP-HiBiT into the vector.

Table 2-10. Reaction mixture for A-tailing purified PCR products.

Reaction component	Volume (µl)
Purified PCR Product	7
10x GoTaq Polymerase Buffer	1
0.2mM dATPs	1
GoTaq DNA Polymerase (Promega)	1

Table 2-11. pGEM-T easy vector and PCR product ligation reaction.

Reaction Component	Standard Reaction (µl)	Positive Control (µl)	Background Control (µl)
2x Reaction Ligation Buffer, T4 DNA Ligase	5	5	5
pGEM-T Easy Vector (50ng)	1	1	1
PCR product*	3	-	-
Control Insert DNA	-	2	-
T4 DNA Ligase	1	1	1
Filtered-dH_2O	10	10	10

*Insert:vector ratio was optimised

2.3 Cell Culture Methods

2.3.1 Glass preparation for cell adherence

To prepare all glass coverslips ready for cell culture, they were first cleaned by submerging them all into a plastic container containing 300 ml 1M hydrochloric acid for one hour with constant shaking. After, all coverslips were washed 5 times with double distilled water (ddH_2O) back to neutral pH. Coverslips are then left in 70 % ethanol overnight, which was replaced with fresh 70% ethanol the following morning, and stored this way in a secured container until further use. Prior to cell culture, each glass was individually placed on cell culture plates (GreinerBioOne) on a sterile tissue culture (TC) hood. Each glass was then pre-treated with 0.1 mg/ml poly-*D*-lysin*e* (PDL; SigmaAldrich) diluted in sterile water*,* a positively charged polymer that aids cell adhesion and were incubated in 37 ^{0}C overnight. The following morning, the PDL solution was removed from the glass. Then, the glass was washed with sterile water 3 times and was allowed to air-dry inside the TC hood. PDL-coated coverslips were coated further with 50ug/ml of laminin and incubated at 37 ^{0}C for 2 hours. Prior to the addition of cells, the laminin- and PDL- coated coverslips were washed with 1 x PBS twice and was allowed to dry for 5 minutes.

2.3.2 Animals

Pregnant C57BL/6 mice were sacrificed at embryonic day 14-18 using schedule 1 CO_2 and cervical dislocation, and was done in accordance with the Animal (Scientific Procedures) Act 1986 set out by the home office. Embryonic mice were decapitated and hippocampal neurons were harvested.

2.3.3 Hippocampal dissection and maintenance

Prior to surgery, all tools were sterilised with 70 % ethanol. The hippocampi were isolated from the brain of each embryo and submerged into ice-cold 1x Gibco's Phosphate Buffered Saline (PBS), which contained no magnesium and calcium. Fresh 1 ml PBS containing isolated hippocampus from the embryos were pipetted into a 15 ml falcon tube, and was subsequently digested with 0.05 % trypsin at 37 ^{o}C for 7 minutes to dissociate all hippocampal neuronal cells. After, 1ml of Dulbecco's Modified Eagle Medium (DMEM; ThermoFisher Scientific) containing pyruvate, 4.5 g/l D-glucose and L-glutamine, which was also supplemented with 10 % (v/v) foetal bovine serum (FBS), was added to the dissociated hippocampi to deactivate the trypsin, and then centrifuged at 800 x g for 3 minutes at RT. The supernatant was removed from the pellets and replaced with 1 ml of NBM supplemented with 2 % B-27 and 0.5 mM GlutaMAX. Using a 1ml pipette, the cell pellet was resuspended carefully by gentle pipetting up-and-down to dissociate

hippocampal neurons. The solution containing dissociated cells was filtered through a cell strainer with a 40 µm pore size (ThermoFisher Scientific) into a fresh falcon tube. Using a haemocytometer, cells were counted, and diluted at the required density (~150, 000 cells/ml) and then plated to 48-well PDL-coated plates. For a 96-well plate format, 20,000 ells/well were plated.

2.3.4 Maintenance of immortal cell line

HEK293 cells were grown in 10cm cell culture dish and were maintained in 10% FBS DMEM (containing pyruvate, 4.5 g/l D-glucose and L-glutamine). To passage, all conditioned media in culture was first discarded and replaced with 10 ml of pre-warmed 1 x PBS (without magnesium and calcium) to wash off any unwanted left-over media from the cells. The PBS was then removed and the cells were dissociated by incubating with 2 ml TrypLE (Fisher scientific) with gentle rocking. The cells were then incubated in 37 ^{0}C and manually rocked, at 1-minute intervals, until all cells have visibly detached and have separated into individual cells. TrpLE was neutralised by adding 7.5 ml 10 % FBS DMEM to the cell container. The cells were further dissociated by gentle rocking or by pipetting up-and-down. If cells were still in large clumps, the cell stock was strained using a 40 µm pore size filter to isolate smaller individual cells. The cell concentration in the original stock was then counted using a haemocytometer and diluted to the desired cell concentration using 10% FBS DMEM. All HEK293 cells were passaged at 80-90% confluency and were not used above passage 15.

2.3.5 Seeding cells for a plate-based assay

Immortal and primary cells were dissociated and seeded as described in 2.3.3, respectively. Cells were counted using haemocytometer and diluted to the desired cell concentration. HEK293 cells were seeded and plated on to 96-well white opaque flat-bottom microplates (Corning) in a 3,000 cells/well dilution in a total volume of 200 µl of 10 % FBS DMEN. For primary hippocampal cells, 20,000 cells were plated in 150 µL of NBM per well. Each experimental group were set-up in duplicates or triplicates.

2.3.6 Lipofectamine transfection of cell cultures

Primary cells were transfected at day in vitro (DIV) 1 with DNA and Lipofectamine 2000 (Invitrogen) at a 1:1 ratio; for immortal cell lines, a 1:3 DNA and lipofectamine ratio was adapted. The different dilutions of transfection reagents required for different plate formats for HEK293 and primary cell cultures are given in Table 2-12. In primary cell cultures, to transfect cells on a

12-well plate, 1 µL of Lipofectamine and 1 µg of DNA plasmid were prepared in 2 separate Eppendorf tubes and were each supplemented with 150 µl Opti-MEM (ThermoFisher Scientific). Lipofectamine and DNA solutions were combined and mixed together by gentle bubbling to make the transfection reagent. To allow DNA-Lipofectamine complexes to form, the mixed transfection reagent was allowed to incubate at RT for 20 minutes in a sterile TC hood. After, 300 µl of media from the cells was discarded and gently replaced with 300 µl transfection reagent, containing DNA-Lipofectamine complexes. The cells were incubated at 37 ^{o}C for 40 minutes before all media from the cells, containing the transfection reagent, were removed and replaced with fresh 1 ml NBM.

For the co-transfections of multiple constructs, the plasmids were first mixed together in an Eppendorf tube by gentle pipetting and was allowed to stand in a TC hood for 10 minutes. Lipofectamine and Opti-MEM mixture was then added onto the plasmid mix in the desired DNA:Lipofectamine ratio (as shown in Table 2-12). Transfection was then carried as same as previously described in section 2.3.6.

Table 2-12. Different amounts of transfection reagents for different plate formats.

	Primary cells		**HEK293 cells**	
	12-well	24-well	12-well	96-well
Number of cells per well	150,000	75,000	275,000	3,000
Transfection reagent (DNA:Lipofectamine ratio)	1:1	1:1	1:3	1:3
Amount of DNA per well (µg/plasmid)	1	0.5	1	0.03
Volume of Opti-MEM required to dilute transfection reagent (µl)	300	150	300	N/A
Total volume of media in cell culture per well (µl)	1000	500	1000	200

2.4 Lentivirus production and transduction

2.4.1 Lentivirus production and purification

HEK293 FT cells, which are fast growing cell line widely used for lentivirus production, were dissociated and seeded on to 10cm culture plates (4 million viable cells/plate) in 10 ml pre-warmed 10 % FBS DMEM as previously described in section 2.3.3. The plate was then incubated at 37 ^{o}C overnight to allow for cell adhesion. To prepare the plasmid mix, 4.56 μg of plasmid, 2.28 μg of Gag Polymerase (encodes the components required for viral packaging and for the reverse transcription) and 1.12 μg of the VSV-G plasmid (encodes the envelope plasmid that enable the infection of host cells) were mixed in a tube by pipetting up-and-down; this is a ratio of 4:2:1, respectively. The plasmid mix was left for 10 minutes at RT. In a separate tube, 400 μl of serum-free DMEM and 24 μl of Lipofectamine 2000 were mixed together, and added on to the tube containing the plasmid mix by gentle bubbling and was allowed to incubate at RT for 20 minutes. After, 400 μl of the transfection mix was added drop-wise on the plate containing cells. The plate was gently swirled side-to-side and was incubated at 37 ^{o}C. After 48 hours post-transfection, conditioned media was removed from the cells and replaced with 10 ml fresh pre-warmed 10 % FBS DMEM. After further 72 hours, the conditioned media containing concentrated virus particles, was carefully removed and stored in a 15 ml falcon tube. Collected viral media (transduction media) was spun at 1000 rpm to pellet cell debris and the supernatant was filtered through a 0.45μm sterile filter and aliquoted in 1ml cryovial tubes, which was subsequently snap frozen using liquid nitrogen and stored in -80 ^{o}C freezer until further use.

2.4.2 Transduction of primary neurons

Primary hippocampal neurons were dissociated and plated (as described in 2.3.3 and 2.3.5, respectively) on a white opaque 96-well plate at DIV0. The 96-well plate format is used as an example here as it was mainly used for the NanoBiT-tau secretion assays; other plate format is described in Table 2-13. In each well, 20,000 cells were plated in 100 μl of NBM. The plate was then incubated overnight in a humidified incubator at 37 ^{o}C. At DIV1, pre-warmed transduction virus media (prepared as described in 2.4.1) was added on top of the conditioned NBM the cells were plated, in a 1:1 ratio of media volume (exact volumes described in Table 2-13). The plate was incubated for 72 hours at 37 ^{o}C to allow efficient transduction to occur. The transduction viral media was removed from each well and exchanged with fresh 150 μl pre-warmed NBM and was placed back into the incubator until DIV13-15. A schematic diagram demonstrating this process is depicted in Figure 16.

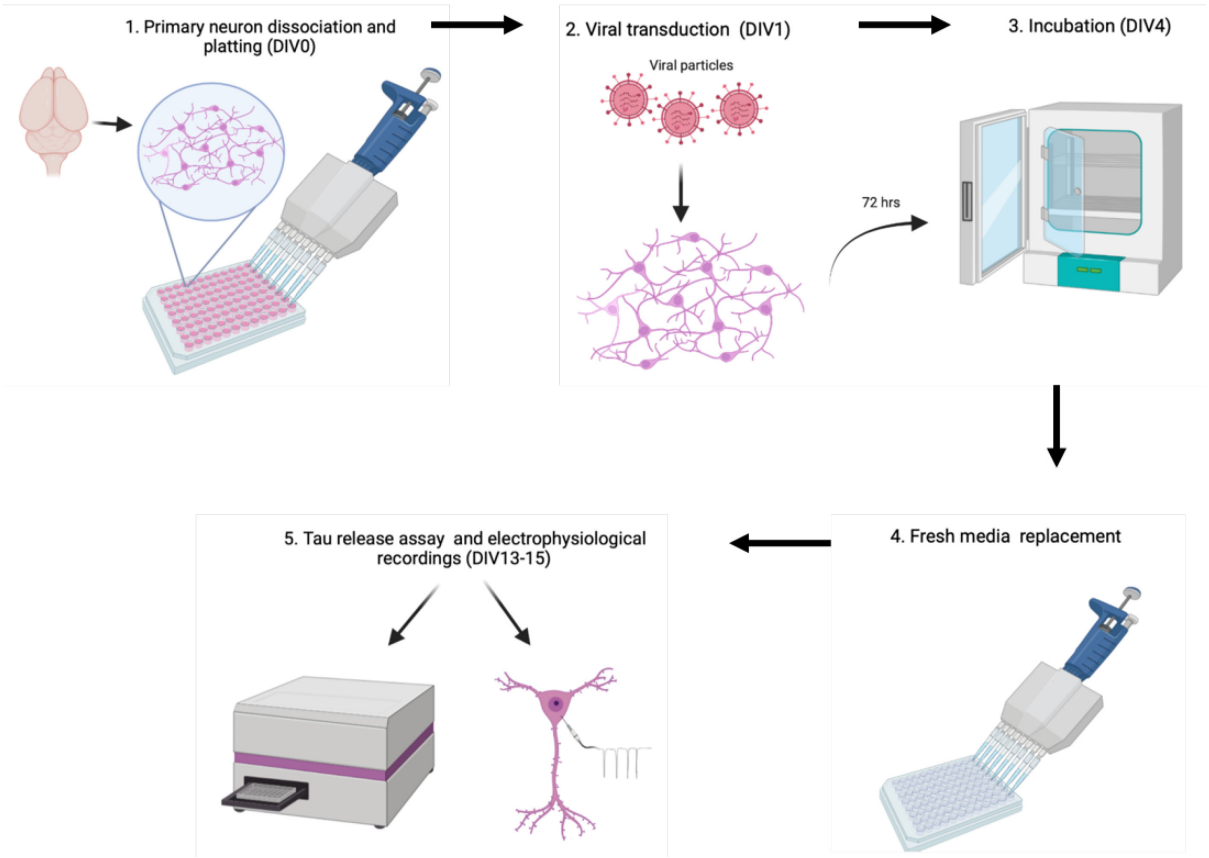

Figure 16. Schematic diagram of lentiviral transduction of primary neurons.

1) Primary hippocampal neurons were dissected and plated at DIV0; 20,000 cells were plated per well on a white opaque 96-well plate in 150 µL of NBM. 2) Neurons were transduced at DIV1 by adding the lentiviral preparations on the conditioned media. 3) Cells were incubated at 37 ^{o}C for 72 hours to allow transduction to occur. 4) Conditioned media was replaced after 72 hours t transduction and was incubated until DIV13-15. 5) All tau secretion assays and electrophysiological recordings were carried out at DIV13-15. Image was produced using biorender

Table 2-13. Volume of transduction media added on to primary neurons for different plate-formats.

Plate format	Number of cells per well	Volume of NBM prior to transduction (μl)	Volume of transduction media added (μl)	Total media (μl)
96-well	20,000	100	100	200
48-well	37,500	200	200	400

2.5 Whole-cell patch clamp electrophysiology

2.5.1 Electrophysiology set-up for primary neurons

Primary hippocampal neurons at DIV13-15 were used for all whole-cell (WC) patch clamp experiments. Glass capillaries (World Precision Instruments 1B150F-4) used for recordings were pulled to approximately 5-8 MΩ resistance. All recordings were made by using a silver chloride electrode with a glass micropipette containing potassium-based gluconate intracellular solution, in mM, potassium gluconate 110, potassium chloride 10, HEPES 10, Phosphocreatine 10, Guanosine-5'-triphosphate 0.4, Mg-ATP 4 and pH balanced to 4.3 using potassium hydroxide. Three different extracellular HEPES-based artificial cerebrospinal fluid (ACSF) solutions were used to perfuse cells during (ingredients are given in Table 2-14). The plain HEPES-based solution was used as a control, also used for 'vehicle' conditions from now on. The plain HEPES-based solution was modified by replacing adding 50 mM KCl or by removing Mg^{2+} content and supplemented with 3 μM Gabazine ($GABA_A$ receptor antagonist; Torcis). The correct osmolarity was checked and the ph of each solution was adjusted to 7.40 using 1M sodium hydroxide. The contents of each solution are given in detail on Table 2-14. The recording stage was perfused with pre-warmed HEPES-based extracellular solution with a bath temperature of 20±2 ^{o}C, at a rate of 2.5 ml/minute.

The patch clamp electrophysiology rig, contained an upright DIC microscope, and monochromatic camera fitted with a FITC filter, was placed in a vibration isolation table. Using a 40x water immersion objective, cells were initially visualized in the brightfield channel and FITC channel was used to check for transduced cells. A three-axis micromanipulator (Scientifica) was used to control the recording pipette. Axopatch^{TM} 200B amplifier, with analogue to digital converter, along with MATLAB and WinEDR software were used for recordings. Transduced neurons that are GFP-expressing were visually selected in the culture for patching.

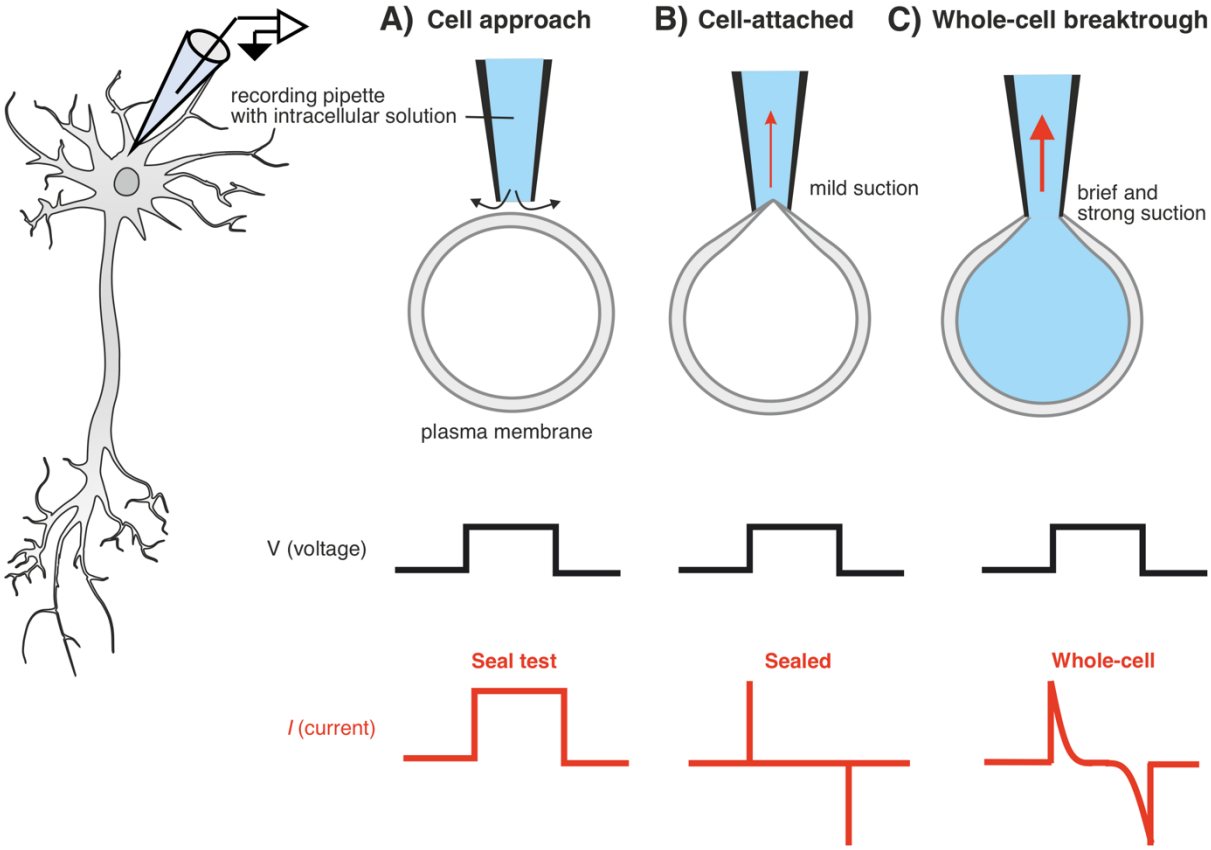

Figure 17. Schematic diagram of whole-cell patch clamp technique.

A) Cell approach consist of outward pressure. B) The pipette is gently lowered into the cell surface and cell- attached is accomplished by releasing the pressure and inducing a mild inward pressure. The cell is held at -70 mV. C) Short burst of strong suction is applied to the membrane until the whole-cell breakthrough is achieved.

Table 2-14. Concentrations of reagents used to make the three different extracellular HEPES-based solution.

	Concentration (mM)		
Reagents	Plain	KCl	(-)Mg^{2+}
NaCl	140	140	140
KCl	2.40	52.40	2.40
Glucose	25	25	25
$CaCl_2$	2	2	2
$MgCl_2$	2	2	0
HEPES	10	10	10
Glycine	0.01	0.01	0.01
pH	7.40	7.40	7.40
Osmolarity (mOsm)	331.81	431.81	325.81

*TTX added to the 'Plain'-HEPES solution in a separate condition.

2.5.2 Resistance test and exclusion criteria

Neurons with healthy morphology or GFP-expressing were selected for patch clamp recordings using visual cues following criteria: good adhesions to the glass coverslip, near the vicinity of other cells with rounded smooth soma surface visible in DIC. At voltage-clamp mode, short bursts of suctions were applied using the pulled glass electrode pipette to break into the membrane allowing the formation of seal (Figure 17). Once, a seal has been obtained, the cell was held at - 70 mV and monitored briefly using a 'resistance test', which involved 2 mV step delivered for 500msec. The individual leak currents at -70 mV, series and input resistance for each cell patched were recorded and analysed using a customised MATLAB script (kindly produced by Dr Mariana Vargas-Caballero's lab) (as shown in Figure 65, Appendix A.2)

The leak currents at -70 mV indicate how much current was needed to inject into the cell to keep the resting membrane potential at -70 mV. Thus, this read-out provides information of how much current are escaping from the cells and therefore how 'leaky'. Series resistance calculates the sum of all resistances between the cells and the amplifier. Input resistance provides a read-out of the total cell resistance; It helps determines the size of the cell and the number of functioning ion channels. Cells were excluded from analysis calculated input resistance exceeded 1000 MΩ.

2.5.3 Measuring the passive and active membrane properties in primary hippocampal neurons

The normal resting membrane potential upon break in was recorded as displayed either in the Multiclamp command setting or in the Axopatch 200B amplifier. In current clamp mode, the cells were injected with currents of 25 pA at 250 ms, starting from -100 pA to a maximum of 500 pA (cell-dependent). Alternatively, 250 pA current injection steps up to 2.25 nA were also carried out in other experiments. Current step injections were applied for each cell to find the rheobase (minimum current required to induce an action potential at infinite duration) at their natural resting membrane potential; the current injections were halted when the patched cell initially fire action potential. Using WinEDR software, action potentials were recorded at baseline and during pharmacological treatments. Data was analysed in MATLAB software using a custom written code (described in Figure 66, Appendix A.2) to find the rheobase and number of action potential (kindly produced by Dr Mariana Vargas-Caballero's lab). The liquid junction potential of -12.5 mV was measured directly was used as a guideline to correct membrane potential values. All membrane potential data presented here are raw values and is not corrected for the liquid junction potential.

2.5.3.1 Analysing action potential dynamics

All recorded traces of neuronal activity were obtained using wEDR, and were analysed by exporting the 5-minute traces into text files. The custom written script (as described in Figure 67, Appendix A.2) was kindly produced by Dr Mariana Vargas-Caballero's lab. The script quantified the total number of action potentials in the recordings. The membrane potentials that is above the threshold of 0 mV were considered as a positive hit. The total number of action potentials quantified in 5 minutes were converted to average firing frequency, in Hertz (Hz). This was done by dividing the total number of action potential fired during the recording and then divided this value by time of recording (e.g., 300 seconds).

The peak potential, which is defined as the point in which the membrane potential reaches its maximum and depolarisation stops, was obtained for each action potential. The maximum amplitude of each action potential, which was considered as total height of the membrane potential, taken from the resting membrane potential to the peak potential.

2.6 Protein Quantification and Analysis

2.6.1 Preparation of cell lysate from immortal and primary cells

All media was aspirated in each well and replaced with ice-cold 1 x PBS (1 ml/well), and subsequently washed with 1 x Tris Buffer Saline (TBS). On ice, 100 µl of 2X sample buffer (made up of 312.5 mM tris pH 6.8, 10 % (v/v) SDS, 50 % (v/v) glycerol, 25 mM dithiothreitol and 0.005 % (v/v) bromophenol blue dye) were then added to each well one-at-a-time. On ice, cells were scraped off the dish using a pipette tip and then the cell lysates were stored at -20 ^{o}C for future use.

2.6.2 SDS-PAGE

Lysates were resolved by sodium dodecyl sulphate-polyacrylamide gel electrophoresis (SDS-PAGE). Short and spacer 1.5 mm (Fisher) glass plates were cleaned with 70% ethanol prior to each use and were assembled into a casting frame, secured into a silicon-mat casting clamp. SDS-PAGE gels were made from resolving and stacking gel mixtures as given in Table 2-15. Resolving gel mixture was poured into the glass plates and were overlaid with water to remove bubbles. Once the overlaid water from the stacking gel was removed, the separating gel mixture was added on top. A 12- or 15-well comb was inserted into the stacking gel carefully. The glass plate frame was transferred into an SDS-PAGE electrophoresis tank containing 1 x Laemmli buffer (25 mM Tris, 192 mM glycine and 1% SDS). The comb was removed and the wells washed with the Laemmli buffer.

Prior to use, all protein samples were incubated at 95 ^{o}C for 5 minutes, then centrifuged at 13,000 x g for 1 minute at RT and subsequently loaded into the SDS-PAGE gels along with 5 µl Page Ruler Plus Prestained Protein ladder (Abcam). The gel was initially set at 20 mA for 10-15 minutes which allowed the proteins to stack, then eventually ran at 35 mA for 1.5 hours once the dye front reached the separating gel.

Table 2-15. Volume of reagents used for making SDS-PAGE gels (12.5%)

Reagents	Separating gel	Stacking gel	Supplier
30% Acrylamide/Bis-acrylamide	3.2 ml	0.35 ml	Sigma-Aldrich
1.5 M Tris + 0.4 % SDS (pH 8.8)	2 ml	-	-
0.5 M Tris + 0.4 % SDS (pH 6.8)	-	0.67 ml	-
dH_2O	2.8 ml	1.67 ml	-
10% Ammonium Persulfate	80 µl	26.6 µl	-
Tetramethlyenediamine	8 µl	2.67 µl	Sigma-Aldrich

2.6.3 Membrane transfer

Sponges, Whatman filter paper and nitrocellulose membrane (Bio-Rad, 0.45 µm) were immersed into transfer buffer, which was prepared from 10 x transfer buffer stock (Tris 0.5 M, glycine 0.4 M), supplemented with 10% (v/v) methanol and ddH_2O. The polyacrylamide gel was first removed from the glass plates and then carefully transferred on top of the nitrocellulose membrane. Using a secured transfer cassette, a 'sandwich' was assembled so that the polyacrylamide gel was between the Whatman paper and nitrocellulose membrane. The transfer cassette was then placed in a tank containing transfer buffer and ice pack (to prevent over-heating) and was allowed to transfer at 100V for 1.5 hours.

2.6.4 Immunoblotting

The nitrocellulose membrane was extracted from the 'sandwich' transfer cassette, and was incubated in blocking solution made from 2.5% (w/v) Bovine Serum Albumin (BSA) in TBS with 0.1% (v/v) Tween-20 (TBS-T) for 1 hour in a rocker. The membrane was washed three times (5 minutes/wash) with TBS-T in a rocker; this washing step was repeated all throughout this section. The membrane was then incubated with the primary antibody (see Table 2-16 for dilutions for each primary antibody), which was in solution with 2.5% (w/v) BSA in TBS-T for 1 hours at RT or overnight at 4 ^{o}C, and was further followed by another washing step. Finally, the membrane was incubated with the appropriate secondary antibody in 2.5% (w/v) BSA in TBS-T (see Table 2-17 for dilutions) for 1 hour at RT. The membrane was further washed with TBS-T as

done previously. The manufacturer's guidelines were used for optimising the incubation time of different primary and secondary antibodies used in the project as listed in Table 2-16 and Table 2-17, respectively.

The membrane was scanned with Odyssey Infrared Imaging Scanner (LICOR) at the 700/800 nm wavelength and Image Studio Scanner Software (LICOR) was used to obtain the image.

Table 2-16. Primary antibodies for immunoblotting

Antibody	Dilutions	Host Species	Supplier (Cat no.)	Incubation time	Molecular Weight (kDa)
Tau	1:1000	Rabbit (polyclonal)	Dako (no. A0024)	1hr at RT or overnight (4°)	55
GAPDH	1:5000	Mouse (monoclonal)	Abcam	1hr at RT or overnight (4°)	36
GFP	1:1000	Mouse (monoclonal)	Santacruz, 9996	1hr at RT or overnight (4°)	27
α-tubulin	1:1000	Mouse (monoclonal)	Sigma	1hr at RT or overnight (4°)	55

Table 2-17. Secondary antibodies for western blotting

Antibody	Dilution	Incubation time	Target Isotype	Reactivity	Host Species	Supplier
Anti-Mouse 680 nm	1:10,000	1 hr at RT	IgG	Mouse	Goat (polyclonal)	LI-COR
Anti-Mouse 800 nm	1:10,000	1 hr at RT	IgG	Mouse	Goat (polyclonal)	LI-COR
Anti-Rabbit 680 nm	1:10,000	1 hr at RT	IgG	Rabbit	Goat (polyclonal)	LI-COR
Anti-Rabbit 800 nm	1:10,000	1 hr at RT	IgG	Rabbit	Goat (polyclonal)	LI-COR

2.6.5 HiBiT-blotting

The Nano-Glo HiBiT Blotting System (Promega, UK) is an antibody-free method for sensitively detecting the presence of HiBiT-tagged proteins following SDS-PAGE and nitrocellulose membrane transfer. This involves the addition of LgBiT protein and furimazine substrate directly to the membrane, and upon complementation of the HiBiT/LgBiT complex a strong luminescence signal can be detected (as depicted in Figure 18). Following nitrocellulose transfer and/or primary/secondary antibody incubations, the nitrocellulose membrane was subjected to 3 washes of TBS-T with gentle rocking, 5 minutes each. To make the blotting reagent, 10X Nano-Glo Blotting Buffer was first diluted 10-fold with dH_2O to make 1 X blotting buffer. Alternatively, 1X TBS-T was used as the diluting blotting reagent. The LgBiT protein was then diluted 100-fold with the 1X blotting buffer and was mixed by inversion. The TBS-T washing solution on the membrane was replaced with LgBiT and blotting buffer solution, and was incubated for 1 hour at RT or overnight at 4 ^{o}C, with gentle rocking. Then, the substrate was carefully added into the LgBiT and blotting buffer solution at a 500-fold dilution and was mixed by hand by gentle swirling then by placing it in a rocker for 5 minutes. The blot was transferred to a chemiluminescence imager with a CCD camera.

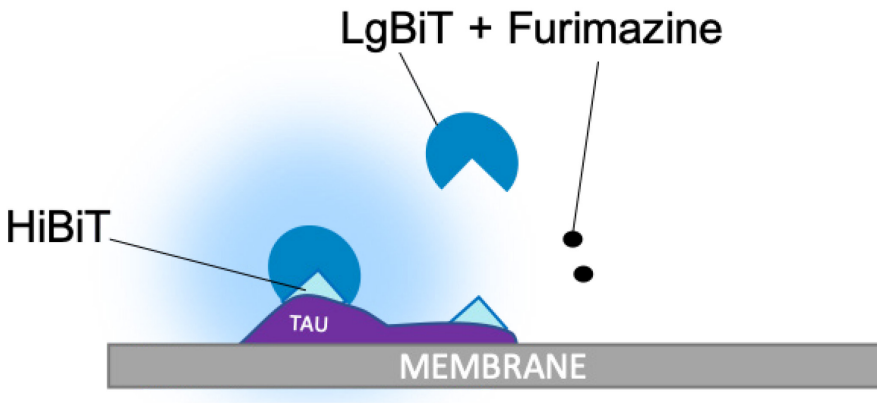

Figure 18. Schematic diagram of HiBiT-blotting.

LgBiT and enzyme substrate (furimazine) is added directly to the nitrocellulose membrane containing bound HiBiT-tagged tau protein. Structural complementation of LgBiT and HiBiT results in the generation of a bioluminescent signal which is detected by chemiluminescence imaging.

2.6.6 Dot-blotting

All dot-blot experiments were performed using a Bio-dot microfiltration apparatus (Bio-rad). Conditioned media and cell lysates from controls or treated (50 mM KCl or 3 µM Gabazine) cultured neurones were collected and lysed using 600 µl of ice-cold RIPA buffer (containing 2 × PBS, 1% (w/v) deoxycholate, 1% (v/v) Triton-X, 0.1% (w/v) SDS and 5 mm EDTA), respectively, and stored on Eppendorf tubes on ice and stored in -20 ^{o}C until use. The conditioned medium and cell lysates were heated to 95 ^{o}C for 5-10 minutes, followed by a 10-minute centrifugation step (13,000 x g) at RT to pellet all cell debris. The microfiltration apparatus was then loaded with 100 µl of 1X TBS to rehydrate the nitrocellulose membrane, followed by the addition of 500 µl supernatant from the conditioned medium and 300 µl from the cell lysates. Samples were allowed to flow through the nitrocellulose membrane by gravity flow for 2 hours; vacuum was applied after if not all samples have drained through the nitrocellulose membrane. Each well was washed with 200 µl of 1X TBS-T three times by vacuum. The nitrocellulose membrane was removed carefully from the microfiltration dot-blot apparatus and was immunoblotted with the desired primary and secondary antibody (as described in section 2.6.4).

2.7 Bioluminescence assays

2.7.1 Live cell assay system

The Nano-Glo Live Cell Assay System (Promega) was used to detect luminescence in living cells. It has two components: The Nano-Glo Live Cell Substrate and NanoGlo- Live Cell Substrate (LCS) dilution buffer. The Nano-Glo Live Cell Substrate is an organic stock solution that contains cell-permeable furimazine (NLuc substrate) diluted into an agent which reduces furimazine auto-luminescence upon the presence or absence of serum. The Nano-Glo LCS dilution buffer is an aqueous solution, which has similar components and functions to PBS or Hank's Balanced Salt Solution, that provides enhanced furimazine stability. It is used to dilute the Nano-Glo Live Cell Substrates in a 20-fold-dilution to make a 5X stock solution of the Nano-Glo Live Cell Reagent to mix with the cell culture medium (as described in Table 2-18). To prepare the Nano-Glo Live Cell Assay reagent, the Nano-Glo LCS dilution buffer was first removed from the freezer, and defrosted to RT. The Nano-Glo Live Cell Substrate, which is stored at -20 ^{0}C (freezer), was defrosted and first spun down using a microcentrifuge, to collect all the solution at the bottom of the tube. The desired amount of reconstituted Nano-Glo Live Cell Reagent was made fresh for every experiment, which was done by combining 1 volume of Nano-Glo Live Cell Substrate with 19 volumes of Nano-Glo LCS Dilution Buffer (a 20-fold dilution).

2.7.2 HiBiT extracellular detection system

Nano-Glo HiBiT Extracellular Detection System buffer solution was warmed to RT. Meanwhile, the experimental plate was removed from the incubator and was allowed to equilibrate to ambient temperature for 10 minutes. LgBiT and substrate was spun down in a centrifuged at 10,000 x g for 1 minute. A master mix of the non-lytic *Nano-Glo HiBiT Extracellular Detection System* buffer was reconstituted by diluting LgBiT and furimazine substrate by ration of 1:100 and 1:50, respectively, in an Eppendorf tube (as described Table 2-18). This was then gently mixed by inverting the tube up-side down 10 times and briefly spun using a microcentrifuge to collect solutions into the bottom of the tube. 20 µl of the reconstituted *Nano-Glo HiBiT Extracellular Detection System* solution was added to 80 µl of conditioned cell media in the experimental plate. The plate was covered and mixed by an orbital shaker for 1 minute 90-100 rotations per minute before reading. The luminescence was measure immediately using a plate reader (e.g., GloMax®-Multi+ Microplate Multimode Reader (Promega) with an integration time of 5 seconds per well.

Table 2-18**. Dilution factor of LgBiT, substrate and buffer for each Nano-Glo system used in the project.**

Nano-Glo Assays	LgBiT	Dilution factor	
		LgBiT: Buffer	Substrate: Buffer
Live Cell Assay System	Cell permeable	N/A	1:20
HiBiT Extracellular Detection System	Cell impermeable	1:100	1:50

2.7.3 Measuring luminescence with a microscope

Cell cultures plated on a glass-bottom dish (35 mm dish, No. 1.5 coverslip with 14 mm glass diameter; MatTek life sciences) for the assay sensitivity experiment was placed under the bioluminescence microscope (see 2.10.2) to first identify transfected cells using the fluorescence filters. The media is removed and replaced with 500 µl pre-warmed DMEM and the cells were allowed to equilibrate to the new media for 10 minutes prior to the addition of luminescence reagents. Fluorescence and brightfield images of transfected cells were obtained first prior to the measurement of luminescence. Luminescence imaging settings were kept the same for all cells from the same experiments.

2.7.4 Assay sensitivity experiments

HEK293 cells were seeded and plated on white opaque 96-well plates (as previously described in 2.3.5) in 10% FBS DMEM. The plates were incubated for 24 hours to allow cells to attach prior to transfection. The transfection reagents consisting of LgBiT and serially diluted GFP-HiBiT-Tau^{E14} mixture were prepared. The GFP-HiBiT-Tau^{E14} plasmid was titrated with a dilution factor listed in Table 2-19. About 30 ng per well of LgBiT plasmid (HSV/TK-LgBiT or CMV-HaloTag-LgBiT) was used to transfect 3,000 cells. For example, for a 1:1 dilution, 30 ng of HSV/TK-LgBiT and 30 ng of GFP-HiBiT-Tau^{E14} plasmid was used to transfect 3,000 cells; for a 1: 1/5 dilution, 30 ng of HSV/TK-LgBiT was and 6 ng of GFP-HiBiT-Tau^{E14} plasmid mixed. Transfection was done as previously described in 2.3.6.

Table 2-19. Dilution factors of transfected CMV-HaloTag-LgBiT and HSV/TK-LgBiT with GFP-HiBiT-Tau^{E14}.

HSV/TK-LgBiT + GFP-HiBiT-Tau^{E14}		**CMV-HaloTag-LgBiT + GFP-HiBiT-Tau^{E14}**	
Dilution factor (n)		Dilution factor (n)	
1: 1	1: 1/1	1: 1	1: 1/1
1: 1/5	1: 1/5	1: 1/4	1: 1/4
1: $1/5^2$	1: 1/25	1: $1/4^2$	1: 1/16
1: $1/5^3$	1: 1/125	1: $1/4^3$	1: 1/64
1: $1/5^4$	1: 1/625	1:$1/4^4$	1: 1/256
1: $1/5^5$	1: 1/3125	1:$1/4^5$	1: 1/1024
1: $1/5^6$	1: 1/15625	1: $1/4^6$	1: 1/4096
1: $1/5^7$	1: 1/78125	1: $1/4^7$	1: 1/16384
1: $1/5^8$	1: 1/390625	1:$1/4^8$	1: 1/65536

Green* indicates limit of detection [CMV]-HaloTag-LgBiT and GFP-HiBiT-Tau^{E14}. Red* indicates limit of detection [HSV/TK]LgBiT and GFP-HiBiT-Tau^{E14}.

2.8 NanoBiT-Tau secretion assays

All NanoBiT-tau secretion assays were performed on DIV13-15.

2.8.1 Detection of basal tau secretion

To detect basal tau secretion, conditioned media at DIV13-15 was assessed for the presence of HiBiT-Tau. This indicates the total level of tau accumulated overtime. The plate was removed from the incubator 10 minutes prior to luminescence read-out. The *HiBiT Extracellular Detection System* solution was prepared as described in section 2.7.2. To read basal tau secretion, 70 µl of conditioned media was first remove from experimental each well, leaving ~80 µl of conditioned. This was then replaced with 20 µl of buffer containing LgBiT and substrate just as described in section 2.7.2. The plate was gently mixed by a rotating mixer and the luminescence was immediately detected.

2.8.2 Measuring activity-dependent tau secretion in cultured primary neurons

Neuronal activity was pharmacologically modulated by treating cells with sterile-filtered and pre-warmed (-)Mg^{2+}-HEPES-based ACSF and plain-HEPES-based ACSF (which was used as vehicle), supplemented with either 3 µM Gabazine (GZ) or 500 nM Tetrodotoxin (TTX), respectively. The plain-HEPES-based ACSF was used as control condition (referred to as 'vehicle'). Conditioned NBM was removed from the cell and stored in a separate plate. Pre-warmed 80 µl of GZ+(-)Mg^{2+}-HEPES and TTX-HEPES-based ACSF were added to the experimental wells in triplicates at a time to prevent drying out of cells. The plate was incubated for 6 hours. The luminescence signals from well was detected after the addition of reconstituted *Nano-Glo HiBiT Extracellular Detection* solution was added to each experimental (as previously described in section 2.7.2).

2.8.3 Inhibition of sulphated proteoglycans biosynthesis

Primary hippocampal neurons were seeded on 96-well plates (as previously described 2.3.5) and were allowed to mature up to DIV13-15. Prior to pharmacological modulation of neuronal activity (as described in section 2.8.1.), cells were pre-treated with warmed 100 NBM supplemented with 2% B-27 and 0.5 mM GlutaMAX and 50 mM sodium chlorate ($NaClO_3$) for 16 hours. Solutions were sterile-filtered and pre-warmed prior to addition to cells. After 16 hours pre-treatment of $NaClO_3$, the conditioned media was removed from each experimental wells and replaced with 80µl of each of the following solutions: (-)Mg^{2+}- HEPES-based ACSF, supplemented with 3 µM GZ with or without 50 mM $NaClO_3$, and plain-HEPES-based ACSF, supplemented with 500 nM TTX with or without $NaClO_3$.As control some cells were treated with just plain-HEPES-based ACSF without

$NaClO_3$. The plate was incubated at 37 ^oC for 6 hours. The Nano-Glo HiBiT Extracellular assay was then used to measure overall luminescence secreted (done as previous described 2.7.2.).

2.8.4 Cell viability assay using Calcein Blue, AM

Calcien Blue AM (ThermoFisher Scientific) a cell-permeable esterase substrate was used to measure enzymatic activity and cell-membrane integrity. When AM esters are cleaved by intracellular esterases, the Calcein AM becomes polarised and are retained by cells, resulting in the generation of a strong fluorescence signal with an excitation/emission of approximately 360/449 nm. To measure overall cell viability in our assays, all conditioned media from cells was aspirated and Calcein AM Blue was dissolved in DPBS (Gibco's) to make up to 10 µM (protected from light) solution. To assess cell viability, 100 µl of 10 µM Calcein AM Blue solution was added each well (96-well plate). After 15-minute incubation, fluorescence signal was measured using a plate-reader. Calcein AM solution was added to 3 empty wells and the signal was used as a blank in the assay; the blank signal was subtracted in all experimental signals.

2.8.5 Measuring membrane-free and vesicular tau in the extracellular space

To distinguish membrane-free and vesicle-bound tau a non-lytic and lytic configuration of the NanoBiT-Tau reporter assay was used as a side-by-side comparison. The non-lytic assay allows the detection membrane-free tau proteins in the extracellular space by adding the LgBiT and substrate (furimazine) directly into the conditioned media. In contrast, the lytic assay, involves the addition of digitonin 50 µg/ml; this gives the total read-out of both membrane-free and membrane-bound tau present in the conditioned media.

For detecting secreted membrane-free and vesicle-bound tau in the conditioned media of primary neurons the following methods were carried out. Primary hippocampal neurons were dissected and plated on 96-well plates (as previously described in section 2.3.3 and section 2.3.5). Neurons were transduced (section 2.4.2) and were the conditioned media was assayed at DIV13-15 for the presence of membrane-free and vesicle-bound tau. The plate was allowed to equilibrate at room temperature prior to use.

Firstly, the conditioned media was removed from each well and 160 µl was split into two wells on a separate white opaque 96 well-plate, labelled 'nonlytic' and 'lytic'; each condition should have 80 µl each. Similarly, two different Eppendorf tubes, labelled 'nonlytic' and 'lytic were prepared. The extracellular HiBiT reagent was reconstituted and the LgBiT and substrate was added (as described in 2.7.2) on both tubes. The 'lytic' tube, was supplemented with digitonin, a non-ionic-detergent, to make a total concentration of 50 µg/ml in solution and mixed by gentle inversion.

Both tubes were briefly spun by a microcentrifuge. Reconstituted ‘non-lytic’ and ‘lytic’ Nano-Glo HiBiT extracellular reagents was added to designated experimental wells. The plate was covered and gently mixed by placing in a rotating rocker for 1 minute at 100 rotations per minute prior to reading the luminescence.

2.9 **Immunocyto**chemistry

2.9.1 Mass cell culture

To fix cells, the media were firstly removed from the cell cultures one-at-a-time and subsequently washed with 1x PBS. For cells cultured on 12-well plates, each well was washed with 500 µl PBS. This was then replaced with 500 µl 4% paraformaldehyde (PFA) supplemented with 20% sucrose in PBS. If coverslips were required immediately, the coverslips were submerged with 500 µl 50mM ammonium chloride (NH_4Cl) in TBS for 5 minutes at RT. The addition of TBS or NH_4Cl helped neutralise unreacted aldehydes and reduced the effect of autofluorescence.

For immunofluorescent staining, cells were firstly permeabilised with 500 µl 0.1% Triton-X100 dissolved in TBS for 5 minutes at RT. To prevent unspecific binding, the cells were then blocked with 10% normal goat serum in TBS for 30-60 minutes at RT. Carefully, glass coverslips were transferred (using clean forceps) on top of the plate lid, covered with hydrophobic parafilm, to allow effective antibody incubation in the later process. Primary antibodies (diluted in 10% normal goat serum; Table 2-20) were carefully pipetted onto the glass cover slips (100 µl per coverslip) and was allowed to incubate for 1 hour at RT or overnight at 4 ^{o}C. The coverslips were then placed back into the wells and were washed with TBS three times for 5 minutes/wash. Cover slips were removed from the wells and placed back into the plate lid. Incubation with the secondary antibodies were then carried out by applying 100 µl on to the coverslips. Secondary antibodies (AlexaFluor 488/555/645), were prepared in 10% normal goat serum/2% BSA in TBS (1:1000 to 10000 dilution) (Table 2-21). To maximise the fluorescent intensity and reduce effect of photobleaching, the coverslips with secondary antibodies were protected from light by covering it with a block-out box. Once incubation was completed, cells were washed with TBS for 5 minutes. On the second wash, instead of washing with TBS alone, cells were stained for their nuclei using Hoechst stain (diluted at 1:1000 to 20000 in TBS) for 5 minutes. The coverslips were washed with TBS for 5 minutes on the third wash. The coverslips were then mounted on a microscope glass slide with ~20 µl Mowiol glue and was allowed to dry prior to imaging.

Table 2-20. Primary antibodies used in immunostaining.

Antibody	Dilution	Incubation	Isotype	Reactivity	Supplier, Product number
MC1	1:300	1 hr at RT	IgG	Mouse, Human	Peter Davies Lab (Jicha et al., 1997)
MAP2	1:50,000	1 hr at RT	IgY	Chicken (polyclonal)	Abcam (no. ab5393)
Tau	1:1000	1 hr at RT	IgG	Rabbit (polyclonal)	DAKO (no. A0024)
HepSS-1	1:1000	1 hr at RT	IgM	Mouse (monoclonal)	Antibodies.com (no. A121769)

Table 2-21. Secondary antibodies used for immunostaining.

Antibody	Dilution	Incubation	Isotype	Isotype	Host Species	Supplier, Product number
AlexaFluor-488	1:1000	1 hr at RT	IgG	Mouse	Goat (polyclonal)	Invitrogen (A-21121)
AlexaFluor-488	1:1000	1 hr at RT	IgG	Rabbit	Goat (polyclonal)	Invitrogen (A-11059)
AlexaFluor-555	1:1000	1 hr at RT	IgG	Mouse	Goat (polyclonal)	Invitrogen (A-21422)
AlexaFluor-555	1:1000	1 hr at RT	IgG	Rabbit	Goat (polyclonal)	Invitrogen (A-21429)
AlexaFluor-555	1:1000	1 hr at RT	IgM	Mouse	Goat (polyclonal)	Invitrogen (A-21426)

2.10 Microscopy

2.10.1 Fluorescence microscopy

Fixed cell images for distal axonal fluorescence distribution analysis were obtained using a Nikon E800 upright fluorescence microscope, equipped with a Plan Fluor 60x 1.40 N.A. Oil immersion objective lens (Nikon Instruments Inc, Japan) and an Imaging OptiMOS sCMOS 1920 x 1080 pixel camera (Photometrics, USA). All off-set, gain and binning settings were kept constant for each experiment. Fluorescence images of the distal part of axons (>350 µm from the cell body) were taken for each healthy cell, which was established by a good nucleus staining. Other images were taken using the Delta Vision Elite microscope using the 60x1.42NA Oil Plan APO objective with the SoftWorks software to modify settings. The fluorescence illumination was achieved using a mercury lamp and FITC/TRITC/DAPI filter sets to resolve the fluorophores used in experiments (as shown in Table 2-22).

Table 2-22. The filter-sets used to resolve the fluorophores used in experiments.

Fluorophore	Filter	Excitation (nm)	Dichroic (nm)	Emission (nm)
Blue	DAPI	375/28	415	460/50
Green	FITC	480/30	505	535/40
Red	TRITC	540/25	565	606/55

2.10.2 Bioluminescence imaging

Bioluminescence images were collected using DM-IRB inverted microscope stand (Leica Microsystems, equipped with a Plan Fluortar 40x 0.50-1.00 N.A. oil objective (Leica Microsystems, Germany) and an Imaging Rolara Thunder EMCCD camera with a 512 x 512 pixel chip (Photometrics, USA). To increase signal/pixel, a reduction optic was fitted using a camera C-mount adaptor fitted with a 0.63x lens to reduce image size. The bioluminescent microscope contains a built-in fluorescence and brightfield imager and were collected using the same imaging system. The fluorescence illuminations were achieved using an HB0103 lamp housing (Leica Microsystems) equipped with a fibre optic connection into the microscope. The stand and camera were placed inside a custom-built light-tight housing and the entire system was mounted on an antivibration table (TMC, USA) to provide stability over long image acquisition times. Camera control and image acquisition was achieved using Micro-manager software (University of California San Francisco, USA), and images were processed and analysed using ImageJ or Fiji (NIH, USA).

2.11 Imaging analysis

2.11.1 Axonal variable fluorescence distribution analysis

Primary neurons were cultured until DIV14 prior to axonal segment analysis. For distal axonal segment analysis, fluorescent images of the distal part of axons (>350 μm from the cell body) were taken. The longest process from each cell was analysed using Image J or Fiji (NIH, USA). Firstly, a segmented line was created over a stretch of a healthy, 'unblebbed' axon. Using this line, plot profiles that correspond to the fluorescence pixel intensity along the axon was generated.

As part of the imaging analysis, all axons underwent visual assessment to ensure that imaging artefacts (e.g., blebbing, out of focus, autofluorescence from cell debris) are minimised. Only axons that demonstrated a good 'clean' stretch of >50 μm axonal length were used in the analysis. This is to ensure that the data analysed are representative of the axon. Each value corresponding to the plot profiles were recorded in Microsoft Excel for Mac 2011. Fluorescence aggregation analysis was performed using a custom script in MATLAB (described in Figure 64, Appendix A.1).

Firstly, the script compared each stretch of treated axon to the corresponding control axons taken from each experimental group. A baseline for each individual axon was generated by subtracting the 10^{th} percentile value from all the values. Axonal points that are positive for aggregation are established when a point lies outside 5 times the mean of the deviation of all control axons from the experiment. The total percentage of plot profile values that lies outside this range for each experimental axon is considered. Then, the script calculates the total number of individual axons that demonstrated >10% aggregated points. These axons ware denoted as positive for aggregation. Axonal fluorescence analysis was done by using a custom script MATLAB (Figure 64 Appendix A.1).

2.11.2 Analysing transduction efficiency in primary neurons

Transduced neurons were fixed and mounted on coverslips as done previously. Images of the cell body of neurons using the Delta Vision Elite microscope and 60x1.42NA Oil Plan APO objective with the SoftWorks software to modify settings. Transduced cells were stained with total tau (DAKO) and Alexa-Fluoro-555 antibodies. Images were taken in the DAPI and TRITC channels which were used to select for group of cells (minimum of 5 in a field of view) with good cell body morphology. The FITC channel was used to take images of transduced neurons on the same plane as TRITC. Different areas from the coverslip was taken for both channels; five images were taken per coverslips and a total of 10 images were obtained per conditions. To quantify transduction

efficiency the total cell body count taken in both TRITC and FITC channels were obtained and a percentage was calculated by dividing the total number of transduced cells by the total number of cells stained for total tau antibody.

2.12 Statistical analysis

All statistical analysis was run on data obtained from at least three independent experiments (unless otherwise stated). GraphPad Prism 6 was used (Ver 6.00m Graph Pad Software Inc.) to generate graphs and make statistical analysis. Statistical significance was evaluated with paired t-test, repeated measures one-way ANOVA followed by Fisher's LSD, or two-way ANOVA followed by Fisher's LSD or Sidak's test, unless otherwise stated. Findings were considered significant as follows: *p<0.05, **p<0.01, ***p<0.005, ****p<0.0001. All error bars presented in graphs represent standard error of mean (SEM).

2.12.1 Defining biological and technical replicates

Biological replicates (N)

Cultures taken from biologically distinct samples (e.g., the same type of organism treated or grown in the same conditions, embryos harvested from different animals) were considered as independent biological repeats (N). For example, primary hippocampal cultures harvested from the embryos isolated from one pregnant mouse was considered as one biological replicate (N=1).

Technical replicates (T)

Technical replicates (T) are repeated measurements taken from the same sample or one biological source. For example, in 96-well plate assays, 2-3 technical replicates were taken for each condition in one biological experiment (T=2-3). Neurons recorded in whole cell patch clamp experiments from the same biological replicate is considered as a technical repeat; usually, 2-8 cells per biological replicate were used for each condition.

2.13 Development of NanoBiT-Tau reporters to assay secretion and re-uptake

To mimic different tau misfolding pathological conditions, AD and FTDP-17, two plasmids constructs are used (Hoover et al., 2010): GFP-Tau^{E14} and GFP-Tau^{P301L}. GFP-Tau^{E14} construct mimics hyperphosphorylation in AD. GFP-Tau^{P301L} construct contains a point mutation at position 301 of the tau protein, causing a change from a proline residue into a leucine. This point mutation is found in patients with familial cases of FTDP (see tauopathies in section 1.1.1).

To allow the detection of misfolded and native tau transfer to be monitored, NanoBiT-tau biosensors were developed in our lab. This is composed of Nanoluciferase (NLuc) which is a 19kDa of a split bioluminescent enzyme, composing of LgBiT (18kDa subunit) and HiBiT (11 amino acid peptide) (Dixon et al., 2016). Structural complementation of these two subunits allow reconstitution of NLuc which generates a strong bioluminescent signal. This assay will provide a mechanistic insight into both pathological and physiological tau release which is currently not possible with the existing fluorescent-based assay. Adding the split-NanoBiT reporters in the different compartments in the system will allow a mechanistic insight in the molecular mechanisms involved in the release and re-uptake wild-type and mutant tau forms in health and disease (Figure 19). LgBiT can be added on the extracellular space to monitor tau release of both wild-type and mutant tau; LgBiT expression vectors can also be expressed in the cytosol to monitor re-uptake (Figure 19).

In this subsection, the molecular cloning strategies and the development process in the generation of NanoBiT-Tau reporter constructs will be outlined. Using extensive molecular cloning techniques GFP-Tau^{WT}, GFP-Tau^{E14}, GFP-Tau^{P301L} which are in pRK5 cloning vectors were tagged with HiBiT to generate GFP-HiBiT-Tau^{WT}, GFP-HiBiT-Tau^{E14}, GFP-HiBiT-Tau^{P301L} expression vectors. Two constructs were also generated to act as positives and negative secretion control (Figure 20A): GFP-HiBiT and a secreted for of GFP-HiBiT (secGFP-HiBiT). GFP-HiBiT is a negative control because its expression will be retained intracellularly. On the other hand, secGFP-HiBiT construct, which contain an interleukin-6 (IL6) signal sequence N-terminal of the GFP coding sequence, encodes a recombinant protein that will be targeted to the secretory pathway, exocytose and should be readily detectable in the extracellular space.

To compliment the investigation focused on the use of GFP-HiBiT-Tau, LgBiT-Tau^{WT}, LgBiT-Tau^{E14}, and LgBiT-Tau^{P301L} constructs were also developed. The aim of generating LgBiT- Tau expression vectors facilitates the study of tau re-uptake mechanisms in wild-type and mutant tau variants. Generation of bioluminescent signal in acceptor cells expressing LgBiT-tau would dictate that 1)

HiBiT-tau has been released into the extracellular space, 2) that HiBiT-tau has been taken-up and 3) that it has interacted with endogenous tau. This system will therefore allow understanding of the mechanisms involve in the initial re-uptake routes of different tau variants and how mutant and wild-type tau variants interact with native tau in acceptor cell.

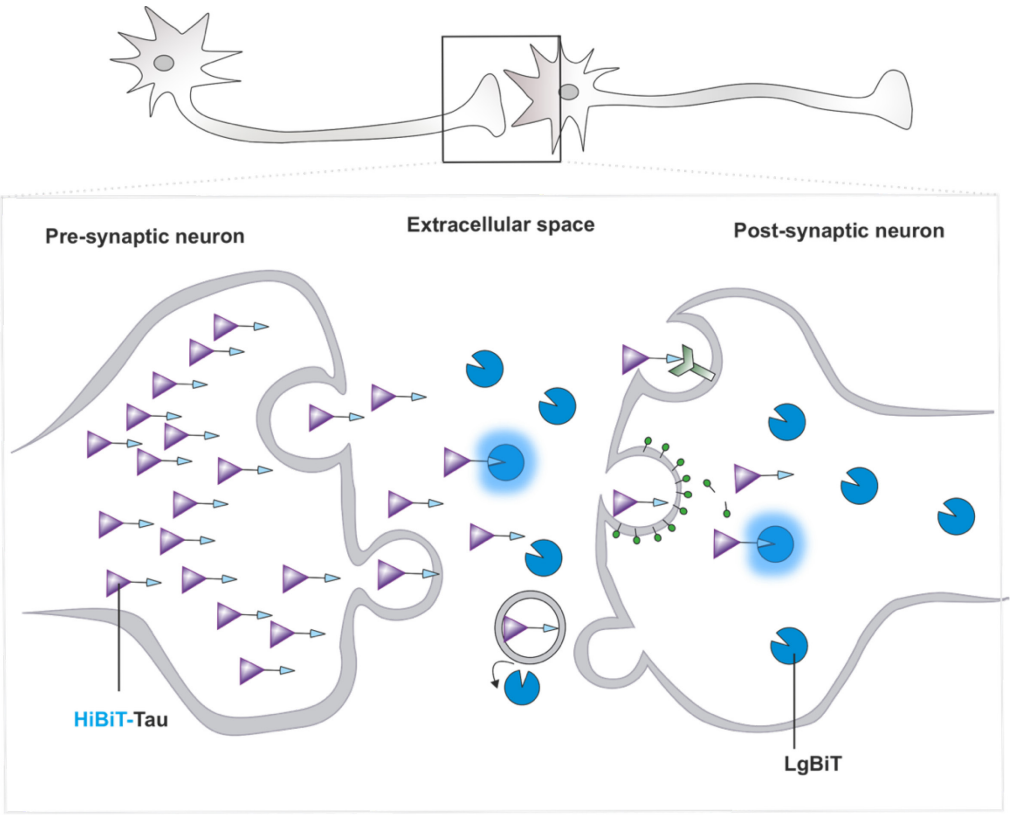

Figure 19. The principle of the NanoBiT-tau complementation assay in the context of extracellular and intracellular detection of tau.

In the pre-synaptic neuron, HiBiT-tagged tau is released via unconventional secretion pathways. Addition of LgBiT and furimazine substrate in the extracellular space detects membrane-free HiBiT-tau. LgBiT can also be expressed in the post-synaptic neuron and any HiBiT-tau are taken up can be detected.

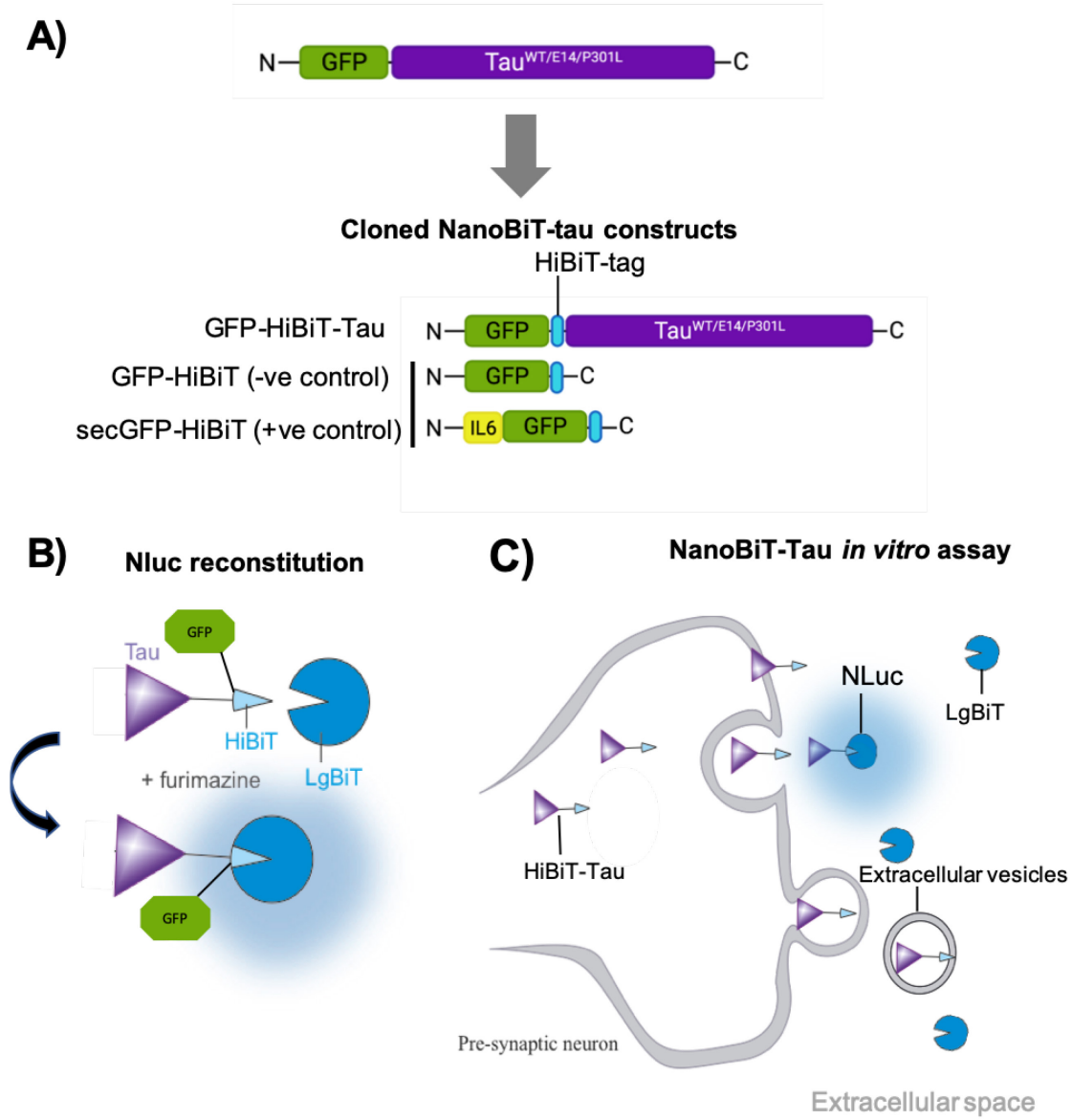

Figure 20. Generation of new NanoBiT-tau constructs for the use of the *in vitro* tau secretion assay.

A) Molecular cloning strategy involved that insertion of HiBiT between GFP and Tau to produce GFP-HiBiT-Tau^{WT}, GFP-HiBiT-Tau^{E14} and GFP-HiBiT-Tau^{P301L} constructs. B) Expression of NanoBiT-tau constructs will produce complementing HiBiT and LgBiT split reporters which generates a strong bioluminescent signal can be detected. C) The placement of NanoBiT-tau and supplementary constructs in the *in vitro* secretion assay; LgBiT is added to the extracellular space to monitor secreted HiBiT-tau.

2.13.1 Generation of NanoBiT-Tau reporter constructs to assay secretion

2.13.1.1 Generation of HiBiT inserts

HiBiT inserts with complementary N- and C-terminus were first generated and amplified using PCR. To do this, two forward and reverse oligonucleotides, (described as primer number 1 and 2 in Table 2-4) were annealed together to generate an insert that contains N- and C- terminal overhangs. The forward primer sequence is 72 nucleotides long (primer number 1 in Table 2-4 and Figure 21A); a 'GATCC' sequence is located in the 5'-end of the primer (yellow), which was used to create a N-terminal overhang once annealed with the reverse primer, followed by nucleotides sequences encoding the HiBiT (blue); finally, an extra adenine 'A' nucleotide is added to finish the sequence in the 3'-end. The reverse primer used was 73 nucleotides long (see Table 2-4 and Figure 21A); to create a C-terminal overhang after the digestion, the reverse primer starts with a 'GATCT' sequence (yellow) in the 5'-end, followed by the HiBiT sequence (blue) that is flanked by two linker nucleotide sequences (red)- these sequences are complementary to the forward primer; finally, a guanine 'G' is located on the 3'- of the primer so that a it can complement with the forward primer to generate the N-terminal overhang.

2.13.1.2 HiBiT-Tau^{E14}

The cloning strategy for GFP-HiBiT-Tau^{E14} is described in Figure 21. The vector backbone, GFP-Tau^{E14}, was digested BamHI to create a linearized vector, allowing the HiBiT insert to complement, which has two similar N- and C-terminal overhangs complementary to the vector plasmid. This allowed the HiBiT insert to be cloned into the linearized vector (Figure 20B). The HiBiT insert can be ligated into different orientation into the linearized vector and can generate two different products. The construct which has correct HiBiT orientation was selected and purified following confirmed sequencing results. This construct was generated by a colleague.

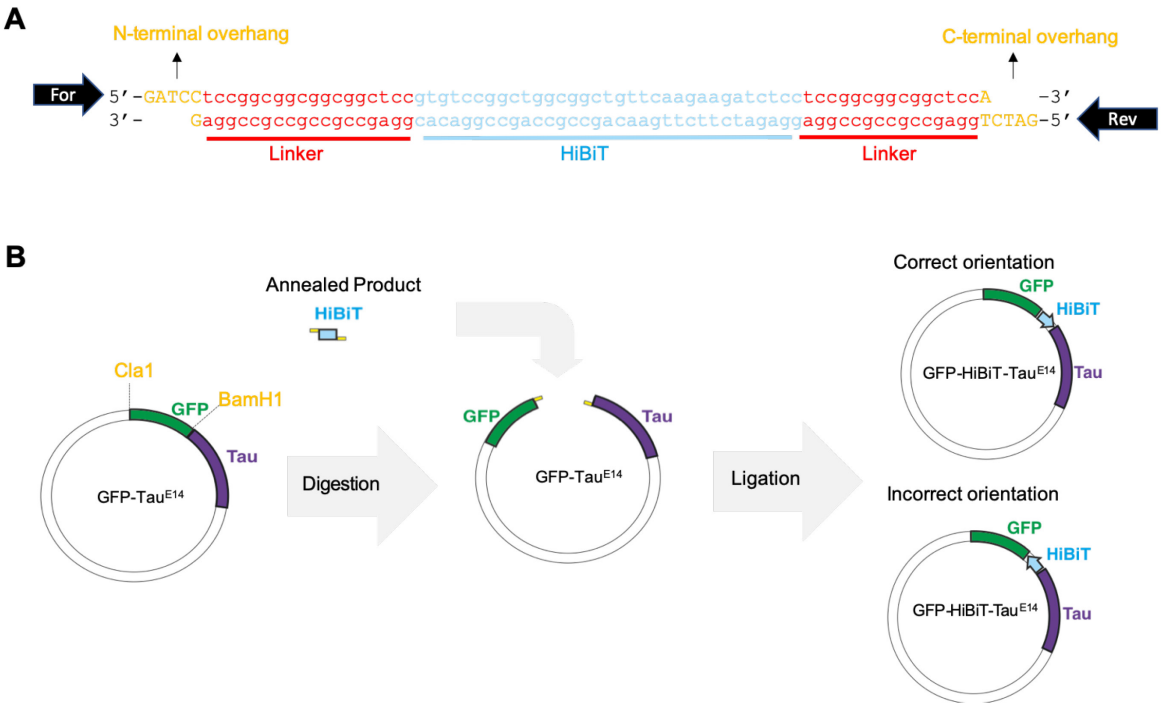

Figure 21. Cloning strategy for the generation of HiBiT oligonucleotide insert and for GFP-HiBiT-Tau^{E14}.

A) The annealing of the forward and reverse primers to form HiBiT insert with N- and C-terminal overhangs. B) Cloning strategy to generate GFP-HiBiT-Tau^{E14}; GFP-Tau^{E14} is digested with BamHI to form a linearized vector that is complementary to the N- and C-terminal overhangs of the HiBiT insert, allowing ligation to occur. Two different orientations are possible with the ligation of HiBiT into the vector backbone. The correct orientation was selected for by restriction digest test and sequencing.

2.13.1.3 HiBiT-Tau^{WT} and HiBiT-Tau^{P301L}

Due to poor cloning efficiency of the HiBiT insert on the GFP-Tau^{WT} and GFP-Tau^{P301L} vector in previous cloning experiments (as described in section 2.13.1.2), an alternative strategy was used to generate the GFP-HiBiT-Tau^{WT} and GFP-HiBiT-Tau^{P301L} constructs. The sequence coding for the GFP-HiBiT was isolated (using primer 3 and 4 from Table 2-4) from the GFP-HiBiT- Tau^{E14} template. The GFP-HiBiT sequence was selectively amplified (cloning strategy and primer designs are described in Figure 22A-B and Table 2-4). Specific forward and reverse primer flanked the GFP-HiBiT from the 5'-end, the primer begins with a 'GGATCC' sequence (in orange Figure 22A), which will encode a BamH1 restriction site. This is followed by the left linker (red), HiBiT (blue) and right linker (red) sequence (Table 2-4).The forward primer recognised the ClaI restriction site and 21 nucleotides, complementary to the anti-sense strand of GFP coding region within the GFP-HiBiT-Tau^{E14} template (Figure 22A). On the other hand, the reverse primer was 101 nucleotides long and bind to the 3'-end of sense strand complementary the downstream sequence of GFP-HiBiT. In order to insert GFP-HiBiT into the vector backbone, a ClaI and BamHI restriction sites flanking the GFP-HiBiT sequence, from upstream and downstream, respectively, needed to be in place.

As the original DNA template used for the PCR had a BamHI restriction site located between the GFP and HiBiT sequence, the reverse primer was designed to carry a single base mutation to render this site unrecognisable by BamH1 RE in later cloning stages. So instead of 'GGATCC' (coding sequence of BamHI site), a 'GGAACC' sequence was incorporated to the primer following the linker sequences. As a consequence of this mutation, this site is not be recognised by BamH1 RE as a potential cut site, allowing the full double-stranded GFP-HiBiT sequence to be amplified alongside a Cla1 and a new BamHI restriction site, located downstream of the HiBiT and linker sequence. To ensure successful change of this site, 23 complementary nucleotides sequences to the GFP was added to the primer sequence at the 5'-end following the 'GGAACC' sequence. After using these forward and reverse primers in a PCR reaction (with Q5 high fidelity DNA polymerase), a GFP-HiBiT insert flanked by ClaI and BamHI restriction sites.

The GFP-HiBiT insert and GFP-Tau^{WT} and GFP-Tau^{P301L} vectors were both digested with ClaI and BamHI to form linearized plasmids that have complementary overhangs, allowing successful ligation. The GFP was excised from the GFP-Tau^{WT} and GFP-Tau^{P301L}. The GFP-HiBiT insert was then ligated into the linearized vectors after the removal of GFP.

To screen for the desired product from the cloning procedure was purified (e.g., GFP-HiBiT-Tau$^{WT/P301L}$), a diagnostic restriction digest test was done using PstI and BglII RE's *in silico* and *in vitro* (Figure 24 and Figure 25). The addition of HiBiT introduced a BglII cut site into the both plasmids. There is no BglII cut site in the original GFP-Tau$^{WT/P301L}$ plasmid hence was used as

negative control for *in vitro* restriction digest. However, there was an extra band not expected in the control plasmid, which could be due to partial digestion. PstI and BglII cuts the new plasmid three times all together therefore, the correct insertion of GFP-HiBiT into the vector backbone is indicated, by the appearance of three DNA lengths at 582, 606 and 5403 (bp); these REs only cut GFP-Tau^{WT} and GFP-Tau^{P301L} plasmids twice. *In silico* digestion of GFP-HiBiT-Tau^{WT} and GFP-HiBiT-Tau^{P301L} show two similar sizes of DNA, at 582 and 606, which appear as a singular band in gel (indicated by two yellow arrows in Figure 24A and Figure 25A). However, A first round using the strategy described above generated diagnostic restriction digest that did not define the expected fragmentation pattern (data not shown).

To carefully validate and investigate the GFP-HiBiT PCR-product used in the cloning procedure, pGEM®-T Easy Vector Systems was used as it allowed the PCR product to be easily cloned for further analysis. This method is discussed in section 2.2.11.The cloning strategy is described in Figure 23. Sequencing results lead to the discovery of a single-point mutation, where an adenine (A) has been replaced with a thymine (T), in the coding sequence of the GFP-HiBiT insert. This mutation was located in the ClaI restriction site of the GFP-HiBiT insert and could lead to amino acid change. To correct the mutation, forward and reverse primers were designed to mutate the T→A (primer used were number 5 and 6 in Table 2-4). The correct GFP-HiBiT insert was then digested with ClaI and BamHI and ligated into the linearized GFP-Tau^{WT} and GFP-Tau^{P301L} plasmids, as done previously. Diagnostic digest of the purified plasmids using PstI and BgII demonstrated that correct construct (e.g., GFP-HiBiT-Tau^{WT} and GFP-HiBiT-Tau^{P301}) was generated as the same banding pattern as showed *in silico* was produced (Figure 25A,B and Figure 24A,B).

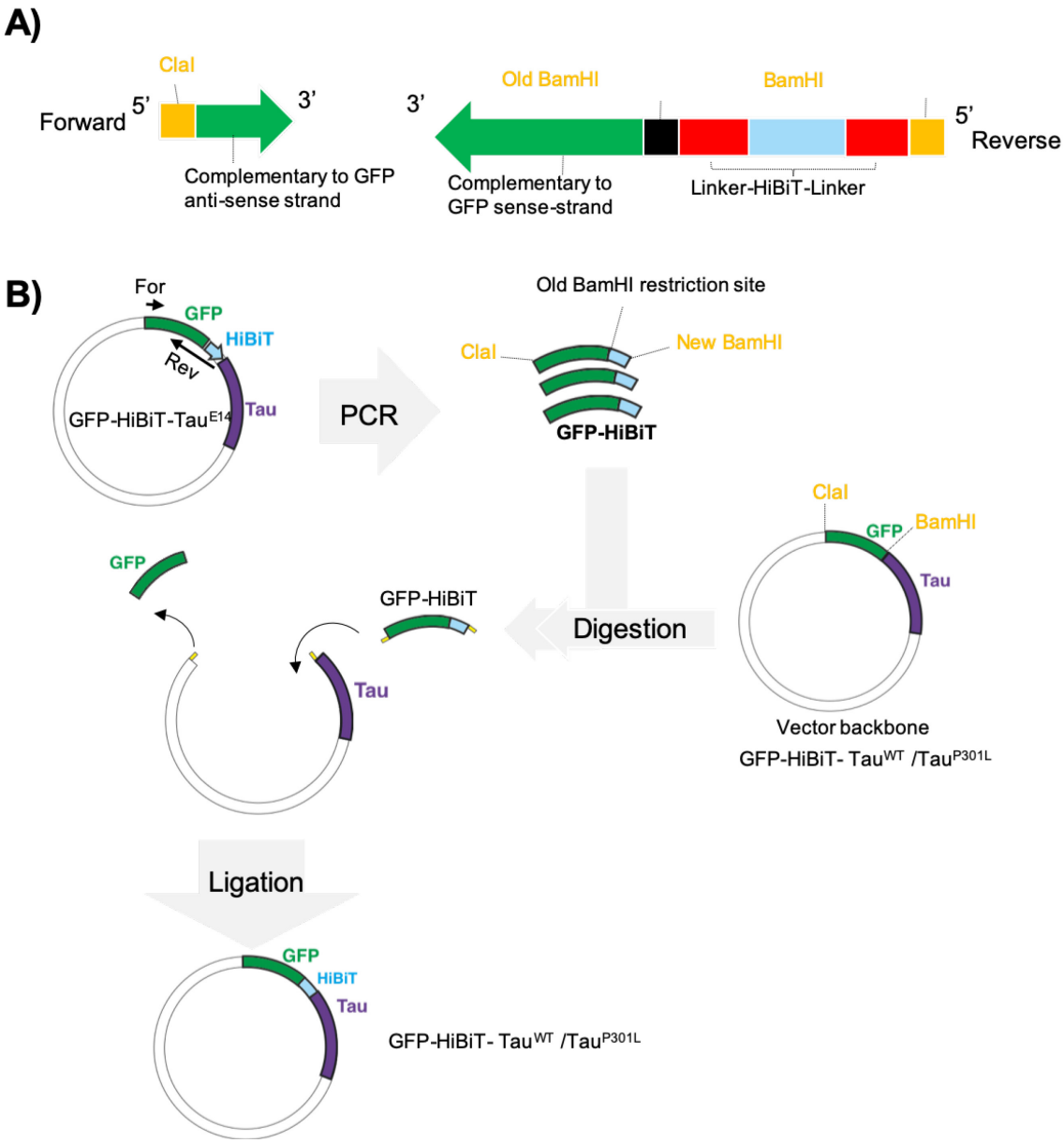

Figure 22. Cloning strategy to generate GFP-HiBiT-Tau^{WT} and GFP-HiBiT-Tau^{P301L}.
A) Features of forward and reverse primers which was used to amplify GFP-HiBiT insert flanked by ClaI and BamHI. B) Cloning work flow to form GFP-HiBiT-Tau^{WT} and GFP-HiBiT-Tau^{P301L}; forward and reverse primers was used in PCR reaction to amplify GFP-HiBiT insert, containing a ClaI and new BamHI restriction site at either side. Vector backbone and GFP-HiBiT insert was digested with ClaI and BamHI. GFP was removed from the vector backbone, followed by ligation to form GFP-HiBiT-Tau^{WT} and GFP-HiBiT-Tau^{P301L}.

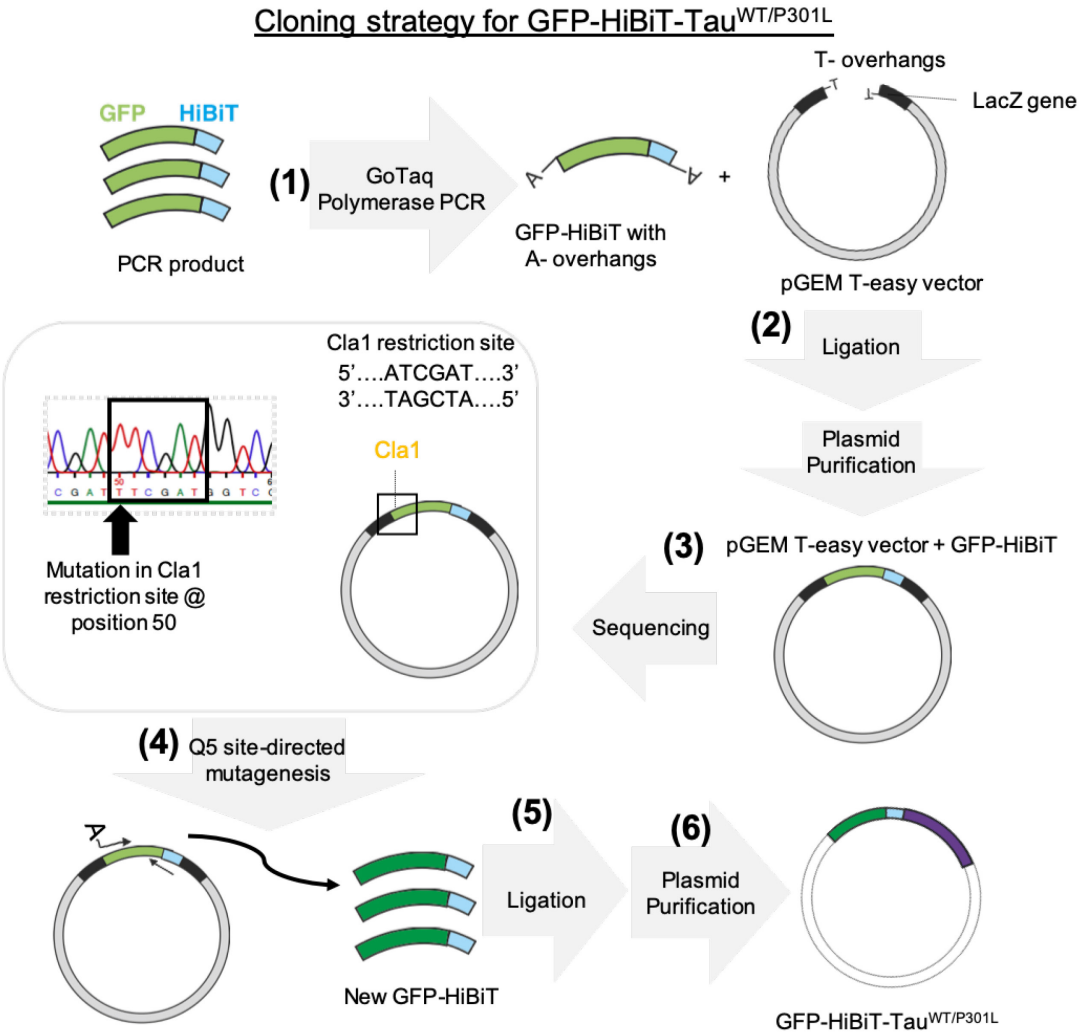

Figure 23. Cloning strategy to correct the mistake in the GFP-HiBiT encoding insert

As fragmentation pattern of cloned products was not what was expected in the initial round of cloning, pGEM T-easy vector system was used to validate PCR product (e.g., GFP-HiBiT). 1) The original insert was amplified via PCR using Go-Taq polymerase. 2) The insert is ligated into a pGEM T-easy vector. 3) the plasmid was purified and sequenced to identify mutation in the construct. The mutation was located in the ClaI restriction site (at 'position 50') where an adenine has been replaced with a thymine. 4) Primers were designed to correct the mutation. 5) New GFP-HiBiT inserts with no mutation was generated and digested with ClaI and BamHI. Digested inserts were ligated into linearized vector backbones of Tau^{WT} and Tau^{P301L}. 6) Plasmids were purified and processed for further investigation.

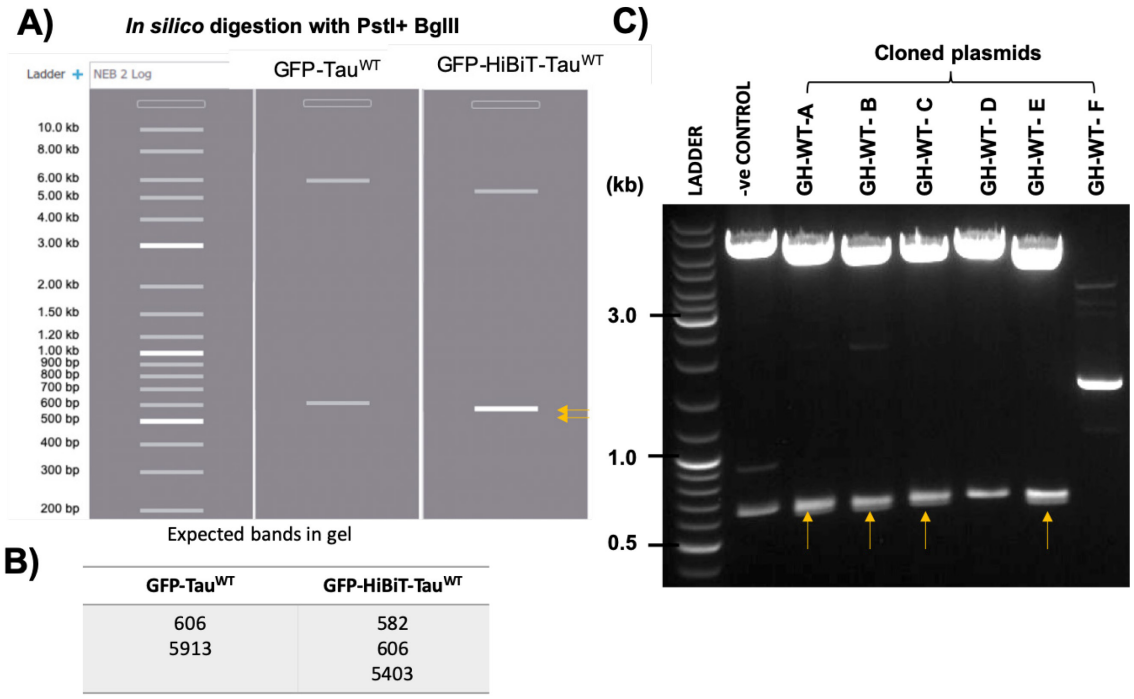

GFP-Tau^{WT}	GFP-HiBiT-Tau^{WT}
606 5913	582 606 5403

Figure 24. Diagnostic test digest to check presence of GFP-HiBiT-Tau^{WT} cloned constructs using PstI and BglII.

A) In silico expected gel pattern and DNA lengths (low panel) when GFP-Tau^{WT} and GFP-HiBiT-Tau^{WT} are digested in silico with PstI and BglII. B) Expected banding pattern in gel. C) Cloned products were digested with PstI and BglII. Yellow arrows indicate the presence of two bands in labelled GH-P A, B, C and -D thus showing successful production of GFP-HiBiT-Tau^{WT} plasmids.

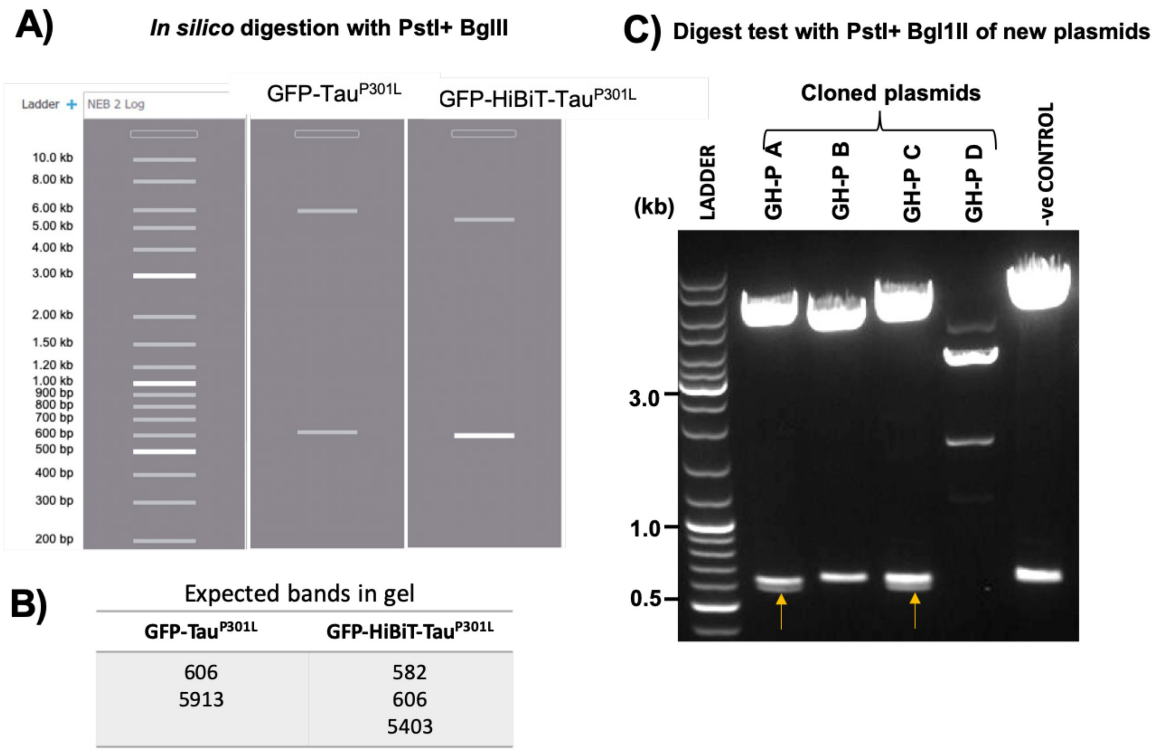

Figure 25. Diagnostic test digest to check for correct GFP-HiBiT-Tau^{P301L} cloned products. A) In silico banding pattern for GFP-TauP301L and GFP-HiBiT-Tau^{P301L} when digested with PstI and BglII. B) *In vitro* restriction digest of cloned products after first attempt at ligating PCR insert HiBiT into the linearized GFP-Tau^{P301L} vector backbone. Yellow arrows indicate the presence of two bands in plasmids labelled GH-P A and C thus showing successful production of GFP-HiBiT-Tau^{P301L} plasmids.

2.13.2 Positive and negative secretion controls

2.13.2.1 GFP-HiBiT

The GFP-HiBiT construct was generated, using the GFP-HiBiT-Tau^{E14} as a template construct (see section 2.2.10). Specific forward and reverse primers were designed to remove tau from the template construct (see primer 7 and 8 in Table 2-4 and Figure 26A-B). This was done by introducing a stop codon 'TGA' down stream of GFP-HiBiT, which stops protein translation after the HiBiT and prevents the tau protein translation. The reverse primer recognises the sense strand just downstream of the HiBiT coding region. To the forward primer was designed so that it bound to the anti-sense strand of the end of the tau coding region beginning at the stop codon attached at the end of tau (orange in Figure 26A). To confirm the removal of tau from the template plasmid, SacII (CCGC/GG) restriction site was used in a restriction digest test *in silico* and *in vitro* (Figure 26C-D); there are two SacII restriction sites in the template plasmid. *In silico* modelling suggested that the deletion of tau from the template plasmid resulted in the removal of a SacII restriction site. Therefore, generation of GFP-HiBiT was confirmed by the appearance of only one band in the gel as indicated by plasmids labelled, SDM-A, -B and -E (yellow arrows in Figure 26D).

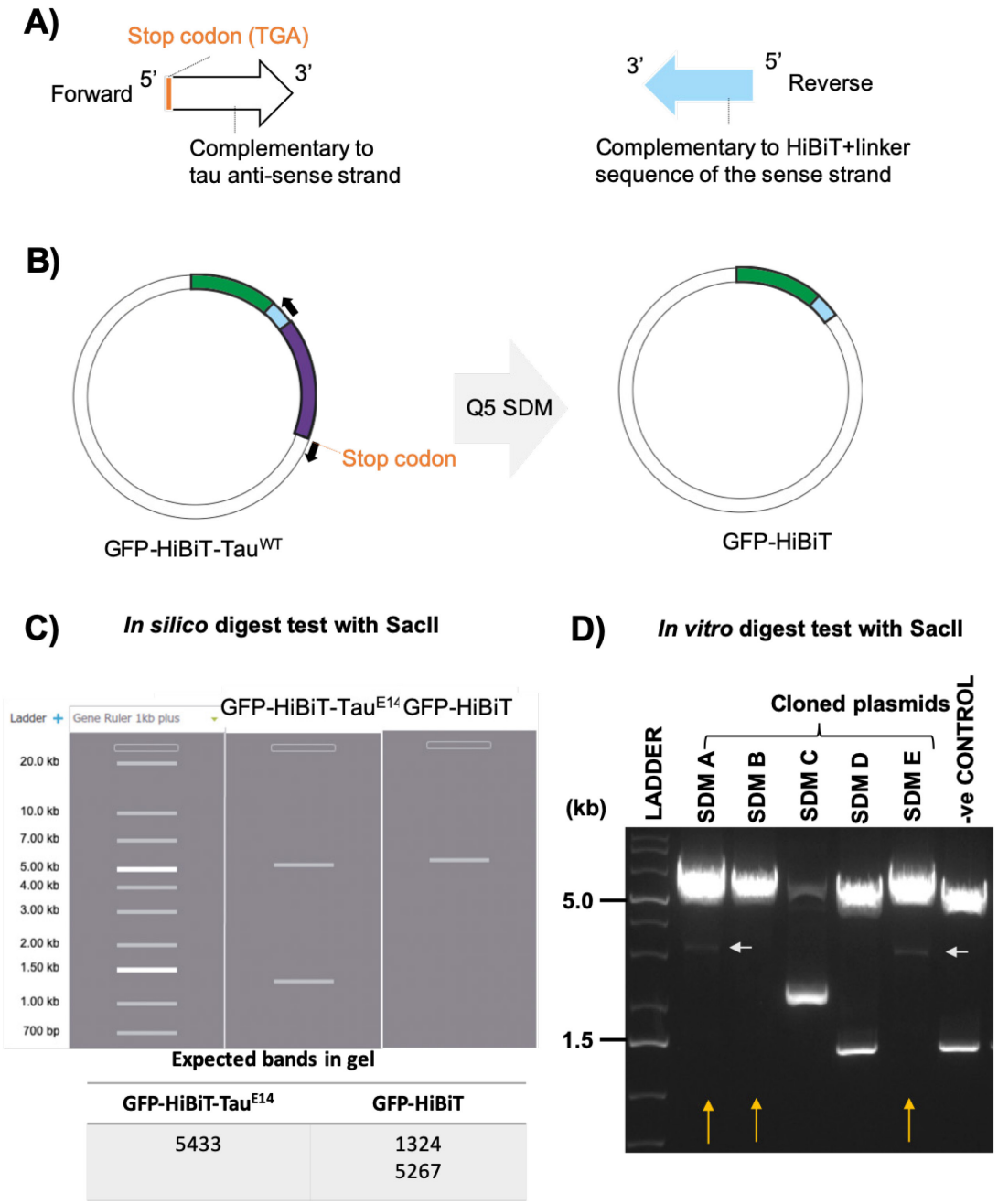

Figure 26. Cloning strategy and digest test results for the generation of GFP-HiBiT control. Schematic diagram of the forward and reverse primer used in Q5 SDM to delete tau from the template (GFP-HiBiT-TauE14). B) Cloning strategy for the generation of GFP-HiBiT control. C) In silico and D) *in vitro* restriction digest test using SacII. Cloned plasmids labelled SDM-A to -E; yellow arrows indicate correct plasmids that has Tau deleted leaving only GFP-HiBiT in the vector backbone; white arrows indicate impartial digestion.

2.13.2.2 secGFP-HiBiT

A positive secretory control (secGFP-HiBiT) was also generated by adding a secretory (IL6)-signal in the original GFP-HiBiT construct. Long forward and reverse primers were designed that encodes the IL6 signal (primer 9 and 10 in Table 2-4) to allow secretory signal sequence to be cloned in to the pRK5-GFP-HiBiT template construct. Using Q5 SDM the IL6-coding sequence was added. Correct insertion of IL6 -encoding sequence in the pRK5-GFP-HiBiT template construct was checked by amplifying just the inserts (e.g., GFP-HiBiT and secGFP-HiBiT). Correct lengths of PCR products were checked using gel electrophoresis. The PCR products for GFP-HiBiT and secGFP-HiBiT produced the correct banding pattern (Figure 27). All plasmid sequences were validated by sequencing.

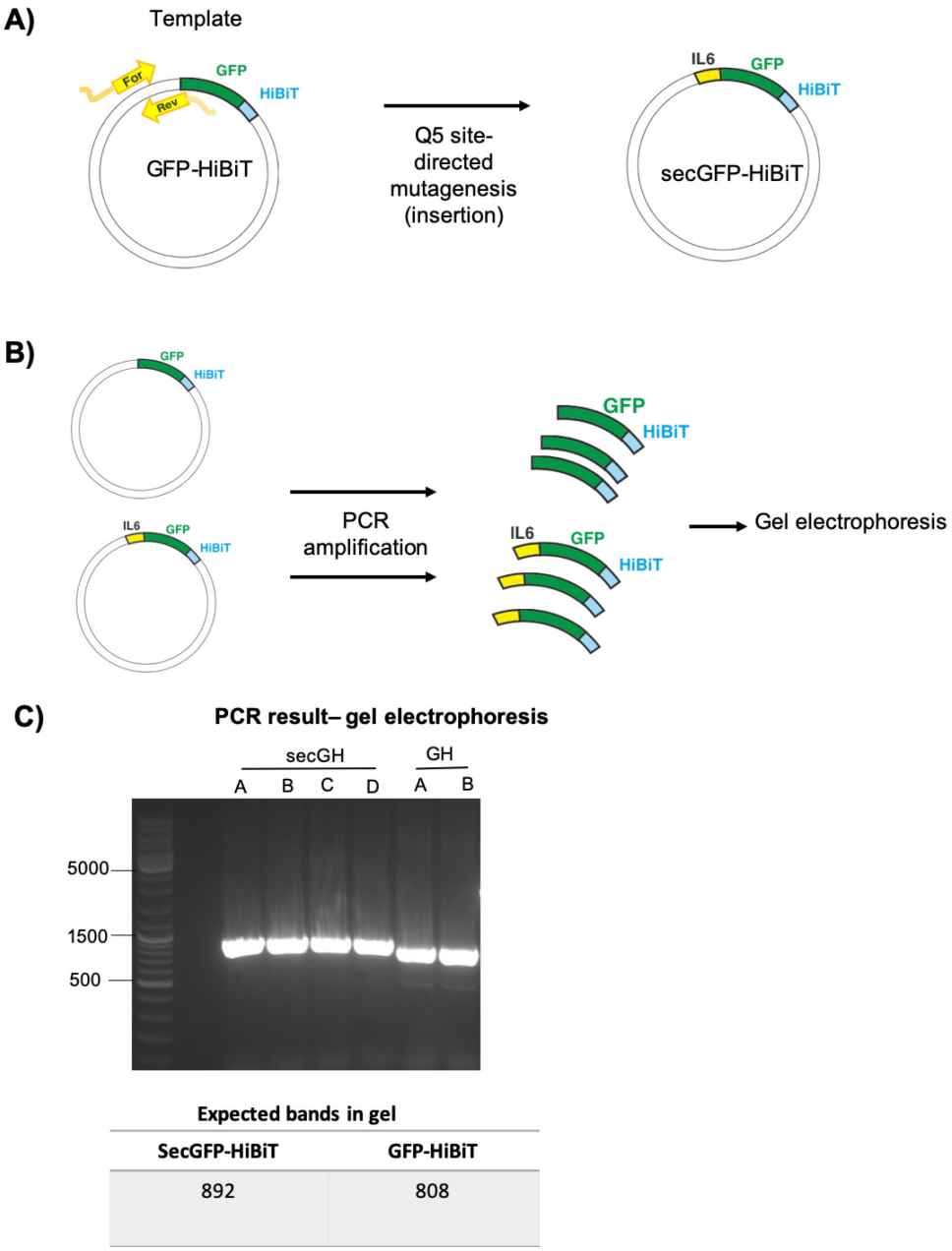

Expected bands in gel	
SecGFP-HiBiT	**GFP-HiBiT**
892	808

Figure 27. Cloning strategy for the generation of secGFP-HiBiT.

A) IL6 signal was added upstream of the original pRK5-GFP-HiBiT template using Q5 site-directed mutagenesis. B) GFP-HiBiT (GH) and secGFP-HiBiT (secGH) were isolated from the template backbone and amplified using PCR. C) Results from PCR products of secGFP-HiBiT and GFP-HiBiT.

2.14 Generation of NanoBiT-Tau reporter constructs to assay re-uptake

2.14.1 LgBiT- Tau^{WT}, LgBiT- Tau^{E14} and LgBiT- Tau^{P301L}

The cloning strategy for the generation of LgBiT-Tau^{WT} and LgBiT-Tau^{P301L} constructs are outlined in Figure 28. LgBiT-Tau^{E14} construct was previously generated by a colleague so the methodology is not outlined in this section. The constructs were confirmed by sequencing.

Firstly, LgBiT was amplified from the donor plasmid using specific forward and reverse primers which flank the coding region and has ClaI and BamHI restriction sites added at the end of the primer DNA, respectively, (primer number 7 and 8 in Table 2-4). These primers added a ClaI and BamHI restriction sites at either side of the sequence encoding the N and C- terminus of LgBiT. LgBiT inserts and GFP-Tau^{WT} and GFP-Tau^{P301L} vector backbones (Figure 28 were digested with ClaI and BamHI. This then facilitates the ligation of the linearize vector backbones and inserts, allowing the generation of LgBiT-Tau^{WT} and LgBiT-Tau^{P301L} constructs. Ligation products were transformed into bacteria and colonies harbouring plasmids with potential successful cloning were selected and subjected to a restriction digest test.

The successful generation of LgBiT-Tau^{WT} construct was identified by the presence of two bands at 509 and 5786 (bp) (successful ligations are indicated by yellow arrows in Figure 29A-B). Successful insertion of LgBiT into Tau^{P301L} vector is indicated by three bands on the gel, at 957, 606 and 4733 (bp)(successful ligations are indicated by yellow arrows in Figure 29C-D).

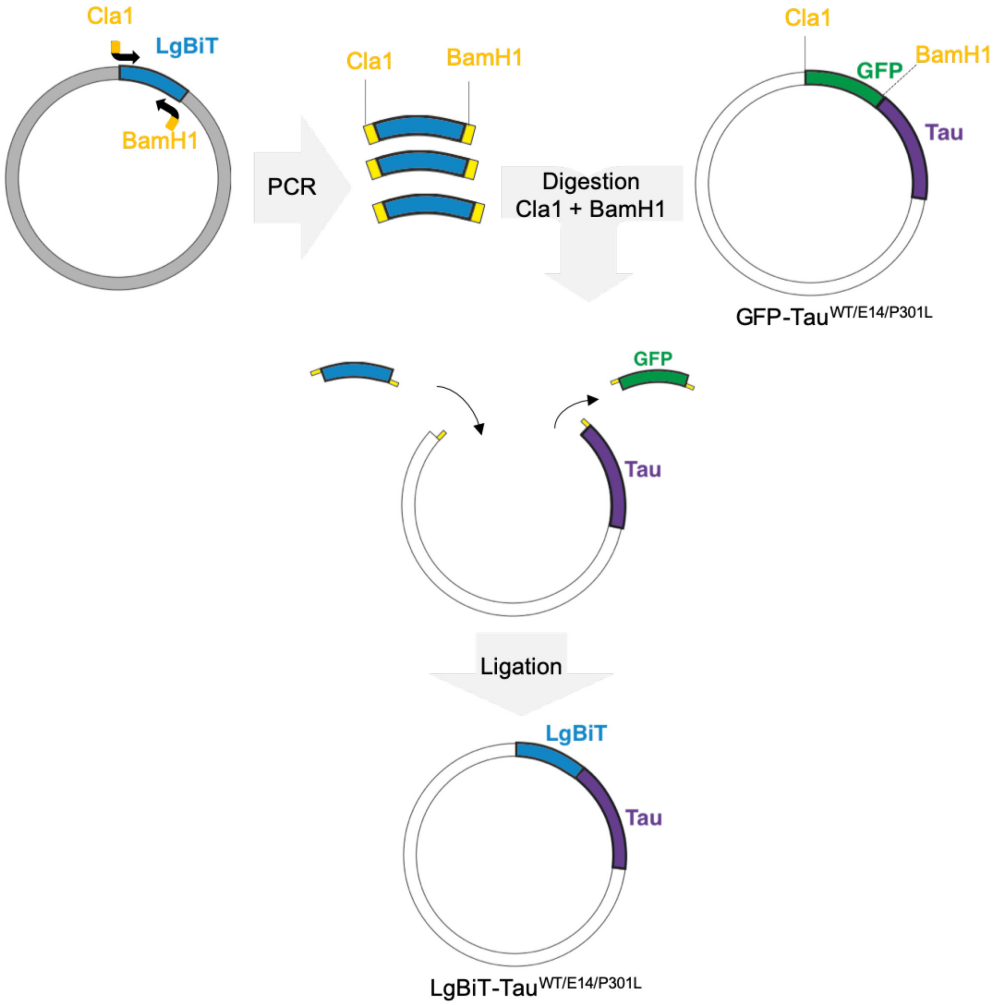

Figure 28. Cloning strategy for the generation of LgBiT-Tau^{WT}, LgBiT-Tau^{E14} and LgBiT-Tau^{P301L} LgBiT was amplified from the vector template using forward and reverse primer which has a ClaI and BamHI restriction site attached at each 5'-end, respectively. LgBiT and GFP-Tau^{WT} and GFP-Tau^{P301L} was digested with ClaI and BamHI. GFP was removed from the vector backbone and LgBiT was ligated into the linearized vector backbone to generate LgBiT- Tau^{WT} and LgBiT- Tau^{P301L}

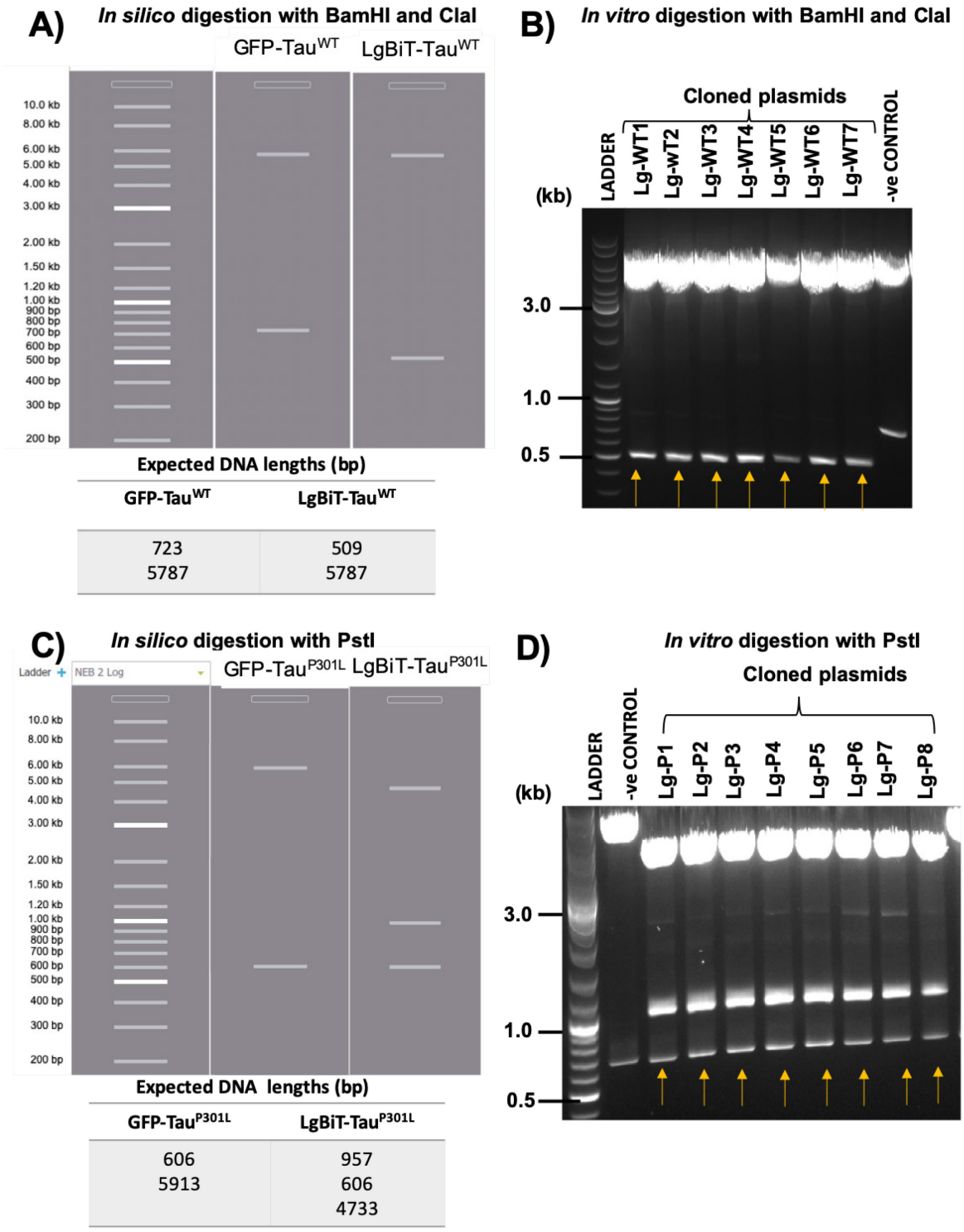

Figure 29. Diagnostic restriction digest using PstI to check for the successful insertion of LgBiT and deletion of GFP in the tau vector backbone.

A) *In silico* and B) *in vitro* digest test of cloned LgBiT-Tau ^{WT} and control (e.g., GFP- Tau^{WT}) plasmids using BamHI and ClaII. C) *In silico* and B) *in vitro* digest-test of cloned LgBiT-Tau^{P301L} and control (e.g., GFP-Tau^{P301L}) plasmids using BamHI and ClaI. Yellow arrows indicate all plasmid constructs that are LgBiT-Tau^{P301L}. Negative control constructs used were GFP-Tau^{WT} and GFP-Tau^{P301L}. Yellow arrows indicate correct cutting pattern.

2.15 Lentiviral constructs generation

NanoBiT-tau constructs were also transferred into a lentiviral vector backbone.

Forward and reverse primers were designed to amplify the cDNA encoding complete GFP-HiBiT-Tau, GFP-HiBiT and secGFP-HiBiT constructs from the pRK5 backbone. Primers were designed so that each of the constructs are flanked with ClaI and XbaI in the N and C-terminus, respectively (primer number 13 and 14 in Table 2-4 were used in the PCR) (Figure 30).

To generate lentiviral GFP-HiBiT construct primer number 17 and 18 in Table 2-4 were used in the PCR to amplify the cDNA encoding GFP-HiBiT. For the amplification of secGFP-HiBiT cDNA from pRK5 parental template primer number 15 and 16 in Table 2-4 were used. Addition of a ClaI and XbaI restriction sight at either end of the amplified product, facilitated the ligation into of GFP-HiBiT-Tau, GFP-HiBiT and secGFP-HiBiT inserts into linearized lentivirus vector. Successfully ligated products were transformed, purified and confirmed by sequencing.

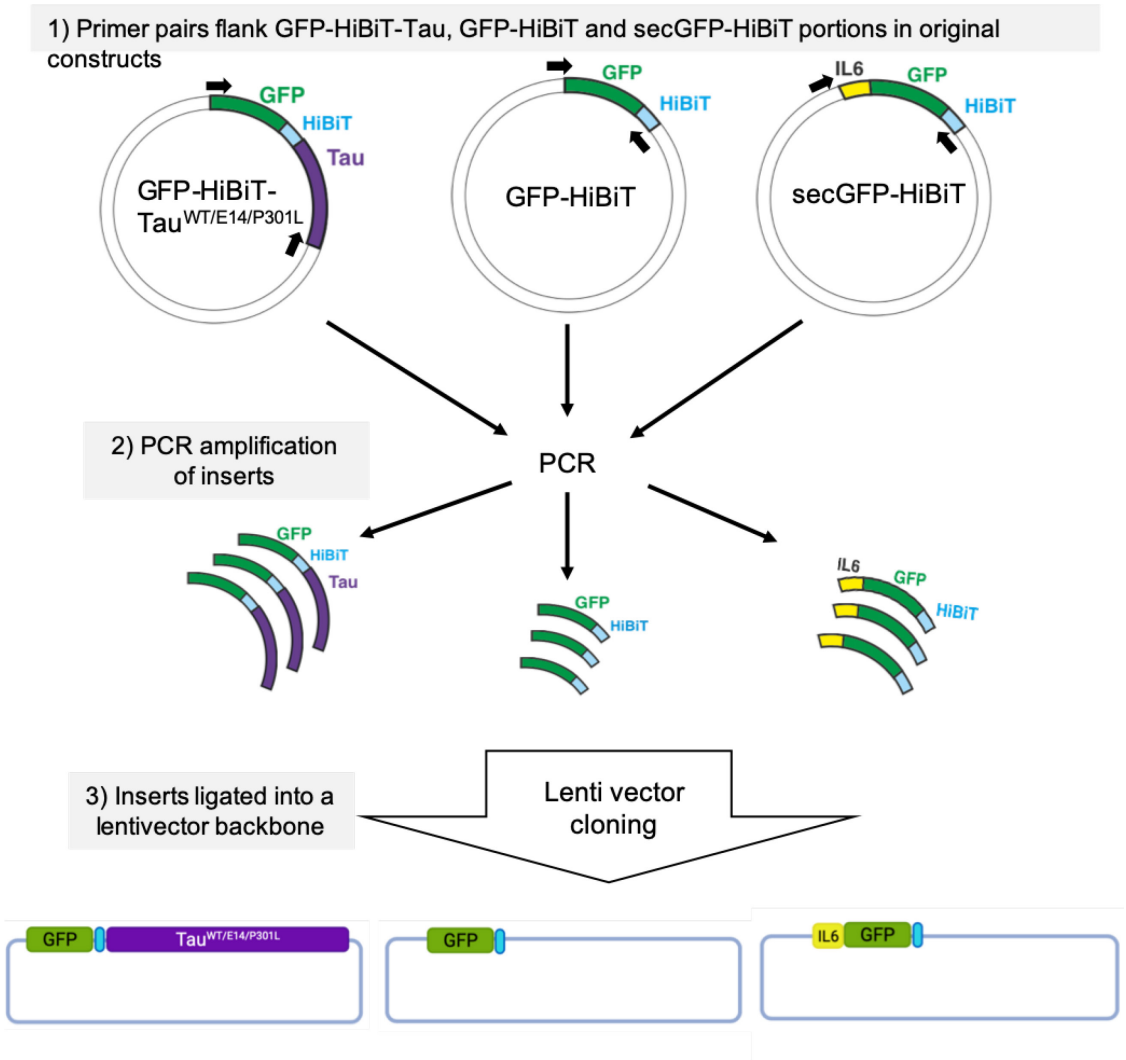

Figure 30. Schematic workflow for the generation of lentiviral constructs.

1) Forward and reverse primers were designed to isolate the GFP-HiBiT-Tau, GFP-HiBiT and secGFP-HiBiT from the pRK5 vector backbone. 2) Inserts were amplified using PCR and following restriction digestion was ligated into a lentivector backbone.

Table 2-23. List of generated NanoBiT-Tau and control constructs.

Plasmid constructs			
	Cloning to pRK5 vector	Cloning to Lentiviral vector	Sequence validation
GFP-HiBiT-Tau^{WT}	✓	✓	✓
GFP-HiBiT-Tau^{E14}	✓	✓	✓
GFP-HiBiT-Tau^{P301L}	✓	✓	✓
LgBiT-Tau^{WT}	✓	N/A	✓
LgBiT-Tau^{E14}	✓	N/A	✓
LgBiT-Tau^{P301L}	✓	N/A	✓
HaloTag-LgBiT	N/A	N/A	✓
LgBiT	N/A	N/A	✓
GFP-HiBiT	✓	✓	✓
secGFP-HiBiT	✓	✓	✓

Chapter 3 Validation of NanoBiT-Tau reporter assay to investigate tau secretion and re-uptake *in vitro*

3.1 Introduction

Multiple assays have been developed to monitor tau transmission across connected neuronal circuits (discussed in 1.9). The cell-to-cell transmission of misfolded tau can be broken down into three main parts: 1) the release of misfolded tau from a donor pre-synaptic cell, 2) the re-uptake of tau into the -post-synaptic cell and 3) the interaction and templating of misfolded tau to the natively folded tau.

In vitro assays that allow the comparison between physiological and pathological tau variants in the study of tau secretion and re-uptake has been difficult to find. Firstly, reliably distinguishing different populations of extracellular tau is made difficult by the presence of both membrane-free tau forms and those encapsulated in extracellular vesicles (vesicle-bound tau). Secondly, most existing biosensors rely on the appearance of misfolded and accumulated tau in the acceptor neurons to indicate cell-to-cell transmission (Hallinan et al., 2019). Thus, there is no means to compare and monitor the transmission of wild-type tau to misfolded forms of tau. To do this, I developed a NanoBiT-tau biosensor to gain insight in the secretion and re-uptake process of both wild-type and misfolded forms of tau.

To ensure that the addition of HiBiT does not affect protein expression and functionality of the newly generated NanoBiT-tau constructs it was first validated using a variety of biomolecular techniques. The validation processes used are outlined in this section. Using biochemical, cellular and imaging techniques, aggregation propensities, protein expression of the NanoBiT-Tau constructs, and the assay sensitivity were assessed in the primary hippocampal neurons.

3.1.1 Cellular and biochemical analysis of the split NLuc reporters

Using molecular cloning techniques, split reporters, HiBiT and LgBiT was added to existing tau constructs. However, the addition of these bioluminescent tags in proteins requires careful validation to ensure that original protein expression and functionality is not modified when they are introduced to the construct.

To test protein functionality, LgBiT-Tau and HiBiT-Tau constructs were co-expressed in HEK293 cells. Figure 31A indicates that the NLuc enzyme was reconstituted by the complementation of HiBiT and LgBiT, which are both intact, functioning and accessible in the expressed proteins, as demonstrated by their ability to generate a luminescence signal. Similarly, expression of GFP protein was unchanged in the HiBiT-Tau constructs as fluorescence signals were identified by imaging. These findings were further confirmed biochemically by western blot which shows the expression of tau and GFP (Figure 31B-C). HiBiT blotting was also carried out (as described in section 2.6.5). This involved the incubation of the nitrocellulose membrane containing HiBiT-tau expressing proteins with LgBiT and substrate. LgBiT and HiBiT complementation results NLuc reconstitution, which subsequently generates strong luminescence signal that can be detected by chemiluminescence imaging indicated that the structural complementation of split NLuc; the presence of protein lysates expressing HiBiT-tagged tau can therefore be visualised in the blot (Figure 31B).

Interestingly, when blotted for total tau, all proteins expressing Tau^{E14} indicated higher molecular weight bands than those expressing Tau^{WT} and Tau^{P301L} (Figure 31B). Varying band thickness and sizes could be due to the different stages of post-translational modifications in which different tau variants undergo. Finally, chemiluminescent imaging was used to check for the expression of HiBiT in the cell lysates (as previously described 2.6.5). HiBiT-containing proteins are demonstrated by the appearance of bright luminescence signals (third panel in Figure 31B).

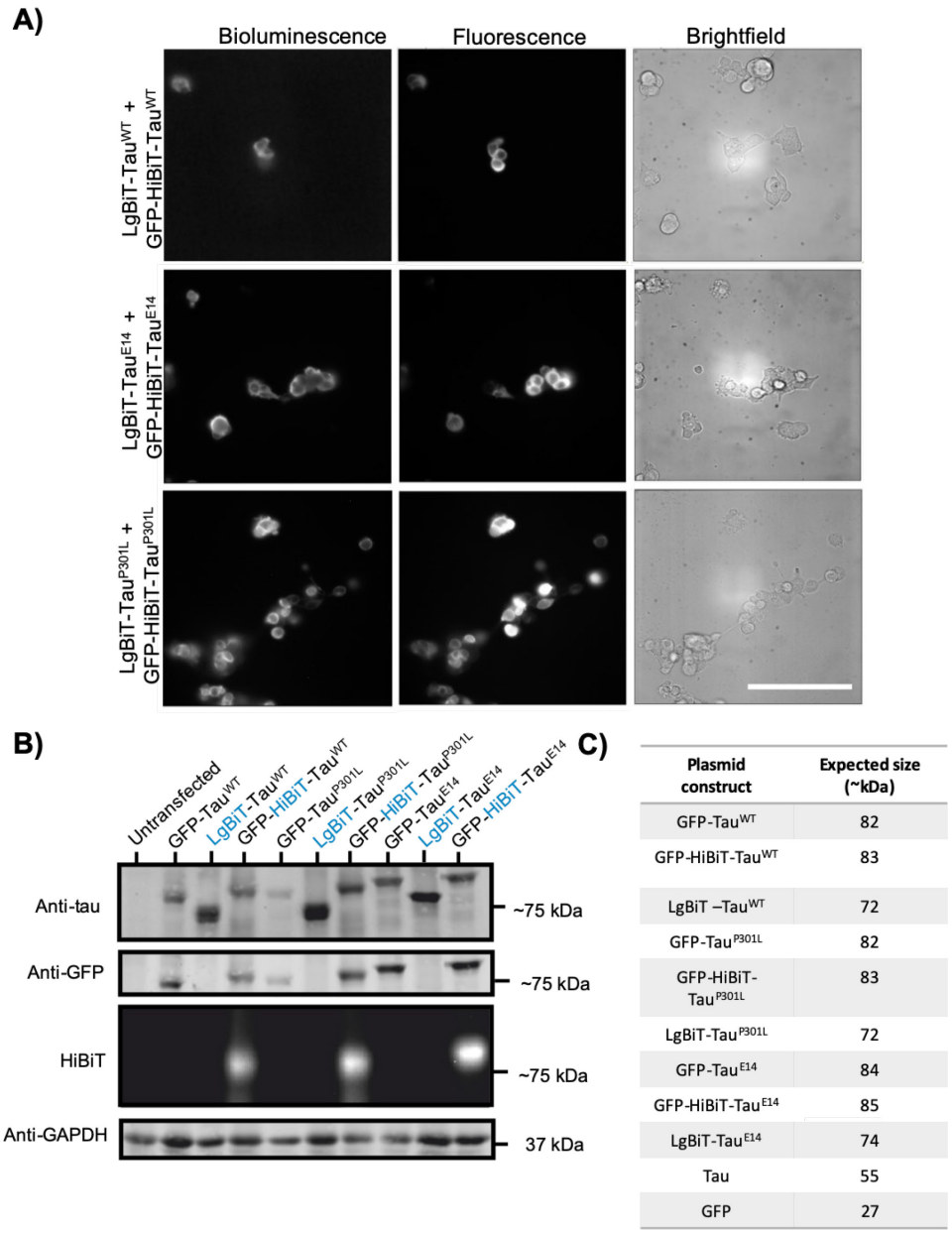

Plasmid construct	Expected size (~kDa)
GFP-Tau^{WT}	82
GFP-HiBiT-Tau^{WT}	83
LgBiT –Tau^{WT}	72
GFP-Tau^{P301L}	82
GFP-HiBiT-Tau^{P301L}	83
LgBiT-Tau^{P301L}	72
GFP-Tau^{E14}	84
GFP-HiBiT-Tau^{E14}	85
LgBiT-Tau^{E14}	74
Tau	55
GFP	27

Figure 31. Expression of NanoBiT-tau constructs in HEK293 cells showed intact fluorescence and bioluminescence function.

A) Fluorescence and bioluminescence signal of HiBiT-tau and LgBiT-tau constructs upon co-transfection in HEK293 cells using the NanoGlo Live Cell assay; scale bar, 100 µm. Bioluminescence signal detection indicate that the HiBiT and LgBiT was able to reconstitute the NLuc enzyme. B) Western blot of the cell lysates extracted from HEK293 cells expressing GFP-HiBiT-Tau and LgBiT-Tau with the different tau variants; blotted for total tau and GFP expression; GAPDH was used as loading control. Presence of HiBiT in protein isolates were assessed using chemiluminescence. LgBiT was added to the nitrocellulose membrane and all HiBiT containing proteins were detected. C) Expected band sizes (kDa) by each construct.

3.1.2 The accumulation of GFP-Tau and NanoBiT-Tau in axons of hippocampal neurons

My group previously established a fluorescent *in vitro* assay to assess the transfer of misfolded and accumulation of tau in distal axons of hippocampal neurons in connected networks (Hallinan *et al.*, 2019). It was found that pathological forms of tau (e.g. GFP-Tau^{E14}) tend to form misfolded tau (as indicated by positive MC1 staining) and accumulate in larger protein inclusions in distal axons, as well as propagate efficiently in connected neuronal networks of primary hippocampal neurons. These large tau protein assemblies, termed 'inclusions' from now on, were visualised by analysing the axonal fluorescence distribution and MC1 staining (Hallinan *et al.*, 2019). Neurons expressing GFP-Tau^{P301L} have also been shown to form misfolded tau proteins upon expression (Pitera *et al.,* 2019). Neurons expressing GFP-Tau^{E14} and GFP-Tau^{P301L} have been shown to form uneven fluorescence distribution along distal parts axons of primary hippocampal neurons that was positive for MC1 staining, whereas Tau^{WT}-expressing neurons formed smooth axonal fluorescence distribution that was MC1-negative (Hallinan *et al.*, 2019).

To demonstrate the formation of inclusions of the different tau variants in hippocampal neurons, fluorescence intensities along the distal axon were compared in neurons expressing the original GFP-Tau constructs and the new GFP-HiBiT-Tau reporters. For this, the constructs were transfected into hippocampal neurons at DIV1 and were cultured to DIV14 (as previously described in 2.11.1). This method led to low transfection efficiency which allowed individual axons to be analysed for fluorescence re-distribution. The distal part of the axons was assessed for tau inclusions; this was classified as the axonal stretch that is >350 µm from the cell body (Figure 32). To assess for the presence of tau inclusions in axons, segmented fluorescence distribution analysis was undertaken for each stretch of axon (this is described in full detail in section 2.11.1).

The axons of neurons expressing GFP-HiBiT-Tau^{WT} and GFP- Tau^{WT} had smooth fluorescence distribution (Figure 32B; Figure 33). GFP-HiBiT-Tau^{WT} and GFP- Tau^{WT} showed no significant difference in the percentage of cells positive for tau inclusions when compared with each other (Figure 33B). In contrast, GFP-HiBiT-Tau^{E14} and GFP- Tau^{E14} expressing neurons showed significant levels of tau inclusions in axons as demonstrated by the punctate fluorescence distribution (Figure 32C,E; Figure 33). Both GFP-HiBiT-Tau^{E14} and GFP- Tau^{E14} expressing axons were positive for tau inclusions in the distal parts (Figure 32C,E; Figure 33). GFP-Tau^{E14} showed strong punctate fluorescence distribution profile in the distal axons when compared to other cells expressing Tau^{WT} and Tau^{P301L} (accumulations of tau are demonstrated by pink arrows in Figure 32C). Interestingly, GFP-HiBiT-Tau^{P301L} and GFP- Tau^{P301L} did not demonstrate the same propensity to accumulate in large assemblies as that of cells disease-associated mutants such as Tau^{E14} (Figure 32D,E; Figure 33).

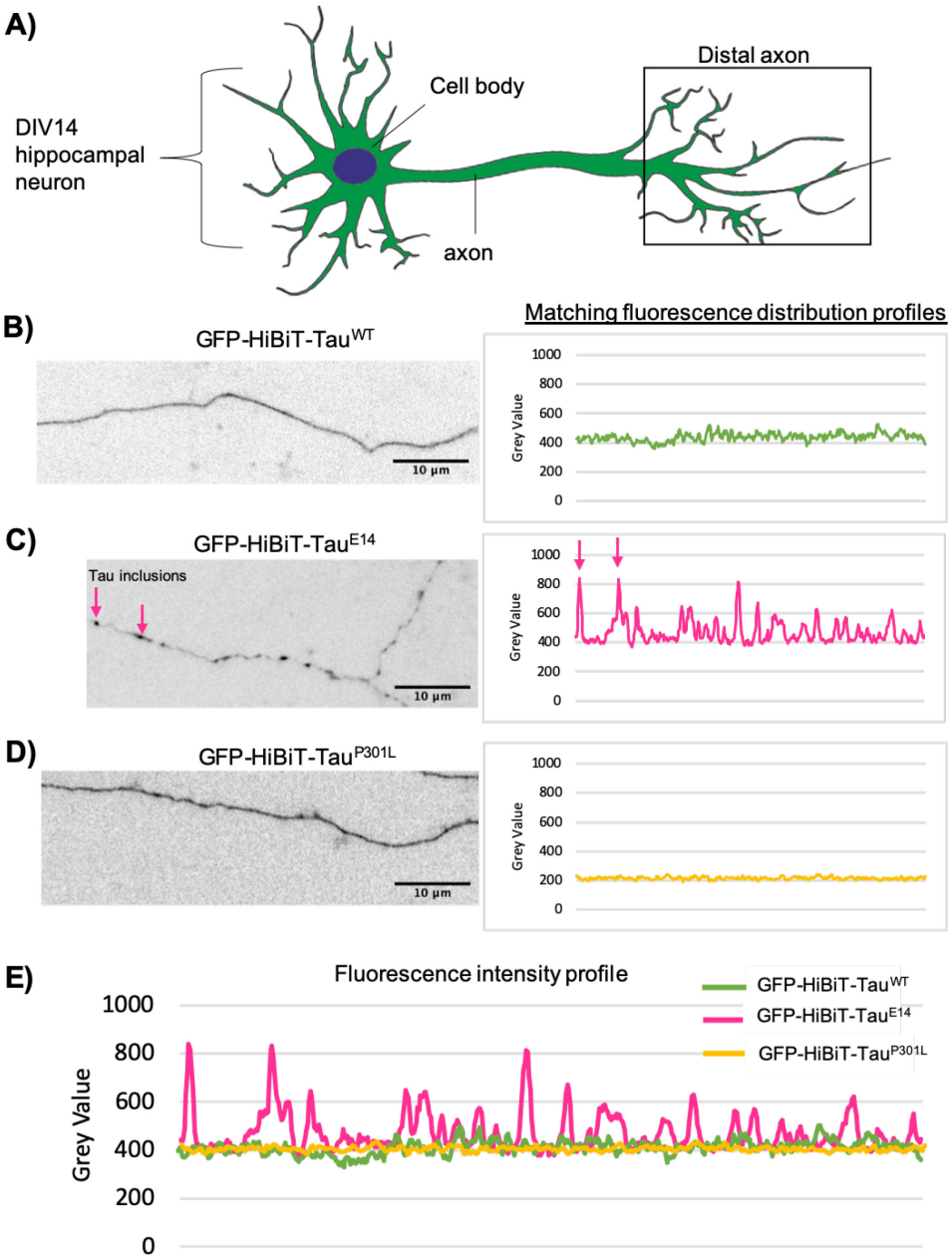

Figure 32. Expression GFP-Tau^{E14}, GFP-Tau^{WT} and GFP-Tau^{P301L} leads to different fluorescence intensity distribution profiles in the distal axon of primary hippocampal neurons.

A) Schematic diagram the 'distal' part of the axon that was used to assess tau accumulation in DIV14 cultured hippocampal neurons. B-C) Representative images of distal axonal fluorescence distribution and matching fluorescence intensity profiles of GFP-HiBiT-Tau^{WT}, GFP- HiBiT-Tau^{E14} and GFP- HiBiT-Tau^{P301L} expressing neurons. GFP-HiBiT-Tau^{E14} demonstrates the presence of large accumulated tau proteins in axons as demonstrated by uneven fluorescence distribution profiles. D) Graph showing side-by-side comparisons in fluorescence intensity between the different tau. N=4.

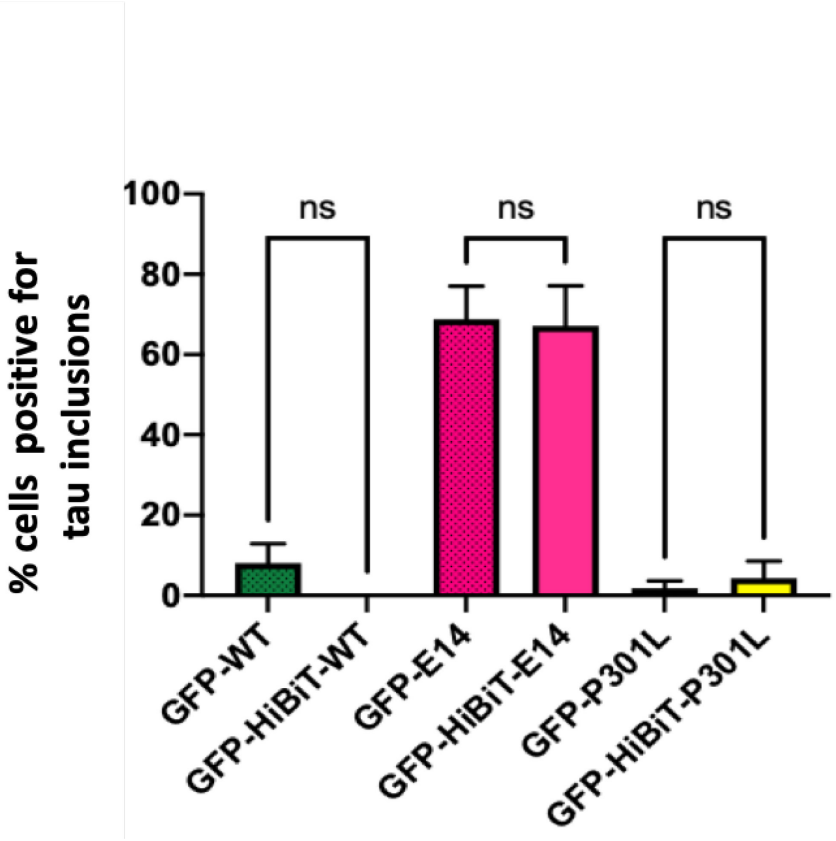

Figure 33. The addition of HiBiT in the NanoBiT-Tau reporters does not alter the ability of different tau variants to form inclusions.

Neurons were transfected with original GFP-Tau and newly generated NanoBiT-Tau constructs at DIV1 and fixed at DIV14. Each transfected cell from the distal axons were analysed for fluorescence distribution. Cells positive for large tau inclusions were assessed and compared within each variant. There was no significant difference between: GFP-Tau^{WT} and GFP-HiBiT-Tau^{WT} (p=0.9746), GFP-Tau^{E14} and GFP-HiBiT-Tau^{E14} (p=0.9449) and GFP-Tau^{P301L} and GFP-HiBiT-Tau^{P301L} (0.9746; two-way ANOVA, followed by Sidak's test; N= 4).

3.2 Validation for the use of NanoBiT-tau reporter assay in the plate-reader and bioluminescent microscope format

The addition of the split NanoBiT reporters to the *in vitro* assay, allow the steps of tau transfer to be monitored. The newer version of the HiBiT and LgBiT complementation assay has never been used to study tau secretion *in vitro* before, it is therefore essential that the assay sensitivity is established in our current system. The LgBiT can be added directly to the extracellular medium and/or expressed in the cytosol of the acceptor cell. This allows tau release and re-uptake to be dissected in connected neuronal networks. To accomplish this, a sensitive bioluminescent assay able to detect low or small changes in signal levels was required. This sensitivity requirement is likely important as only a small fraction of tau protein will be released into the extracellular medium, meaning that less tau will likely be taken-up to the post-synaptic neuron (Figure 19). An important determinant of this sensitivity is the noise from background luminescence. This noise may derive from 1) background signal generated from the uncomplemented LgBiT protein in the absence of HiBiT, 2) autoluminescence from the furimazine substrate, and 3) machine and detector noise.

3.2.1 Establishing NanoBiT-tau assay sensitivity in a plate-reader format

To investigate and optimise the dynamic range of the NanoBiT-tau assay, the assay sensitivity was established using two methods of measuring luminescence signal: the plate-reader and the bioluminescence microscope. A sensitive assay is defined by its ability to detect low signals above background levels. To test the sensitivity of the plate-reader assay, the expression of LgBiT was controlled in HEK293 cells. This was done by using two commercially available LgBiT-expressing vectors that have higher expression than others; one is driven by a weaker herpes simplex virus thymidine kinase (HSV/TK) promoter, named as HSV/TK-LgBiT from now on, and the other is driven by a stronger mammalian expression vector, known as the human cytomegalovirus (CMV) promoter, which will be called CMV-HaloTag-LgBiT from now on (Damdindorj et al., 2014).

Firstly, I established the lowest luminescence signal the plate-reader assay can detect. To do this, HSV/TK-LgBiT and CMV-HaloTag-LgBiT constructs were expressed in HEK293 cells. These were co-expressed with a GFP-HiBiT-Tau^{E14} construct which was titrated by reducing the amount of DNA transfected in cells (schematic diagram to describe the process is in Figure 34B). This method controls the amount of complemented NLuc generated and allows the level of bioluminescent signals to be manipulated in the assay. The x-axis in Figure 34C,D represents that DNA ratio of the co-transfected LgBiT and GFP-HiBiT-Tau^{E14} component. As a background control the expression of LgBiT only (depicted as 1:0 ratio in Figure 34C,D) was used. The luminescence signal generated by

the uncomplemented LgBiT enzyme was used a marker for assay detectability; any positive hits were considered as the luminescence signals that are above the background noise.

The signal to background noise ratio was first tested in CMV-HaloTag-LgBiT constructs. However, expression of this construct in HEK293cells generated a really high background noise. To test whether the assay can detect lower luminescence background signals in the assay, I lowered the amount of uncomplemented LgBiT in the assay by using HSV/TK-LgBiT construct to drive lower protein expression in HEK293 cells. The maximal signal sensitivity and background noise generated was compared in assays using CMV-HaloTag-LgBiT and HSV/TK-LgBiT constructs.

HSV/TK-LgBiT expression has a maximal signal sensitivity that is similar to CMV-HaloTag-LgBiT. When cells are saturated with high GFP-HiBiT-Tau^{E14} expression, the system is pushed to the maximum limit of signal detection. The plate-reader assay reaches maximum signal detection at around a magnitude of 10^7 relative light units (RLU) when cells co-expressed HSV/TK-LgBiT and GFP-HiBiT-Tau^{E14}. Expression of CMV-HaloTag-LgBiT with GFP-HiBiT-Tau^{E14} also generated similar magnitude of maximal luminescence detected in the plate reader assay. However, at lower dilution factors of GFP-HiBiT-Tau^{E14}expression, the differences in assay background can be identified between HSV/TK-LgBiT and CMV-HaloTag-LgBiT. The lowest luminescence signal that can be detected above background upon the expression of CMV-HaloTag-LgBiT is indicated by the green arrow in Figure 34C; the luminescence generated upon expression of this construct resulted in higher background signal is 91169 (RLU), is proportional to the first detectable signal which is found with the dilution factor 1/4096. Due to this higher background signal, the threshold of detection limit for CMV-HaloTag-LgBiT requires a lot higher expression of CMV-HiBiT-Tau^{E14} to be detectable above background. In comparison, expression of HSV/TK-LgBiT resulted in significantly higher sensitivity at a dilution factor of 1/15625 ($p=0.0098$); a mean signal of 35550 +/- 17657 (RLU) can be significantly detected above the assay background of 4978 +/- 910.2 (RLU) as indicated by red arrow in Figure 34D. CMV-HaloTag-LgBiT has a detection limit threshold (given as a dilution factor) of 1 in 4096 (red arrow in Figure 34C), whereas HSV/TK-LgBiT has a detection limit of 1 in 15,625 (green arrow in Figure 34C).

In context of the main questions of the project, the assay becomes 4-fold more sensitive with the use of HSV/TK-LgBiT than CMV-HaloTag-LgBiT, as its capable of detecting 1 unit of HiBiT-tagged tau for every 15,625 expressed by the cell; this means that only 1 in 15,625 tau needs to be released into the extracellular space to be detected above background signal. A LgBiT that results in a better assay signal detection with low background noise, is preferable as it means that low or small changes in signals could be detected. For our results, the HSV/TK-LgBiT has a better signal to

noise ratio than CMV-HaloTag-LgBiT in the plate-reader, therefore the plate-reader system will stand more of a chance of detecting these small changes of tau release above background noise.

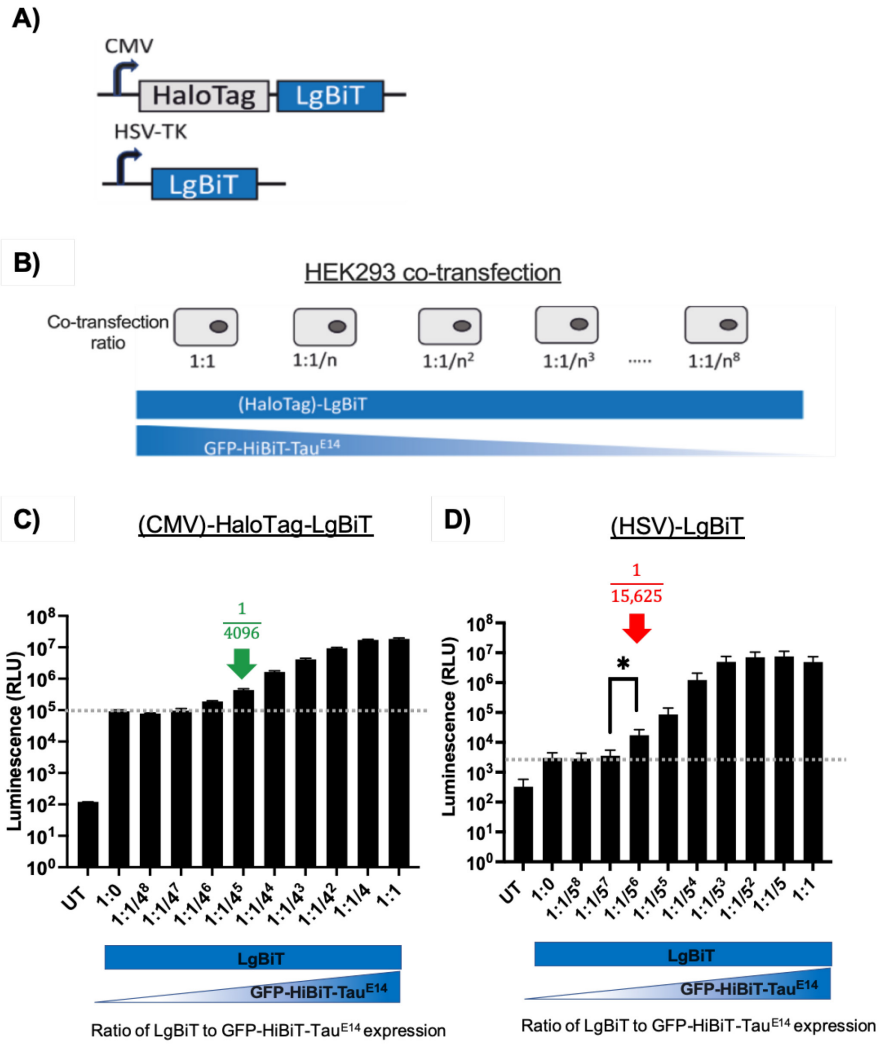

Figure 34. Establishing assay sensitivity by titrating complementation of GFP-HiBiT-Tau^{E14} and HaloTag-LgBiT/LgBiT.

A) Schematic diagram of the CMV-HaloTag-LgBiT construct and the HSV/TK-LgBiT construct. B) HEK293 cells were co-transfected with GFP-HiBiT-Tau^{E14}, which was serially diluted, and CMV-HaloTag-LgBiT or HSV/TK-LgBiT. C) Bioluminescent signals generated (given as arbitrary relative luminescence (RLU) units, presented as a log scale) from the structural complementation of HaloTag-LgBiT:GFP-HiBiT-Tau^{E14} showed that signal can be detected above background noise (grey dotted line); green arrow represents the minimal signal detected above background; no statistical analysis; T=3, N=1. C) Expression of HSV-LgBiT:GFP-HiBiT-Tau^{E14} in HEK293 cells lead to greater signal:noise ratio; minimal signal detected above background is indicated by the red arrow; one-way ANOVA, Dunnet's comparison test, p=0.0098, N=3.

3.2.2 Testing the sensitivity of luminescence microscope for the detection of NanoBiT-tau reporter assay

Besides customising the NanoBiT-tau reporter assay in a plate-reader format to monitor secretion, the use of a bioluminescence microscope was also explored in the project, to allow the visualisation of both the tau secretion and re-uptake process. To do this, hippocampal neurons cultured in microfluidic devices can be used monitor the release and the re-uptake of WT and mutant forms of tau (further discussed in section 7.3.2 and 7.3.1). Using the bioluminescence microscope, the differences in signal-to-noise ratio between the two LgBiT-containing constructs were investigated. Firstly, the maximal signal intensities were compared between the two different LgBiT vectors. When CMV-HaloTag-LgBiT and HSV/TK-LgBiT expression vectors were independently co-expressed with GFP-HiBiT-Tau^{E14} in HEK293 cells, both fluorescence and bioluminescence signals were detected, indicating the reconstitution of NLuc enzyme and functioning GFP. However, the overall luminescence signal intensity of the reconstituted NLuc enzyme containing CMV-HaloTag-LgBiT expression vector is higher when compared to the NLuc enzyme containing HSV/TK-LgBiT expression vector (Figure 35C,D).

As uncomplemented LgBiT and/or HiBiT can generate a certain level of auto-luminescence generating a background noise, it was also important to check what level this is in all assay format to ensure that signals can be detected above background signal noise. To check this in the bioluminescence microscope format, CMV-HaloTag-LgBiT and HSV/TK-LgBiT expression vectors were co-expressed with GFP, which resulted in the production of the uncomplemented LgBiT protein in cells (see lower panels in Figure 35). No background bioluminescence signal could be identified with the expression of uncomplemented LgBiT, when expressed in HEK293 cells from the CMV-HaloTag-LgBiT and HSV/TK-LgBiT expression vectors. In contrasts, the plate-reader detected almost two-orders of magnitude difference in luminescent signal, with around 10^5 RLU for CMV-HaloTag-LgBiT and ~10^3 RLU for HSV/TK-LgBiT, demonstrating a clear difference in background signal. Although the luminescence microscope was capable of detecting difference in maximal signal intensities between the expression of CMV-HaloTag-LgBiT and HSV/TK-LgBiT, the plate-reader assay was capable of detecting good maximum intensities but generate low background noise.

In summary, as the aim of the project is to detect low level of secreted HiBiT-tagged tau in the extracellular media, it was essential to use an assay that has a good dynamic range of bioluminescence detection capabilities. Using these two LgBiT constructs that were driven by different promoters, the expression levels LgBiT in cells were manipulated. This allowed the sensitivity and the signal-to-noise to be investigated in different assay formats. These findings

showed that the plate-reader has a superior dynamic range of luminescence detection compared to the luminescence microscope. Therefore, the plate-reader assay was used to for further investigation in tau secretion.

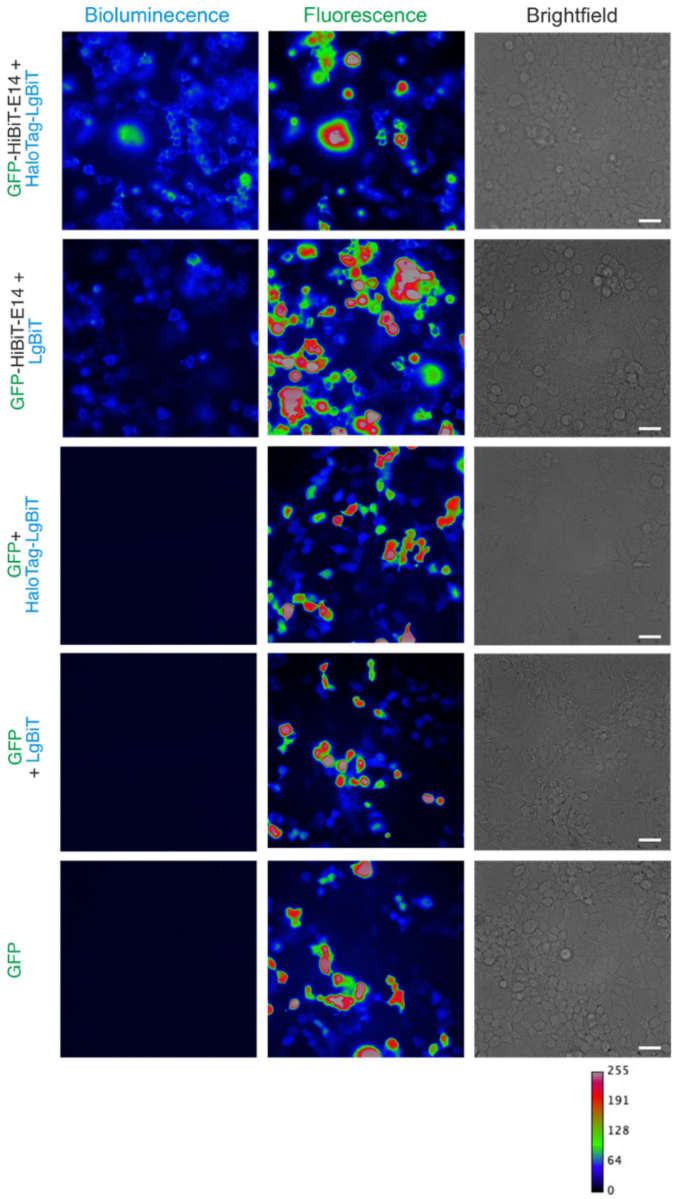

Figure 35. Testing the sensitivity of the bioluminescence microscope.

Cells were transfected 2 hours after seeding and were imaged after 48 hours. The Nano-Glo live cell assay were carried out which involves the addition of the substrate to the cells. Luminescence signals were captured using a bioluminescent microscope after co-expression of constructs CMV-HaloTag-LgBiT or HSV/TK-LgBiT with GFP-HiBiT-TauE14 and GFP. Similar background signal was generated when un-complemented CMV-HaloTag-LgBiT and HSV/TK-LgBiT were co-expressed with GFP. For each sample/cell culture, 20 images were taken with 1 ms pauses in between; luminescence signal was collected for 5 seconds per image. All signals from the stack of 20 images were summed to generate one photo panel. Scale bar = 20 µm. N=1.

3.3 Establishing NanoBiT-tau reporter assay for the detection of tau release in cultured hippocampal neurons

3.3.1 GFP-HiBiT-tau expression is improved with lentiviral transduction

To improve the chance of detecting low level tau secretion in the assay, lentiviruses on the GFP-HiBiT-Tau constructs were used to transduce primary neurons instead of transfection. A caveat to transfecting neurons is that overexpression of the tau proteins could have implications on cellular and molecular machineries that may affect physiological tau secretion. Furthermore, transfection also does not yield a high proportion of GFP-HiBiT-tau-expressing neurons; from 150,000 cells plated, only 7-15 cells are transfected, which gives <1% transfection rate. To overcome these limitations in the NanoBiT-Tau reporter assay, lentiviral-derived vectors expressing HiBiT-Tau (e.g., GFP-HiBiT-Tau^{WT}, GFP-HiBiT-Tau^{E14} and GFP-HiBiT-Tau^{P301L}) were used.

Firstly, the tau expression levels of cultured primary hippocampal neurons were assessed after transduction with lentivirus-derived GFP-HiBiT-Tau^{WT}. At DIV14, cells were fixed and stained for total tau (red, Figure 36A) using an antibody that recognises C-terminal part of tau, at amino acid 243-441, and Hoechst nuclear stain (blue, Figure 36A). As all GFP-HiBiT-Tau constructs contain a GFP coding sequence in the N-terminus, protein translation results in the production of a green fluorescent protein; visualisation of this fluorescent signal indicated successful expression GFP-HiBiT-tau in cells. The fluorescence intensities were compared between untransduced (yellow arrow, Figure 36A) and transduced cells (white arrow, Figure 36A) in the different channels. The total tau stain between untransduced and transduced cell indicates similar fluorescence intensities (Figure 36A, top left panel). This show that transduced tau is expressed within physiological levels in primary hippocampal neurons.

Next, the differential protein expression was analysed between tau variants, and no significant difference was found between GFP-HiBiT-Tau^{WT} and GFP-HiBiT-Tau^{E14} when relative expression of total-tau over endogenous-tau was compared (Figure 36B-C). Densitometry analysis was not carried out on GFP-HiBiT-Tau^{P301L} as total-tau blot indicated no band where it would be expected (Figure 36B-C). HiBiT-blotting revealed a band at ~60 kDa in the cell lysates taken from primary cultures expressing GFP-HiBiT-Tau^{P301L} (white arrow in Figure 36B) which is not the expected molecular weight. Interestingly, GFP-HiBiT-Tau^{P301L} expression in HEK293 cells revealed the expected molecular weight of ~83kDa (Figure 31A). Microscopy images of neurons expressing the GFP-HiBiT-Tau^{P301L} indicated that cultured neurons are capable of expressing mutant tau variant *in vitro* but at very low levels (Figure 37). The localisation of GFP-HiBiT-Tau^{P301L} expression was directly compared to GFP-HiBiT-Tau^{WT} in the nucleus and cytosol. While GFP-HiBiT-Tau^{WT}-

expression indicated a localisation that is more directed to the cytoskeletal compartment, HiBiT-Tau^{P301L} expression appeared to be more diffused to both the nucleus and cytoplasm. As further investigations were required to establish what caused this protein modification in neurons expressing GFP-HiBiT-Tau^{P301L}, it was decided not to use these tau variants in side-by-side comparisons with others in future assays.

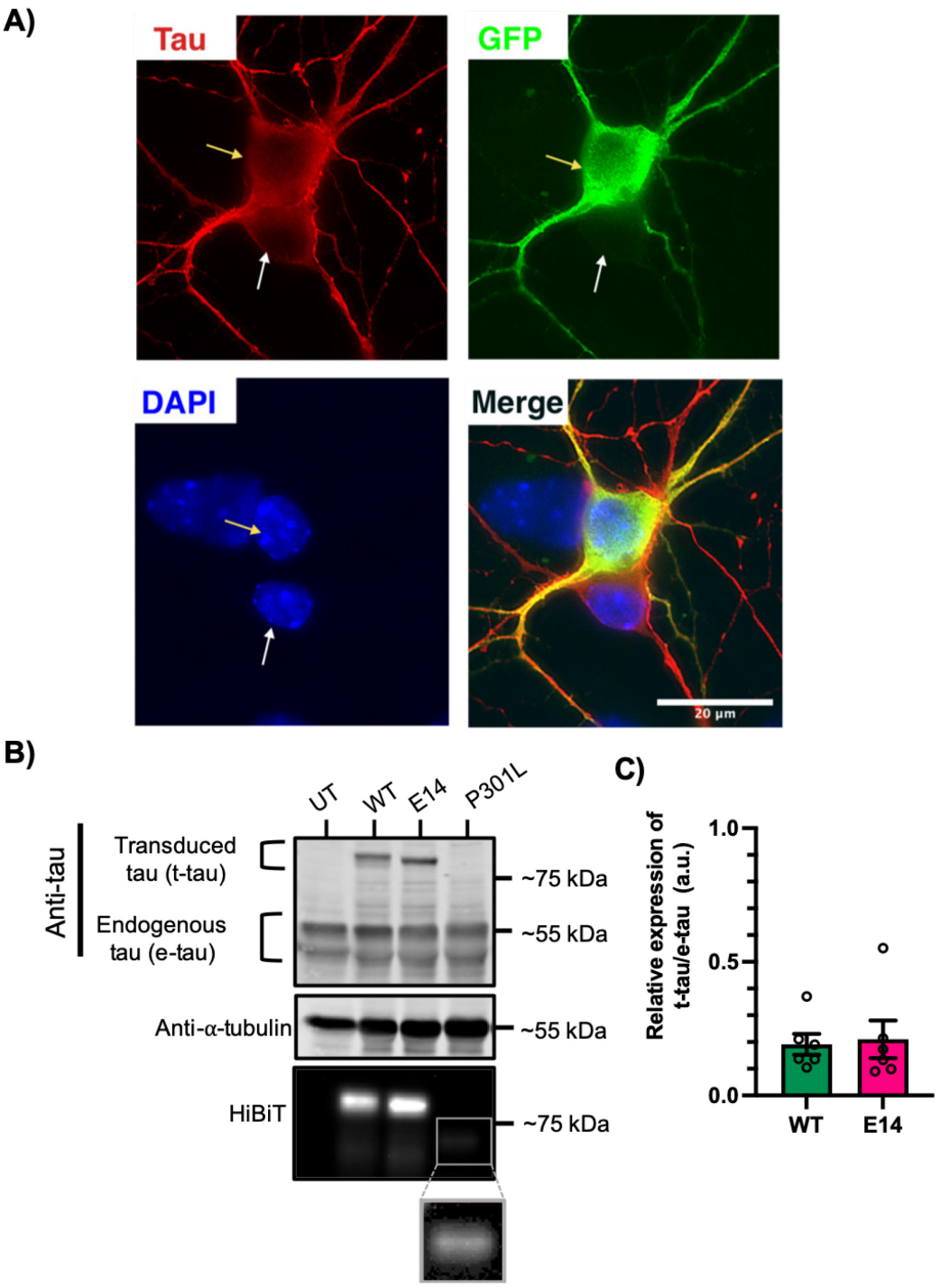

Figure 36. Differential protein expression of HiBiT-tau constructs in primary hippocampal neurons.

A) Representative images of DIV14 hippocampal neurons transduced with lentiviruses that expresses GFP-HiBiT-Tau^{WT}. Cultures were fixed at DIV14 and stained with anti-tau antibody (red) and DAPI (blue). GFP signal indicates transduced neuron expressing GFP-HiBiT-Tau^{WT}. The red channel indicates the presence of total tau in all neuron. Arrows indicate the difference between a transduced (yellow arrows) and an untransduced (white arrows) neuron. B) Western-blot showing presence of transduced tau (t-tau) and endogenous tau (e-tau) in lysates of cultured

neurons. The membrane was blotted with anti-tau (DAKO) and α-tubulin. The presence for HiBiT in the protein lysates were detected through chemiluminescence imaging (lower panel); the image was taken after 3-minute exposure. C) Densitometry of immunoblot showing relative expression of transduced-tau over endogenous-tau between GFP-HiBiT-Tau^{WT} and GFP-HiBiT-Tau^{E14}. There was no significant difference in relative expression between GFP-HiBiT-Tau^{WT} and GFP-HiBiT-Tau^{E14} (p=0.3099; two-tailed paired t-test, N=6).

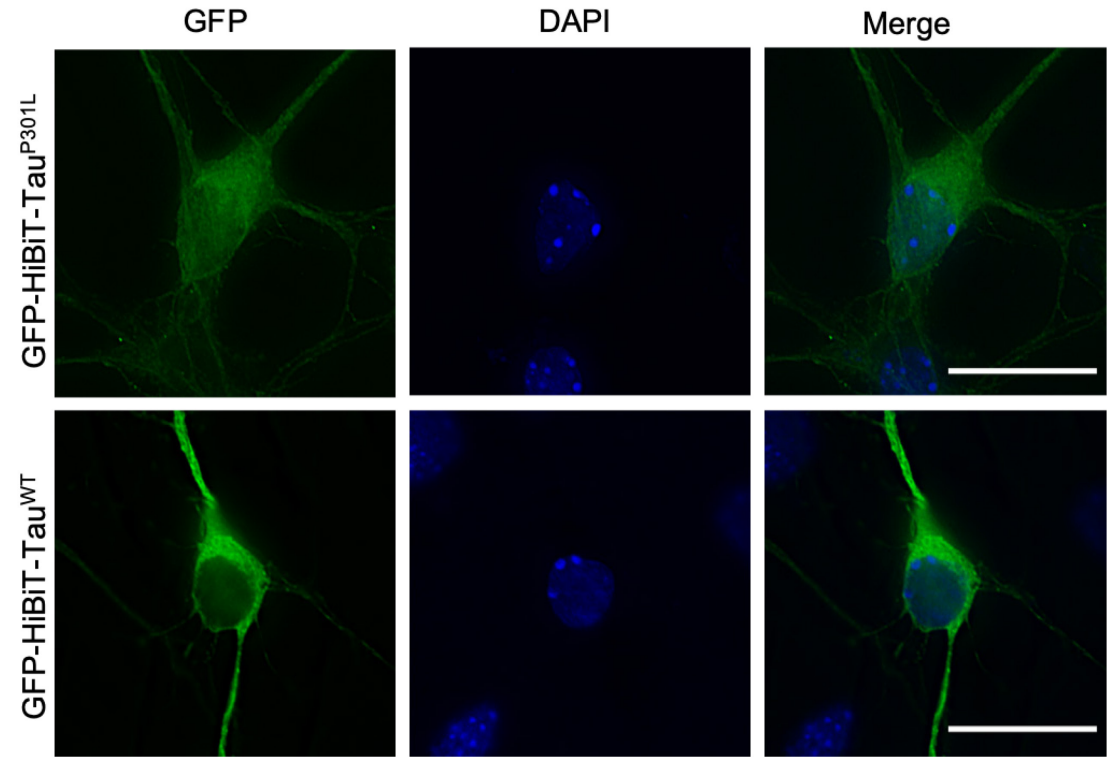

Figure 37. Expression of GFP-HiBiT-Tau^{P301L} leads to a more diffuse phenotype in neurons. GFP-HiBiT-Tau^{P301L} (top panel) and GFP-HiBiT-Tau^{WT} expression in fixed DIV13-16 hippocampal neurons. GFP-HiBiT-Tau^{P301L} demonstrated diffused distribution to the rest of the cell body including localisation in the nucleus. GFP-HiBiT-Tau^{WT} - expression (bottom panel) is more localised in the cytoskeleton, with the presence of GFP signal more distinct between the cell body and nucleus. Taken at 60X magnification. Scale bar= 20μm. N=3.

3.3.2 The use of lentiviral transduction of HiBiT-tau does not alter ability of tau to form inclusions *in vitro*.

To compare the ability of neurons to develop tau inclusions in axons following lentiviral expression GFP-HiBiT-Tau^{WT} and GFP-HiBiT-Tau^{E14}, GFP-HiBiT-Tau^{P301L} constructs immunocytochemistry were used. Similar to previous findings, both GFP-HiBiT-Tau^{WT} and GFP-HiBiT-Tau^{P301L} demonstrated a smooth fluorescence distribution in their axons (Figure 38). In contrast, GFP-HiBiT-Tau^{E14} indicated strong aggregation propensity to the other tau variants, which supports previous findings (Hallinan et al., 2019).This shows that lentiviral transduction of the HiBiT-tau reporters does not alter the ability to form tau inclusions in axons.

All lentiviral transduction of GFP-HiBiT-Tau^{WT}, GFP-HiBiT-Tau^{E14}, and GFP-HiBiT-Tau^{P301L} will be referred to as HiBiT-Tau^{WT}, HiBiT-Tau^{E14} and HiBiT-Tau^{P301L}, respectively, from now on.

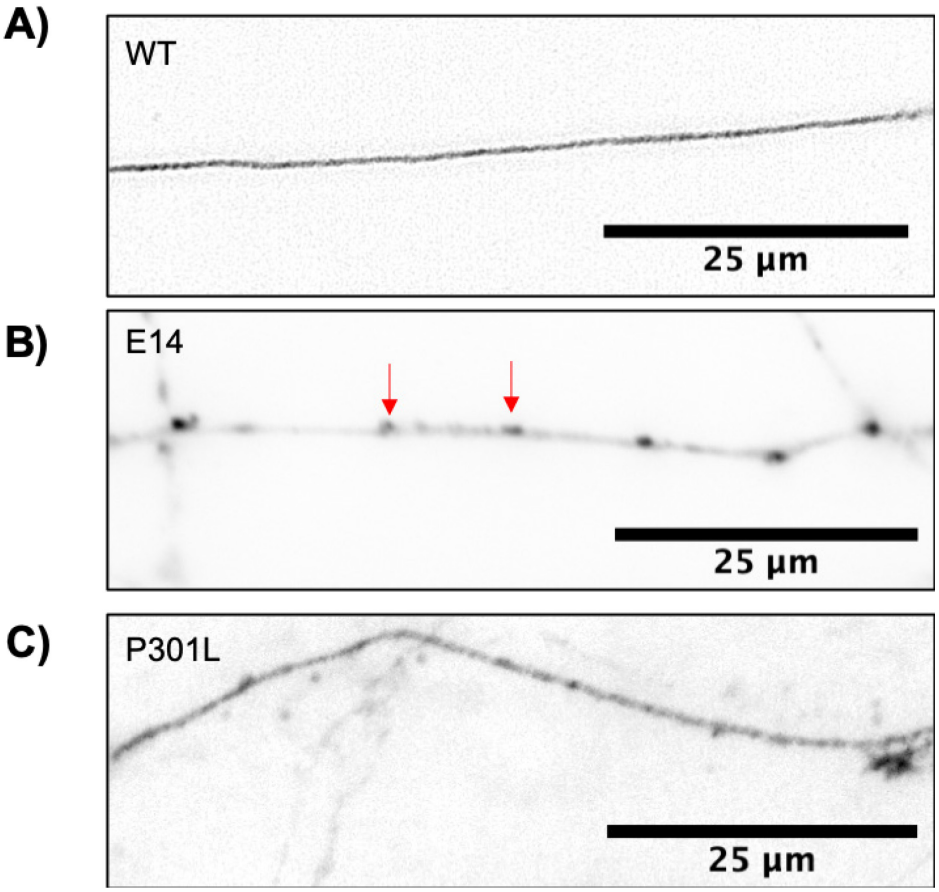

Figure 38. Lentiviral transduction of HiBiT-tau reporters does not modify the axonal phenotypes of the different tau variants upon expression in neurons.

A-C) Representative inverted images of the axons of DIV14 hippocampal neurons transduced with lentiviral vectors to express GFP-HiBiT-Tau^{WT} (WT), GFP-HiBiT-Tau^{E14} (E14), and GFP-HiBiT-Tau^{P301L} (P301L). Images taken in the distal part axons. Pink arrows illustrate the presence of tau inclusions (red arrows). N=3.

Table 3-1 Validation process of the NanoBiT-Tau reporter constructs

Plasmid constructs	Western blot		Fluorescence	Bioluminescence	
	Tau	HiBiT-blot		Luminometer	Bioluminescent microscope
GFP-HiBiT-Tau^{WT}	✓	✓	✓	✓	✓
GFP-HiBiT-Tau^{E14}	✓	✓	✓	✓	✓
GFP-HiBiT-Tau^{P301L}	✓	✓	✓	✓	✓
LgBiT-Tau^{WT}	✓	N/A	N/A	✓	✓
LgBiT-Tau^{E14}	✓	N/A	N/A	✓	✓
LgBiT-Tau^{P301L}	✓	N/A	N/A	✓	✓
HaloTag-LgBiT	✓	N/A	N/A	✓	✓
LgBiT	N/A	N/A	N/A	✓	✓
GFP-HiBiT	N/A	N/A	✓	✓	N/A
secGFP-HiBiT	N/A	N/A	N/A	✓	N/A

3.4 Conclusion

In this chapter, I carefully validated the newly generated NanoBiT-tau reporter constructs using a wide range of molecular biology and cellular techniques (as summarised in Table 3-1). By comparing with previously established tau constructs used to study tau aggregation and propagation (Hoover et al., 2010; Hallinan et al., 2019; Pitera et al., 2020). To ensure that the different components in the NanoBiT-tau biosensor were not modified from the molecular cloning process and can be expressed in primary hippocampal neurons, validation assays were undertaken. Firstly, biochemical analysis using western blot was able to validate the protein expression of the different components in the HiBiT-Tau and LgBiT-Tau constructs. The expression of GFP and tau were assessed using anti-GFP and anti-tau antibodies. The expression of HiBiT was also assessed. The variation in protein expression levels may be due to the different preparation of the DNA constructs and the rate of protein degradation. Furthermore, the differences in banding pattern (with all tau^{E14}-containing proteins demonstrating higher molecular weight than other tau variants) may be due to variations in post-translational modifications of different tau species.

In addition, the expression of HiBiT-tau and LgBiT-Tau in HEK293 cells resulted in the production of strong bioluminescence signals which indicated the successful HiBiT and LgBiT reconstitution of the NLuc enzyme. The ability to form tau inclusions were also assessed in primary hippocampal neurons upon the expression of the newly generated HiBiT-tau constructs. These results showed that the addition of HiBiT did not modify the ability of HiBiT-Tau^{WT} and HiBiT-Tau^{E14}-expressing neurons to form tau inclusions in axons *in vitro* at DIV14. The percentage of cells positive for tau inclusions were similar between HiBiT-Tau^{WT}, HiBiT-Tau^{P301L} and HiBiT-Tau^{E14}-expressing neurons versus cells expressing Tau^{WT}, Tau^{P301L} and Tau^{E14}, respectively. These results were similar to what has been previously reported in the lab using GFP-Tau^{WT} and GFP-Tau^{E14} (Hallinan et al., 2019). Most importantly, the sensitivity of the NanoBiT-Tau biosensor in different assay formats were also assessed. The plate-reader to be the optimal method of measuring tau secretion in cultured primary neurons as it showed a greater dynamic range in luminescence detection.

To conclude, the generation of HiBiT-tau and LgBiT-tau constructs resulted in a functional NanoBiT-Tau biosensor capable of assaying wild-type and mutant tau release and re-uptake in a highly sensitive manner. As the primary focus of the project shifted the focus to investigate tau secretion, only HiBiT-tau reporter constructs will be used from here on.

3.4.1 Discussion: HiBiT-Tau protein expression and localisation

Different post-translation modifications have been reported in literature including phosphorylation, glycosylation, acetylation, ubiquitination and tau cleavage. The patterns and occurrences of post-translation modifications may play a role in differential expression patterns and localisation of different tau forms. In this study, Tau^{WT} and Tau^{E14} protein expression differed to Tau^{P301L} when total tau expression was blotted for in primary hippocampal neuronal lysates. Lower molecular weight protein was detected in neurons expressing Tau^{P301L}. Interestingly, the protein expression levels of Tau^{P301L} in primary hippocampal neurons was not detectable when blotted for total tau. However, when HiBiT expression was blotted by the addition of LgBiT and furimazine on the membrane low-level Tau^{P301L} expression was detected using chemiluminescence imaging. In comparison to the other tau variants which demonstrated expected molecular weight of 80-90 kDa, HiBiT-Tau^{P301L} proteins were detected at an unexpected banding pattern of ~60 kDa. Intriguingly, the molecular weight between these different tau variants did not differ to each other when protein lysates from HEK293 cells were used; Tau^{WT} and Tau^{E14} and Tau^{P301L} demonstrated very similar molecular weights of 80-90 kDa. Sequence validation of the lentiviral HiBiT-Tau^{P301L} construct used to generate lentiviral particles for neuronal transduction indicated the correct coding sequence which suggest that the lack of Tau^{P301L} protein expression is not due to mutations on the HiBiT-Tau sequence. It may be possible that mutations could be present in the lentiviral vector backbone. Future work could look into sequencing the whole plasmid construct to detect potential mutations.

Biochemical validation using western blot did not lead to the expected protein molecular weight. Potential mechanism for this lack of Tau^{P301L} expression could be due to variable post-translation modification resulting in the misprocessing of the tau protein (Figure 5). Truncation is one of the most prominent modifications of tau (Gu et al., 2020; Plouffe et al., 2012) and can occurs in multiple sites along the tau protein in both physiological and pathological conditions (as seen Figure 39). In pathological conditions, several lines of studies have showed the different tau fragments has the ability to drive tau pathology in AD and other tauopathies. Indeed, there is evidence to suggest that early C- and N-terminal tau cleavage may be important markers of AD progression (Horowitz et al., 2004; Limorenko and Lashuel, 2022). It has been reported that tau fragments at position D13, E391, and D421 promote tau aggregation and accumulate in AD brains as well as correlate with the progression of the tau pathology (García-Sierra et al., 2003; Horowitz et al., 2004). C-terminal cleavage of tau at residue D421, triggered by caspase-3, can influence the ability of tau to bind and stabilise microtubules and also lead to filament formation(García-Sierra et al., 2003). Others have proposed that N-terminal truncation may lead to more severe AD pathology (Horowitz et al., 2004). These reports suggests that different truncations of tau may

have varying pathological activities. Furthermore, in a recent study using a combination of microdialysis and biochemical analysis, heparin-induced tau accumulates detected in the interstitial fluid from transgenic mice were mainly truncated forms with varying sizes (e.g., monomers, oligomers and fibrils) (Giamblanco et al., 2020). They found that expression of Tau^{P301L} mutant not only promoted the formation of oligomers and but also resulted in tau fibril breakage consequently forming different sizes. It is possible that the expression of this Tau^{P301L} mutant leads to the generation of smaller molecular weight tau fragments as a consequence of truncation, which may explain why there were a lack of larger tau accumulates observed in the distal axons of primary hippocampal neurons in the assay. This may also explain the presence of 60 kDa tau protein in the Tau^{P301L} cell lysates. Tau cleavage may also be a protective mechanism by promoting the removal of abnormal tau as well as promote abnormal tau accumulation. Whether tau truncation occur before, during or after the onset of tau accumulates still remains to be investigated.

The lack of tau inclusions in hippocampal neurons may also be explained by differences in tau clearance by the ubiquitin-proteasomal system and the autophagy-lysosomal pathways in different tau variants. This is plausible as occurrence of post-translational modifications may have varying effect in these tau degradation processes (Alquezar et al., 2021). Long-lived and larger protein inclusions that are not degraded via proteasomal pathway are processed through the autophagy pathway. It has been observed that impairment in autophagy function can lead to the delay of tau clearance and enhances tau accumulation (Wang et al., 2010). Tau^{P301L} proteins may be degraded at a faster rate than other tau variants hence very small amount of tau expression can be observed in hippocampal neurons.

Figure 39. The products of tau cleavage in health and disease. Cleaved tau in (A) healthy state and (B) diseased state. There are a large number of cleaved tau detected in the diseased state. Adapted from Limorenko et al., 2022.

3.4.1.1 Cells expressing Tau^{P301L} protein showed a smooth fluorescence intensity distribution profile similar to cells expressing Tau^{WT} protein

Interestingly, Tau^{P301L}-expressing neurons did not display significant accumulation of large tau inclusions in the distal axons and demonstrated smoother fluorescence distribution phenotypes. Although the hyperphosphorylated and disease-associated mutated tau have been shown to induce the formation of large tau inclusions in literature (Hallinan et al., 2019; Pitera et al., 2019), we showed that Tau^{P301L} expressing neurons did not accumulate in larger tau inclusions in distal axons; Tau^{P301L} expressing cells demonstrates a smooth fluorescence intensity. The lower fluorescence intensities of Tau^{P301L}-expressing neurons and its diffused appearance could be because smaller molecular species of tau are generated in the expression of this tau mutant; the *in vitro* fluorescence assay (Hallinan et al., 2019) may be biased in detecting larger aggregates in the axons of neurons, and it is possible that smaller tau aggregates exist but are undetectable in this fluorescence-based assay. Previous findings in the lab have shown that Tau^{P301L} expressed in primary neurons readily misfolds in axons, as indicated by MC1 staining, when compared to Tau^{WT} at DIV14 (Pitera et al., 2019). As I did not directly assess for tau misfolding, it is possible these

Tau^{P301L} expressing neurons do not form large tau aggregates but rather form misfolded tau proteins that are undetectable in the fluorescence *in vitro* assay.

3.4.1.2 Somatodendritic mislocalisation of tau

Furthermore, the overall distribution of fluorescence in the soma of HiBiT- Tau^{P301L} expressing neurons were also different to other tau variants. Higher magnification images comparing the fluorescence distribution in the soma of neurons expressing HiBiT-Tau^{P301L} and HiBiT-Tau^{WT} may indicate some key differences in tau localisation between different tauopathies. The diffused fluorescence signal observed in the soma and nuclear region of HiBiT-Tau^{P301L} expressing neurons could suggests that tau is mislocalised to the nucleus (Figure 37). The differences in the fluorescence intensities between the cell body and the nucleus were more striking in neurons expressing HiBiT-Tau^{WT} and HiBiT-Tau^{E14} compared to HiBiT-Tau^{P301L} neurons. This variation could be due to the presence of different conformationally distinct tau strains between these sub-types of tau variants. As previously discussed in section 1.4.3, distinct tau monomers encode strains. These tau strains can determine the pattern of tau pathology propagation, rate of disease progression and fibril formation which is why tauopathies are so heterogenous (Kaufman et al., 2016; Sanders et al., 2014). As tau strains have distinct conformations, this may also dictate their relative cellular localisation.

Since HiBiT-Tau^{P301L} protein demonstrated a more diffused pattern of localisation in the somatodendritic region when compared to WT, it is likely that expression of HiBiT-Tau^{WT} and HiBiT-Tau^{P301L} will generate different tau entities and strains, the structural morphology and protein-protein interaction will also differ. Saunders et al., (2014) beautifully showed that distinct strains of tau propagate *in vivo*, through multiple generations and extractions. In this study, tau strains were isolated and propagated in a biosensor stable cell line expressing the tau repeat domain containing two disease associated mutations (P301L/V337M) which was fused to a yellow fluorescent protein (RD-YFP). Characterisation of 20 different polyclonal cells expressing RD-YFP showed variable inclusion morphology. Interestingly, they found that re-introducing these tau strains into naïve cell lines results in the replication of the same structural phenotype (Sanders et al., 2014). Biochemical characterisation of these clones allowed the differentiation of tau strains based on tau inclusion size. Different clones propagated more efficiently than others, whereas others showed to fragment into smaller species. These clones also demonstrated different solubility. Isolation of the two clonal lines that stably propagated aggregates of distinct conformation was further studied; these strains were named DS9 and D10. Interestingly, re-expressing strain DS9 resulted in the appearance of nuclear speckles in stable cell lines (Sanders et al., 2014). Later studies showed that sub-strains also exists within each of these strains and that

each can trigger unique tau pathology *in vivo* (Sharma et al., 2018). Intriguingly, just as previously shown all DS9-derived clones isolated from DS9 tau monomer strain also showed morphological characteristics and generated nuclear speckles (Sanders et al., 2014). Application of lysates derived CBD and AD patients also produced distinct strains and structural morphologies in the biosensor cell line, all of which produced different degrees of nuclear speckles.

The interest in understanding Tau and its interaction with the nucleus are growing, particularly because of evidence showing that RNA and DNA not only bind but also induce efficiently fibrillization of intracellular tau. What the role of tau is in the nuclear region remains to be investigated but it has been suggest that nuclear tau could protect DNA integrity, participate in DNA repair mechanisms and ribosomal gene translation and assembly (Antón-Fernández et al., 2022; Diez and Wegmann, 2020). More recently however, stress-induced Tau mislocalisation to the nucleus has been proposed to be disease-associated (Eftekharzadeh et al., 2018). This study showed that pathogenic tau can mislocalise to nuclear pore complexes, where it can disrupt nuclear pore complex formation in AD brains and *in vitro* models (Eftekharzadeh et al., 2018). Pathological tau is shown to directly interact with components of nuclear pore complex (e.g., Nup98, Nip62), important for controlling the intracellular trafficking of proteins and RNA, which causes accelerated aggregation and fibrilization of tau in the cytoplasm.

Disruption in nuclear transport has also been shown in other familial neurodegenerative diseases such as amyotrophic lateral sclerosis, FTD, Huntington's disease (Antón-Fernández et al., 2022). Based on this, it may be that neurons expressing Tau^{P301L} are more stressed because of the production of smaller toxic tau oligomers, which become mislocalised to the somatodendritic regions as well as in the nucleus, where they then may induce further neuronal disruption. To determine whether similar processes have occurred in my assay, higher resolution co-localisation images would be required to confirm whether mutant-tau does indeed mislocalise and bind to nuclear components. However, Eftekharzadeh and colleagues has already shown data demonstrating greater colocalisation of phosphorylated tau with nuclear pore complex in human AD (Braak VI) brain tissue (Eftekharzadeh et al., 2018)..

Considering that HiBiT-Tau^{P301L}-expressing neurons did not clearly demonstrate a similar protein expression to the other tau variants, it was not be used for side-by-side comparisons in future tau secretion assays. However, as fluorescence imaging of HiBiT-Tau^{P301L} expressing neurons were still detectable visually, cultured hippocampal neurons expressing HiBiT-Tau^{P301L} were still used for electrophysiological recordings.

Chapter 4 Differential secretion of wild-type and mutant tau

4.1 Introduction:

The functional role of tau is well established in the intracellular space as a regulator of microtubule assembly and dynamics, however its role in the extracellular space still remains unknown. The fact that tau can be found in the CSF of both controls and AD patients (Hampel et al., 2010) suggests that tau is secreted by cells into the extracellular space in both physiological and pathological conditions. This is supported by multiple lines of evidence which have detected tau in various conditioned media such as cell lines overexpressing tau (Chai et al., 2012), primary neurons (Bright et al., 2015; Karch et al., 2012; Pooler et al., 2013), ISF and CSF of mice (Yamada et al., 2011; Yamada et al., 2014) and humans (Magnoni et al., 2012).

There are two main forms of tau that are found in the extracellular space: vesicular tau (1.7.4) and membrane-free tau (1.7.3). A large proportion of tau in the extracellular space is mainly membrane-free (Chai et al., 2012; Karch et al., 2012) with only a small proportion detected inside extracellular vesicles (Dujardin et al., 2014; Saman et al., 2012; Simón et al., 2012a). Extracellular vesicles, such as exosomes and ectosomes, can also be split into two main types; tau could be encapsulated inside the vesicle membrane or attached extracellularly (reviewed in section 1.7.4).

Various lines of evidence have shown that tau is secreted by primary neurons in both physiological and pathological conditions independent of cell death (Pooler et al., 2013; Wu et al., 2016). In pathological conditions, the release of misfolded tau is the initiating step for the spreading of tau pathology. There is evidence showing that tau phosphorylation state may affect secretion propensities in immortal cell lines (e.g., CHO and SH-SY5Y) (Katsinelos et al., 2018). In this study, pseudo-hyperphosphorylated tau, Tau^{E14}, was preferentially secreted over the WT and dephosphorylated tau proteins, Tau^{AP}. Briefly, Tau^{AP} mimics hypophosphorylation because 14 serine and threonine sites are mutated into alanine. Although Katselinos et al., (2018) found that hyperphosphorylated forms of tau are preferentially secreted in CHO and Sh-SY5Y cell lines, it still remains unclear whether this is the same for cultured primary hippocampal neurons. Furthermore, are tau secretion propensities affected by the type of tau variant expressed by cells? If that is the case, what influences secretion propensities? Do primary hippocampal neurons release a specific tau forms (e.g., membrane-free tau or vesicular tau) more preferentially than others in physiological and pathological conditions? Understanding these questions may give us a

better understanding of the molecular process involved in the tau secretion of different tau variants and how this may contribute to the overall progression of tau pathology.

Aims:

- To investigate differential secretion propensities between two different tau variants that mimics physiological and pathological processes. To mimic the hyperphosphorylation that is a hallmark of AD, Tau^{E14} was used. This this mutant has robustly shown to misfold and aggregate *in vitro* (Hallinan et al., 2019). As a control, a non-misfolding and non-aggregating tau, Tau^{WT} variant, was used.
- The NanoBiT-Tau biosensor was used to assess membrane-free and vesicular tau that is released into the extracellular space from cultured primary hippocampal neurons expressing either the wild-type or mutant tau.

4.2 Endogenous tau is secreted in basal conditions

Pooler and colleagues (2013) previously showed that endogenous tau is released into the extracellular space from cultured cortical neurons in physiological conditions. In this section, I determined whether tau is secreted in cultured hippocampal neurons at basal conditions. To do this, the conditioned media were collected from DIV14 cultured neurons and blotted for the presence of tau using a dot-blot assay (described in section 2.6.6). Hippocampal neurons were cultured on multiple-well plates (four technical replicates were obtained for each experiment). In each well, the conditioned media from the cultured neurons were collected and applied on nitrocellulose membrane to bind all the endogenous tau proteins that has been released into the extracellular space. The total tau was probed by using an antibody that recognises the C-terminal part of tau (amino acids 243-441) (Figure 40). As the conditioned media was not subjected to a lysis buffer, only membrane-free tau present in the extracellular space was detected in the dot-blot assay. Figure 40 showed that membrane-free tau is indeed secreted from mature cultured hippocampal neurons. Furthermore, the membrane was also blotted for the presence of intracellular protein, glyceraldehyde 3-phosphate dehydrogenase (GAPDH), which is an intracellular enzyme of about 37 kDa that is responsible for the catalysis of glycolysis. As GAPDH is constitutively expressed intracellularly in all tissues in large amounts, it was used as a cell lysis control (bottom panel in Figure 40). The presence of GAPDH in the extracellular space would indicate the level of cell lysis in the cultures. As the detected tau in the conditioned media was independent of presence of GAPDH, the membrane-free tau detected therefore did not derive from a cell lysis.

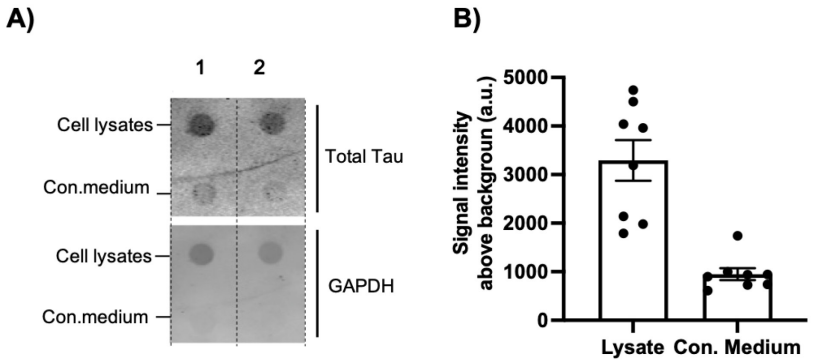

Figure 40. Endogenous tau is secreted from cultured primary hippocampal neurons in physiological conditions.

Conditioned media and cell lysates from DIV 14 neurons were collected and assessed for the presence of membrane-free tau and intracellular tau using a dot-blot assay. A) Representative examples from two technical replicates of cultured hippocampal neurons from two different experiments; showing the presence of tau in cell lysates

and conditioned media. Anti-tau (DAKO) and anti-GAPDH antibody were blotted used to detect tau and as a cell-lysis indicator, respectively. B) Densitometry from 8 technical replicates (T = 8) taken from a total of two biological experiments (N = 2).

4.3 Wild-type and mutant tau secretion

4.3.1 The NanoBiT-Tau lytic assay allows the detection of membrane-bound tau

The NanoBiT-Tau reporter assay (as described in section 3.3) was customised to allow measurements of membrane-free and vesicular tau that is secreted into the extracellular space. To accomplish this, a non-lytic and lytic modality of the NanoBiT-Tau reporter assay (as demonstrated by Figure 41A) was used (as described in section 2.8.5).

Prior to use in primary cultures, the NanoBiT-Tau non-lytic and lytic assay was first trialled on HEK293 cell cultures expressing HiBiT-Tau^{E14} and GFP-HiBiT. After 24 hours post-transfection, the cells were either treated the non-lytic or lytic assay (methods described in section 2.8.5). The luminescence signals were detected after the addition of LgBiT in both assays. To ensure that luminescence signals detected in the assay were due to the secretion of HiBiT-tagged proteins rather than the release of intracellular proteins from cell lysis, the expression of GFP-HiBiT was used as an internal negative secretion control. As GFP-HiBiT do not have a signal peptide, it is not targeted for secretion and so remains inside the cytosol of cells.

The expression of GFP-HiBiT in 'non-lytic' group indicate the level of background generated from uncomplemented HiBiT and LgBiT in the NanoBiT-Tau assay (Figure 41). In the non-lytic assay, the signal generated from cells expressing HiBiT-Tau^{WT} was detectable above the signal from GFP-HiBiT-expressing cells, our findings show that HiBiT-Tau ^{WT} secretion can be detected above background. Addition of the lytic assay resulted in the release of intracellular GFP-HiBiT and HiBiT-Tau^{WT} into the extracellular space leading to an increase in NLuc structural complementation; as a result, there is an increase in overall bioluminescent signal in the lytic assay in the HiBiT-containing cells. These findings show that addition of digitonin is capable to lysing the cell membrane and all of the membrane-bound organelles (Figure 41).

The untransfected group was treated with LgBiT and substrate only. The fact that there is low level signal in this group suggests that the LgBiT and substrate generate only a small amount of background signal in the assay.

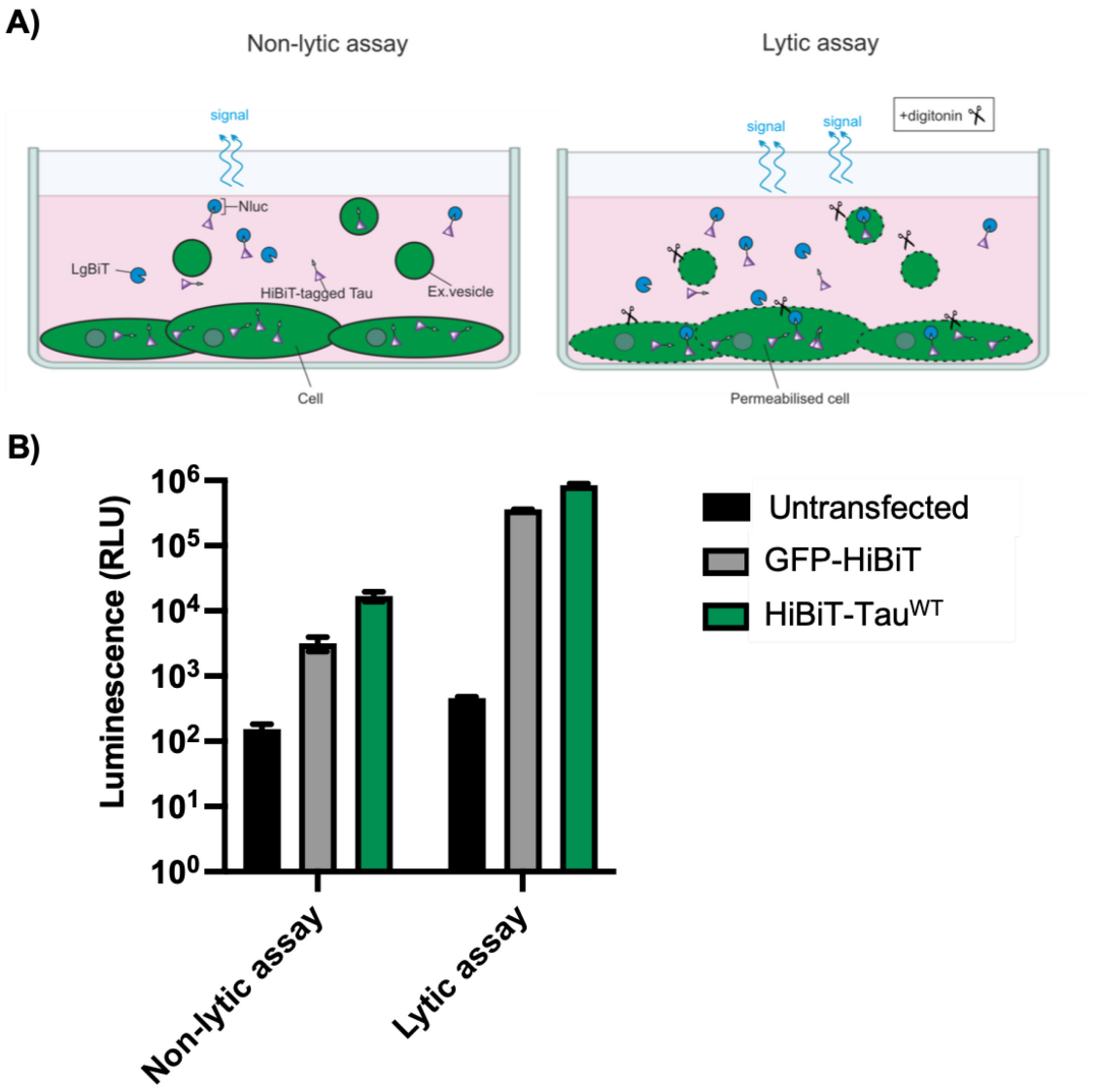

Figure 41. Non-lytic and lytic NanoBiT-Tau reporter assay used to detect different membrane-free and vesicular-tau.

A) Schematic diagram of the non-lytic and lytic assay used to differentiate between level of secreted free-tau and vesicular-tau. The non-lytic assay does not lyse the membrane. The addition of both LgBiT and furimazine in to the conditioned media detects all membrane-free tau in the extracellular space. In the lytic assay, LgBiT and substrate mixture is supplemented by the 50 µg/µl digitonin. As digitonin lyse cell membranes, the signal detected in the lytic assay indicates the total level of intracellular and extracellular tau, including those packaged in extracellular vesicles. B) HEK293 cells were transfected with GFP-HiBiT (negative control) and HiBiT-Tau^{E14}. After 24 hours post-transfection, non-lytic and lytic assay was carried out in parallel and the luminescence signal (given as relative light units, RLU) was detected immediately using a plate-reader; T=3, N=1.

4.3.2 Tau release is within the dynamic range of assay detection

To ensure that tau secretion can be detected within the dynamic range of the NanoBiT-Tau reporter assay, the positive control, secretory GFP-HiBiT (secGFP-HiBiT), and a negative control (GFP-HiBiT) was utilised in parallel alongside the expression of HiBiT-Tau construct. Murine hippocampal neurons were transduced to express HiBiT-Tau^{WT}, HiBiT-Tau^{E14}, secGFP-HiBiT and GFP-HiBiT. Luminescence signals were detected after the addition of LgBiT and substrate (as previously described in 2.7.2). All raw data was normalised to the signal generated by cells expressing secGFP-HiBiT within each separate experiment. This was used as a positive control because the secretory IL6 signal target the encoded protein for cellular secretion into the extracellular space; this signal was used to compare the relative secretion of other HiBiT-tagged proteins.

The positive control generated significantly higher bioluminescent signal relative to the negative control ($p=0.0004$) and the tau variants (Figure 42); this information sets the maximum signal detection in our assay. In contrast, both HiBiT- Tau^{WT} and HiBiT-Tau^{E14} showed significantly reduced luminescence signal when compared to the positive control (Figure 42) which indicates that tau secretion does not go above the maximum assay signal the assay is able to detect. Furthermore, the relative luminescence of HiBiT-Tau^{WT} ($p=0.0388$) and HiBiT-Tau^{E14} ($p=0.0076$) were significantly higher when compared to the negative control (GFP-HiBiT) showing that secretion for both Tau^{WT} and Tau^{E14} can be detected above assay background (as previous shown in HEK293 cells Figure 41) and that it is well within the dynamic range of detection in the assay (Figure 42).

Due to the small sample numbers, HiBiT-Tau^{WT} and HiBiT-Tau^{E14} did not show significant differences in relative luminescence in this instance. However, the Tau^{E14} did show higher relative luminescence signal (0.29 a.u. ± 0.043) when compared to HiBiT-Tau^{WT} (0.22 a.u. ± 0.073) which is trending to significance ($p = 0.0562$; Figure 42). It suggests therefore, that HiBiT-Tau^{E14} could be secreted preferentially by murine hippocampal neurons. Further experiments were added to detect differential secretion between HiBiT-Tau^{WT} and HiBiT-Tau^{E14} in primary hippocampal neurons (results shown in section 4.3.4).

Overall, this data shows that tau secretion can be detected and is within the dynamic range of detection in the assay. Next aim of this project would be to dissect the difference between HiBiT- Tau^{WT} and HiBiT-Tau^{E14} in their secretion in the extracellular space and quantify the proportion of membrane-free and vesicle-bound tau.

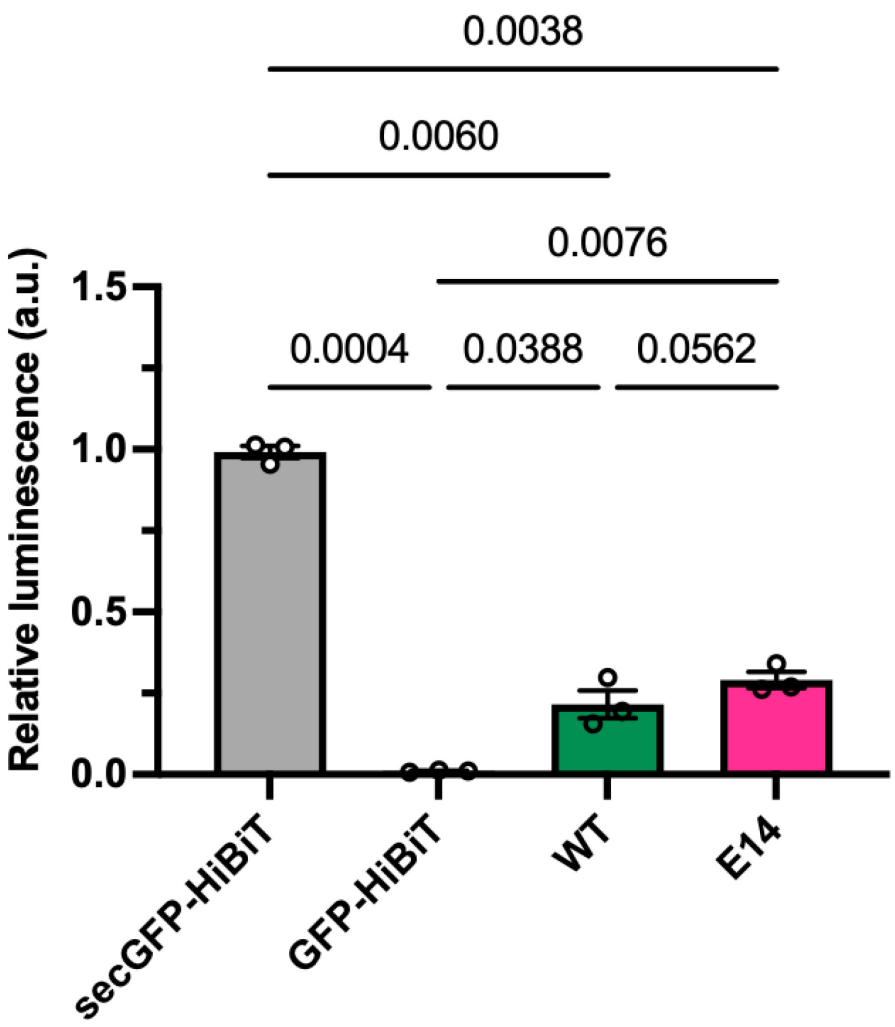

Figure 42. Tau secretion is within the dynamic range of the assay detectability.

Primary hippocampal neurons were cultured in a 96-well plate and transduced with lentiviral vectors expressing secretory-GFP-HiBiT (secGFP-HiBiT), GFP-HiBiT, HiBiT- Tau^{WT} and HiBiT-Tau^{E14}. Non-lytic NanoBiT-Tau assay was carried out at DIV13-15. Luminescent measurements were taken after the addition of LgBiT and substrate to the media and raw values were normalised to the secGFP-HiBiT within each individual experiment. The graph indicates luminescence relative to secGFP-HiBiT, given as arbitrary units (a.u.). There is significant difference between positive control (luminescence generated from cells expressing secGFP-HiBiT) and HiBiT-Tau^{WT} and HiBiT-Tau^{E14} showing that tau secretion is within the dynamic range of assay detection. Signal generated HiBiT-Tau^{WT} and HiBiT-Tau^{E14} ^{is} also detected above assay background (as indicated by the signal generated from negative control, GFP-HiBiT). Repeated measures one-way ANOVA, followed by uncorrected Fisher's LSD; N=3.

4.3.3 The majority of WT and mutant tau are secreted as a free protein

To detect the different forms of tau secreted (e.g., membrane-free and vesicular-tau) in the extracellular space in in cells expressing WT and mutant tau, the non-lytic and lytic modalities of the NanoBiT-tau biosensor were used (as described in 2.8.5). The conditioned media at DIV13-15 from each well was split into two parallel conditions: a) non-lytic and b) lytic. The lytic assay was employed to distinguish the populations of tau that is in vesicular tau and membrane-free tau, whereas non-lytic assay detects soluble and membrane-free tau only.

There is a significant difference between the non-lytic and lytic assay in HiBiT-Tau^{WT} ($p=0.0148$; Figure 43A). Similarly, the lytic assay was also able to detect greater proportion of HiBiT-Tau^{E14} in the extracellular space when compared to the non-lytic assay ($p=0.0155$; Figure 43B). These results show that in both HiBiT-Tau^{WT} and HiBiT-Tau^{E14}-expressing cultured hippocampal neurons, the majority of tau found in the extracellular are membrane-free tau; vesicular-tau only accounts for approximately third of the tau present in the extracellular space. There are no observable differences in the ratio of secreted membrane-free and vesicular tau between HiBiT-Tau^{WT} and HiBiT-Tau^{E14}.

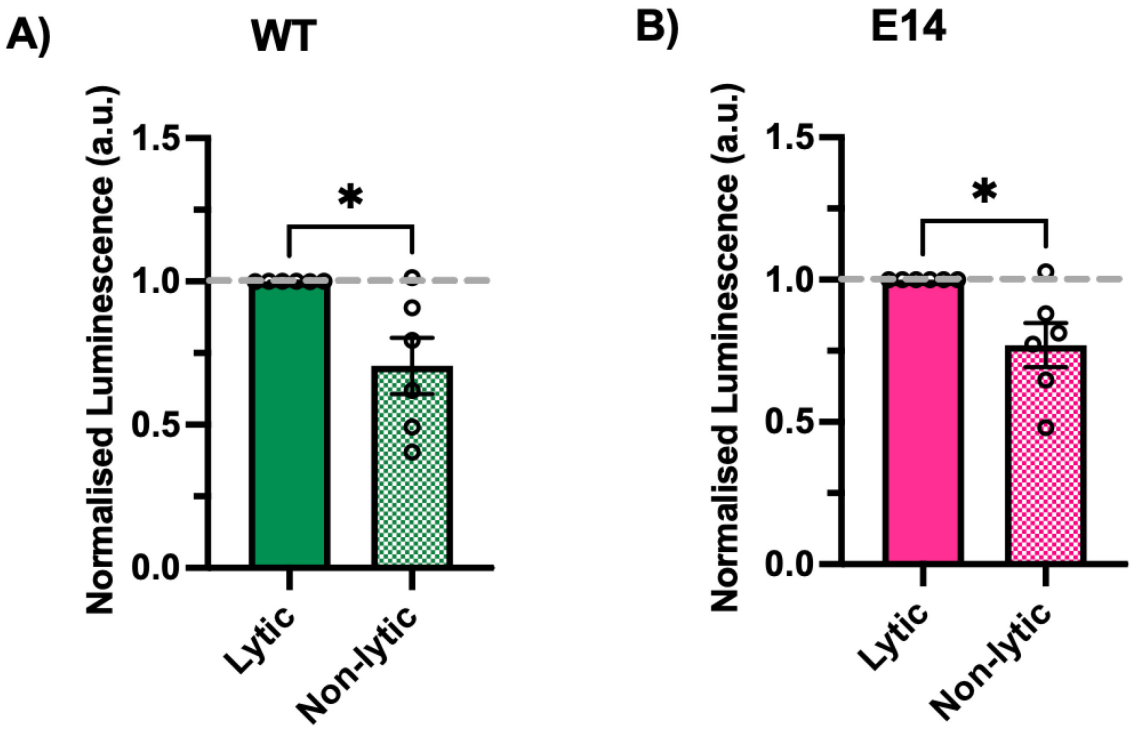

Figure 43. Membrane-free and vesicle-bound tau are both secreted in physiological and pathological conditions.

HiBiT-Tau^{WT} and HiBiT-Tau^{E14} -expressing neurons secrete both free-tau and vesicular-tau in the extracellualr space. Conditioned medium were collected from DIV13-15 cultured hippocampal neurons expressing either HiBiT-Tau^{WT} (green) and HiBiT- Tau^{E14} (pink) proteins. Half of the coditioned medium were split into two parrallel conditions for the non-lytic and lytic assay to detect the presence of free-tau and vesicular-tau. Control neurons were transduced with GFP-HiBiT. The conditioned media from these cultures were collected and treated with non-lytic or lytic treatment; luminencent signals produced were quantified and used as background control for all raw values. All values presented in the data therefore take into account the autoluminesncent background generated from uncomplemented HIBiT and LgBiT and the addition of digitonin in the assay. Background subtracted data was normalised to the lytic-assay values (set to 1). A) There is a significant difference between non-lytic and lytic luminenscence signal in HiBiT-Tau^{WT} (p=0.0148, paired t-test, N=6). B) There is also significant difference between non-lytic and lytic luminenscence signal in HiBiT-Tau^{E14} (p=0.0155, paired t-test, N=6).

Table 4-1. Proportion of secreted free-tau and vesicular-tau in WT and E14 cultured hippocampal neurons

	Free-tau (%)	Vesicular-tau %	SD
WT	70.5	29.5	± 23.97
E14	77.0	23	± 18.94

4.3.4 Mutant tau is preferentially secreted by hippocampal neurons

As cells expressing HiBiT-Tau^{E14} demonstrated a greater propensity to accumulate in the distal axons when compared to neurons expressing HiBiT-Tau^{WT}, I assessed whether the secretion propensities between these two tau variants also varied, previous work by Hallinan and colleagues showed that co-culture of hippocampal neurons expressing GFP-Tau^{E14} and GFP-Tau^{WT} in three-chamber microfluidic device indicated that the propagation of tau misfolding and the formation of accumulates in distal axons was more efficient in neuronal networks co-cultured with GFP-Tau^{E14} when compared to GFP-Tau^{WT} alone (Hallinan et al., 2019). Therefore, this suggests that the transfer and release of mutant tau from pre-synaptic neurons were more efficient in neurons expressing GFP-Tau^{E14}. Thus, I hypothesised that Tau^{E14} may be preferentially secreted over Tau^{WT}. To test this hypothesis, the level of tau detected in the extracellular space of cultured hippocampal neurons expressing HiBiT-Tau^{WT} and HiBiT-Tau^{E14} in basal conditions. To do this, the non-lytic NanoBiT-tau biosensor was used to measure basal tau secretion (as described in 2.8.1). The conditioned media from neuronal cultures were collected and assayed at DIV13-15. The total amount of tau secreted in the extracellular space were measured and analysed using the non-lytic NanoBiT-Tau assay (as previously discussed and validated in section 4.3.2).

These results showed that HiBiT-Tau^{WT} and HiBiT-Tau^{E14} are both secreted by hippocampal neurons at low level that is detectable above assay background (as seen in Figure 42). There is significant increase in pseudo-hyperphosphorylated tau secretion (p=0.0039) when compared to control. This difference was not due to differential protein expression levels between the HiBiT-Tau^{WT} and HiBiT-Tau^{E14} (data shown in Figure 36). To determine protein expression, western blot analysis was done to the cell lysates obtained from cells expressing HiBiT-Tau^{WT} and HiBiT-Tau^{E14}(data is described in section 3.3.1 and Figure 36). Furthermore, to ensure that this difference in secretion propensities is not due to the induction of neurodegeneration from HiBiT-Tau ^{E14} expression, Calcein Blue AM assay was used to detect cell viability for each cell culture (as

outlined in 2.8.4). Results showed no significant difference in cell viability between cells expressing HiBiT-Tau^{WT} and HiBiT-Tau^{E14} ($p>0.9999$, Figure 44B).

Overall, these findings show that pseudo-hyperphosphorylated tau is preferentially secreted by murine hippocampal neurons when compared to wild-type forms of tau at basal conditions. This suggests that hyperphosphorylation may play a role in secretion propensities in this cultured system, which is similar to what has already been shown in other studies (Katsinelos et al., 2018).

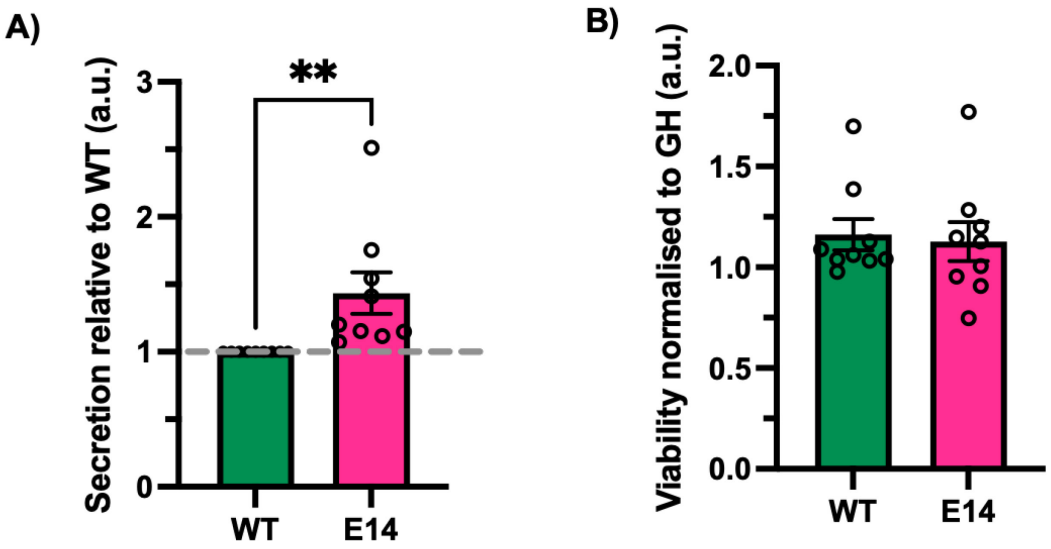

Figure 44. Differential tau secretion between HiBiT-Tau^{WT} and HiBiT-Tau^{E14} in cultured hippocampal neurons is independent of cell death.

The basal tau released in the conditioned media of cultured hippocampal neurons expressing mutant and wild-type tau over the course of two weeks were assessed using the non-lytic NanoBiT-Tau assay. All assays were done at DIV13-15. A) Relative secretion of membrane-free HiBiT-Tau^{WT} and HiBiT-Tau^{E14} in cultured hippocampal neurons. There is significant difference between HiBiT-Tau^{WT} and HiBiT-Tau^{E14} ($p=0.0039$, one-tailed paired t-test, N=9) in secretion levels in primary hippocampal neurons. B) Calcein AM Blue was used to assess cell viability between HiBiT-Tau^{WT} and HiBiT-Tau^{E14}; signals were normalised to the control GFP- HiBiT (GH) signal. No significant difference in cell viability ($p>0.9999$, two-tailed, paired t-test, N=9) between HiBiT- Tau^{WT} and HiBiT-Tau^{E14}.

4.4 Conclusion

In this chapter, we investigated the differential secretion between two variants of tau: Tau^{WT} and Tau^{E14}. The NanoBiT-Tau biosensor was able to detect the secretion of both variants in primary neurons above background and within the dynamic range of the assay. I established a non-lytic and lytic reporter system with this biosensor that allowed the detection of both membrane-free and vesicular tau in cultured primary hippocampal neurons expressing either Tau^{WT} or Tau^{E14}.

Our results showed no differences in the proportion of membrane-free and vesicular tau between WT and mutant. In accordance to previous findings, these results suggest that Tau^{WT} and Tau^{E14} is preferentially secreted as a membrane-free protein rather than packaged in vesicles (Dujardin et al., 2014; Pernègre et al., 2019; Pooler et al., 2013). However, membrane-free was considerably lower than what has been reported in literature (Dujardin et al., 2014) which is further discussed in Chapter 6. It is also important to note that all HiBiT-Tau proteins that are highly accessible to structurally complement with the LgBiT in the extracellular space were measured in this assay. This include all HiBiT-tau that are freely soluble, attached to the outer cell surface extracellular membrane. Therefore, the level of membrane-free tau is likely overestimated in this assay.

As the majority of extracellular tau identified in the conditioned media of Tau^{WT} and Tau^{E14}-expressing neurons were mainly membrane-free, I decided to focus on these forms of tau in this project.

The results showed that tau is secreted in physiological conditions by healthy and intact cells, which is in accordance to what has previously been shown in literature (Pooler et al., 2013; Yamada et al., 2014). However, how and why tau is secreted in these conditions is still unclear. It is possible that the state of tau may affect secretion propensity in primary hippocampal neurons. In line with what has previously been shown in cell lines, pseudo-hyperphosphorylated tau was found to be preferentially secreted by hippocampal neurons over WT (Katsinelos et al., 2018). Although we did not fully assess whether phosphorylation states of tau may affect tau secretion, as this would require a direct comparison with a tau variant that is dephosphorylated (e.g., Tau^{AP}), there is already evidence of this in literature (Katsinelos et al., 2018). These results therefore suggest that when tau becomes hyperphosphorylated, hippocampal neurons increase their level of release into the extracellular space that is independent of cell death. Alternatively, the differences in the secreted tau levels detected in the extracellular space between HiBiT-Tau^{WT} and HiBiT-Tau^{E14} expressing neurons could also be due variable protein expression (caused by different transduction efficiency). To control for this, every new viral preparation of the HiBiT-Tau^{WT} and HiBiT-Tau^{E14} were done in parallel and were validated by assessing the protein expression of the different tau variants using western blot and imaging analysis (as shown in

Figure 36A-B). The protein expression of transduced HiBiT-Tau^{WT} and HiBiT-Tau^{E14} were assessed by blotting with an anti-tau antibody and LgBiT. To quantify the relative protein expressions between viral preparation of the NanoBiT-tau constructs, densitometry analysis was obtained by normalising the expression of transduced tau to the endogenous tau (Figure 36B). No significant differences were observed between cultures expressing HiBiT-Tau^{WT} and HiBiT-Tau^{E14} across different biological replicates (Figure 36C). Therefore, the differences in the secretion levels between these two tau variants is not due to the variation in tau expression. Driving the increase in the release of these hyperphosphorylated forms of tau could be a protective mechanism to reduce the intracellular accumulation of misfolded tau proteins and accumulates, subsequently increasing its accumulation in the extracellular space.

Interestingly, previous work from our lab have shown that tau hyperphosphorylation leads to efficient propagation of tau misfolding and formation of tau accumulates (Hallinan et al., 2019). Co-culture of 'donor' Tau^{E14}-expressing neurons with 'acceptor' Tau^{WT}-neurons, using microfluidic devices, lead to efficient propagation of misfolding and formation of accumulates in healthy connected neuronal networks (Hallinan et al., 2019). The axons of 'acceptor' Tau^{WT}-expressing neurons developed misfolding even before aggregation can be identified in 'donor cells'. For this to have occurred these misfolded forms of tau must have been released and taken-up in the connected neuronal network. The fact that Tau^{E14} are preferentially secreted by hippocampal neurons explains why in these connected networks the tau^{E14} variant led to robust and efficient propagation of misfolding and aggregation.

To conclude, our NanoBiT-tau reporter assay was able to established the secretion propensities of different tau variants at basal conditions. How secretion propensities of tau are modulated with neuronal activity remains to be investigate.

Chapter 5 Establishing the effects of neuronal activity in the secretion of wild-type and mutant tau

5.1 Introduction

Although the functional significance of extracellular tau is largely unknown, there is a lot of evidence showing that it can be secreted by neurons *in vitro* and *in vivo* independent of cell death (Pooler et al., 2013; Yamada et al., 2014; Wu et al., 2016). Why this phenomenon occurs in physiological conditions is still currently unknown. However, neuronal activity may play an important role in the secretion of tau in both physiological and pathological conditions (Pooler et al., 2013; Yamada et al., 2014; Wu et al., 2013). Pooler et al., (2013) previously demonstrated that depolarising primary cortical neurons can induce the secretion of membrane-free tau. The secretion process has been shown to be calcium-dependent. *In vivo*, neuronal and synaptic activity increased in tau secretion in the interstitial fluid of tau transgenic mouse brain in the absence of neurodegeneration (Yamada et al., 2014). In diseased conditions, neuronal activity has been reported to increase the secretion of pathogenic tau (Wu et al., 2016). Here, they show that the secretion and re-uptake of pathogenic tau species contribute to the spreading and propagation of tau pathology in connected neuronal networks (Wu et al., 2016). In this regard, the formation of synaptic contacts has been proposed to mediate the cell-to-cell spreading of tau pathology in connected neuronal networks (Calafate et al., 2015; Yamada et al., 2014). Cell-to-cell transmission of tau may be more efficient in synapses because tau have greater affinity to these cell-surface proteins and lipids.

Due to its lack of secretory signal peptide, cytosolic tau protein is thought to be secreted into the extracellular space via unconventional protein secretion (1.7.3). To test the hypothesis, that an unconventional protein secretion process mediates the release of tau in both physiological and pathological conditions. One way tau can be secreted into the extracellular space is by direct translocation across the plasma membrane using sulphated proteoglycans such as HSPGs (Katsinelos et al., 2018; Merezhko et al., 2018) (discussed in detail in 1.7.3.1). Sulphated proteoglycans are highly abundant in the plasma membranes of neurons and have an emerging role in the regulation of axonal guidance, neuronal connectivity and synapse development (see review by Condomitti et al., 2018). There are numerous studies showing that tau can bind to sulphated proteoglycans pre-and post-synaptically (Holmes et al., 2013; Katsinelos et al., 2018; Merezhko et al., 2018; Rauch et al., 2018). Specifically, HSPGs have been shown to play an important role in the spread of tau pathology in neuronal networks (Holmes et al., 2013; Rauch et

al., 2018). Given that HSPGs have been associated with re-uptake of pathogenic tau species (Raunch et al., 2018; Holmes et al., 2013), it is possible that tau can also be secreted in this way. Indeed, pharmacological inhibition surface HSPG biosynthesis, using sodium chlorate and heparinase III, has been shown to be effective in reducing tau secretion in primary hippocampal neurons and immortal cell lines (Katsinelos et al., 2018; Merezhko et al., 2018). Although there is evidence showing that hyperphosphorylated tau proteins are secreted preferentially via HSPG-mediated direct translocation across the plasma membrane (Katsilenos et al., 2018), it is unclear how neuronal activity play a role in this process.

In line with previous findings (Pooler et al., 2013; Yamada, 2017), we showed that tau can be secreted by cultured hippocampal neurons in physiological conditions; and that in pathological conditions, pseudo-hyperphosphorylated tau (Tau^{E14}) proteins are preferentially secreted by neurons. However, it remains to be investigated whether neuronal activity may affect the secretion propensities of different tau variants and what mechanisms are used to mediate the release of different tau variants in health and disease.

If neuronal activity does indeed enhance the propagation of tau pathology (Wu et al., 2016), then one would assume that the release of mutant tau forms are also accelerated. Given that there are increasing evidence for the role of sulphated proteoglycans in mediating the spread of tau pathology (Holmes et al., 2013; Katsinelos et al., 2018; Merezhko et al., 2018; Rauch et al., 2018), we speculated whether it may also be involved in activity-dependent secretion of tau. Based on these observations, we hypothesised that neuronal activity may be a key driver for tau secretion propensities and that mutant tau forms of tau may be preferentially secreted during enhanced neuronal activity. In certain conditions, the presence of sulphated proteoglycans may therefore enhance the secretion of pathogenic tau seeds and therefore accelerating tau propagation.

5.1.1 Aims:

- Using the NanoBiT-Tau biosensor, we investigated how neuronal activity affects the secretion of wild-type and mutant in primary neurons. Neurophysiological properties of neurons expressing WT and mutant tau were measured at basal and stimulated conditions using whole-cell patch clamp. As a proof-of-concept, pharmacological agents were firsts tested to ensure that the desired effect in neuronal activity is induced. Passive and activate intrinsic properties were measured.
- To elucidate the molecular mechanisms involved in the secretion process of wild-type and mutant tau in primary hippocampal neurons, the cell surface expression of sulphated proteoglycans was reduced using sodium chlorate ($NaClO_3$). We tested how ablation of cell surface sulphated proteoglycans affect activity-dependent secretion.

5.2 Proof-of-concept: pharmacological stimulation of neuronal activity

5.2.1 Can potassium chloride enhance neuronal activity in cultured neurons?

The ability of commonly used pharmacological agents to induce neuronal activity were assessed in cultured primary hippocampal neurons using whole-cell patch clamp electrophysiology. Acute application of 50 mM potassium chloride (KCl) has been a standard practice for enhancing neuronal activity via depolarisation-driven process in cultured neurons (Pooler et al., 2013; Ismael et al., 2021; Sorkolov et al., 2015). Elevated extracellular KCl leads to the depolarisation of the membrane due to increased concentration of potassium ions entering the cell. This activates L-type voltage sensitive calcium channels (L-type VSCCs) leading to an influx of calcium (see review by Rienecker et al., 2020). Calcium influx mediated by L-type VSCCs, activates multiple downstream signalling processes such as the activation of calmodulin kinase, mitogen activated protein kinase and calcineurin pathways. These then activates CREB-mediated transcription of activity-regulated genes eventually leading to an increase in neuronal activity (Rienecker et al., 2020).

5.2.1.1 Passive intrinsic membrane properties of neurons

To demonstrate whether acute 50 mM KCl treatment stimulates neuronal activity, passive intrinsic membrane properties were measured with ACSF (vehicle) at normal physiological levels of KCl (2.4 mM KCl), or after the immediate addition of additional 50 mM KCl. Passive membrane properties that were recorded include input resistance, series resistant, leak currents at -70 mV, and resting membrane potential (RMP). To describe briefly, input resistance helps determine the size and maturity of the cell and the permeability of ion channels. The series resistance, which indicate the sum of all resistances between the amplifier and the cell, provides an indication of the quality of the patch. Data obtained for series resistance (not shown) was used as a quality control. Leak current is the amount of current injection required to hold a cell at a given membrane potential.

As expected, the input resistance of cells treated with 50 mM KCl showed significant reduction when compared to vehicle ($p = 0.0346$; Figure 45A). Considering that the cells are all the same maturity, this reduction in input resistance may suggest that KCl-treated cells have higher ionic movements. Furthermore, the leak current at –70 mV in KCl-treated cells was also more negative when compared to vehicle ($p = 0.0032$); Figure 45B), with a leak current of -1515 pA ± 210 pA. In contrast, the average leak current in vehicle was -70 pA ±- 13 pA. KCl application also significantly increased the RMP of cells ($p= 0.0005$; Figure 45C), indicating membrane depolarisation, with an average membrane potential of -9.38 mV ± 2.23 mV.

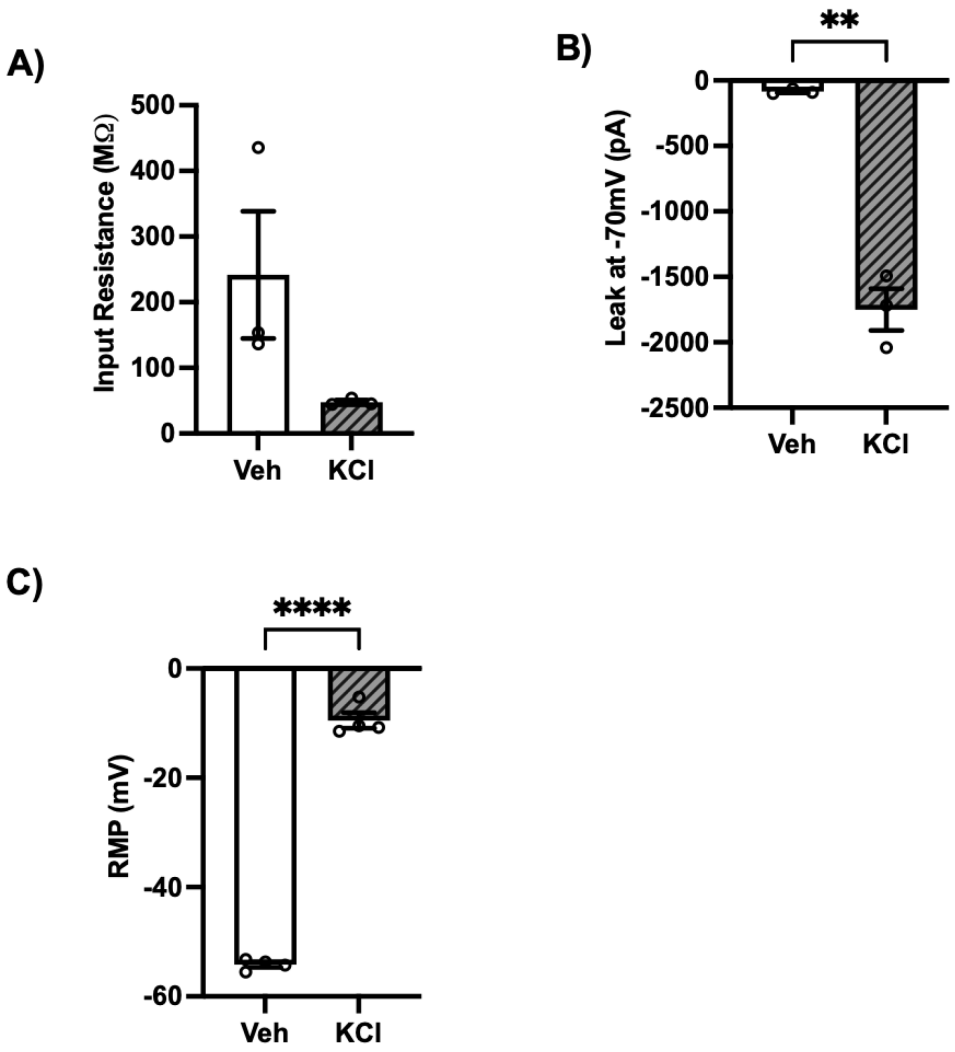

Figure 45. Passive electrical properties of hippocampal neurons after acute 50 mM KCl treatment.

Whole-cell patch clamp experiments of DIV13-15 cultured hippocampal neurons acutely treated (0 - 1 hour) with or without 50 mM KCl. A) Input resistance, B) Leak currents at –70 mV, and C) resting membrane potential (RMP) between vehicle and KCl-treated cells. Application of 50 mM KCl leads to significant changes in passive membrane properties. There is a significant difference in leak currents at -70mM (p = 0.0032; paired t-test, N=3) and RMP (p = 0.0005; paired t-test, N=3) between vehicle and KCl treated cells. $p^{**} < 0.01$, $p^{****} < 0.001$.

5.2.1.2 Changes in active membrane properties upon KCl treatment

To demonstrate that active membrane properties are modified with KCl treatment, the rheobase and the firing frequency before and after treatment were measured. Current injection up to 500 pA did not elicit the firing of action potentials in cells exposed to high KCl (Figure 46A-B). In contrast, control neurons fired action potentials in response to current injections of between 25 pA to 150 pA. To test whether action potentials can be elicited at higher current injections, a stimulus of up to 2.25 nA was applied to cells (Figure 46A-B). Again, KCl-treated cells did not fire any action potentials (Figure 46C-D). However, if the RMP of a KCl-treated cell is corrected to – 70 mV prior to the current injections, KCl-treated cells were able to generate a single action potential for each current injection step (Figure 47A-B). In contrast, vehicle demonstrated a higher number of action potential generated (Figure 47C-D). Furthermore, spontaneous activity was visible in vehicle conditions, where the RMP remained stable and between –70 mV to –60 mV. However, after the addition of 50 mM KCl, spontaneous activity was halted and the RMP became depolarised (Figure 48).

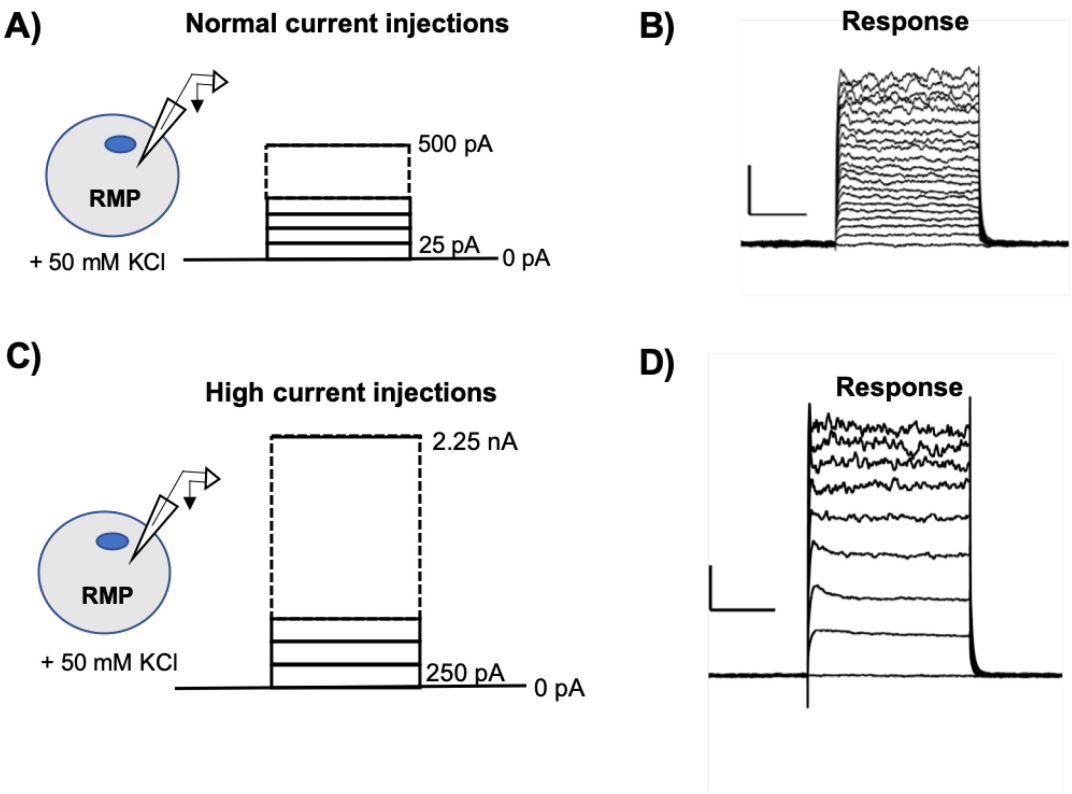

Figure 46 Different current injections to generate action potential in cells treated with or without 50 mM KCl.

A-B) Current injection steps of 25 pA applied to cells up to 500 pA to obtain a rheobase value at the cell's normal RMP. C-D) Higher current injection steps of 250 pA applied to cells up to 2.25 pA to obtain rheobase at maximum current whilst cells are held in their normal RMP. The trace is representative from 3 individual cells (T=3). Scale bar = 100 ms, 20 mV. These recordings were carried out by Hannah Warming and analysed by myself.

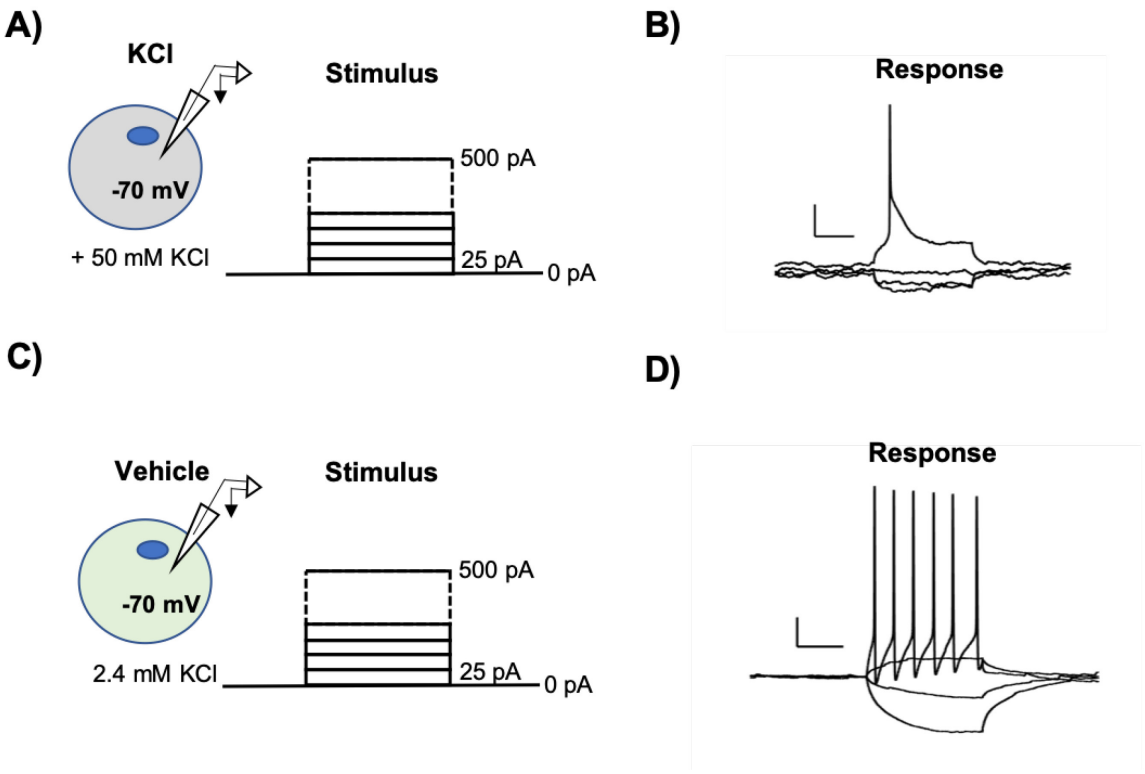

Figure 47 Response to current injections when cell's RMP is held at -70 mV with or without 50 mM KCl.

Increasing current injection steps of 25 pA were applied to cells up to 500 pA to obtain the rheobase value. The RMP of each cell was held at -70 mV prior to current injections. A-B) The stimulus and response given from cells treated with 50 mM KCl. C-D) The stimulus and the response from vehicle cells, which demonstrate greater number of action potentials. The trace is representative from 3 individual cells (T=3). Scale bar = 100 ms, 20 mV. These recordings were carried out by Hannah Warming and analysed by myself.

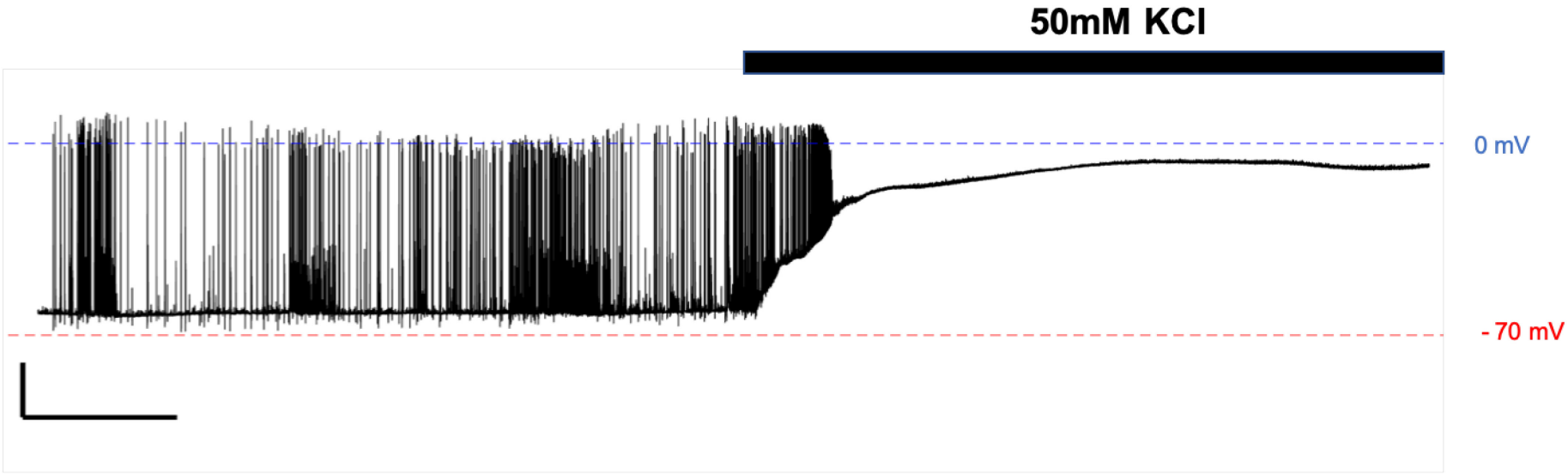

Figure 48. Acute application of KCl elevates the resting membrane potential.

Primary hippocampal neurons demonstrate spontaneous activity in basal conditions. The addition of 50 mM KCl resulted in depolarisation of the resting membrane potential but an increase in the number of action potential was not recorded. Scale bar = 100 sec, 20 mV. Representative image taken from one of 10 individual cells (T=10) recorded from across 3 biological repeats (N=3).

5.2.1.1 A brief conclusion and discussion for the use of KCl to elevate neuronal activity

High concentrations of KCl have been widely used to induce neuronal depolarisation in a wide range of tau release studies (Ismael et al., 2021; Pooler et al., 2013; Yamada et al., 2014). In this study, application of 50 mM KCl in the extracellular space of neurons led to membrane depolarisation but did not increase the number of action potentials generated by neurons. Although depolarisation of the membrane potential (RMP shifted to -10 mV) was accomplished, acute KCl application immediately silenced spontaneous activity of cultured primary hippocampal neurons. This may be explained by that fact that at -10 mV of RMP, there is persistent inactivation of sodium voltage-gated ion channels, which subsequently enters the cell in the refractory period where it is unable to fire any action potentials.

Furthermore, other passive intrinsic membrane properties such as input resistance and leak current were also altered in KCl treatment. Lower input resistance suggests that there is greater membrane conductance occurring in KCl-treated cells. Lower leak current could suggest the following: 1) the ion channels in KCl-treated cells could be more permeable which may explain the change in input resistance, 2) the membrane integrity of KCl-cell could be impaired allowing ions to leak through the membrane, and 3) a greater amount of negative current is required to maintain the cell at –70 mV; this is explained by the fact that the RMP of KCl-treated cells were more positive, so naturally would require more current injections to maintain RMP at -70 mv. These changes in passive intrinsic properties may reflect on why KCl-treated cells demonstrated lower excitability and why the generation of action potentials are impaired.

Although elevated extracellular KCl is a method widely used to induce global membrane depolarisation in cultured neurons, our electrophysiological data showing altered passive and active intrinsic properties, suggests that it may be a poor representative of what happens *in vivo*. There are also the questions of cell health. Studies have shown that cells treated with 50 mM KCl has no effect in cell viability *in vitro* (Ismael et al., 2021; Pooler et al., 2013), however these studies did not assess the electrophysiological properties of cultured neurons. Lactate dehydrogenase, which was widely used to measure membrane integrity and cell viability, does not necessarily provide a good indication of membrane properties. This shows the importance of assessing electrophysiological properties of cells when subjected to pharmacological manipulation.

5.2.2 Gabazine-mediated stimulation of neuronal activity

As application of KCl did not elicit an increase in action potential in cultured mature hippocampal neurons, we next targeted γ-Aminobutyric acid type A ($GABA_A$) receptors, which are pentameric ionotropic ion channels that typically generate inhibitory currents in adult pyramidal cells (Sigel and Steinmann, 2012). Gabazine, which is a selective and competitive antagonist of $GABA_A$ receptors, reduces network inhibition, and therefore enhance neuronal activity in cultured neurons (Sigel and Steinmann, 2012; Xue et al., 2010). $GABA_A$ receptors are permeable to chloride ions; they are the main inhibitory receptors found in the central nervous system, and modulate excitatory activity of neurons (Sigel and Steinmann, 2012). $GABA_A$ receptor blockade using gabazine results in allosteric inhibition in channel opening that leads to a reduction in membrane permeability to chloride ions. This therefore attenuates GABA-mediated synaptic inhibitory inputs to neurons causing enhanced excitation in cultured neurons (Sigel and Steinmann, 2012).

The effects of gabazine were tested as another alternative stimulant. In order to detect activity-dependent tau secretion, I first determined whether gabazine application can elicit the desired response that elevated KCl treatment could not, which is to induce an increase in neuronal activity. Furthermore, establishing the time-dependent effects of gabazine in primary neurons would help determine the length of time required to collect secreted tau in the conditioned media in stimulated conditions.

To test whether the release of tau into the extracellular space is modulated by neuronal activity we first determined the effects of gabazine exposure in primary neurons. Two range of time-points of gabazine exposure were tested: 0-6 hours and 16 hours. Passive and active intrinsic membrane properties were recorded as previously described to determine if gabazine altered these measures of cell function. In addition, TTX, a voltage-gated sodium channel blocker, was also used to inhibit action potentials.

5.2.2.1 Gabazine application does not alter the passive and active membrane properties of primary hippocampal neurons

Our results showed that 0-6 hours and 16-hours exposure to 3 µM gabazine treatment did not affect the passive membrane properties of recorded neurons (Figure 49). No significant differences in RMP between vehicle and gabazine-treated cells was found after 0-6 hours of treatment ($p = 0.3580$) and at 16 hours ($p = 0.4815$) (Figure 49C). However, gabazine-treated cells showed a more negative leak current at -70 mV when compared to vehicle at 0-6 hours of treatment ($p = 0.0211$; Figure 49B). In 0-6 hours gabazine exposure, vehicle had an average leak current of -70.39 pA ± 21.43 pA, whereas gabazine-treated cells had -108.71 pA ± 20.73 pA. The

difference in leak current is lost between gabazine and vehicle after 16 hours of treatment ($p > 0.9999$; Figure 49B). These results suggest that gabazine-treated cells require greater current injections to keep their membrane potential at –70 mV, but that the effect is temporary. A more negative leak current could suggest that gabazine alters membrane conductance.

The rheobase of vehicle and gabazine-treated cells were also determined at by injecting step currents of 25 pA up to 500 pA, whilst in their normal physiological membrane potential (Figure 50A-C). The rheobase were recorded at different time-points of treatment; the results show no significant differences between vehicle and gabazine-treated cells after 0-6 hours ($p=0.8282$) and 16 hours ($p=0.4632$) treatments (Figure 50A).

5.2.2.2 The firing frequency of cells are increased upon gabazine application

To determine the level of activity in neurons, the number of action potentials were assessed before and after application of gabazine (represented as firing frequency, in Hertz). After 0-6 hours of gabazine exposure, a significant increase in the number of action potentials ($p = 0.0293$) were observed when compared to vehicle (Figure 51A,B). At 16 hours of gabazine treatment, there was no longer a significant difference in frequency between vehicle and gabazine-treated cells ($p>0.9999$; Figure 51A,C). This suggests that the increase in frequency is time-dependent and returns to baseline. The average firing frequency in vehicle remained consistent at both time-points. Representative samples of the number of action potential fired by cells can be seen in the traces presented in Figure 51B,C. These findings showed that acute 6 hours of gabazine treatment is sufficient in stimulating an increase in neuronal activity in cultured primary neurons, but the effect may be lost by 16 hours of exposure. This suggests that homeostatic scaling could be occurring in these neurons.

At basal levels, cultured hippocampal neurons demonstrated spontaneous activity which is enhanced with the addition of gabazine (Figure 52A). This enhancement is seen at onset of gabazine perfusion, and sustained throughout the recording. In contrast, application of 500 nM TTX inhibit all activity (Figure 52B). Prior to the addition of TTX, patched cells demonstrated spontaneous activity, and as expected this is immediately inhibited after the addition of TTX into the recording bath chamber (Figure 52B) indicating proof-of-concept. TTX can therefore be used as a negative control for assessing activity-dependent tau release.

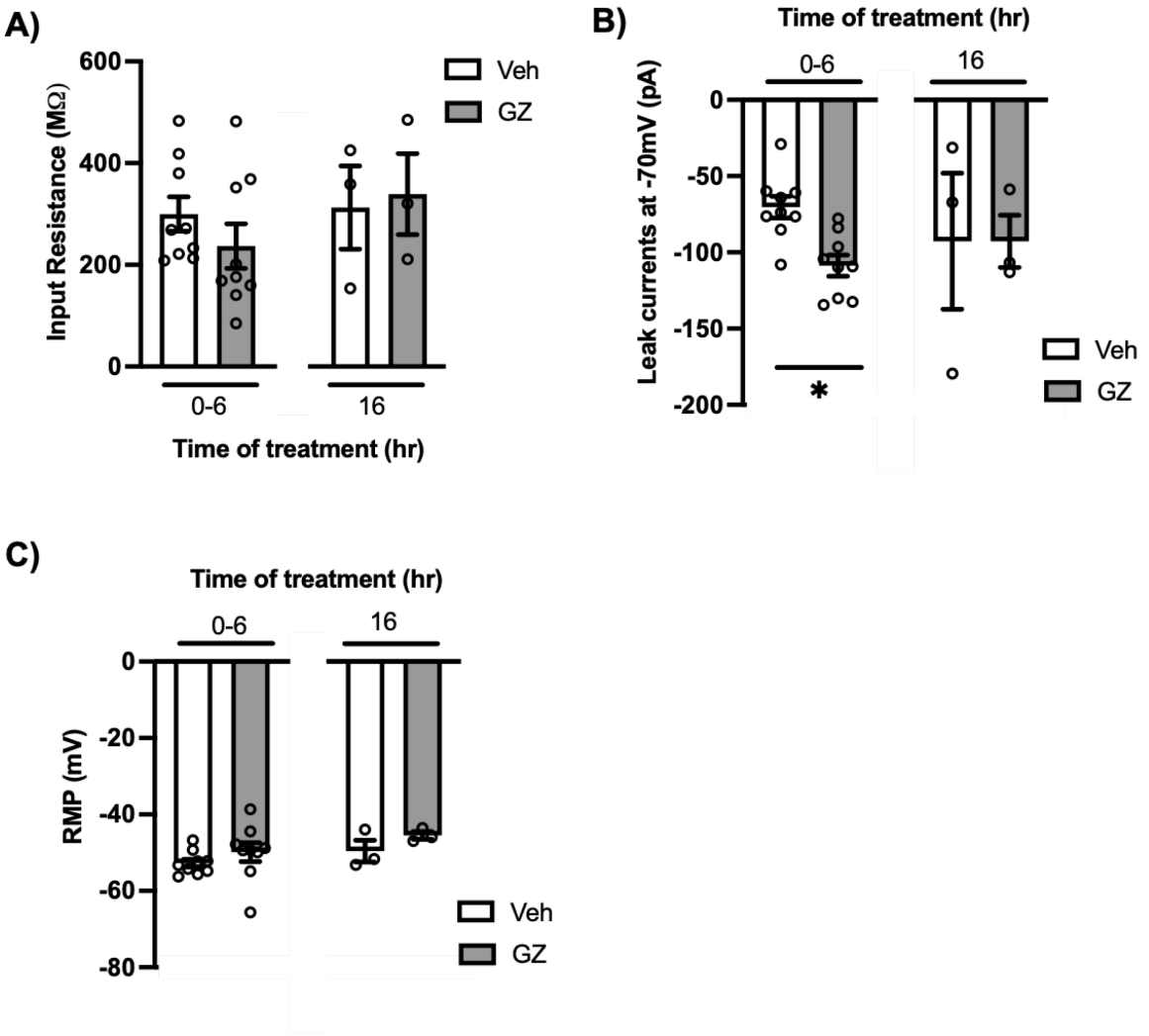

Figure 49. Passive intrinsic properties of neurons treated with acute and chronic gabazine.

Whole-cell patch clamp recordings of hippocampal neurons treated with or without 3 µM gabazine (GZ) at two different time points: 0-6 and 0-16 hours analysed to measure (A) input resistance, (B) leak currents at –70 mV, and (C) resting membrane potential (RMP). There was no significant difference in input resistance and RMP between vehicle and gabazine at both time points. There was a significant difference between vehicle and gabazine at 0-6 hours ($p = 0.0211$; repeated measures two-way ANOVA, followed by Sidak's multiple comparisons test; $p^* < 0.05$, N=9 (6 hours), N=3 (16 hours).

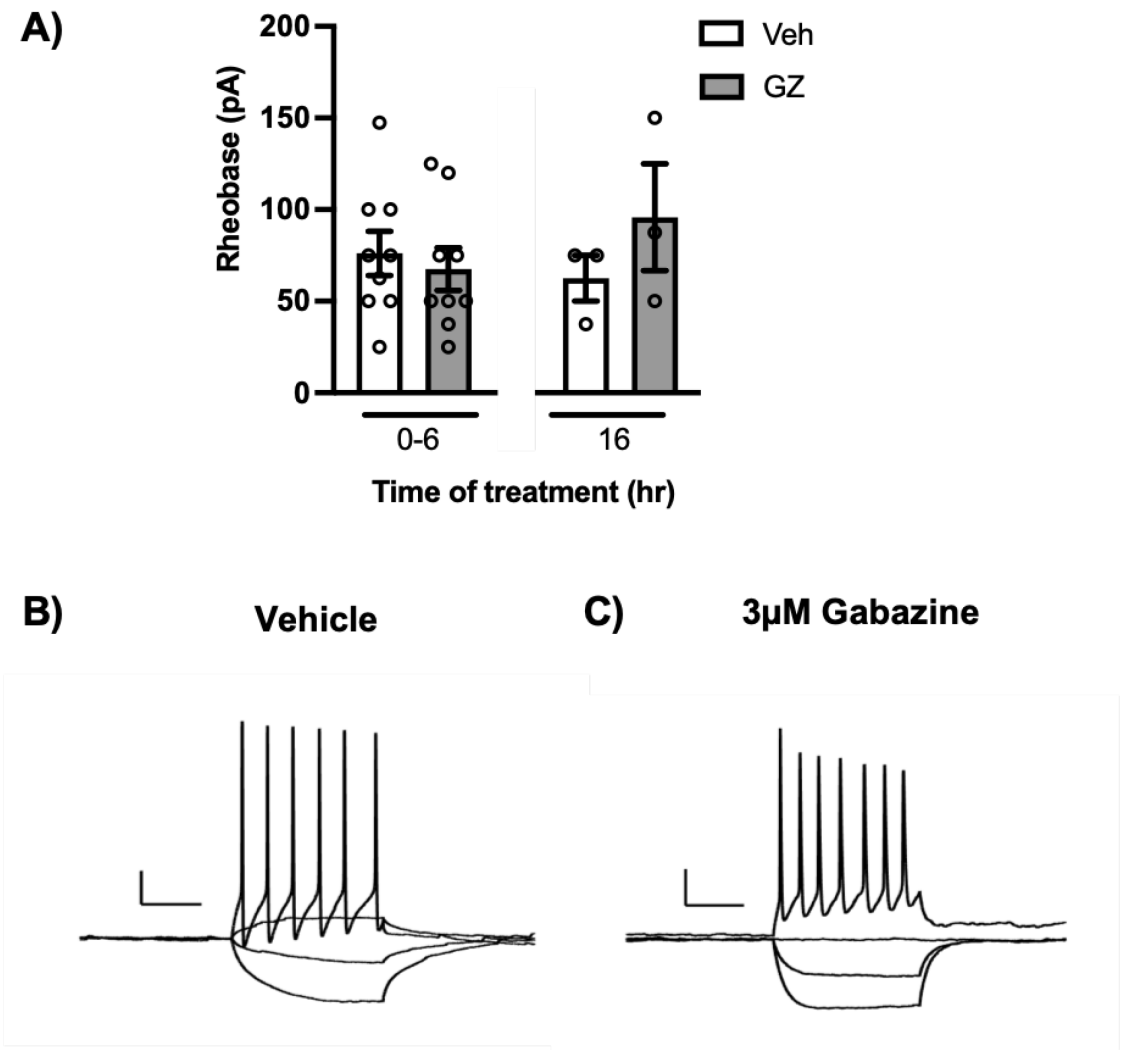

Figure 50 Rheobase of cultured hippocampal neurons with or without gabazine treatment.

Whole-cell patch clamp recordings in current-clamp mode was used to assess the minimal current required to induce an action potential at infinite duration between vehicle and gabazine-treated cells. A) Rheobase of patched cells with or without treatment of 3 μM gabazine (GZ) at selected time points:0-6 and 16 hours. B-C) example traces of cell spiking during current injection steps in vehicle and gabazine-treated cells. There is no significant difference in the rheobase between vehicle and gabazine-treated neurons at 0-6 hours ($p=0.8282$) and 16 hours ($p=0.4632$) treatment. Repeated measures two-way ANOVA, followed by Sidak's multiple comparisons test; N=9 (6 hours), N=3 (16 hours). Scale bar= 50 ms, 20 mV.

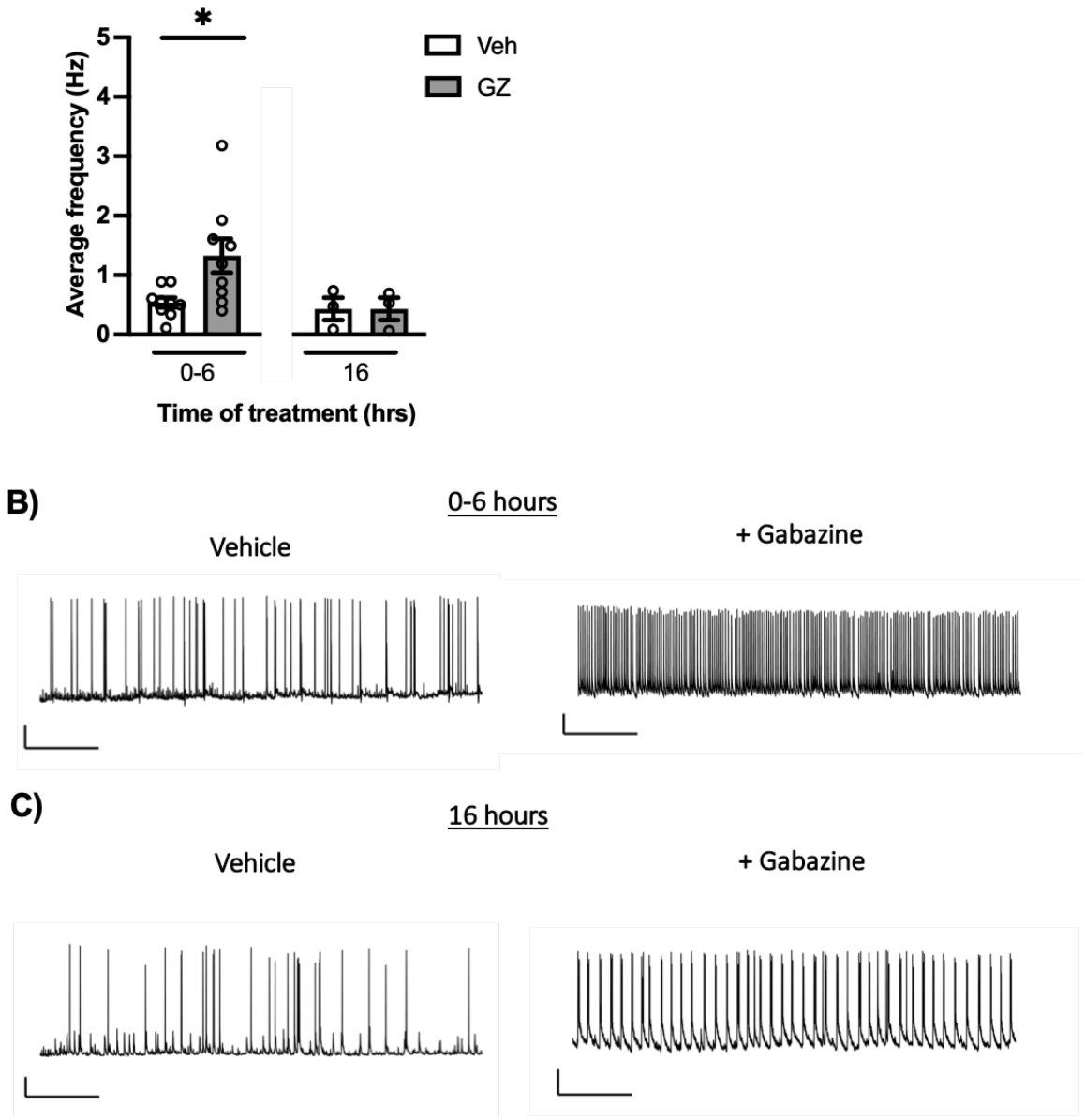

Figure 51. Gabazine application induced a time-dependent increase in neuronal activiy. Whole-cell patch clamp recordings of DIV13-15 hippocampal neurons in current-clamp mode. A) Differences in the average firing frequency during 0-6 and 16 hours of gabazine treatment. B-C) Representative traces of hippocampal neurons recorded with or without gabazine (GZ) treatment, taken from 5 minute recordings. Gabazine treament for 0-6 hours led to a significant increase in the average firing frequency (Hz) ($p = 0.0293$). Repeated measures two-way ANOVA, followed by Sidak's multiple comparisons test; $p^* < 0.05$, N=9 (6 hours), N=3 (16 hours). Scale bar= 50 ms, 20 mV.

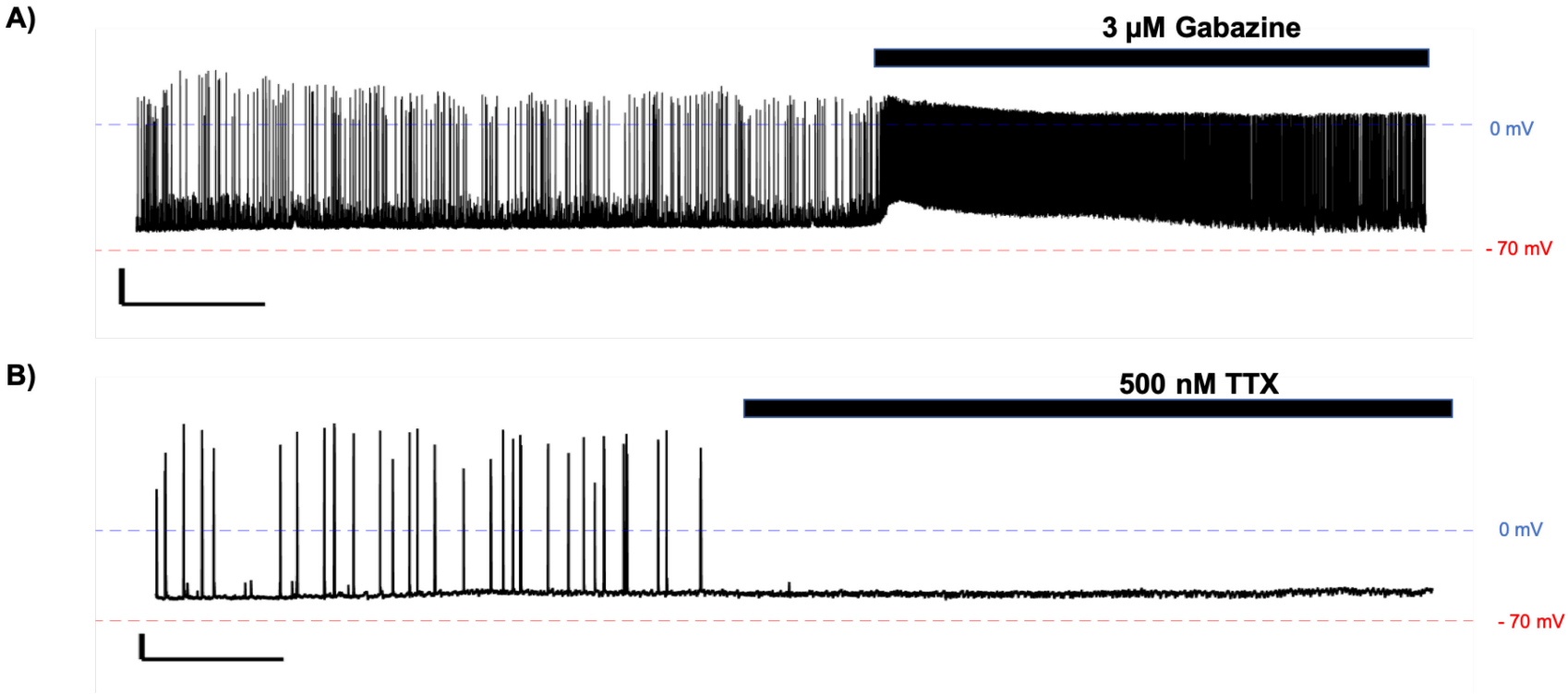

Figure 52. Modulation of neuronal activity in cultured primary hippocampal neurons using gabazine and TTX.

Whole-cell patch clamp recordings in current-clamp mode showing 15-minute trances of spontaneous and gabazine-induced neuronal activity. Primary hippocampal neurons demonstrate spontaneous activity in basal conditions. Application of 3 µM gabazine and 500 nM lead to an increase in the firing of action potentials, whereas 500 nM TTX lead to inhibition of spontaneous activity. A) Representative trace indicating before and after the application of 3 µM gabazine. B) The effect of the application of 500 nM TTX in spontaneous activity. Representative images taken from neurons treated with gabazine (T=12, N=3) and with TTX (T=3). Scale bar = 100 sec, 20 mV.

5.2.2.3 A brief conclusion and discussion on the use of gabazine to stimulate neuronal activity

As characterised by others, acute application of gabazine can stimulate neuronal activity. Gabazine exposure induced an immediate increase in the number of action potential which was sustained after 0-6 hours of gabazine application. Blockage of $GABA_A$ receptors resulted in the sustained phasic and tonic inhibition of $GABA_A$ receptors, which subsequently led to global reduction in inhibitory inputs in neurons. After prolonged exposure to gabazine (for 16 hours), homeostatic regulation of neuronal activity becomes activated causing no further increase in neuronal firing. This is not surprising as neurons are known to have homeostatic plasticity and can change neuronal activity patterns in response to a specific stimulus (Mody, 2005). The mechanisms involved in homeostatic synaptic plasticity, or 'synaptic scaling' remain to be determined. However, it has been suggested that neurons can alter the ion-channel properties, particularly voltage-dependent conductance, or by number or properties of ionotropic and metabotropic receptors that mediate synaptic transmission (Jarvis and Zamponi, 2007; Turrigiano and Nelson, 2000). Activation of homeostatic plasticity may therefore explain the differences in activity at 0-6 and 16-hour time-points.

To summarise, 0-6 hours of gabazine exposure induced the greatest increase in neuronal activity. To get the best chance of monitoring any difference in activity-dependent secretion of wild-type and mutant tau in hippocampal neurons, we decided to expose cells in this time-frame.

5.3 Activity-dependent secretion of wild-type and mutant tau

5.3.1 Passive and active intrinsic properties of wild-type and mutants tau-expressing neurons

Firstly, to ensure that any electrophysiological changes are due to pharmacological treatments and not because of differences in tau variant expressed by neurons, the passive and active intrinsic membrane properties of neurons expressing HiBiT-Tau^{WT}, HiBiT-Tau ^{E14} and HiBiT-Tau^{P301L} at basal conditions were assessed. The input resistance and leak currents at -70 mV between the tau variants were similar and did not show significant differences (Figure 53A,B). The RMP of cells expressing HiBiT- Tau^{WT}, HiBiT- Tau^{E14} and HiBiT- Tau^{P301L} were similar and no differences were found (Figure 53C). Furthermore, the rheobase of cells expressing wild-type and mutant cells in unstimulated conditions were also similar to each other and did not show significant differences, suggesting that active membrane properties are also not altered by expression of mutant tau forms (Figure 53D).

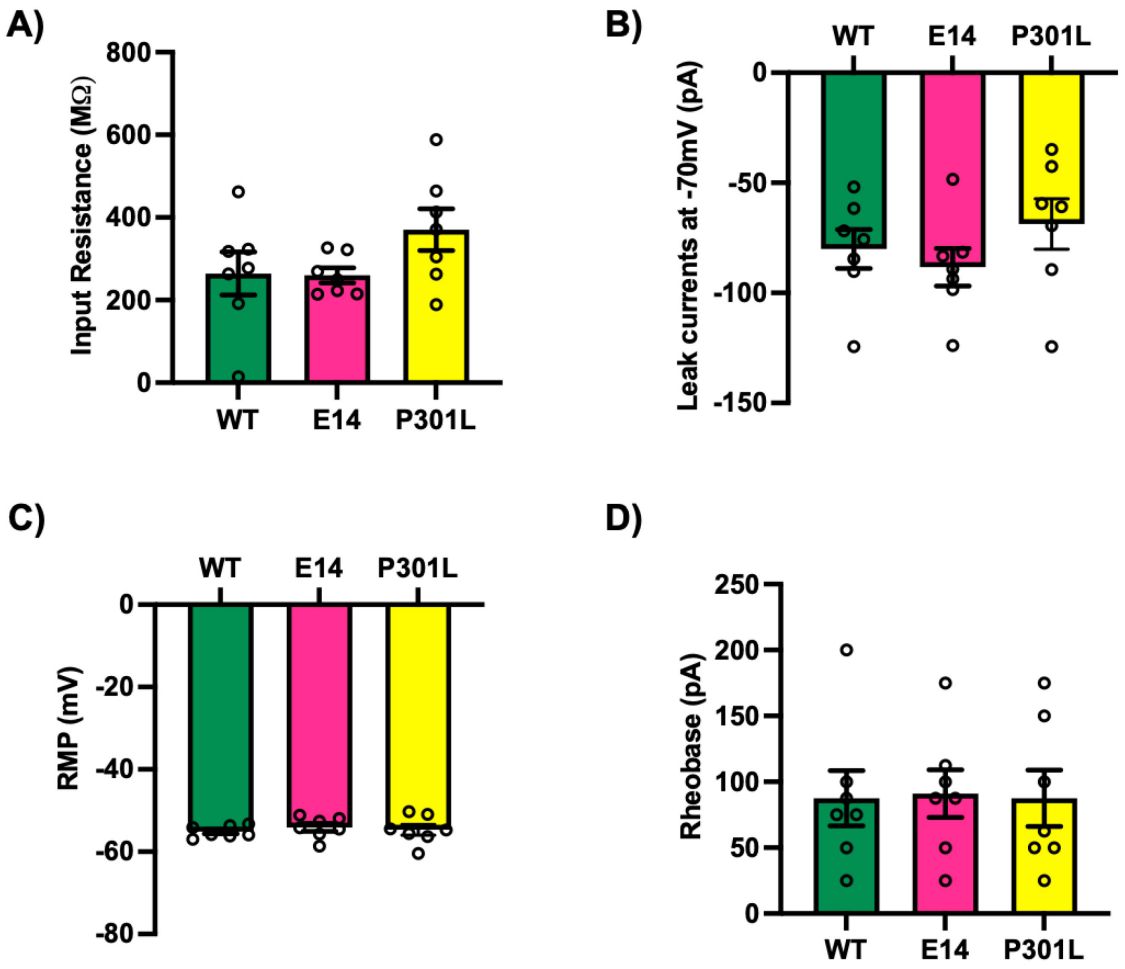

Figure 53. Passive and active intrinsic properties of neurons expressing wild-type and mutant tau in unstimulated conditions.

Primary hippocampal neurons were transduced with lentiviruses to induce the expression of HiBiT-Tau^{WT}, HiBiT-Tau^{E14} and HiBiT-Tau^{P301L}. At DIV13-16, whole-cell patch clamp recordings were used to record difference in passive and active membrane intrinsic properties in basal conditions. A) Input resistance, B) leak currents at -70mV, C) Resting membrane potential (RMP) and D) rheobase from cells are not altered by expression of different tau variants. Repeated measures one-way ANOVA, followed by Uncorrected Fisher's LSD test; N=7.

5.3.2 Gabazine increases the activity of HiBiT-Tau^{WT} and HiBiT-Tau ^{E14} expressing neurons

Before investigating the differential tau secretion between tau variants, I first established whether gabazine can induce an increase in activity in cultured primary hippocampal neurons after 0-6 hours exposure. Using whole-cell patch clamped, the frequency of action potentials generated by neurons expressing HiBiT-Tau^{WT} and HiBiT-Tau ^{E14} were assessed before and after 0-6 hours of gabazine exposure. As the HiBiT-Tau^{WT} and HiBiT-Tau ^{E14} were the conditions that showed similar protein expression when cell lysates of cells expressing HiBiT-Tau^{WT} and HiBiT-Tau ^{E14} were assessed by western blot, they were the only conditions compared in this sub-section.

Baseline measurements were taken to compare the level of spontaneous activity in HiBiT-Tau^{WT} and HiBiT-Tau ^{E14} -expressing neurons prior to stimulating neuronal activity with gabazine. Conditions without gabazine were referred to as 'vehicle' from now on. At baseline, HiBiT-Tau^{WT}-expressing neurons were significantly more active than HiBiT-Tau^{E14} cells ($p = 0.0366$); the average firing frequency of HiBiT-Tau^{WT}-expressing neurons were 2-fold higher than HiBiT-Tau ^{E14} (Figure 54A,B,D). In addition, although the significant difference is lost between HiBiT-Tau^{WT} and HiBiT-Tau ^{E14} in stimulated conditions ($p = 0.0735$), on average the frequency in HiBiT-Tau ^{E14} neurons (0.69 Hz ± 0.46 Hz) (Figure 54A,C,E) were still lower when compared to HiBiT-Tau^{WT} neurons (0.94 Hz ± 0.69 Hz). The trend to significance may suggest that mutant tau neurons may be less active than WT (Figure 54C,E).

Our results show that 0-6 hours gabazine exposure leads to significant increase in neuronal firing in neurons expressing HiBiT-Tau^{WT} ($p = 0.0241$; Figure 54A,B-C).) and HiBiT-Tau ^{E14} ($p = 0.0127$; Figure 54D-E) when compared to baseline measurements.

To conclude, these results indicate that application of gabazine for 6 hours was chosen as the time-point to stimulate neurons as it led to an immediate and sustained increase in firing frequency in cultured hippocampal neurons

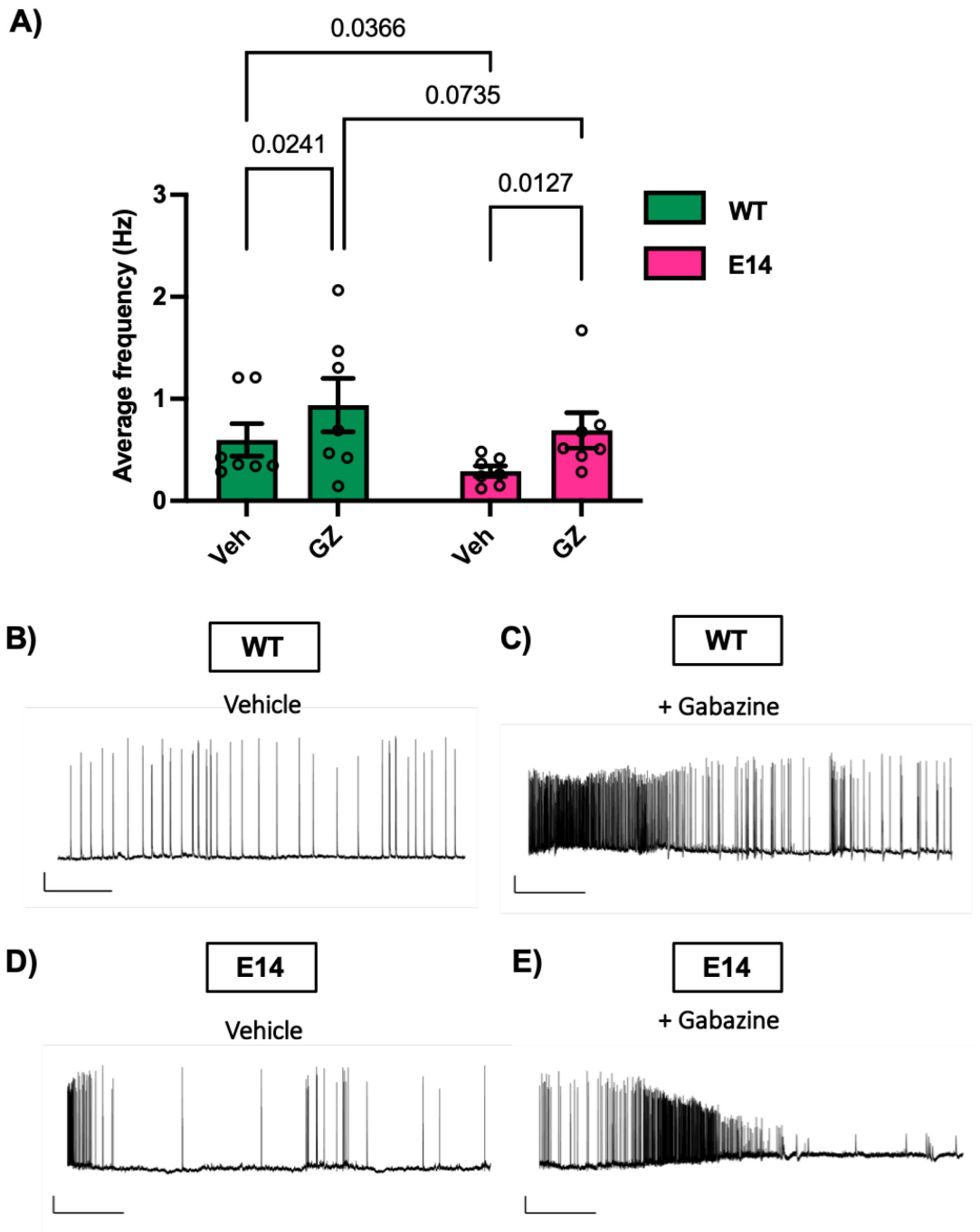

Figure 54. Average firing frequency between HiBiT-Tau^{WT} and HiBiT-Tau^{E14} before and after gabazine application

Whole-cell patch clamp recordings of DIV13-15 hippocampal neurons in current-clamp mode. A) Average firing frequency before (vehicle) and after 0-6 hours of 3 µM gabazine (GZ) exposure in cultured hippocampal neurons expressing HiBiT-Tau^{WT} and HiBiT-Tau^{E14}. B-C) Representative recordings from expressing HiBiT- Tau^{WT} before and after gabazine treatment. D-E) Representative recordings from cells expressing HiBiT-Tau^{E14} with or without gabazine. Repeated measures two-way ANOVA, followed by Uncorrected Fisher's LSD test; N=7.

5.3.2.1 Action potential properties of cells expressing Tau^{E14} is altered during neuronal activity

Whole-cell patch clamp recordings before and after gabazine exposure indicated some differences in the action potential properties in cells expressing WT and mutant tau. To further explore why there is a difference in firing frequency at basal and stimulated conditions, I further assessed the properties of cells expressing HiBiT-Tau^{E14} and HiBiT-Tau^{WT} in vehicle and stimulated conditions. To do this, peak and amplitude action potentials were assessed in these neurons before and after application of gabazine (Figure 55A). Briefly, the peak potential was defined as the point in which the membrane potential reaches its maximum and depolarisation. The maximum amplitude of each action potential, which was considered as total height of the membrane potential, taken from the RMP to the peak.

Application of gabazine reduced the average peak potential in cells expressing HiBiT-Tau^{E14} when compared to vehicle ($p = 0.0442$, Figure 55B). In contrast, the average peak potential ($p = 0.1704$) was unchanged in HiBiT-Tau^{WT} cells after gabazine application. Similar findings were observed when action potential amplitudes were assessed. The action potential amplitude was significantly decreased in HiBiT-Tau^{E14} during stimulation ($p = 0.0070$) when compared to vehicle (Figure 55C) whereas the amplitude of HiBiT-Tau^{WT} was unaffected ($p = 0.5339$; Figure 55C). Differences in average peak and amplitude potentials between HiBiT-Tau^{WT} and HiBiT-Tau^{E14} were also compared in stimulated conditions. HiBiT-Tau^{E14} cells demonstrated lower maximum amplitude potentials when compared to HiBiT-Tau^{WT} in the gabazine conditions ($p = 0.0128$ comparison not shown in graph). These findings show that action potential properties are altered in HiBiT-Tau^{E14}-expressing neurons in stimulated conditions.

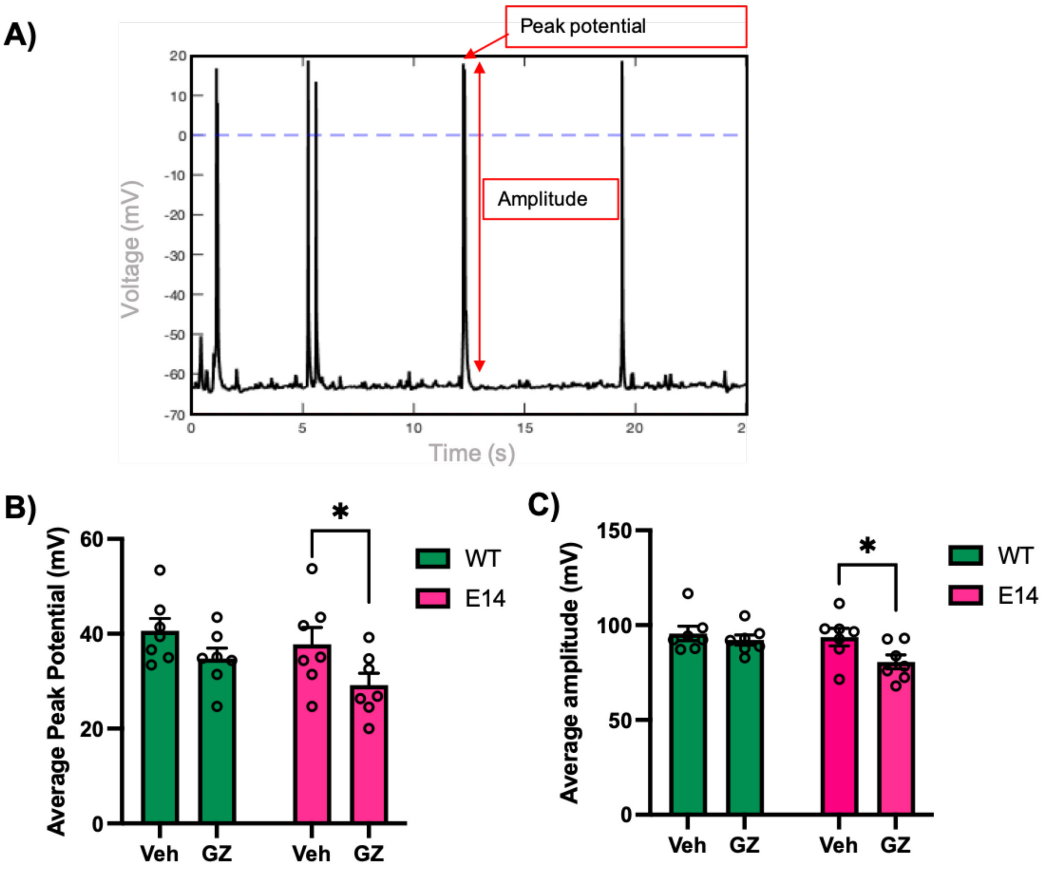

Figure 55 Average peak potential and amplitude of neurons expressing tau variants in GZ treatment.

A) Schematic diagram of how peak potentials and amplitudes are measured for each individual action potential in a recording. The peak potential (B) and action potential amplitude (C) were obtained for all recordings of cells expressing different tau variants. Peak potential ($p = 0.0442$) and action potential amplitude ($p = 0.0070$) was significantly decreased in HiBiT-Tau^{E14} upon stimulation. Peak potential ($p = 0.1704$) and action potential amplitude ($p = 0.5339$) showed no significance between vehicle and GZ-treatment in HiBiT-Tau^{WT}. Repeated measures two-way ANOVA, followed by Uncorrected Fisher's LSD test; $p^* < 0.05$, N=7.

5.3.3 Neuronal activity modulates the secretion of wild-type and mutant tau

Based on the findings so far, neuronal stimulation enhances the firing of action potentials in HiBiT-Tau^{WT}- and HiBiT-Tau ^{E14}-expressing cultured neurons. To determine whether WT and mutant tau secretion is activity-dependent, primary hippocampal neurons expressing the different HiBiT-tau variants were pre-treated with gabazine and TTX for 6 hours (described in detail in 2.8). The NanoBiT-Tau biosensor was employed to assess the level of secreted membrane-free tau in the extracellular space in stimulated and inhibited conditions.

Our findings showed that enhancing neuronal activity increases the secretion HiBiT-Tau^{WT} ($p = 0.0434$; Figure 56A). Similarly, increasing neuronal activity in HiBiT-Tau^{E14} neurons, can also lead to elevated levels of tau in the conditioned media, which was trending to significance ($p = 0.0586$; Figure 56B). In contrast, blocking neuronal activity with TTX did not change the level HiBiT-Tau^{WT} ($p = 0.6262$) and HiBiT-Tau^{E14} ($p = 0.9115$) detected in the extracellular space when compared to baseline (vehicle). These findings indicate that neuronal activity blockade is not enough to completely inhibit the secretion of tau. Therefore, non-activity dependent secretion pathways may be involved in this process.

To confirm whether the tau detected in the conditioned media is secreted via activity-dependent processes, as opposed to the release of intracellular tau from cellular damage, a cell viability assay was also performed following the tau secretion assay (as described in section 2.8.4.). Calcein Blue AM, which is a cell-permeant esterase substrate, was used to detect intracellular esterase activity and therefore served as a probe for cell membrane integrity and viability in cells. In healthy and viable conditions, Calcein Blue substrates are retained within cells and react with intracellular esterases, leading to the generation of a strong fluorescent signal. Dead cells lack esterase activity so only viable cells are labelled and detected. The cell viability assay indicated no significant difference between treatments and cell-type therefore any differences seen in tau secretion are therefore not due to cellular damage (Figure 56C).

To summarise, stimulating neuronal activity increases tau secretion in both physiological and pathological conditions. It suggests that some of WT and mutant tau secretion is mediated by activity-dependent secretory pathways; as TTX did not reduce tau in the extracellular space in both conditions, it is likely that other secretory mechanisms that do not involve activity may also mediate the release of tau into the extracellular space. Interestingly, electrophysiological recordings suggest that HiBiT-Tau^{E14} –expressing neurons are less active and indicated altered action potential properties when compared to HiBiT-Tau^{WT}. More importantly, the fact that mutant tau displayed lower firing rate but higher extracellular tau levels suggests that mutant tau activity-dependent secretion maybe underestimated in this cultured system.

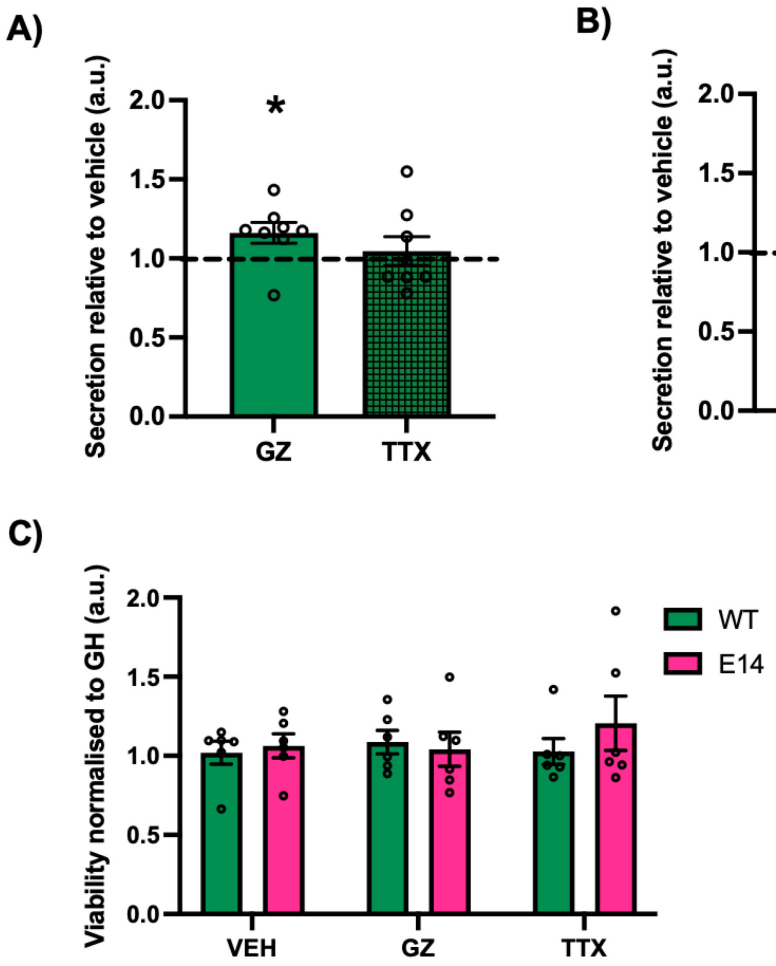

Figure 56. Activity-dependent secretion of HiBiT-Tau^{WT} and HiBiT-Tau^{E14} is not due to cell death. Relative tau secretion in neuron cultures expressing HiBiT-Tau^{WT} and HiBiT-Tau^{E14} before (vehicle) and after treatment of 3 µM gabazine and 500 nM tetrodotoxin (TTX) for 0-6 hours. Raw values were background subtracted and normalised to the GFP-HiBiT-expressing cells (GH). A) In HiBiT-Tau^{WT}-expressing cells, secretion is significantly increased with gabazine application (p = 0.0434) but no difference with TTX (p = 0.6262) was observed when compared to vehicle. B) Gabazine increased tau secretion in cells expressing HiBiT-Tau^{E14} (p = 0.0586) but no difference in TTX (p = 0.9115) when compared to control. Repeated measures one-way ANOVA, followed by Uncorrected Fisher's LSD test; N=8. C) Cellular viability between treatments and conditions were assessed using Calcein Blue AM. There was no difference in cell viability between vehicle, gabazine and TTX treated cultures (repeated measures two-way ANOVA, followed by Sidak's test; $p^* < 0.05$N=8).

5.3.4 Secretion and action potential dynamics of HiBiT-Tau^{P301L} -expressing neurons

As HiBiT-Tau^{P301L} neurons did not display the same level of protein expression comparable to HiBiT-Tau^{WT} and HiBiT-Tau^{E14}, it was excluded from previous comparisons, but has been investigated separately. To test whether HiBiT-Tau^{P301L} secretion is also activity-dependent, passive and active intrinsic properties were also initially assessed. Our findings showed the firing frequency of cells expressing HiBiT-Tau^{P301L} significantly increased with upon neuronal stimulation with gabazine for 0-6 hours ($p = 0.0312$; Figure 57A-B). Interestingly, HiBiT-Tau^{P301L} did not change upon enhanced neuronal activity; there was no significant difference in tau secretion between gabazine and vehicle ($p= 0.1997$, Figure 57C). This showed that enhancing neuronal activity does not lead to an increase in HiBiT-Tau^{P301L} secretion, unlike neurons expressing HiBiT-Tau^{E14} . Furthermore, inhibition of neuronal activity using TTX did not completely prevent tau secretion completely; there was no significant difference in the relative tau secretion between TTX and vehicle ($p = 0.4733$; Figure 57C). The cell viability assay showed that the treatments did not impair membrane integrity or cause cell death (Figure 57D). Interestingly, the average peak and amplitude potentials of neurons expressing Tau^{P301L} significantly decreased with gabazine treatment ($p = 0.0312$; Figure 58A-B). As this alteration in amplitude and peak potential were also reported on neurons expressing Tau^{E14} in stimulated conditions, this finding suggests that Tau^{P301L} may induce similar physiological effects in neurons. As neurons expressing WT tau did not display similar alteration during gabazine treatments, lower peak and amplitude potentials may be an early pathogenic marker for diseased neurons.

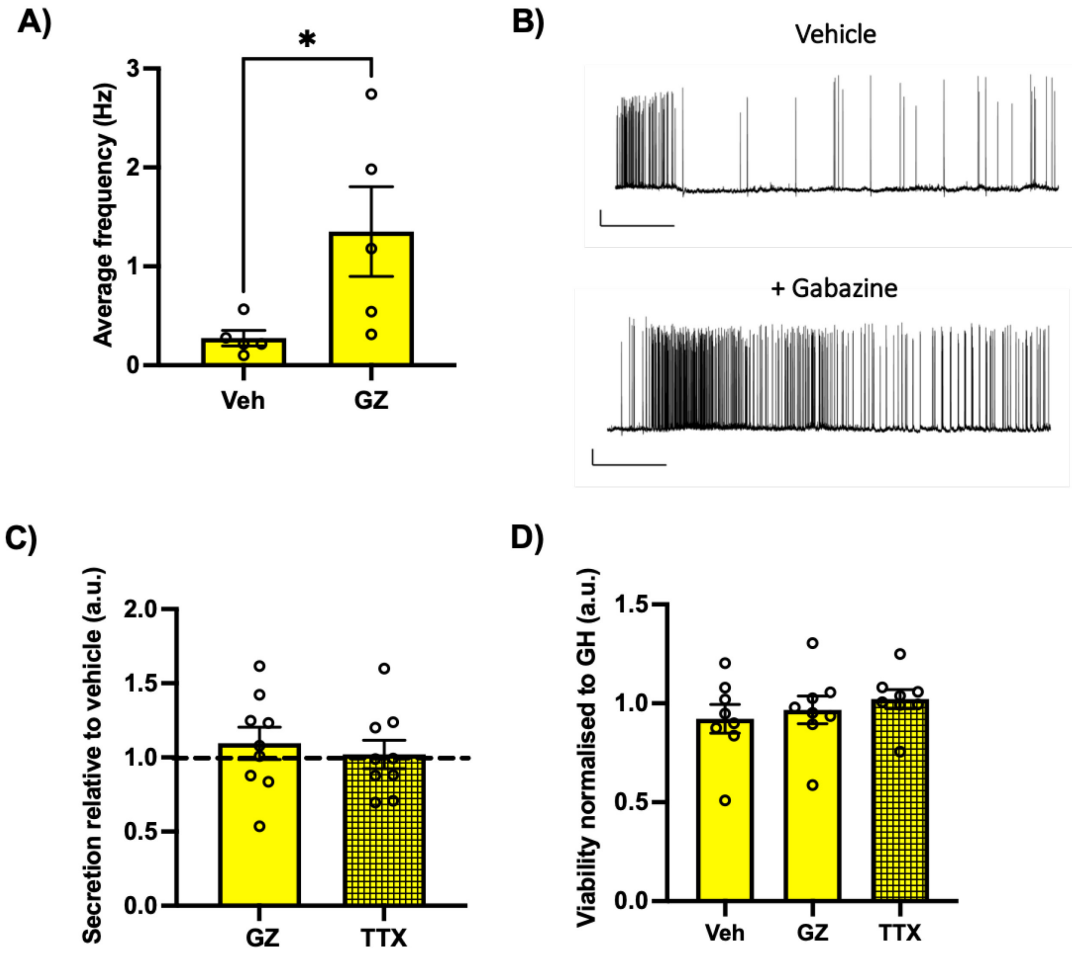

Figure 57. Secretion of Tau^{P301L} is not activity-dependent.

Whole-cell patch clamp and non-lytic NanoBiT-Tau secretion assay was used to record firing frequency and tau released into the extracellular space in the presence and absence of gabazine and TTX 0-6 hours application. A) Average firing frequency of cells expressing HiBiT-Tau^{P301L} is significantly increased (p= 0.0312, paired t-test, N=5) after 0-6 hours of gabazine application when compared to vehicle. B) Representative trace of action potentials recorded in vehicle and after gabazine exposure. C) Relative tau secretion of Tau^{P301L} (normalised to the signal from GFP-HiBiT-expressing cells) was assessed with or without 6 hours of gabazine and TTX application. No significant difference in tau secretion was observed between gabazine (p = 0.1997) and TTX (p = 0.4733) when compared to control. Repeated measures one-way ANOVA, followed by Uncorrected Fisher's LSD test; *p* < 0.05,* N=9. D) Cellular viability assay using Calcein Blue AM between control, gabazine and TTX treated cultures shows no significant differences in cell viability. Repeated measures one-way ANOVA, followed by Sidak's test; N=8.

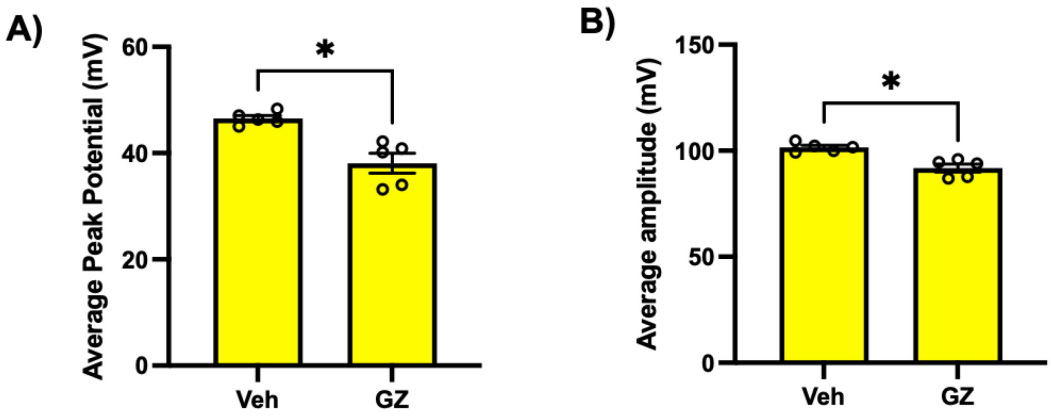

Figure 58. Gabazine application alters action potential properties of neurons expressing HiBiT-Tau^{P301L}.

Average peak potentials (A) and action potential amplitudes (B) of neurons expressing HiBiT-Tau^{P301L}. The average peak potential and the amplitude are significantly decreased with after 0-6 hours of gabazine exposure (p=0.0312); paired t-test, $p^* < 0.05$, N=5) when compared to vehicle.

5.4 Tau^{WT} and Tau^{E14} are direct translocated through the plasma membrane

We investigated whether wild-type and mutant forms of tau are using sulphated proteoglycans to escape cells by translocation across the plasma membrane of primary hippocampal neurons in the presence and absence of neuronal activity. Cell viability assay was also carried out alongside the tau release assay to ensure that detected tau in the conditioned media was not due to the release of intracellular tau from degenerated neurons.

5.4.1 Inhibition of sulphated proteoglycans causes a reduction in activity-dependent tau secretion in both WT and E14

To investigate the role of sulphated proteoglycans in activity- and non-activity -dependent tau secretion, sulphated proteoglycans biosynthesis was inhibited in cells expressing HiBiT-Tau^{WT} and HiBiT-Tau^{E14}. This was done by applying $NaClO_3$ which pharmacologically inhibits the formation of 3'p phosphoadenosine 5'-phosphosulfate, the universal donor for sulfotransferase, by competitively binding to 3'-phosphoadenosine-5'-phosphosulfate synthase. This effectively blocks the sulphation of all GAGs.

Firstly, we found that application of gabazine, TTX and $NaClO_3$ did not lead to cell death. There were no significant differences in Calcein AM signal in the different treatments suggesting that the released tau detected in the assay were from intact neurons rather than from degenerated neurons.

Application of $NaClO_3$ lowered the relative activity-dependent tau secretion in both tau variants. There was significant reduction in the presence of HiBiT-Tau^{WT} ($p = 0.0016$) and HiBiT-Tau^{E14} ($p = 0.0118$) in the conditioned media in cells treated with both gabazine and $NaClO_3$ (Figure 59A). In HiBiT-Tau^{WT} neurons, there was 68 % reduction in the relative tau secretion when cells were treated with $NaClO_3$ and gabazine compared to vehicle. About 32 % of HiBiT-Tau^{WT} can still be detected in the extracellular space which suggests that the removal of sulphated proteoglycans did not completely block the activity-dependent secretion of HiBiT-Tau^{WT} (Figure 59A). Similar findings were observed in HiBiT-Tau^{E14}; addition of $NaClO_3$ and gabazine resulted in significant reduction in the presence of HiBiT-tau ^{E14} in the conditioned media when compared to vehicle levels ($p = 0.0118$; Figure 59B); blockade of sulphated proteoglycans in neuronally stimulated neurons reduced tau levels down to ~42 % from baseline. Similar to previous findings, application of gabazine lead to an increase in both HiBiT-Tau^{WT} and HiBiT-Tau^{E14} (Figure 59A,B).

To investigate the role of sulphated proteoglycans in non-activity-dependent secretion of tau we employed the use of TTX in the presence or absence of $NaClO_3$. Inhibition of neuronal activity and sulphated proteoglycan biosynthesis, using TTX and $NaClO_3$, led to significant reduction in secretion of HiBiT-Tau^{WT} when compared to vehicle-HiBiT-Tau^{WT} ($p = 0.011$; Figure 59B). Similar findings were observed in HiBiT-Tau^{E14} neurons when compared to vehicle-HiBiT-Tau^{E14} ($p = 0.0118$; Figure 59B).

Interestingly, TTX and $NaClO_3$ application did not completely inhibit the release of both wild-type and mutant tau into the extracellular space; at least 28 % of HiBiT-Tau^{WT} and 30 % of HiBiT-Tau^{E14} were still detectable in the conditioned media of Tau^{WT} and Tau^{14} expressing neurons, respectively.

To summarise, application of $NaClO_3$ reduced basal and activity-dependent secretion of both variants. $NaClO_3$ and TTX application also lowered non-activity-dependent secretion of both wild-type and mutant tau. However, inhibition of sulphated proteoglycans did not entirely ablate tau secretion in both conditions. These findings suggest that sulphated proteoglycans may be involved in activity- and non-activity-dependent secretion of both wild-type and mutant tau in cultured hippocampal neurons. Multiple secretory pathways are therefore mediating the release of tau into the extracellular space in physiological and pathological conditions.

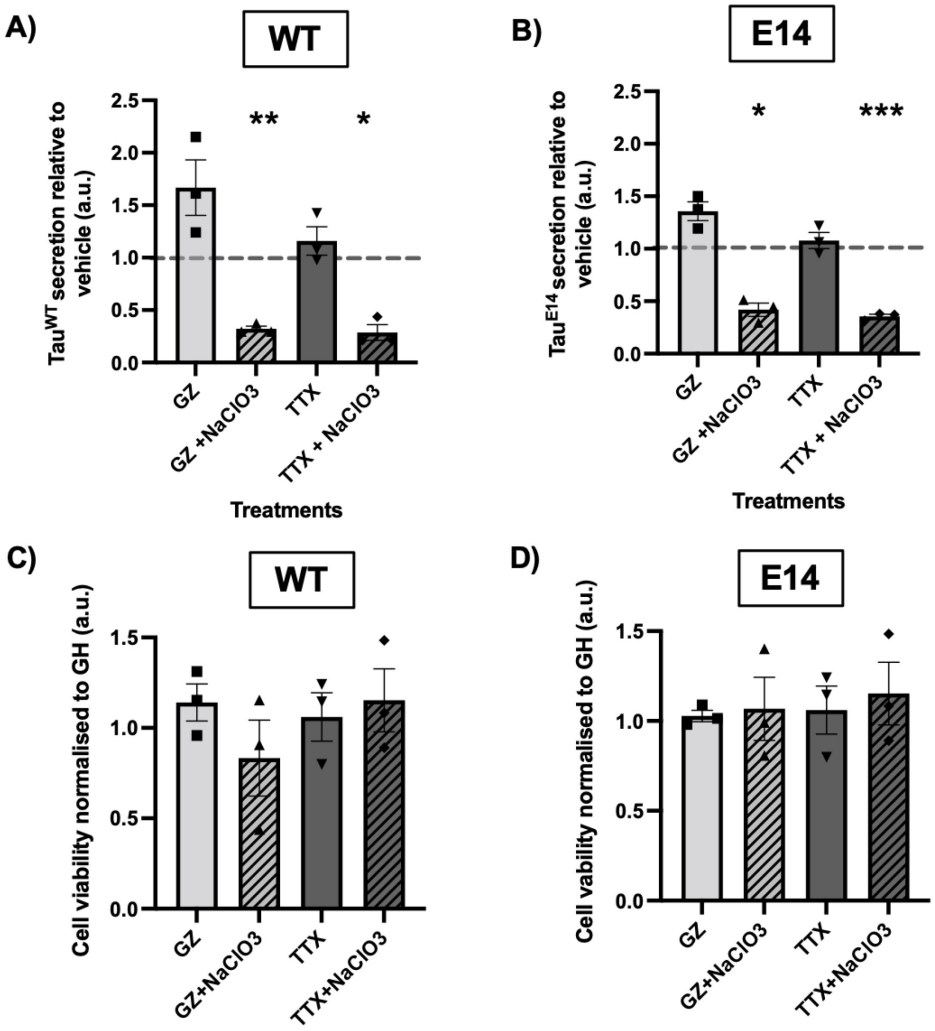

Figure 59. Inhibition of sulphated proteoglycans reduces activity-dependent and non-activity-dependent secretion of wild-type and mutant tau.

A-B) Relative secretion of HiBiT-Tau^{WT} (A)and HiBiT-Tau^{E14} (B) in cultured hippocampal neurons with or without the presence of 3 µM gabazine (GZ), 500 nM TTX and 50 mM $NaClO_3$. All data were normalised to vehicle; this was referred to as baseline control (dotted line). HiBiT-Tau^{WT} basal secretion is reduced upon application of Gabazine and $NaClO_3$ ($p = 0.0016$) when compared to the control. TTX and $NaClO_3$ application was able to reduce baseline HiBiT-Tau^{WT} secretion ($p = 0.0110$). HiBiT-Tau^{E14} secretion was also significantly reduced with GZ and $NaClO_3$ ($p = 0.0118$) when compared to baseline levels. Application of TTX and $NaClO_3$ lead to significant reduction in baseline tau secretion levels ($p = 0.001$). Repeated measures one-way ANOVA followed by Uncorrected Fisher's LSD test; *$p* < 0.05, p** < 0.01, p***< 0.001,$* N=3). C-D) Cell viability assay using Calcein Blue AM in HiBiT-Tau^{WT} and HiBiT-Tau^{E14} expressing neurons treated with or without $NaClO_3$ during neuronal stimulation and inhibition. No significant differences were observed between each condition (repeated measures one-way ANOVA followed by Sidak's test, N=3).

5.5 Conclusion

5.5.1 Proof-of-concept: not all pharmacological agents enhance neuronal activity

This work investigated how different pharmacological manipulations can modulate neuronal activity in cultured hippocampal neurons. As a proof-of-concept electrophysiological effects of KCl-induced depolarisation and $GABA_A$-receptor-mediated induction of neuronal activity were assessed on cultured hippocampal neurons. We found that gabazine-mediated inhibition of $GABA_A$ receptors were able to enhance neuronal activity in cultured hippocampal neurons. Using electrophysiological recordings and the NanoBiT-tau biosensor we found that 6 hours exposure to 3 µM gabazine resulted in sustained increase in neuronal activity in cultured primary hippocampal neurons, which was not observed in potassium chloride treated-cells.

5.5.2 Activity- and non-activity-dependent secretion of wild-type and mutant tau

In both HiBiT-Tau^{WT} and HiBiT-Tau^{E14} cultures, neuronal activity was significantly enhanced with gabazine application, showing that the cells are healthy and active. The NanoBiT-Tau reporter assay showed that gabazine-mediated neuronal stimulation led to an increase in the level of HiBiT-Tau^{WT} and HiBiT-Tau^{E14} detected in the extracellular space of cultured hippocampal neurons. Analysis of cell viability showed activity-dependent tau secretion detected in our assays were independent of cell death. Together, these findings suggest that enhanced neuronal activity increased extracellular tau, indicating activity-dependent secretion, which was not seen when activity was inhibited with TTX.

All cells expressing HiBiT-Tau^{WT}, HiBiT-Tau^{E14} and HiBiT-Tau^{P301L} demonstrated spontaneous activity in unstimulated conditions. Action potential analysis suggests that HiBiT-Tau^{WT} cultures were more active than HiBiT-Tau^{E14} in basal conditions. Interestingly, we showed that HiBiT-Tau^{E14} is preferentially secreted by neurons than HiBiT-Tau^{WT} in similar conditions.

In stimulated conditions, HiBiT-Tau^{E14} neurons were less active than HiBiT-Tau^{WT}. Interestingly, given that HiBiT-Tau^{E14} cells were less active than HiBiT-Tau^{WT} in gabazine-treated conditions, when relative tau secretion levels are compared to baseline, higher levels of HiBiT-Tau^{E14} were detected in the extracellular media than HiBiT-Tau^{WT}. Taking these into consideration, the fact that HiBiT-Tau^{E14} neurons were less electrically active than HiBiT-Tau^{WT} suggests that activity-dependent secretion of misfolded tau may be underestimated in our assay. Our data also show action potential dynamics maybe altered in cells expressing HiBiT-Tau^{E14}, which was not observed in the wild-type.

5.5.2.1 TauP301L secretion in cultured hippocampal neurons

The tau secretion results obtained from neurons expressing HiBiT-Tau^{P301L} needs to be taken with caution as biochemical analysis previously showed a lack of Tau ^{P301L} protein expression in primary neurons (demonstrated in Figure 36A,B); the molecular weight of the tau protein lysate did not have the expected banding pattern suggesting that tau misprocessing and truncation may have occurred following expression of HiBiT-Tau^{P301L} primary hippocampal neurons (further discussed in 3.4.1). This could suggest for a lower overall protein expression of tau in these neurons which may explain the lack of extracellular membrane-free tau observed in culture. Furthermore, this can also be explained by the differences in turnover rates between different tau variant. Tau^{P301L} expression may induce higher protein turnover in neurons. Recent findings have shown that the expression of tau mutant expressing double mutation of Tau$^{P301L/S302F}$ in organotypic slices has really high turnover rates, with an average overall half-life of 7 days (Croft et al., 2021)**.** In this study, analysis of tau inclusion formation and turnover rate showed that the Tau^{P301L} and double Tau$^{P301L/S302F}$ mutants rapidly formed neuronal tau inclusions (12-96 hours) and that the dynamic of tau turnover Tau$^{P301L/S302F}$ mutant had significantly longer half-life (~7 days). In contrast, the WT tau variant did not form tau inclusions and had a turnover rate of ~3 days (Croft et al., 2021). This rapid formation of tau inclusions is reminiscent of the half-life of tau inclusion formation *in vivo* in transgenic mice models. This research could therefore explain why there is such a low level of Tau^{P301L} detected in the extracellular space. Equally, the reduce tau^{P301L} detected in the extracellular space could also be due to lack of protein expression as demonstrated in the lack of signal that is comparable to Tau^{WT} and Tau^{E14} in the western blot analysis of the cell lysates extracted from cultured primary hippocampal neurons. Further investigations are required to assess what caused this reduced protein expression of Tau^{P301L}.

Although the mechanisms underlying the biochemical changes and cell expression of Tau^{P301L} *in vitro* still remains to be investigated, I was able to assess the electrophysiological properties of these cells in basal and stimulated conditions because whole-cell patch clamp recordings required visual selection of GFP-expressing neurons using the microscope. The neurons that were recorded for these experiments therefore expressed HiBiT-Tau^{P301L}.

5.5.3 Abnormal phosphorylation and mutation may cause action potential dynamics disruption

I find that hyperphosphorylation and abnormal mutation of tau disrupts action potential dynamics when compared to WT conditions. Neurons expressing tau with abnormally pseudo-phosphorylated and disease-associated P301L mutation had lower action potential frequency in basal conditions when compared to control. Upon the addition of gabazine to enhance neuronal activity, mutant tau-expressing neurons were also unable to increase the firing frequency to the same extent as in control neurons as we all lowered action potential peak and amplitude, there was a significant reduction in peak potential and action potential amplitude in Tau^{E14} and Tau^{P301L}-expressing cells. The fact that these changes in action potential properties were only found in mutant forms of tau and not WT could suggest that it might be an underlying marker of pathology. These results suggest that pathological tau proteins that are associated with AD and tauopathy development may be causing a disruption in cellular and network activity. Indeed, there is evidence showing that mutant tau expression can alter action potential dynamics (Hatch et al., 2017) and mediate synaptic dysfunction (Hoover et al., 2010) *in vivo* and *in vitro.* Indeed, others have also shown the pathological consequences of hyperphosphorylation and tau mutation at P301L *in vivo* and *in vitro.* (Ahmed et al., 2016; Cowan et al., 2010; Hasegawa et al., 1998; Hoover et al., 2010; Rodríguez-Martín et al., 2013). These studies have shown that pathological forms of tau could be contributing to the disruption of microtubule integrity, impairment of axonal transport and glutamatergic receptors that governs network activity, which could be contributing to the observed action potential dynamics changes in different conditions. Hatch et al., (2017) were able to rescue disruptions in action potential dynamics by suppressing pathological tau expression (by doxycycline treatment) and by pharmacologically stabilising microtubules. The molecular mechanisms of Tau dysfunction are still unclear but changes in ion channel conductance and composition in these cells could mediate these changes. Hyperphosphorylation and mutation of tau could disrupt microtubule integrity and impair axonal transport by mislocalisation of tau proteins in dendritic compartments (Hoover et al., 2010). This in turn causes synaptic targeting and anchoring of AMPA and NMDA receptors to be disrupted, which subsequently lead to damaged of dendritic spines and overall synaptic dysfunction. The underlying molecular mechanisms that may cause action potential disruption is further discussed in Chapter 6.

5.5.4 Tau is directly translocated across the plasma membrane in healthy and diseased conditions

Intriguingly, our data suggests that non-activity-dependent secretion processes may also account for the membrane-free tau found in the extracellular space in our assays. Blocking neuronal activity using TTX did not result in complete ablation of tau secretion in our assay. The level of WT and mutant tau in the conditioned media did not change from baseline when neuronal activity was completely inhibited. This suggests that non-activity dependent processes are also at play in the secretion of both wild-type and mutant tau.

Furthermore, by enhancing and blocking neuronal activity in the presence and absence of sodium chlorate, which inhibited sulphated proteoglycan biosynthesis, we were able to investigate the molecular mechanisms that may facilitate activity-dependent secretion of both wild-type and mutant tau. We hypothesised that wild-type and mutant tau may escape cells by direct translocation across the plasma membrane. Our data showed that blocking sulphated proteoglycans biosynthesis can reduce activity-dependent secretion of both HiBiT-Tau^{WT} and HiBiT-Tau^{E14}, therefore this process may be mediated by sulphated proteoglycans. Equally, inhibition of neuronal activity and sulphate proteoglycan biosynthesis also decreased HiBiT-Tau^{WT} and HiBiT-Tau^{E14} secretion. These findings suggest the sulphated proteoglycans may mediate both activity-dependent and non-activity dependent secretion of wild-type and mutant tau.

There is increasing interest in understanding the role of tau/HSPG binding in disease pathogenesis as well as a potential therapeutic target for drug developments. Tau/HSPG relationship is particularly intriguing as tau is a heparin-binding protein and that heparin-application has been shown to induce efficient tau fibrillisation *in vitro* (Pérez et al., 1996). Furthermore, the fact that HSPGs have also been shown to mediate both of the release and re-uptake of tau in physiological and pathological conditions (Katsinelos et al., 2021; Merezhko et al., 2018; Rauch et al., 2018) suggests that tau/HSPG binding may have a role in intracellular propagation of pathological processes. Tau and HSPG binding may also affect tau aggregation and contribute to in-direct hyperphosphorylation of tau by activation of kinases, which may therefore further assist on the pathological processes (Avila et al., 2016; Hasegawa et al., 1997; Townsend et al., 2020). Taken together, sulphated proteoglycans are emerging players in the progression of tau pathology which warrants further investigations.

To summarise, neuronal activity can modulate the secretion of wild-type and mutant tau. Secretion of tau is mediated by both activity and non-activity dependent pathways. Sulphated proteoglycans may mediate the translocation of tau across the plasma membrane to the extracellular space and exacerbate the formation of pathological tau species. Sulphated

proteoglycans could therefore be a good target for future therapeutic interventions to slow the transmission of tau misfolding and aggregation in connected neuronal networks.

Chapter 6 Discussion

6.1.1 NanoBiT-tau reporter assay allows the sensitive detection of tau cell-to-cell transmission in cultured neurons

In this project, a sensitive NanoBiT-tau biosensor was generated and validated to dissect the different steps that lead to tau cell-to-cell transmission in physiological and pathological conditions. In contrast to fluorescence-based *in vitro* assays, such as the one developed in our lab (Hallinan et al., 2019), the NanoBiT-Tau biosensor assay allows the detection of events that occur prior to tau misfolding and seeded aggregation. The NanoBiT-Tau biosensor is unique in that it does not rely on the presence of aggregates in adjacent cells to indicate that tau release and re-uptake has taken place. This therefore allows the cell-to-cell transmission of both WT and mutant tau to be investigated side-by-side. This is made possible by the availability of different forms of LgBiT; firstly, the addition of membrane impermeable LgBiT into the extracellular medium, allows membrane-free tau to be detected and distinguished from vesicular-tau; secondly, expression of LgBiT in post-synaptic cells allows the re-uptake of both wild-type and mutant tau to be monitored as it enters the cytosol; finally, this assay can also be used to detect the early events of seeded aggregation – the interaction of misfolded tau and endogenous tau in acceptor cells can be assayed.

Due to the time constraints of the project, the NanoBiT-tau biosensor assay was only used for the detection of tau secretion. Although the mechanisms of tau re-uptake were not explored using the NanoBiT-Tau report assay, this technology has recently been used to study cholesterol-dependent tau re-uptake and aggregation in HEK293 cells and primary neurons (Tuck et al., 2022). In this study, hTau^{P301L} tagged with HiBiT (tau-HiBiT) were incubated with heparin to form tau-HiBiT aggregates. To measure the entry of these tau-HiBiT aggregates, LgBiT was expressed in HEK293 biosensor cell line (Frost et al., 2009). Tau-HiBiT aggregates were able to be taken-up by cells expressing LgBiT. This was confirmed by the generation of bioluminescence signal from the complementation of HiBiT and LgBiT that resulted in the generation of NLuc enzyme. Besides the dependence to cholesterol, they also entry of exogenously prepared tau to mouse and human neurons are dependent on interactions with transmembrane proteins such as LRP1 and HSPG, further corroborating previous findings (Holmes et al., 2013; Rauch et al., 2018; Rauch et al., 2020). Extracting cholesterol using methyl-beta- cyclodextrin from the plasma membrane of primary neurons significantly reduced tau entry, without overt cytotoxicity.

In comparison to fluorescence-based biosensors, NanoBiT-Tau reporter assay offers many advantages such as high signal-to-noise ratio, sensitivity, fast experimental application, customisable to different assay formats and straight forward data analysis (see review by Hall et al., 2021). To my knowledge, our study is the first one that used the HiBiT and LgBiT biosensor to monitor the differential secretion of tau variants in the context of neuronal activity in physiological and pathological conditions. This assay was also the first to establish the link between neuronal activity and the secretion of tau via direct translocation of tau across the plasma membrane sulphated proteoglycans.

6.1.2 Hyperphosphorylated tau is preferentially secreted by neurons

This project provides evidence that tau is secreted by primary hippocampal neurons in both physiological and pathological conditions, which corroborates previous findings (Pooler et al., 2013; Wu et al., 2016; Yamada et al., 2014). Our findings indicate differential secretion propensities between wild-type and pseudo-hyperphosphorylated tau. Primary hippocampal neurons preferentially secrete pseudo-hyperphosphorylated tau over WT tau in basal conditions and this difference is not because of neurodegeneration. In support of this finding, there is evidence showing that hyperphosphorylation can increase the propensity of tau to be secreted into the extracellular space of CHO, HeLa and SY-SHSY cells (Katsinelos et al., 2018; Plouffe et al., 2012). Although this study does not compare secretion propensities between hyperphosphorylated and dephosphorylated versions of tau, this has already been done by Katsinelos et al., (2018). Here, they compared the secretion propensities of wild-type, pseudo-hyperphosphorylated and dephosphorylated tau in CHO and SY-SHSY cells. They found a significant reduction in the presence of dephosphorylated tau, whereas pseudo-hyperphosphorylated tau significantly increased when conditioned media were assessed by Katsinelos et al., (2018).

The role of phosphorylation in tau secretion is still unclear, however it is known that hyperphosphorylation of tau is strongly associated with AD. There are about 40 disease-related phosphorylation sites that have been identified in AD (Hanger et al., 2007). One example is the phosphorylation of threonine 181 (pT181), which is a widely used clinical biomarker for AD (Hampel et al., 2010). Interestingly, there is also evidence showing that dephosphorylated tau is preferentially secreted by primary cortical neurons in physiological conditions (Pooler et al., 2013). Taking these together, it is possible that tau secretion occurs as a physiological protective mechanism built in cells. Neurons may preferentially secrete hyperphosphorylated and misfolded tau to lower the accumulation of intracellular aggregates. In fact, certain phosphorylation sites on some variants may target tau to become secreted at an accelerated rate compared to others. Furthermore, different tau variants could have distinct secretory routes; the mechanism of tau release could be dependent on multiple factors such as the types of cells used, tau isoforms, phosphorylation, truncation, and neuronal activity. Phosphorylation state of tau may also influence the mechanism in which tau pathology propagates in connected neuronal networks. A better understanding of the secretion process of different tau conformers are therefore critical in treating such a heterogeneous disease.

Furthermore, two forms of tau were identified in the conditioned media of cultured primary hippocampal neurons in both WT and mutant tau: soluble free tau and vesicular tau. In line with

previous studies (Pooler et al., 2013; Yamada et al., 2014), the NanoBiT-Tau assay was able to detect a greater proportion of membrane-free tau in the extracellular space than vesicular tau. Interestingly, we detected a higher amount of vesicular-tau in the extracellular space when compared to what has been reported in other studies. In literature, ~98 % secreted tau in the extracellular space are membrane-free with only about ~2% are reported to be vesicular-tau (Dujardin et al., 2014; Wang et al., 2017). This may be because of the differences in methodology in which these tau release assays were carried may also explain these differences. In some studies, Enzyme-Linked Immunosorbent Assays (ELISAs) were used to detect tau secretion (Dujardin et al., 2014; Wang et al., 2017). Although it is well-established, ELISAs involve multiple incubation and washing steps, and therefore some tau may be lost in this way (see review by Hall et al., 2021). Furthermore, multiple centrifugation steps are required for the separation of extracellular vesicle proteins such as ectosomes and exosomes from cell culture supernatants, and it is likely that some may be lost in this way. The NanoBiT-tau assay is advantageous in that it by-passes all these wash or centrifugation (Hall et al., 2021). LgBiT can be added directly into the isolated conditioned media and the luminescence signal generated from the reconstituted NLuc can be read immediately; this is able to detect the total HiBiT-tau that are membrane-free. This assay can also be customised so that tau released via extracellular vesicles can be detected.

6.1.3 Neuronal activity regulates tau secretion in physiological and pathological conditions

We showed that an increase in neuronal activity leads to elevated tau levels in the extracellular space in both physiological and pathological conditions which is consistent with previous findings *in vitro* and in vivo (Pooler et al., 2013; Wu et al., 2016; Yamada et al., 2014)(Figure 60). Interestingly, electrophysiological recordings suggest that cells expressing hyperphosphorylated tau mutant were less active when compared to WT. To my knowledge, there is currently no study that compares the neurophysiological activity of primary cultured neurons expressing Tau^{WT} and Tau^{E14}, and linked it with tau secretion; most tau secretion studies that induced neuronal activity assume that these neurons expressing WT and disease-associated mutants are equal in activity and therefore comparable in tau secretion. Considering that pseudo-hyperphosphorylated tau is readily detected in the extracellular space, one would assume that this would also correspond to greater activity. After all, network hyperexcitability have been observed in the initial stages of AD and in AD mouse models which have been closely associated with hyperphosphorylation (Busche et al., 2008; Palop and Mucke, 2009; Wu et al., 2016). This was not the case in our study. Expression of pseudo-hyperphosphorylated tau in primary neurons led to less neuronal activity when compared to controls.

This finding was intriguing as tauopathies are closely associated with increase network excitability (Targa Dias Anastacio et al., 2022). However, there is evidence showing that expression of mutant P301L *in vivo* can led to significant reduction in neuronal activity when compared to control (Busche et al., 2019). By using two-photon calcium imaging in awake mice, they found that dual expression of P301L tau and APP/PS1 in a mouse model revealed that tau could potentially be silencing neuronal activity and have a strong ability to over-ride Aβ-mediated hyperexcitability (Busche et al., 2019). This was further corroborated by others showing that tangle-bearing neurons are less active than those that did not have tangles (Marinković et al., 2019). This finding suggests that pathological tau species may be able to drive the reduction in neuronal activity *in vivo.* It is still unclear why cells expressing hyperphosphorylated tau demonstrate reduced activity. But there are studies showing hyperphosphorylated tau reduces hippocampal excitability in cultured hippocampal neurons and AD mouse models (Hatch et al., 2017; Hoover et al., 2010). Hatch et al., (2017) showed that hyperphosphorylated tau can reduce the excitability of CA1 hippocampal neurons by relocating the axon initial segment (AIS), which is where action potentials are generated. Hoover et al., (2010) has also showed that hyperphosphorylated tau become mislocalised to dendritic spines and can impair AMPA and NMDA receptor trafficking or synaptic anchoring. These glutamatergic receptors are important as they govern excitatory synaptic transmission (Hoover et al., 2010). It is possible that hyperphosphorylation of tau in diseased conditions may be a compensatory mechanism that is activated to suppress aberrant excitatory/inhibitory imbalance that occur during the initial stages of AD.

This reduced activity may explain why in stimulated conditions there was less tau detected in the extracellular space, even though hyperphosphorylated tau was readily detectable in basal conditions when compared to control. This therefore suggests that the secretion of hyperphosphorylated tau is underestimated in our assay. These neurophysiological changes associated with hyperphosphorylation may also be a marker for diseased neurons.

The exact molecular mechanisms of activity-dependent secretion remain to be determined. However, the fact that increasing neuronal activity can upregulate tau secretion suggests that the release mechanisms could be mediated by the fusion of pre-synaptic vesicles, carrying both WT and disease-associated tau, to the plasma membrane resulting in the release of membrane-free tau to the extracellular space. In support of this, there is evidence that tau could be acting as a signalling molecule by binding to post-synaptic receptors (Gómez-Ramos et al., 2008) which may explain why it would be released in pre-synaptic vesicles like neurotransmitters. Moreover, a recent tau interactome study has shown that the interaction between tau and proteins involved synaptic vesicle fusion is upregulated in response to neuronal stimulation (Tracy et al., 2022). They also found that the tau-interactome changes depending of the expressing tau conformer

suggesting that the secretion mechanisms involved in activity-dependent secretion may be distinct between different tauopathies. How tau hijacks these pre-synaptic vesicles remain to be investigated. In addition, there are also increasing evidence showing that tau release could be mediated by the fusion of intracellular membrane organelles such as autophagosomes, lysosomes and late endosomes via exocytosis (Chen et al., 2020; Fontaine et al., 2016; Pilliod et al., 2020; Rodriguez et al., 2017). Although some tau secretion is activity-dependent, our findings show that some secretion may be occurring via non-activity-dependent pathways.

Pharmacological blockade of all neuronal activity using TTX did not affect baseline levels of tau in the extracellular space in Tau^{WT} and Tau^{E14} cultures. This result coroborates what has been seen *in vivo* (Yamada et al., 2014). In physiological conditions, application of TTX by reverse microdialysis also did not reduce the presence of endogenous tau in the ISF of freely moving mice (Yamada et al., 2014). Interestingly, they compared the release of tau and Aβ in the ISF of mice over the course of 27-hours TTX treatment. They found faster reduction in Aβ ISF levels below baseline when compared to tau which remained stable over the course of 27 hours. It has been proposed that, the balance between cellular release and clearance of tau may be mediating this stable release of tau into the ISF. This suggests that in vivo tau has a slow protein turnover rate. Therefore, to observe the TTX-mediated effects on tau release, the time window chosen would need to be expanded. This may explain why 6 hours of TTX treatment, did not reduce tau secretion at baseline levels in cultured primary hippocampal neurons expressing either Tau^{WT} and Tau^{E14}. Alternatively, it could also suggest that non-activity-dependent mechanisms may also be at play in the secretion of tau in physiological and pathological conditions. What secretion pathways could be mediating the non-activity dependent release of tau still needs to be elucidated.

6.1.4 Consequences of abnormal phosphorylation and tau mutation in neuronal networks

Findings in this project showed that action potential dynamics are altered in cells expressing mutant forms (e.g., Tau^{E14} and Tau^{P301L}) of tau during enhanced neuronal activity. Baseline measurements showed that the action potential amplitude and peak are unaffected in cells expressing wild-type and pseudo-phosphorylated tau. However, induction of neuronal activity resulted in a significant reduction in both action potential amplitude and peak potential in cells expressing mutant tau forms but not WT. Although few have investigated the electrophysiological changes that occur upon the expression of different tau mutants *in vitro* and correlates it to tau secretion, there is some evidence showing the pathogenic tau forms can alter intrinsic neuronal excitability of neurons, impair action potential dynamics and modulate short-term and long-term plasticity *in vitro* and *in vivo* (Fá et al., 2016; Hill et al., 2019; Hill et al., 2020; Ondrejcak et al., 2018). Hill et al., (2019) recently showed that injection of tau oligomers into cortical neurons

taken from mice brain slices caused impairments in synaptic transmission and reduced action potential amplitude and kinetics (Hill et al., 2019). The mechanisms underlying the reduction in peak and amplitude potentials in Tau^{E14}-expressing cells remain unclear. However, in the case of Tau^{E14} which is able to efficiently misfold and accumulate into larger protein inclusions at the distal axons of DIV14 neurons, it is possible that the formation of these tau proteins in the soma of the axon may restrict the current flow from the axon initial segment (AIS), where action potentials are initially generated (Hatch et al., 2017). The generation of action potential is largely dependent on many factors and is regulated by the function of voltage-gated ion channels, which are ion-selective pores that span the cell membrane. Action potential is generated in the AIS which is enriched with ankyrins, ion channels and spectrin proteins (Leterrier, 2018). Re-location of the AIS may also cause changes in action potential dynamics in mutant-tau expressing neurons observed in this study. Similar observations were reported by Grubb and Burrone (2010), showing an activity-dependent distal shift of the AIS baseline location in cultured DIV12-14 cultured hippocampal neurons . This is further corroborated by other studies showing that the expression of pseudo-hyperphosphorylated tau has been shown to reduce action potential firing and amplitude by shifting the position of the AIS further down the axon; this was correlated to reduced neuronal firing (Hatch et al., 2017). Considering that the AIS scaffold has close association with microtubules and actins, disruption caused by hyperphosphorylated and mutant tau may cause this interaction to breakdown. Alternatively, disruption or changes to voltage-gated sodium and potassium ions, enriched in the AIS to allow action potential generation, is also a possibility.

Abnormal phosphorylation and mutation of tau may also have an impact in impairing microtubule integrity and axonal transport. Phospho-mimetic tau has been shown to bind with less affinity to microtubules, exhibiting more motile tau (Rodríguez-Martín et al., 2013). Neurons expressing abnormally phosphorylated and mutated tau has been shown to become mislocalised to dendritic compartment, causing suppression of excitatory synaptic transmission (Hoover et al., 2010). Based on this study, before overt neurodegeneration is observed in AD transgenic mice model, Tau^{P301L} and pseudo-phosphorylated tau has been shown to localise in dendritic spines. This caused reduction in AMPA and NMDAR receptors insertion in the post-synaptic membrane, as well as impaired the clustering of NMDAR. As a consequence, the mini excitatory post-synaptic currents amplitude and frequency were reduced significantly which subsequently resulted in impaired synaptic function in AD mice. Furthermore, previous studies have shown that DIV14 hippocampal neurons expressing phospho-mimetic Tau^{14} display early selective axonal transport deficits, as a consequence of a build of misfolded tau proteins in the distal axonal segment (Hallinan et al., 2019). As tau support microtubule dynamics, it's dysfunction may lead to axonal transport deficits that precede synaptic loss. Expression of mutant Tau^{E14} lead to a reduction in

the total number of lysosome available in the distal axons and also compromised bi-directional lysosomal transport (Hallinan et al., 2019). Importantly, there are also evidence showing hyperphosphorylated tau, which become misfolded, is less able to interact to microtubules (Cowan et al., 2010). As a consequence of impaired microtubule-tau binding, the maintenance of microtubule dynamics and cytoskeleton breakdown *in vivo*, causing deleterious effects in Drosophila flies. Notably, suppression of phosphorylation lead to restored cytoskeletal defects in flies (Cowan et al., 2010).

Accumulating amount of evidence have showed that pathogenic forms of tau can also cause synaptic dysfunction by disrupting pre-synaptic vesicle and plasma membrane fusing (Hoover et al., 2010; Tracy and Gan, 2018; Wu et al., 2021; Zhou et al., 2017). Flies expressing disease-associated FTDP-17 tau mutant has been shown to mislocalise in pre-synaptic sites and bind synaptic vesicles via a presynaptic vesicle membrane protein called synaptogyrin-3, causing the crosslinking of pre-synaptic actin polymers, which in turn restrict the mobilisation of synaptic vesicles. This therefore impaired synaptic transmission during prolonged neuronal activity (McInnes et al., 2018; Zhou et al., 2017). The fact that we found significant formation of tau accumulates in distal part of axons of mutant tau and observed changes in neuron's electrophysiological functions may suggest potential disruptions in the cell-to-cell communication and synaptic function.

6.1.5 Molecular mechanisms that mediates the secretion of tau in physiological and pathological conditions

6.1.5.1 Direct translocation of tau across the plasma-membrane

My data suggests that sulphated proteoglycans may mediate the release of Tau^{WT} and Tau^{E14} in stimulated and unstimulated conditions. Application of sodium chlorate was able to significantly reduce the level of tau secreted in the extracellular space in cells expressing wild-type and pseudo-hyperphosphorylated tau. This shows that sulphated proteoglycans are involved in both activity-and non-activity-dependent secretion of tau in physiological and pathological conditions. Multiple secretory pathways have been proposed to have the role in the secretion of tau into the extracellular space (reviewed in section 1.7). The release of membrane-free tau may be mediated by direct-translocation of tau across the plasma membrane. As inhibition of sulphated proteoglycans significantly reduced the amount of both wild-type and mutant tau at and in the presence of neuronal stimulation baseline by ~70% suggests that sulphate proteoglycans have a direct role in mediating the secretion process. This is in line with previous findings that showing the sulphated proteoglycans (i.e., HSPGs) mediate tau release (Katsinelos et al., 2018). The fact

that tau secretion is significantly affected by the presence of sulphated proteoglycans suggests that wild-type and mutant tau proteins may be interacting with these structures prior to release into the extracellular space. Previous work has shown that HSPG and tau interaction lead to re-uptake (Holmes et al., 2013; Rauch et al., 2018). If tau can efficiently be internalised via HSPG-mediated mechanisms, then there is a possibility that tau is also using this pathway to be secreted.

The role of HSPG-mediated tau secretion is currently understudied. Much of the knowledge in the role of tau and HSPG mediated interaction come from re-uptake studies. Our data is the first to correlate the HSPG-mediated secretion to the effects of neuronal activity. Firstly, we find that inhibition of proteoglycans biosynthesis was not enough to ablate the secretion of both WT and mutant tau in basal conditions which suggests that non-HSPG mediated pathways may be at play. It may be that different tau variants have variable dependency in HSPG-mediated secretion. In support of this, Puangmalai et al., 2020 found that knock out of HSPG biosynthetic enzyme exostin-2 and pharmacological application of HSPG antagonists were able to abolish the uptake of AD, DLB derived tau oligomers, but not PSP derived tau oligomers. Although this study did not look at whether this is same for tau secretion, findings from tau re-uptake studies could be transferable to tau secretion as both processes could occur concurrently. It is also possible that different cell types may have different secretion machineries and varying levels of HSPG-dependent secretion and uptake mechanisms. Blocking this pathway may have implications tau propagation as heparin and heparin derivatives has been shown to competitively inhibit cellular tau uptake as well as reduce tau-induced neurotoxicity (Wang et al., 2018).

6.1.5.2 Role of sulphated proteoglycanss in the formation of tau inclusions and phosphorylation

One of best evidence supporting the role of sulphated proteoglycans in mediating the secretion of tau is the fact that heparin and other polyanions are capable of binding to tau and induce the formation of fibrils *in vitro* (Goedert et al., 1996). Heparan sulphate, which is closely related to heparin, has been found to accumulate and co-localise with NFTs in the brains of AD and Down's syndrome patients (Snow et al., 1990), and when conjugated to proteoglycans are able to contribute the propagation of tau via prion-like mechanisms (Holmes et al., 2013). In normal conditions, heparan sulphates are predominantly located in the cell surface, however, in disease conditions, they accumulate intracellularly before the detection of tau pathology and accumulation with NFTs (Snow et al., 1990). This suggests that sulphated proteoglycans may play a role in the early pathogenic mechanisms of tauopathy (Snow et al., 1990). Although studies on

HSPG-dependent tau secretion from neurons are currently limited (Katsinelos et al., 2018; Merezhko et al., 2018), the general topic of tau-HSPG interaction has garnered a lot of attention in recent years particularly because it has consistently shown that HSPG-tau binding could mediate tau fibril cellular uptake and propagation of tau pathology (Holmes et al., 2013; Rauch et al., 2018; Stopschinski et al., 2018).

Sulphated proteoglycans and tau interaction have implications in fibril formation and phosphorylation, and therefore may have effects in tau secretion. Firstly, the binding of tau to HSPGs may lead to pathological structural changes just as shown with heparin application (Arrasate et al., 1997). Heparin-induced conformational changes have been shown to cause abnormal folding in tau causing further exposure of phosphorylation sites, thus subsequently accelerating tau aggregation (Avila et al., 2016; Townsend et al., 2020). Interestingly, treatment of heparinase and chondroitinase was able to reduce twisting of AD-derived PHF filaments (Arrasate et al., 1997). There is also evidence showing that heparin-induced tau fibrillisation can become fragmented into oligomers and monomers when it interacts with HSPGs (Giamblanco et al., 2020; Goedert et al., 1996; Townsend et al., 2020). It may be possible that mutant tau interactions with HSPG may contribute to the destabilisation tau fibrils which would normally sequester misfolded tau proteins and therefore mitigate tau neurotoxicity. Tau interaction with the plasma membrane and HSPGs at the cell surface could act as nucleation sites for tau aggregation and pathogenic tau seeds production which may in turn assist in the propagation of tau pathology in neuronal networks. This could happen pre- and post-synaptically located HSPGs. Moreover, recent evidence have shown that the sulphation patterns of co-factor heparin is able to regulate tau aggregation kinetics (Townsend et al., 2020). Using thioflavin T fluorescence assay, which is commonly used to monitor fibril formation, the removal of 2-*O*-sulphated heparin sulphates significantly slowed down the rate of aggregation when compared to the removal of other sulphation patterns such as *N*- or 6-*O*-sulphated heparin sulphates (Townsend et al., 2020).

In addition, tau/HSPG binding could also be exacerbating the tau pathology by indirectly causing tau hyperphosphorylation. There is evidence of heparin stimulating tau hyperphosphorylation through activation of cyclin-dependent kinase (cdc28), cAMP-dependent protein kinase, GSK3β and several stress-activated protein kinases (SAP kinases) *in vitro* (Hasegawa et al., 1997; Naini and Soussi-Yanicostas, 2018). The differences in the secretion between WT and mutant tau may be explain by greater interaction of hyperphosphorylated tau with HSPGs at the cell surface membrane. This recruitment could further exacerbate hyperphosphorylation through activation of kinases which in turn increases phosphorylation of tau and the production of pathological tau seeds which are released into the extracellular space (Hasegawa et al., 1997; Naini and Soussi-Yanicostas, 2018). This increase in hyperphosphorylation may cause intracellular stress and as a

protective mechanisms, cells increase secretion into the extracellular space to reduce intracellular mutant tau load.

It is important to note that the morphology of heparin-induced fibrils does not completely recapitulate those found in the brains of patient with AD and other tauopathies. This is supported by a significant amount of evidence from cryo-EM studies which have shown that heparin nucleated tau fibrils have distinct conformation and activity from fibrils seeded from brain-derived tau (Despres et al., 2019; Falcon et al., 2019; Fitzpatrick et al., 2017). The advantage of our study is that neurons are allowed to generate their own intracellular tau inclusions without the need to apply heparin to induce the accumulation of tau in the axons. This therefore allows a more controlled comparative study of tau secretion at physiological and pathological conditions. It should be noted that AD brain contains of mainly phosphorylated tau which is higher in negative charge than normal tau, which is therefore likely to repel polyanionic GAGs. It is still unclear what the role of GAG-protein interactions are in the formation of tau fibrils. These findings will be important and may have implications with the development of AD progression as sulphation patterns of GAGs are known to change with aging, which is the principal risk factor for the progression of AD. Taken together, HSPGs is an emerging player in the progression of tau pathology which warrants further investigations.

6.1.5.3 Role of plasma membrane in tau secretion

The fact that disrupting plasma membrane components such as cholesterol, sphingomyelin and phosphatidylinositol 4,5-bisphosphate [PI(4,5)P2] is sufficient in reducing tau secretion (Katsinelos et al., 2018; Merezhko et al., 2018), suggests that tau and lipid interaction may have a role in direct translocation process. Although lipid and tau interaction were not tested in the study, there is accumulating evidence showing that tau can modulate plasma membrane properties and form pore-like structures that may mediate release (Ait-Bouziad et al., 2017; Lasagna-Reeves et al., 2014; Patel et al., 2015). Tau can form stable protein-lipid complexes that are capable of modulating plasma membrane structures (Ait-Bouziad et al., 2017). Tau can also form pore-like structures in the lipid bilayer, forming tau ‘ion’ channels that are able to modulate cell conductivity (Patel et al., 2015). Others have also reported the ability of tau to form spherical APF which can form pore-like structures in membranes (Lasagna-Reeves et al., 2014). It has been proposed that these structures can potentially occur such as cell, nuclear, or organelle membranes and may mediate ionic leaks. Although these studies are promising, they do not have evidence showing direct penetration or translocation of tau during the secretion process, it highlights the important of tau and plasma membrane interaction. More studies are required to further elucidate the role of phospholipids and plasma membrane structures in tau secretion.

6.1.5.4 Non-activity dependent secretion pathways

Furthermore, as inhibition of both sulphated proteoglycans biosynthesis and neuronal activity was not enough to stop tau secretion processes, it is likely that other non-activity-dependent and HSPG-independent secretory mechanisms are also at play in the secretion process. One possible way this can be mediated is via fusion of pre-synaptic vesicles containing membrane-free tau to the plasma membrane. Pooler et al., (2013) showed that inhibition of the pre-synaptic vesicle and plasma membrane docking process by application of tetanus toxin can reduced activity-induced secretion of endogenous tau. Moreover, recent analysis of the tau interactome changes during neuronal activity has implicated the involvement of the pre-synaptic vesicle fusion machinery (Tracy et al., 2022). They showed that neuronal stimulation enhances tau association of SNARE (e.g., synpatotagmin 1, Mint1) and synaptic vesicle proteins (e.g., synapsin 1). One thing to note about these studies is that KCl-induced depolarisation was used to stimulate neurons. As shown from my results, different pharmacological agents have distinct neurophysiological effects on membrane properties of cells and it is possible that different secretion machineries may be activated in response to different pharmacological stimulants. In addition, these studies have only been done in physiological conditions and how activity-dependent secretion of in pathological conditions has not been fully investigated. It would be interesting to know how the tau interactome changes in different disease states and whether distinct triggers secretory pathways are triggered in response to neuronal activity.

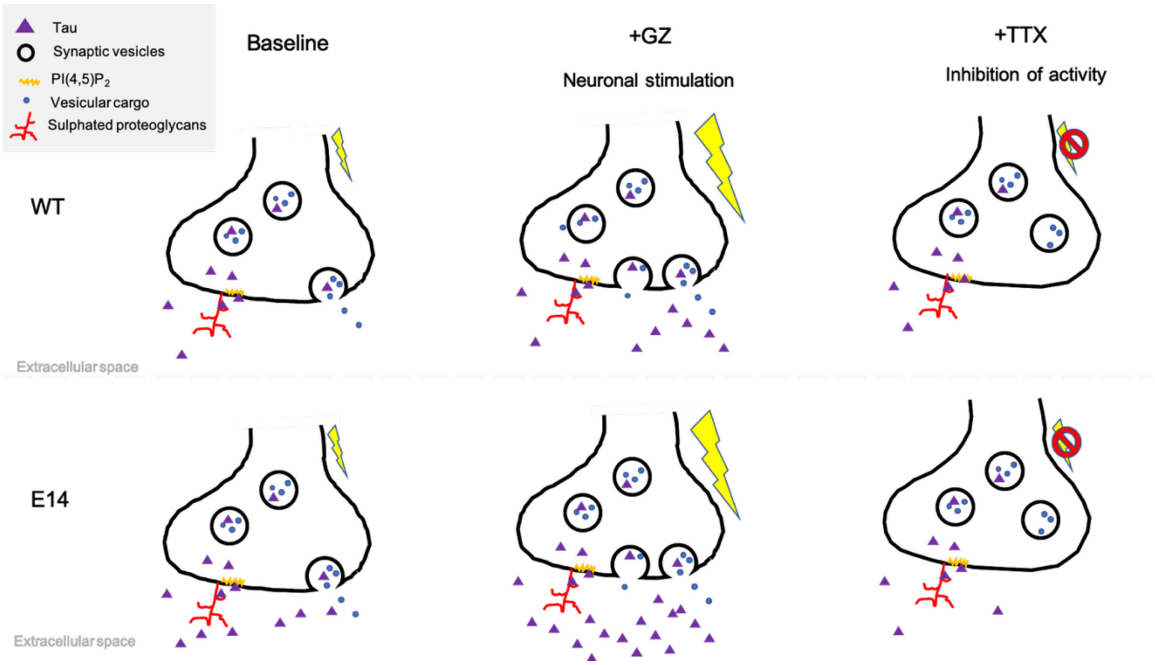

Figure 60 Summary of findings showing activity-dependent secretion of both WT and mutant tau.

At basal conditions, tau is secreted via unconventional pathway. Tau^{E14}-expressing neurons preferentially secreted by neurons than Tau^{WT}. Gabazine application result in increased neuronal stimulation which lead to an increase in the release of membrane-free tau in the extracellular space. Application of TTX results in blockade of neuronal activity; Tau^{WT} and Tau^{E14} secretion remain similar to baseline.

Chapter 7 Future directions

7.1 What other pathways mediate the release of membrane-free tau?

We showed that sulphated proteoglycans mediate some but not all of tau secretion that occurs during neuronal activity in both physiological and pathological conditions. It is likely that other unconventional secretion pathways are recruited to secrete different forms of tau into the extracellular space.

There is increasing evidence showing that the release of synaptic vesicles derived from intracellular membranes organelles (such as autophagosome, lysosomes, late endosomes) could also contribute to the extracellular pool of membrane-free tau in both physiological and pathological conditions (Chen et al., 2020; Fontaine et al., 2016; Pilliod et al., 2020; Rodriguez et al., 2017). Identifying what type of synaptic vesicles are mediating the release of mutant tau would also be valuable. Selectively blocking these secretory pathways may help slow down cell-to-cell transmission of tau pathology.

It is also likely that different secretory mechanisms are involved during activity-dependent secretion. A recent study has characterised tau-interacting proteins that are increased during activity-induced tau secretion (Tracy et al., 2022). This study showed that tau association with SNARE-complex proteins (e.g., synaptotagmin 1, Mint1) and synaptic vesicle protein such as synapsin 1 is upregulated during neuronal stimulation (Tracy et al., 2022). Interestingly, they showed that different disease-associated tau conformers may have distinct pattern of tau-protein interactions. Differences in tau-protein interactomes between FDT-associated mutations, such as Tau^{P301L} and Tau^{V337M} (mutation in position 337 of MAPT gene leads to valine →methionine change), when compared to normal conditions. Tau^{V337M} mutant had an increased interaction with proteins associated with spliceosomal complex and synaptic vesicles proteins when compared to Tau^{P301}. Loss of tau protein interactions were also reported in both tau variants; these were mainly associated with ribosomal and mitochondrial proteins. These patterns were distinct to physiological conditions (Tracy et al., 2022). Identifying these specific tau-interactome signatures for distinct tau conformers will be important in understanding the molecular mechanisms of tau secretion in different tauopathies. Considering that pre-synaptic vesicles fusion may play an important role in activity-dependent secretion of mutant tau, selectively inhibiting these disease-specific SNARE-protein complexes may therefore reduce activity-dependent tau secretion in

pathological conditions. The NanoBiT biosensor could be used for high-throughput drug screening for treatments that can reduce the secretion of seed-competent tau.

Tau-phospholipid interactions also seem important as it has tau has been shown to be recruited into the plasma membrane before it is released into the extracellular space by HSPGs (Katsinelos et al., 2018; Merezhko et al., 2018). In this regard, the release of disease-associated tau via direct translocation across the plasma membrane may first require interaction with PI(4,5)P2, sphingolipids and cholesterol in the cytosolic part of the plasma membrane. As there is evidence showing that tau can produce pore-like structures on plasma membranes (Ait-Bouziad et al., 2017; Lasagna-Reeves et al., 2014), further investigations could look in to the relationship between tau and phospholipids and how these structures may mediate tau translocation without the need for sulphated proteoglycans.

7.2 Large-scale comparative studies between different tau conformers

The NanoBiT-tau biosensor that we established in the plate-reader format is highly sensitive and compatible for high-throughput screening for studying a wide-range of different disease-associated tau mutants. This would allow large-scale comparative studies to probe for differential tau secretion pathways that might exist between different tau conformers in tauopathies. There are currently 112 known MAPT mutations (Figure 61); the NanoBiT-Tau biosensor we established could be used to compare the secretion and re-uptake propensities of these tau variants in a high-throughput setting.

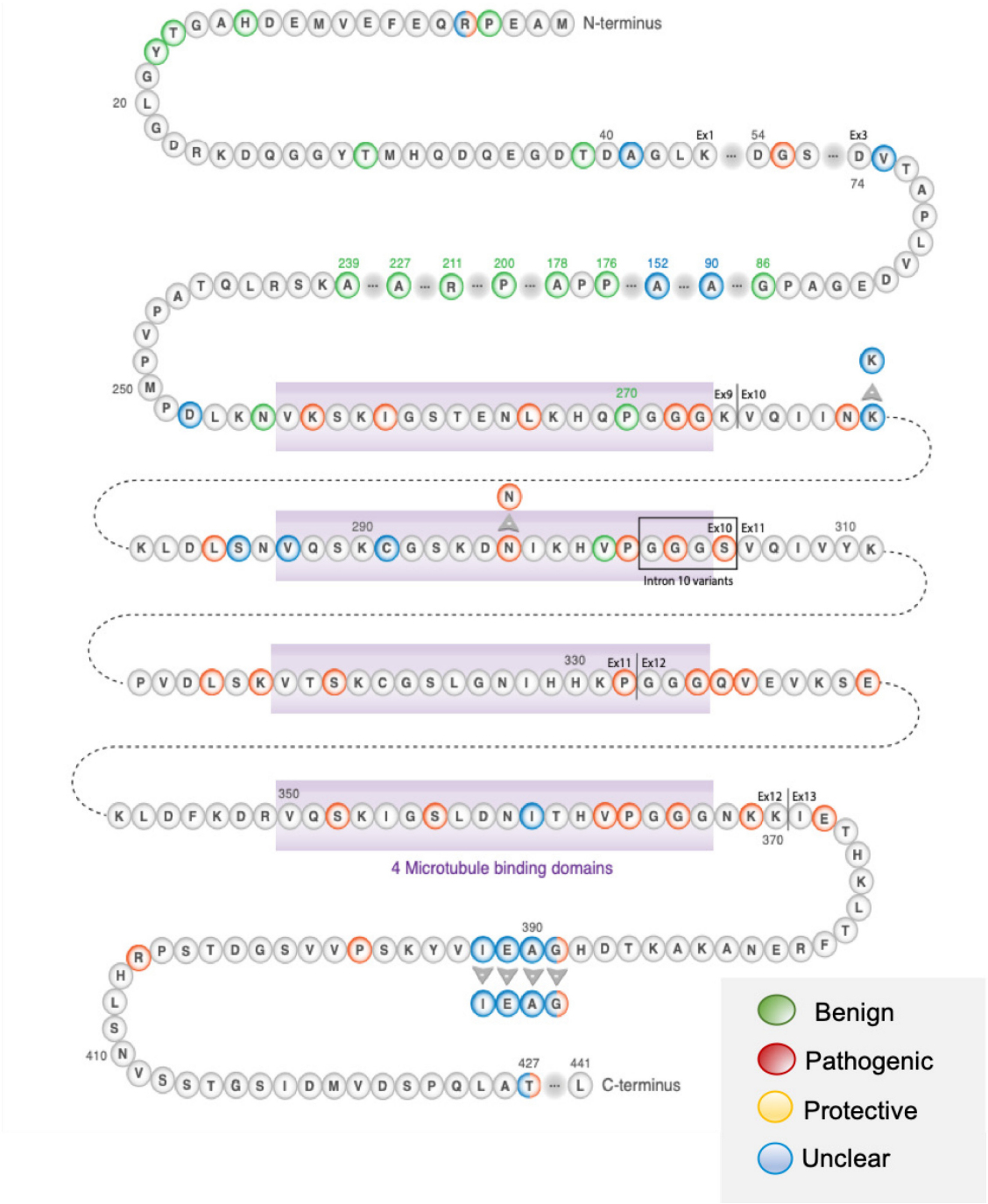

Figure 61. MAPT mutations based on the full-length isoform 441.

Image adapted from ALZFORUM

7.3 What are the mechanisms of tau re-uptake in physiological and pathological conditions?

7.3.1 How to investigate the events that precedes tau misfolding and aggregation in physiological and pathological conditions

Although we had the means to study tau re-uptake, due to the time constraints of the project, the NanoBiT-tau reporter assay was only used to study tau secretion. I previously described the molecular cloning process for the generation of LgBiT-Tau^{WT}, LgBiT-Tau^{E14}, and LgBiT-Tau^{P301L} constructs (Link chapter). We also previously validated the NanoBiT-tau reporter assay and establish the sensitivity required to enable tau secretion and re-uptake to be detected (Figure 62A). In this regard, this assay can be used to investigate the molecular mechanism of tau re-uptake and can be compatible with different formats such as plate-reader and bioluminescence imaging.

This assay allows mechanisms involved in cell-to-cell transmission of WT and mutant tau. Firstly, the molecular mechanisms of tau re-uptake can be investigated using this assay (Figure 62Bi). LgBiT can be expressed by 'acceptor' neurons to detect both WT and mutant tau as it enters the cytosol. LgBiT can also be expressed with a HaloTag to allow these post-synaptic 'acceptor' cells to be fluorescently labelled and distinguished from pre-synaptic 'acceptor' neurons. Only membrane-free tau available to complement with LgBiT in the cytosol are detected. This will provide a mechanistic view of how WT and mutant tau species are taken-up in the cytosol. This technology has already been used in cell lines and primary neurons to study cytosolic entry of tau at physiological levels and how cholesterol affects this process (Tuck et al., 2022).

Secondly, this assay can also be used to investigate the events that precede seeded tau aggregation (Figure 62Bii). HiBiT-tau and LgBiT-tau constructs can be expressed by neurons to monitor tau misfolding and aggregation in a connected neuronal network. For example, HiBiT-Tau^{E14} and mutant LgBiT-Tau^{WT} can be expressed in pre-synaptic and post-synaptic neurons, respectively. HiBiT-tau^{E14} released from pre-synaptic cells can then be taken-up by adjacent cells expressing natively-folded tau tagged with LgBiT. The initial template misfolding of tau can therefore be detected. This method is advantageous in that it allows the cells to generate their own misfolded tau proteins and aggregates, that are then secreted in to the extracellular space in their own way.

Finally, the availability of both HiBiT-Tau^{WT} and LgBiT-Tau^{WT} also enables the cell-to-cell transmission of tau in a physiological state to be monitored (Figure 62Bii). Fluorescence-based

biosensors that have been used previously (Hallinan et al., 2019) required the presence of tau misfolding and aggregation in the post-synaptic cell to show that pathogenic tau species have been taken up; as WT tau does not readily aggregate in primary hippocampal neurons, there is no way of detecting whether it has been taken up in the post-synaptic neuron and if it has interacted with endogenous tau. This LgBiT and HiBiT-based biosensor will therefore give us a better mechanistic insight in the cell-to-cell transmission of tau in physiological conditions.

Overall, the NanoBiT-tau biosensor allows a mechanistic insight to the secretion and re-uptake of tau in physiological and pathological conditions.

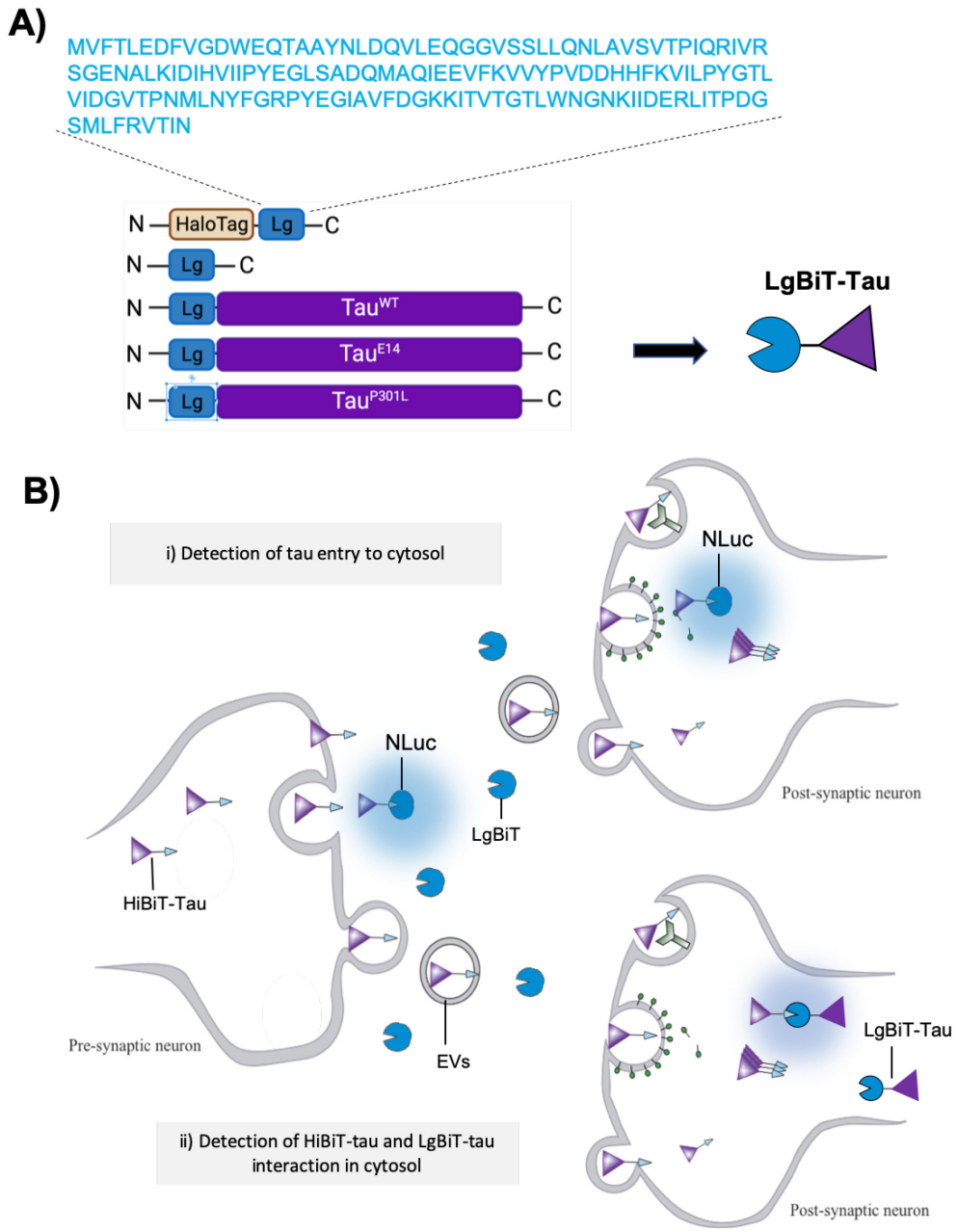

Figure 62. Illustration of LgBiT-tau constructs generated to investigate tau re-uptake.

A) LgBiT-Tau^{WT}, LgBiT-Tau^{E14}, LgBiT-Tau^{P301L}, HaloTag-LgBiT and LgBiT constructs to be used in re-uptake experiments. B) NanoBiT-Tau reporters can be used to detect both release and re-uptake in a connected neuronal network. Two different re-uptake mechanisms can be investigated: i) the exact molecular mechanisms of tau entry to the cytosol can be investigated by the expression of LgBiT in the post-synaptic neuron. This will detect tau in the cytosol that are membrane-free; ii) the interaction of WT and mutant tau that was released from the extracellular space and taken up, with endogenous tau that is expressed by adjacent cells can be investigated. HiBiT-tau and endogenously expressed tau tagged with LgBiT can be detected in this assay. EVs = extracellular vesicles such as ectosomes and exosomes.

7.3.2 Modelling tau release and re-uptake in connected neuronal networks

Work previously done in our lab has shown that tau misfolding and formation of accumulates propagate efficiently in a connected neuronal network using primary hippocampal neurons grown on microfluidic devices (Hallinan et al., 2019). To do this, GFP-Tau^{E14}-expressing cells (green) were co-cultured with RFP-Tau^{WT} (red) on the main channels on a microfluidic device (as seen on Figure 63 A-C). The use of microfluids for tau propagation studies are advantageous as this allows different populations of cells to be fluidically isolated. Furthermore, certain microfluidic designs can be used to control neurite outgrowth in cultured neurons (Holloway et al., 2019) allowing for a better *in vitro* model for the unidirectional connectivity found in certain areas of the brain. Unidirectional outgrowth of neurons was found to be successful with designs such as the 'arrow head' (as seen Figure 63D).

Microfluidics and NanoBiT-Tau biosensors can therefore be used together to monitor the release and re-uptake of different tau variants at a single-cell resolution. This set-up is unique in that cells expressing HiBiT-tau can be cultured in the first channel (green cells; Figure 63C), and another subset of cells expressing LgBiT- or LgBiT-tau can be cultured in the second channel (red cells; Figure 63C). These two sub-sets of neurons can be treated as they are fluidically isolated. The secretion and re-uptake of different tau variants can therefore be monitored. To monitor release, LgBiT can be added directly on to the second chamber and all HiBiT-tau released can be detected.

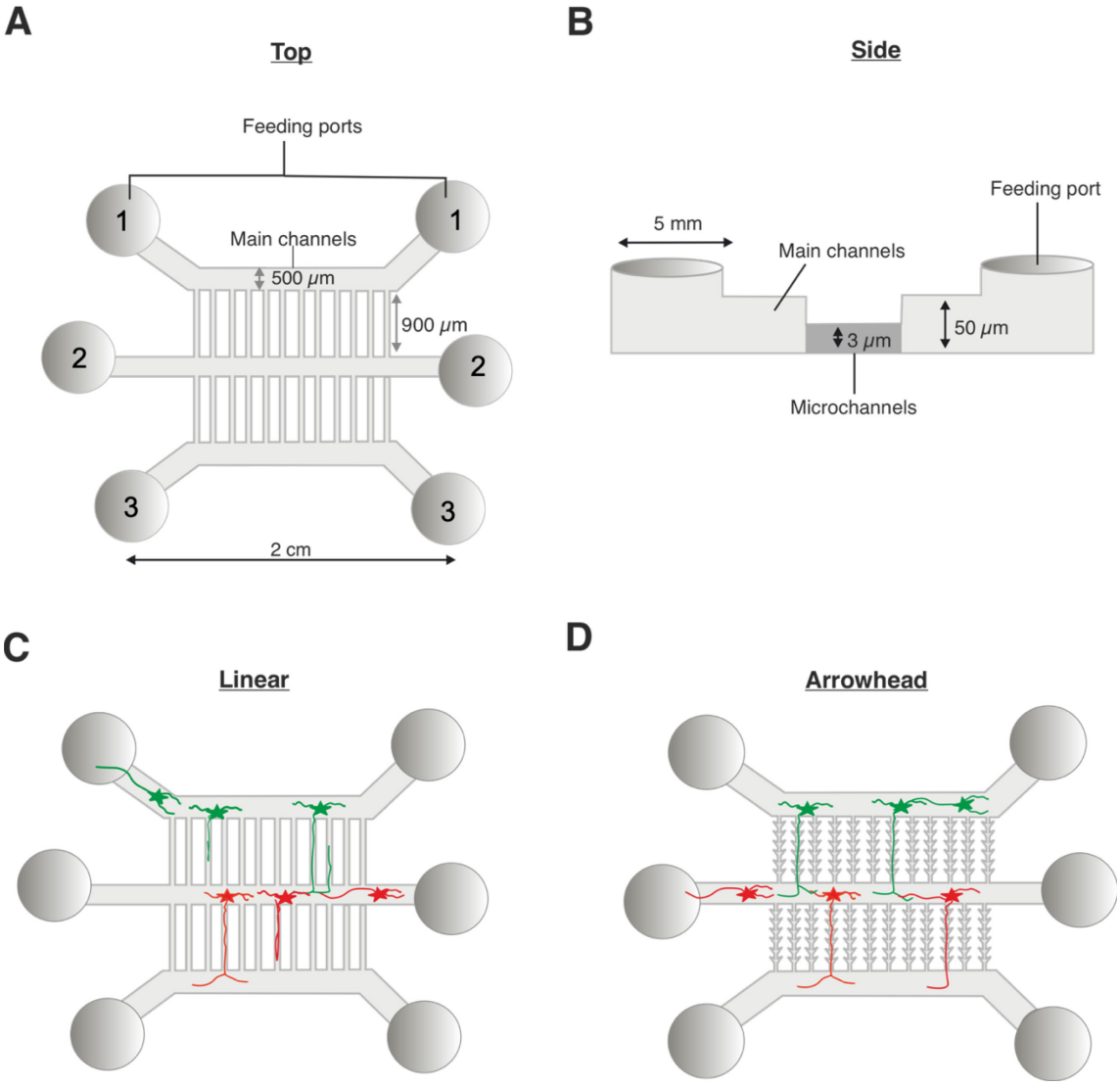

Figure 63 Illustration of microfluidic device designs available to monitor tau secretion and re- uptake.

A-B) the microfluidic device dimensions are shown on the top (A) and side (B) views. C) Linear microfluidic devices can be used in tau secretion assays. Neuronal outgrowth is not unidirectional in this device and neurons can grow back to the main channels. D) The arrowhead microfluidic device can be used in both tau secretion and re-uptake assays, as it orientates neuronal outgrowths in one direction.

Appendix A Plasmid sequence validation

A.1 MATLAB script used for assessing tau aggregation

```
controlbase=prctile(control,10);
controlzero=control-controlbase;
max=max(controlzero);
include=max<171;
controlzero2=controlzero(:,include);
deviation=std(controlzero2);
mean=mean(deviation);
logicctl=controlzero>5*mean;
sumcontrol=sum(logicctl);
[n,x]=size(control);
percentagecontrol=sumcontrol/n;
finalcontrol=sum(percentagecontrol>0.1)/x*100;

expbase=prctile(exp,10);
expzero=exp-expbase;
logicexp=expzero>5*mean;
sumexp=sum(logicexp);
[m,y]=size(exp);
percentageexp=sumexp/m;
finalexp=sum(percentageexp>0.1)/y*100;

exp1base=prctile(exp1,10);
exp1zero=exp1-exp1base;
logicexp1=exp1zero>5*mean;
sumexp1=sum(logicexp1);
[m,y]=size(exp1);
percentageexp1=sumexp1/m;
finalexp1=sum(percentageexp1>0.1)/y*100;

```

Figure 64. MATLAB script used to analyse axonal aggregation *in vitro*.

Plot profile values for were generated for each transfected axon. Controls axon used were transfected with GFP-TauWT and was used to generate a baseline range. Any values or aggregated points that lie outside 5 times the standard deviation was considered an aggregated point. Collectively, if all positive aggregated points exceed >10% of the total axon value, then it was considered as an axon positive for aggregation.

A.2 MATLAB scripts used for whole-cell electrophysiology

The individual leak currents at -70 mV, series and input resistance for each cell patched were recorded and analysed using a customised MATLAB script as shown in Figure 65 (kindly produced by Dr Mariana Vargas-Caballero's lab). To find the rheobase and number of action potential custom written code in Figure 66 was used. The total number of action potentials for each recording trace were assessed using the script described in **Error! Reference source not found.** The maximum and peak potential for each action potential was also measured.

```
pathname = ['/Volumes/My Passport/Dianne/WC_data_patch_2021/Transduced_Cells/'];
excel_fileName = ['/Users/dml1n18/OneDrive - University of Southampton/Patchclamp/Dianne_PC_log_1.xlsx'];
Data_log_spiking = dataset('xlsfile', excel_fileName);

excel_row_number = 232 %set row for analysis here
experiment_number = excel_row_number-1;

directory = Data_log_spiking.Directory(experiment_number)
directory = directory{1};
run_number = Data_log_spiking.Run_Restest(experiment_number);
str_run_number = num2str(run_number);
cd([pathname directory])

numfiles = 20; %use first 20 sweeps of a restest file *** EDIT IF <20SWEEPS
mydata = cell(1,numfiles); mid = cell(1,numfiles); base = cell(1,numfiles);
for k=1:numfiles %loops from 1 to "numfiles"

load(sprintf(['sweep' str_run_number '_%d.mat'],k)) %loads sweep_struct.data

if length(sweep_struct.data)== 3000
all_data(:,k) = sweep_struct.data; %adds all sweeps of the run into a matrix
else end
end

AverageTrace = mean(all_data');
%peak = max(all_data(:));
figure(1), plot(AverageTrace) %plots mean trace of Restest

leak = mean(AverageTrace(1:500)) %average of first 500 samples = leak
mid = mean(AverageTrace(1500:1900)); %average during voltage step
Peak = max(AverageTrace);
InputRes = abs((2/(mid-leak))*1000)
SeriesRes = abs((2/(Peak - leak))*1000)
```

Figure 65 MATLAB script used to assess membrane properties such as leak current, input and series resistance.

This script was generated by Dr Mariana Vargas-Caballero's lab.

```
pathname = ['/Volumes/My Passport/Dianne/WC_data_patch_2021/Transduced_Cells/'];
excel_fileName = ['/Users/dml1n18/OneDrive - University of Southampton/Patchclamp/Dianne_PC_log_1.xlsx'];
Data_log_spiking = dataset('xlsfile', excel_fileName); %Changed CD

for excel_row_number = 232 %change this to analyse each row
    excel_row_number
    experiment_number = excel_row_number-1;

    time = Data_log_spiking.Exposure_time(experiment_number);
    include = Data_log_spiking.Include(experiment_number);

    if include == 1 %& time == 48
        directory = Data_log_spiking.Directory(experiment_number);
        directory = directory{1};

        cd([pathname directory])


        run_number = Data_log_spiking.Run_Family_currents(experiment_number);
        str_run_number = num2str(run_number);
        [filelist,tvector,sampint,numfiles] = file_list_DML(run_number);%Changed File_list_Hannah
        filename = [pathname 'Analysis_files/Spike_analysis_' directory '_' str_run_number ];
        load(['sweep' str_run_number '_1.mat'])

        mydata = cell(1,numfiles);
        for k=1:numfiles
            load(sprintf(['sweep' str_run_number '_%d.mat'],k)) %loads sweep_struct.data
            mydata{k} = (sweep_struct.data);
        end

        stim_type = Data_log_spiking.Stim_type(experiment_number)

        if stim_type == 1
            middle1 = 5001;
            middle2 = 10000; %This sets the start & end of current injection period
            %based on sample number - the data the script will check for
            %APs.
            current_steps = [-100: 25: 1000];%Tells Matlab your current injections
            %start at -100pA, in steps of 25pA up to a max. of 1000pA.

%
        elseif stim_type == 2   %This is for your "long" data, 40,000 samples
            middle1 = 10001;
            middle2 = 30000;
            current_steps = [-100: 25: 1000];
        end


        hold on
        max_value_all = [];
        min_value_all = [];
        for i = 1:numfiles
            sweep1 = mydata{i};
            [max_value, index] = max(sweep1(middle1:middle2));
            max_value = mean(sweep1(index+middle1-1:index+middle1+1));

            max_value_all = [max_value_all max_value];


            [min_value, index] = min(sweep1(middle1:middle2));
            min_value = mean(sweep1(index+middle1-1:index+middle1+1));
            min_value_all = [min_value_all min_value];
        end



        voltage_change = max_value_all- min_value_all;
        current_steps = current_steps(1:size(voltage_change,2));
        negative_stim_change = current_steps<0;
        positive_stim_change = current_steps>=0;
        new_voltage_change = [voltage_change(negative_stim_change)*-1 voltage_change(positive_stim_change)];
        spiking_yes_no = new_voltage_change > 60; %%Changed AP threshold

        [y,index] = find(spiking_yes_no==1)
        rheobase_confirm = 0
        rheobase = -1;
        if isempty(index) ~= 1
            rheobase = current_steps(index(1))
            hold on


            figure(50)
            hold off
            set(gcf,'Position',[ 680   384   560   420])
            plot(mydata{index(1)-1},'k')
            hold on
            plot(mydata{index(1)},'r')


            rheobase_confirm = input('Is the cell spiking in red trace? 1 = yes/0 = no, enter 5 to exit','s');

        end

        if rheobase_confirm == '5'
            break
        end

        new_current_steps = [current_steps(negative_stim_change) current_steps(positive_stim_change)];

        figure(100), hold on,
        set(gcf,'Position',[92   385   560   420])

        plot(new_current_steps, new_voltage_change,'k','LineWidth',1.5)%plot control in black


        save('filename', 'new_current_steps', 'new_voltage_change', 'rheobase', 'rheobase_confirm')
    end

end
grid on
```

Figure 66 MATLAB script for assessing rheobase.

The script was generated by Dr Mariana Vargas-Caballero's lab.

```
ydata=table2array(data(:,2)); %Extracts column 2 (y data) to string of doubles
ydata(isnan(ydata))=[];          % Removes NaN values from the string

MinValue = min(ydata); %Finds minimum mV value = "baseline"
mean_MinValue = mean(ydata); %finds the mean of ydata as 'baseline' to ignore noise
Threshold = 0

xdata=table2array(data(:,1));    %Extract X data = time in seconds;
xdata(isnan(xdata))=[];             %Remove NaN values

[N ,AP_samples] = spike_times(ydata,Threshold); %AP_samples = when each AP peaks (sample number)
differences = diff(AP_samples); %How many sample numbers between each AP peak
intervals = (differences*0.001)';    %Convert sample numbers to interval time (in seconds)
%^ Assuming sample frequency of 1KHz (1 per msec)
%For 20kHz change to *0.0005 (1 per 0.05msec)- use is used 0.05msec
%For data recorded at 1 per msec sampling interval use *0.001 (1kHz)

num_APs = length(AP_samples);
peak_potentials=[];

for i = 1:num_APs   %for each action potential in order, find the sample number

    sample_number = AP_samples(i);

    peak_potential = ydata(sample_number);  %Extract the AP peak value at that sample number
    peak_potentials = [peak_potentials peak_potential]; %Add peak values to matrix

end

AP_samples_in_seconds = AP_samples*0.001; %Converts AP index into seconds for plotting

AP_amplitudes = peak_potentials - mean_MinValue; %subtract baseline to get total amplitude of mV change

Min1=[]; Min2=[]; Min3=[]; Min4=[]; Min5=[]; %Create empty matrix for each minute of recording
%The following loop adds data to its relevant matrix, separated by  minute

for i=1:num_APs;
    if AP_samples_in_seconds(i) < 60    %If AP falls between 0-60seconds
        min1_AP_amp = AP_amplitudes(i); %Add corresponding amplitude to matrix for Min1
        Min1 = [Min1 min1_AP_amp];      %Matrix contains ALL amplitudes from first minute

    elseif AP_samples_in_seconds(i) <120 && AP_samples_in_seconds(i) >=60   %if 60-120 sec...
         min2_AP_amp = AP_amplitudes(i);
        Min2 = [Min2 min2_AP_amp];      %Matrix contains ALL amplitudes from second minute & so on

         elseif AP_samples_in_seconds(i) <180 && AP_samples_in_seconds(i) >=120
         min3_AP_amp = AP_amplitudes(i);
        Min3 = [Min3 min3_AP_amp];

         elseif AP_samples_in_seconds(i) <240 && AP_samples_in_seconds(i) >=180
         min4_AP_amp = AP_amplitudes(i);
        Min4 = [Min4 min4_AP_amp];

         elseif AP_samples_in_seconds(i) <300 && AP_samples_in_seconds(i) >=240
         min5_AP_amp = AP_amplitudes(i);
        Min5 = [Min5 min5_AP_amp];
    end
end

%Generate average & Stdev per minute:
Amp_Minute1 = mean(Min1); Amp_Minute2 = mean(Min2);
Amp_Minute3 = mean(Min3); Amp_Minute4 = mean(Min4);
Amp_Minute5 = mean(Min5);

std_min1 = std(Min1); std_min2 = std(Min2); std_min3 = std(Min3);
std_min4 = std(Min4); std_min5 = std(Min5);

%prints all averages as a single vector
Avg_amplitude_per_minute = [Amp_Minute1 Amp_Minute2 Amp_Minute3 Amp_Minute4 Amp_Minute5]

%Print all stdev - use for analysis if needed
std_per_minute = [std_min1 std_min2 std_min3 std_min4 std_min5]


Min_pp_1=[]; Min_pp_2=[]; Min_pp_3=[]; Min_pp_4=[]; Min_pp_5=[]; %Create empty matrix for each minute of recording
%The following loop adds data to its relevant matrix, separated by  minute
```

Figure 67 MATLAB script for the analysis for the number of action potentials, peak potential and maximum potential.

The script was generated by Hannah Warming and modified by myself.

A.3 Lentiviral constructs for transduction

All constructs that were generated and used on this project were validated by sequencing analysis. The plasmid vectors listed in appendix A were used for the generation of lentiviral particles to transduce primary hippocampal neurons. The lentiviral expression vector was also denoted as 'E60'. All detailed plasmid information is located on Table 2-1.

A.3.1 GFH-HiBiT-Tau

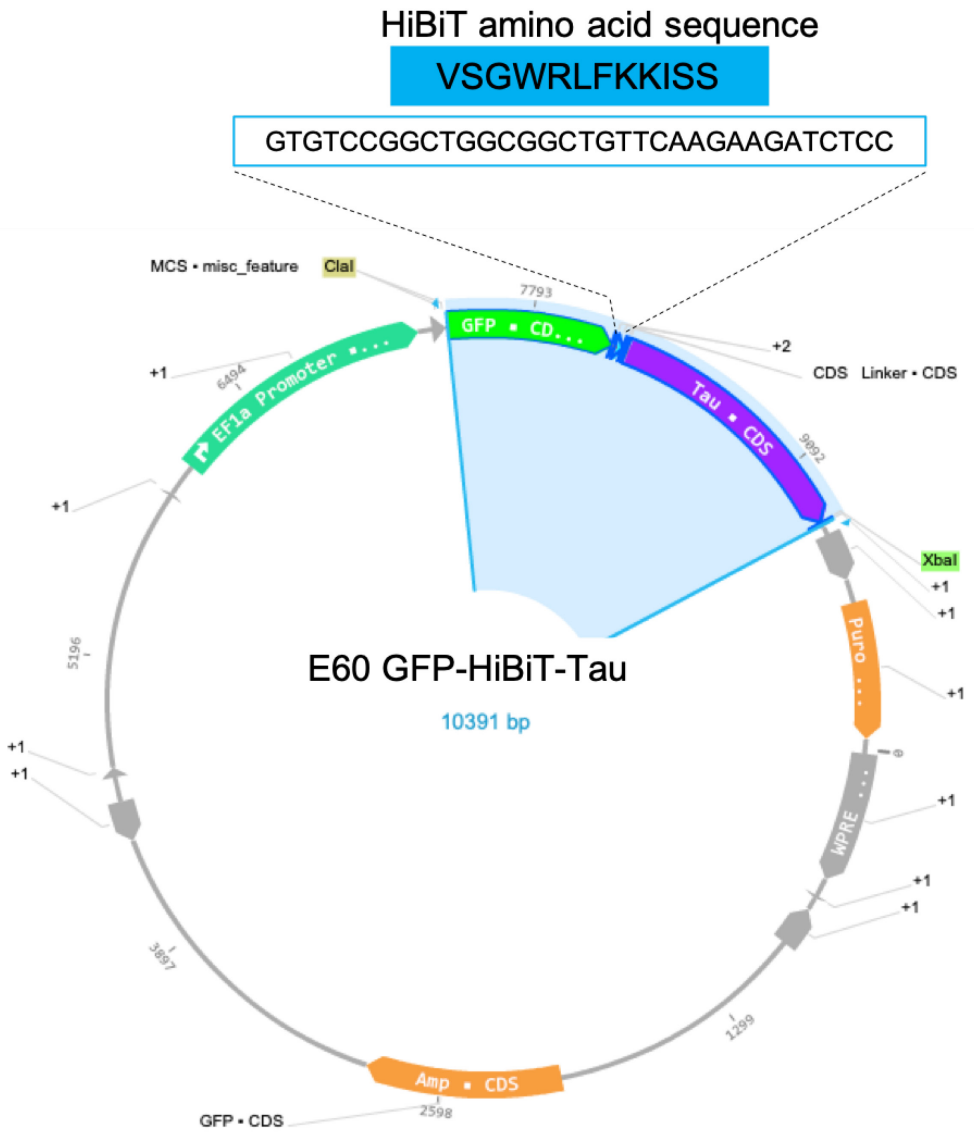

Figure 68. Plasmid map for GFP-HiBiT-Tau constructs on a lentiviral expression vector.

Green encodes for green fluorescent protein; blue encodes for HiBiT; purple indicates Tau encoding sequence. ClaI and XbaI restriction sites flank GFP-HiBiT-Tau (purple) encoding sequences. Generated using Genome Compiler.

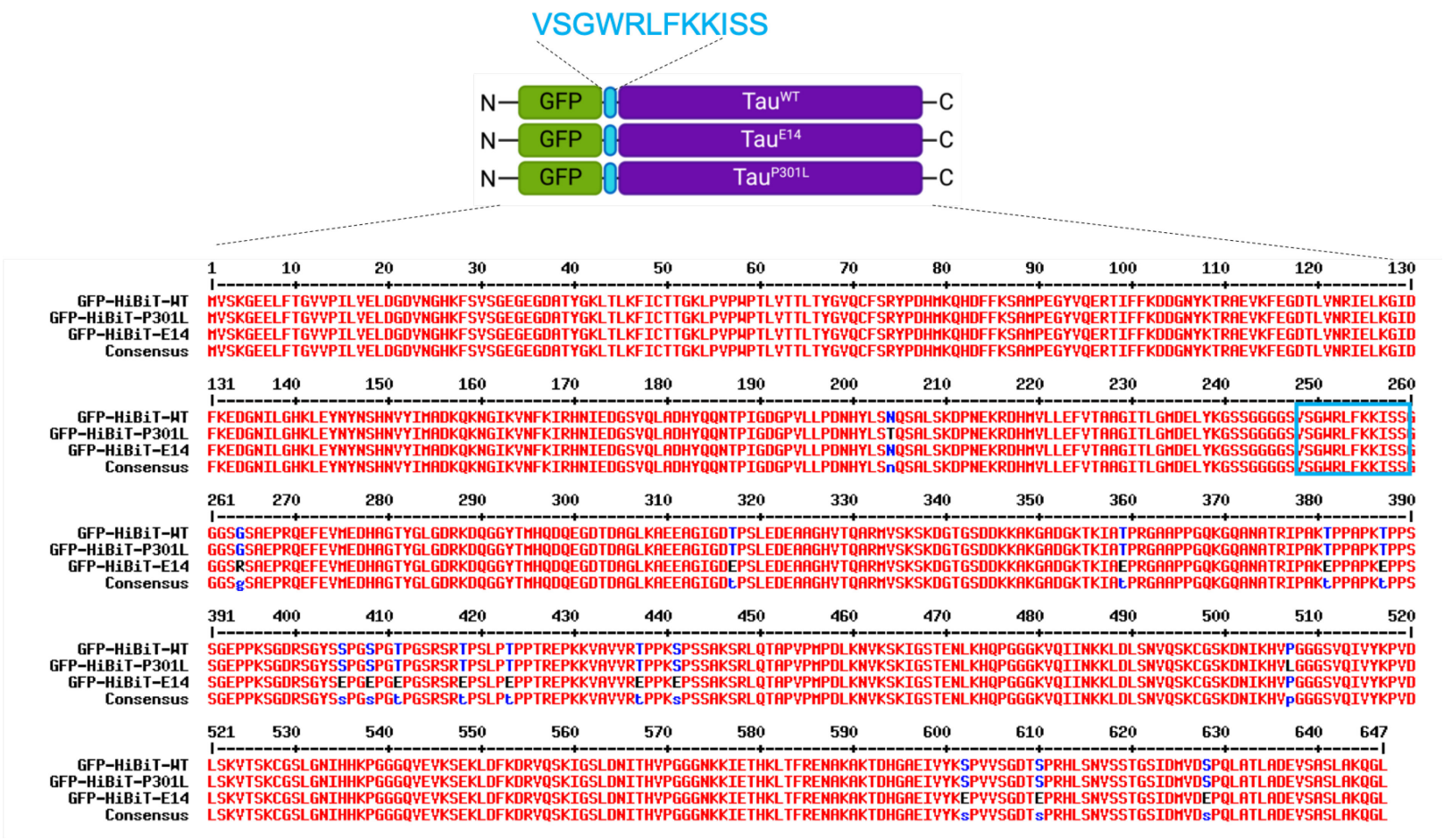

Figure 69. Sequence alignment of the different GFP-HiBiT-Tau variants.

A.3.2 Secretory controls

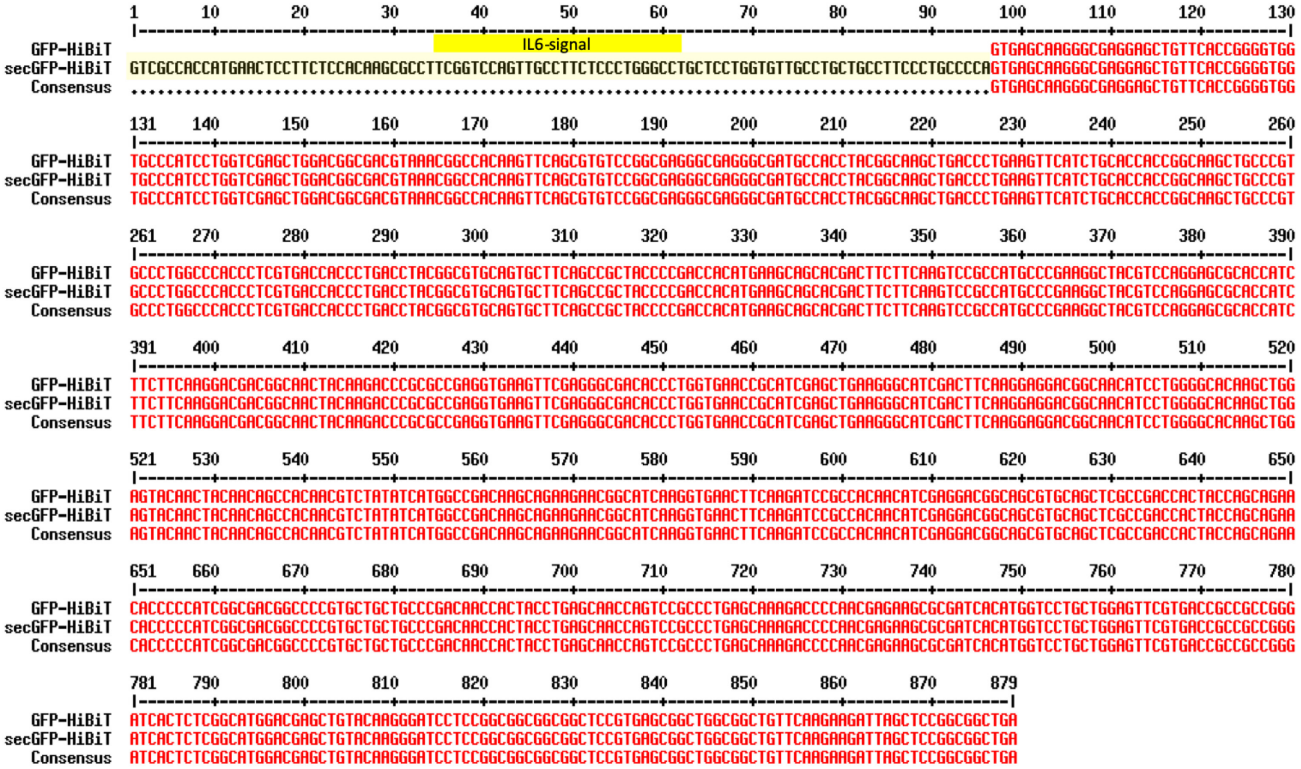

Figure 70. GFP-HiBiT and secGFP-HiBiT sequence alignment

This indicates the sequence validation alignment for the lentivirus plasmids used in the project. GFP-HiBiT and secGFP-HiBiT is on a lentiviral expression vector. Red indicate similarities in nucleotide sequences. Yellow indicate IL6 sequence on secGFP construct.

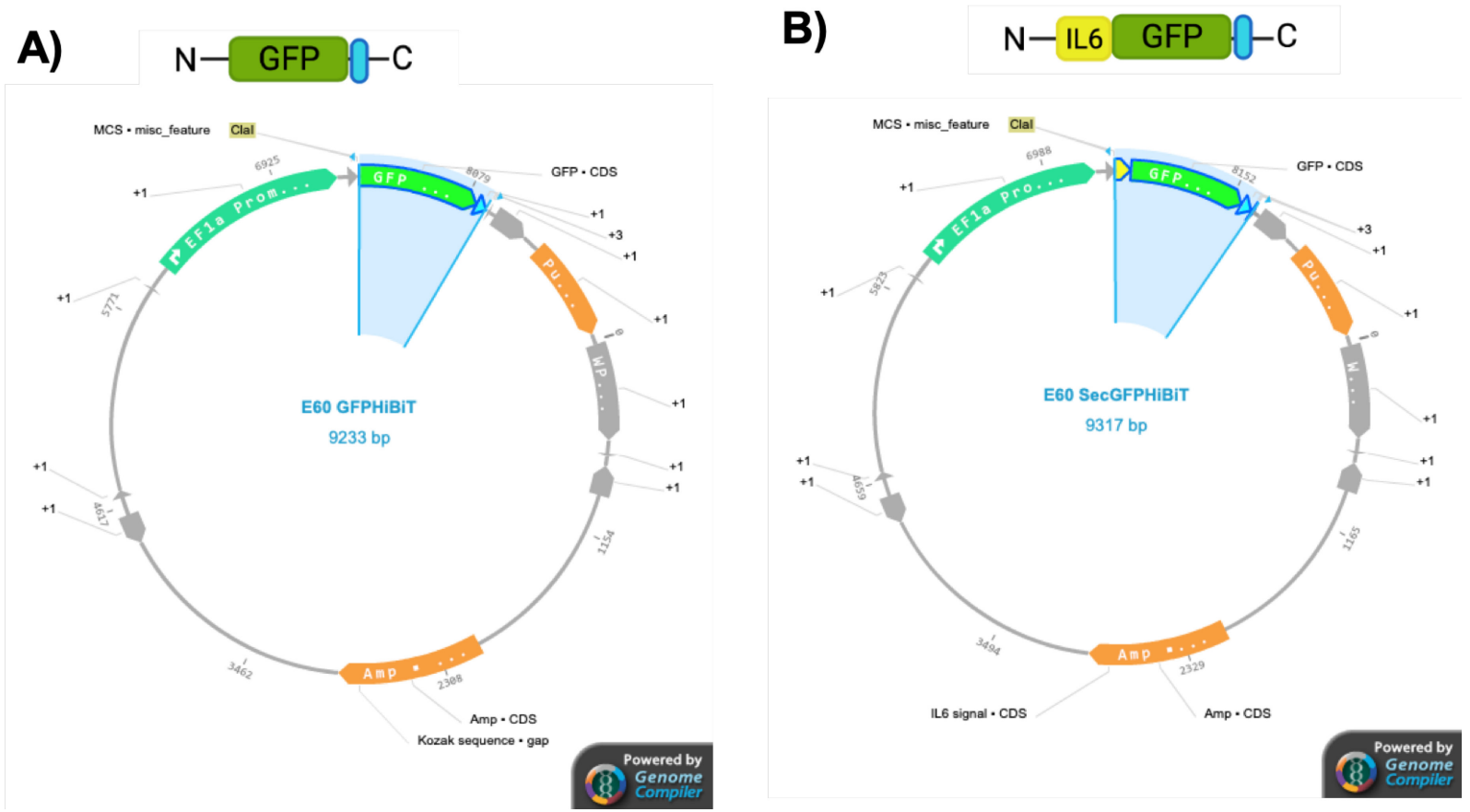

Figure 71 Plasmid map for GFP-HiBiT and secGFP-HiBiT on a lentiviral expression vector.

A.4 Buffers and Solutions

A.4.1 Tissue Culture:

Neurobasal Medium (50ml)

- 48.875 ml neurobasal media (Gibco)
- 1 ml B-27plus supplement (Gibco)
- 125µl Glutamax (Gibco)

A.4.2 Molecular Biology:

LB Agar (1L)

- 20 g Agar
- 10 g NaCl
- 10 g Tryptone
- 5 g Yeast extract
- dH_2O to 1 L. Adjust to pH 7.0 with 5 M NaOH and Autoclave.
- Supplement with 1 ml (100 µg/ml Ampicillin) prior to pouring.

LB media (1L)

- 10 g Tryptone
- 10 g NaCl
- 5 g Yeast extract
- 950 ml ddH_2O
- Adjust to pH 7.0 with 5 M NaOH and make up to 1L with ddH_2O and autoclave.
- Supplement with 1 ml (100 µg/ml Ampicillin) prior to use.

SOC Outgrowth (NEB)

- 2% (w/v) Vegetable Peptone
- 0.5% (w/v) Yeast Extract
- 10 mM NaCl
- 2.5 mM KCl
- 10 mM MgCl2
- 10 mM MgSO4
- 20 mM Glucose

10X TAE Buffer (1L)

- 48.4 g Tris base (40 mM final 1X concentration)
- 11.4 ml glacial (17.4 M) acetic acid
- 20ml 0.5 M EDTA
- dH2O to 1L

A.4.3 Protein Analysis

5x Sample Buffer (SDS-PAGE)

- 350mM Tris pH6.8
- 30% glycerol
- 10% SDS
- 600mM DTT
- 0.012% BPB

SDS PAGE gels

Table 7-1 SDS page ingredients for resolving and stacking gel

Resolving gel		Stacking gel	
Reagent	Volume (1 gel)	Reagent	Volume (1 gel)
Acrylamide	2ml	Acrylamide	260µl
1.5M Tris + 0.4% SDS	1.5ml	0.5M Tris + 0.4% SDS	500µl
ddH_2O	2.5ml	ddH_2O	1.25ml
10% APS	60µl	10% APS	20µl
TEMED	6µl	TEMED	2µl

10x Laemmi Buffer (Running Buffer; 1L)

- 30.0 g Tris base (25 mM)
- 144.0 g glycine (192 mM)
- 10.0 g SDS (0.1% w/v)
- Dissolve in 1L ddH_2O and check pH ~8.5
- To make 1x Running Buffer add 100ml of 10X stock solution of Laemmli buffer to 900ml dH_2O.

10x TBS

- 20mM Tris pH7.5
- 140mM NaCl
- Up to 1L with dH_2O

1x TBS-T (1L)

- 100 ml 10x TBS
- 5 ml Tween-50 (Sigma)
- Up to 1L with dH_2O

10x PBS

- 1.37 M NaCl
- 27 mM KCl
- 100 mM Na_2HPO_4,
- 18 mM KH_2PO_4.

A.4.4 Electrophysiology

Intracellular K+ gluconate solution (~290 mOsm)

- 110mM Potassium gluconate
- 10mM KCl
- 10mM HEPES
- 10mM K2Phosphocreatine
- 0.4mM GTP
- 4mM Mg^{2+}-ATP
- 20mM KOH to adjust pH to 7.2

Bibliography

Abounit, S., Wu, J. W., Duff, K., Victoria, G. S. and Zurzolo, C. (2016). Tunneling nanotubes: A possible highway in the spreading of tau and other prion-like proteins in neurodegenerative diseases. *Prion* **10**, 344–351.

Ahmed, R. M., Devenney, E. M., Irish, M., Ittner, A., Naismith, S., Ittner, L. M., Rohrer, J. D., Halliday, G. M., Eisen, A., Hodges, J. R., et al. (2016). Neuronal network disintegration: common pathways linking neurodegenerative diseases. *J. Neurol. Neurosurg. Psychiatry* **87**, 1234–1241.

Ait-Bouziad, N., Lv, G., Mahul-Mellier, A. L., Xiao, S., Zorludemir, G., Eliezer, D., Walz, T. and Lashuel, H. A. (2017). Discovery and characterization of stable and toxic Tau/phospholipid oligomeric complexes. *Nat. Commun.* **8**, 1–16.

Albert, M., Mairet-Coello, G., Danis, C., Lieger, S., Caillierez, R., Carrier, S., Skrobala, E., Landrieu, I., Michel, A., Schmitt, M., et al. (2019). Prevention of tau seeding and propagation by immunotherapy with a central tau epitope antibody. *Brain* **142**, 1736–1750.

Alquezar, C., Arya, S. and Kao, A. W. (2021). Tau Post-translational Modifications: Dynamic Transformers of Tau Function, Degradation, and Aggregation. *Front. Neurol.* **11**, 1826.

Alzheimer's Society (2014). *Dementia UK Second edition - Overview*.

Andreadis, A., Brown, W. M. and Kosik, K. S. (1992). Structure and novel exons of the human tau gene. *Biochemistry* **31**, 10626–10633.

Antón-Fernández, A., Vallés-Saiz, L., Avila, J. and Hernández, F. (2022). Neuronal nuclear tau and neurodegeneration. *Neuroscience*.

Armstrong, A., Mattsson, N., Appelqvist, H., Janefjord, C., Sandin, L., Agholme, L., Olsson, B., Svensson, S., Blennow, K., Zetterberg, H., et al. (2014). Lysosomal network proteins as potential novel CSF biomarkers for Alzheimer's disease. *NeuroMolecular Med.* **16**, 150–160.

Arrasate, M., Pérez, M., Valpuesta, J. M. and Avila, J. (1997). Role of glycosaminoglycans in determining the helicity of paired helical filaments. *Am. J. Pathol.* **151**, 1115–1122.

Asai, H., Ikezu, S., Tsunoda, S., Medalla, M., Luebke, J., Haydar, T., Wolozin, B., Butovsky, O., Kügler, S. and Ikezu, T. (2015). Depletion of microglia and inhibition of exosome synthesis halt tau propagation. *Nat. Neurosci.* **18**, 1584–1593.

Austefjord, M. W., Gerdes, H.-H. and Wang, X. (2014). Tunneling nanotubes: Diversity in morphology and structure. *Commun. Integr. Biol.* **7**, e27934.

Avila, J., Jiménez, J. S., Sayas, C. L., Bolós, M., Zabala, J. C., Rivas, G. and Hernández, F. (2016). Tau Structures. *Front. Aging Neurosci.* **8**, 262.

Barghorn, S., Davies, P. and Mandelkow, E. (2004). Tau Paired Helical Filaments from Alzheimer's Disease Brain and Assembled in Vitro Are Based on β-Structure in the Core Domain. *Biochemistry* **46**, 1694–703.

Berriman, J., Serpell, L. C., Oberg, K. A., Fink, A. L., Goedert, M. and Crowther, R. A. (2003). Tau filaments from human brain and from in vitro assembly of recombinant protein show cross-beta structure. *Proc. Natl. Acad. Sci. U. S. A.* **100**, 9034–8.

Bolós, M., Llorens-Martín, M., Jurado-Arjona, J., Hernández, F., Rábano, A. and Avila, J. (2016). Direct Evidence of Internalization of Tau by Microglia In Vitro and In Vivo. *J. Alzheimer's Dis.* **50**, 77–87.

Braak, H. and Braak, E. (1991). Neuropathological stageing of Alzheimer-related changes. *Acta Neuropathol.* **82**, 239–59.

Braak, H., Thal, D. R., Ghebremedhin, E. and Del Tredici, K. (2011). Stages of the Pathologic Process in Alzheimer Disease: Age Categories From 1 to 100 Years. *J. Neuropathol. Exp. Neurol.* **70**, 960–969.

Bright, J., Hussain, S., Dang, V., Wright, S., Cooper, B., Byun, T., Ramos, C., Singh, A., Parry, G., Stagliano, N., et al. (2015). Human secreted tau increases amyloid-beta production. *Neurobiol. Aging* **36**, 693–709.

Buée, L., Bussière, T., Buée-Scherrer, V., Delacourte, A. and Hof, P. R. (2000). Tau protein isoforms, phosphorylation and role in neurodegenerative disorders. *Brain tResearch Rev.* **33**, 95–130.

Bugiani, O., Murrell, J. R., Giaccone, G., Hasegawa, M., Ghigo, G., Tabaton, M., Morbin, M., Primavera, A., Carella, F., Solaro, C., et al. (1999). Frontotemporal Dementia and Corticobasal Degeneration in a Family with a P301S Mutation in Tau. *J. Neuropathol. Exp. Neurol.* **58**, 667–677.

Busche, M. A., Eichhoff, G., Adelsberger, H., Abramowski, D., Wiederhold, K. H., Haass, C., Staufenbiel, M., Konnerth, A. and Garaschuk, O. (2008). Clusters of hyperactive neurons

near amyloid plaques in a mouse model of Alzheimer's disease. *Science (80-.).* **321**, 1686–1689.

Busche, M. A., Wegmann, S., Dujardin, S., Commins, C., Schiantarelli, J., Klickstein, N., Kamath, T. V., Carlson, G. A., Nelken, I. and Hyman, B. T. (2019). Tau impairs neural circuits, dominating amyloid-β effects, in Alzheimer models in vivo. *Nat. Neurosci.* **22**, 57–64.

Calafate, S., Buist, A., Miskiewicz, K., Vijayan, V., Daneels, G., de Strooper, B., de Wit, J., Verstreken, P. and Moechars, D. (2015). Synaptic Contacts Enhance Cell-to-Cell Tau Pathology Propagation. *Cell Rep.* **11**, 1176–1183.

Calafate, S., Flavin, W., Verstreken, P. and Moechars, D. (2016). Loss of Bin1 Promotes the Propagation of Tau Pathology. *Cell Rep.* **17**, 931–940.

Chai, X., Dage, J. and Citron, M. (2012). Constitutive secretion of tau protein by an unconventional mechanism. *Neurobiol. Dis.* **48**, 356–366.

Chen, Q., Zhou, Z., Zhang, L., Wang, Y., Zhang, Y. W., Zhong, M., Xu, S. C., Chen, C. H., Li, L. and Yu, Z. P. (2012). Tau protein is involved in morphological plasticity in hippocampal neurons in response to BDNF. *Neurochem. Int.* **60**, 233–242.

Chen, J. J., Nathaniel, D. L., Raghavan, P., Nelson, M., Tian, R., Tse, E., Hong, J. Y., See, S. K., Mok, S.-A., Hein, M. Y., et al. (2019). Compromised function of the ESCRT pathway promotes endolysosomal escape of tau seeds and propagation of tau aggregation. *J. Biol. Chem.* **294**, 18952–18966.

Chen, X., Li, Y., Wang, C., Tang, Y., Mok, S. A., Tsai, R. M., Rojas, J. C., Karydas, A., Miller, B. L., Boxer, A. L., et al. (2020). Promoting tau secretion and propagation by hyperactive p300/CBP via autophagy-lysosomal pathway in tauopathy. *Mol. Neurodegener.*

Chien, D. T., Bahri, S., Szardenings, A. K., Walsh, J. C., Mu, F., Su, M.-Y., Shankle, W. R., Elizarov, A. and Kolb, H. C. (2013). Early Clinical PET Imaging Results with the Novel PHF-Tau Radioligand [F-18]-T807. *J. Alzheimer's Dis.* **34**, 457–468.

Chinnery, H. R., Pearlman, E. and McMenamin, P. G. (2008). Cutting Edge: Membrane Nanotubes In Vivo: A Feature of MHC Class II + Cells in the Mouse Cornea. *J. Immunol.* **180**, 5779–5783.

Chun, W., Waldo, G. S. and Johnson, G. V. W. (2010). Split GFP Complementation Assay for Quantitative Measurement of Tau Aggregation In Situ. In *Methods in molecular biology (Clifton, N.J.)*, pp. 109–123.

Clavaguera, F., Bolmont, T., Crowther, R. A., Abramowski, D., Frank, S., Probst, A., Fraser, G., Stalder, A. K., Beibel, M., Staufenbiel, M., et al. (2009). Transmission and spreading of tauopathy in transgenic mouse brain. *Nat. Cell Biol.* **11**, 909–913.

Clavaguera, F., Akatsu, H., Fraser, G., Crowther, R. A., Frank, S., Hench, J., Probst, A., Winkler, D. T., Reichwald, J., Staufenbiel, M., et al. (2013). Brain homogenates from human tauopathies induce tau inclusions in mouse brain. *Proc. Natl. Acad. Sci.* **110**, 9535–9540.

Clavaguera, F., Hench, J., Goedert, M. and Tolnay, M. (2015). Invited review: Prion-like transmission and spreading of tau pathology. *Neuropathol. Appl. Neurobiol.* **41**, 47–58.

Courade, J.-P., Angers, R., Mairet-Coello, G., Pacico, N., Tyson, K., Lightwood, D., Munro, R., McMillan, D., Griffin, R., Baker, T., et al. (2018). Epitope determines efficacy of therapeutic anti-Tau antibodies in a functional assay with human Alzheimer Tau. *Acta Neuropathol.* **136**, 729–745.

Cowan, C. M., Bossing, T., Page, A., Shepherd, D. and Mudher, A. (2010). Soluble hyper-phosphorylated tau causes microtubule breakdown and functionally compromises normal tau in vivo. *Acta Neuropathol.* **120**, 593–604.

Croft, C. L., Wade, M. A., Kurbatskaya, K., Mastrandreas, P., Hughes, M. M., Phillips, E. C., Pooler, A. M., Perkinton, M. S., Hanger, D. P. and Noble, W. (2017). Membrane association and release of wild-type and pathological tau from organotypic brain slice cultures. *Cell Death Dis.* **8**, e2671–e2671.

Croft, C. L., Goodwin, M. S., Ryu, D. H., Lessard, C. B., Tejeda, G., Marrero, M., Vause, A. R., Paterno, G., Cruz, P. E., Lewis, J., et al. (2021). Photodynamic studies reveal rapid formation and appreciable turnover of tau inclusions. *Acta Neuropathol.*

Crotti, A., Sait, H. R., McAvoy, K. M., Estrada, K., Ergun, A., Szak, S., Marsh, G., Jandreski, L., Peterson, M., Reynolds, T. L., et al. (2019). BIN1 favors the spreading of Tau via extracellular vesicles. *Sci. Rep.* **9**, 9477.

Crowther, R. A. and Goedert, M. (2000). Abnormal tau-containing filaments in neurodegenerative diseases. *J. Struct. Biol.* **130**, 271–279.

Damdindorj, L., Karnan, S., Ota, A., Hossain, E., Konishi, Y., Hosokawa, Y. and Konishi, H. (2014). A Comparative Analysis of Constitutive Promoters Located in Adeno-Associated Viral Vectors. *PLoS One* **9**, 106472.

Dawson, H. N., Ferreira, A., Eyster, M. V., Ghoshal, N., Binder, L. I. and Vitek, M. P. (2001). Inhibition of neuronal maturation in primary hippocampal neurons from tau deficient mice. *J. Cell Sci.* **114**, 1179–1187.

De Calignon, A., Polydoro, M., Suá Rez-Calvet, M., William, C., Adamowicz, D. H., Kopeikina, K. J., Pitstick, R., Sahara, N., Ashe, K. H., Carlson, G. A., et al. (2012). Propagation of Tau Pathology in a Model of Early Alzheimer's Disease. *Neuron* **73**, 685–697.

Despres, C., Di, J., Cantrelle, F. X., Li, Z., Huvent, I., Chambraud, B., Zhao, J., Chen, J., Chen, S., Lippens, G., et al. (2019). Major Differences between the Self-Assembly and Seeding Behavior of Heparin-Induced and in Vitro Phosphorylated Tau and Their Modulation by Potential Inhibitors. *ACS Chem. Biol.* **14**, 1363–1379.

DeVos, S. L., Corjuc, B. T., Oakley, D. H., Nobuhara, C. K., Bannon, R. N., Chase, A., Commins, C., Gonzalez, J. A., Dooley, P. M., Frosch, M. P., et al. (2018). Synaptic Tau Seeding Precedes Tau Pathology in Human Alzheimer's Disease Brain. *Front. Neurosci.* **12**, 267.

Diez, L. and Wegmann, S. (2020). Nuclear Transport Deficits in Tau-Related Neurodegenerative Diseases. *Front. Neurol.* **11**, 1056.

Dinh, N.-D., Chiang, Y.-Y., Hardelauf, H., Waide, S., Janasek, D. and West, J. (2014). Preparation of neuronal co-cultures with single cell precision. *J. Vis. Exp.* 51389.

Dixon, A. S., Schwinn, M. K., Hall, M. P., Zimmerman, K., Otto, P., Lubben, T. H., Butler, B. L., Binkowski, B. F., Machleidt, T., Kirkland, T. A., et al. (2016). NanoLuc Complementation Reporter Optimized for Accurate Measurement of Protein Interactions in Cells. *ACS Chem. Biol.* **11**, 400–408.

Dujardin, S., Bégard, S., Caillierez, R., Lachaud, C., Delattre, L., Carrier, S., Loyens, A., Galas, M.-C., Bousset, L., Melki, R., et al. (2014). Ectosomes: A New Mechanism for Non-Exosomal Secretion of Tau Protein. *PLoS One* **9**, e100760.

Dujardin, S., Commins, C., Lathuiliere, A., Beerepoot, P., Fernandes, A. R., Kamath, T. V., De Los Santos, M. B., Klickstein, N., Corjuc, D. L., Corjuc, B. T., et al. (2020). Tau molecular diversity contributes to clinical heterogeneity in Alzheimer's disease. *Nat. Med.* **26**, 1256.

Duyckaerts, C., Uchihara, T., Seilhean, D., He, Y. and Hauw, J. J. (1997). Dissociation of Alzheimer type pathology in a disconnected piece of cortex. *Acta Neuropathol. 1997 935* **93**, 501–507.

Eftekharzadeh, B., Daigle, J. G., Kapinos, L. E., Coyne, A., Schiantarelli, J., Carlomagno, Y., Cook, C., Miller, S. J., Dujardin, S., Amaral, A. S., et al. (2018). Tau protein disrupts

nucleocytoplasmic transport in Alzheimer's disease. *Neuron* **99**, 925.

Elbaum-Garfinkle, S., Ramlall, T. and Rhoades, E. (2010). The role of the lipid bilayer in tau aggregation. *Biophys. J.* **98**, 2722–2730.

England, C. G., Ehlerding, E. B. and Cai, W. (2016). NanoLuc: A Small Luciferase Is Brightening Up the Field of Bioluminescence. *Bioconjug. Chem.* **27**, 1175–1187.

Fá, M., Puzzo, D., Piacentini, R., Staniszewski, A., Zhang, H., Baltrons, M. A., Li Puma, D. D., Chatterjee, I., Li, J., Saeed, F., et al. (2016). Extracellular Tau Oligomers Produce An Immediate Impairment of LTP and Memory. *Sci. Rep.* **6**,.

Falcon, B., Zhang, W., Murzin, A. G., Murshudov, G., Garringer, H. J., Vidal, R., Crowther, R. A., Ghetti, B., Scheres, S. H. W. and Goedert, M. (2018). Structures of filaments from Pick's disease reveal a novel tau protein fold. *Nature* **561**, 137–140.

Falcon, B., Zivanov, J., Zhang, W., Murzin, A. G., Garringer, H. J., Vidal, R., Crowther, R. A., Newell, K. L., Ghetti, B., Goedert, M., et al. (2019). Novel tau filament fold in chronic traumatic encephalopathy encloses hydrophobic molecules. *Nature* **568**, 420–423.

Fischer, I. and Baas, P. W. (2020). Resurrecting the Mysteries of Big Tau. *Trends Neurosci.* **43**, 493–504.

Fischer, D., Mukrasch, M. D., von Bergen, M., Klos-Witkowska, A., Biernat, J., Griesinger, C., Mandelkow, E. and Zweckstetter, M. (2007). Structural and Microtubule Binding Properties of Tau Mutants of Frontotemporal Dementias †. *Biochemistry* **46**, 2574–2582.

Fitzpatrick, A. W. P., Falcon, B., He, S., Murzin, A. G., Murshudov, G., Garringer, H. J., Crowther, R. A., Ghetti, B., Goedert, M. and Scheres, S. H. W. (2017). Cryo-EM structures of tau filaments from Alzheimer's disease. *Nature* **547**, 185–190.

Flavin, W. P., Bousset, L., Green, Z. C., Chu, Y., Skarpathiotis, S., Chaney, M. J., Kordower, J. H., Melki, R. and Campbell, E. M. (2017). Endocytic vesicle rupture is a conserved mechanism of cellular invasion by amyloid proteins. *Acta Neuropathol.* **134**, 629–653.

Fontaine, S. N., Zheng, D., Sabbagh, J. J., Martin, M. D., Chaput, D., Darling, A., Trotter, J. H., Stothert, A. R., Nordhues, B. A., Lussier, A., et al. (2016). DnaJ/Hsc70 chaperone complexes control the extracellular release of neurodegenerative-associated proteins. *EMBO J.* **35**, 1537–1549.

Fraser, P. E. (2014). Prions and prion-like proteins. *J. Biol. Chem.* **289**, 19839–40.

Friedhoff, P., Schneider, A., Mandelkow, Eva-Maria, A. and Mandelkow*, E. (1998). Rapid Assembly of Alzheimer-like Paired Helical Filaments from Microtubule-Associated Protein Tau Monitored by Fluorescence in Solution. *Biochemistry* **37**, 10223–30.

Frost, B. and Diamond, M. I. (2010). Prion-like mechanisms in neurodegenerative diseases. *Nat. Rev. Neurosci.* **11**, 155–159.

Frost, B., Jacks, R. L. and Diamond, M. I. (2009). Propagation of Tau Misfolding from the Outside to the Inside of a Cell. *J. Biol. Chem.* **284**, 12845–12852.

Fu, H., Hardy, J. and Duff, K. E. (2018). Selective vulnerability in neurodegenerative diseases. *Nat. Neurosci.* **21**, 1350–1358.

García-Sierra, F., Ghoshal, N., Quinn, B., Berry, R. W. and Bínder, L. I. (2003). Conformational changes and truncation of tau protein during tangle evolution in Alzheimer's disease. *J. Alzheimers. Dis.* **5**, 65–77.

Ghag, G., Bhatt, N., Cantu, D. V., Guerrero-Munoz, M. J., Ellsworth, A., Sengupta, U. and Kayed, R. (2018). Soluble tau aggregates, not large fibrils, are the toxic species that display seeding and cross-seeding behavior. *Protein Sci.* **27**, 1901–1909.

Ghetti, B., Oblak, A. L., Boeve, B. F., Johnson, K. A., Dickerson, B. C. and Goedert, M. (2015). Invited review: Frontotemporal dementia caused by microtubule-associated protein tau gene (MAPT) mutations: a chameleon for neuropathology and neuroimaging. *Neuropathol. Appl. Neurobiol.* **41**, 24–46.

Giamblanco, N., Fichou, Y., Janot, J. M., Balanzat, E., Han, S. and Balme, S. (2020). Mechanisms of Heparin-Induced Tau Aggregation Revealed by a Single Nanopore. *ACS Sensors* **5**, 1158–1167.

Ginsberg, S. D., Che, S., Counts, S. E. and Mufson, E. J. (2006). Shift in the ratio of three-repeat tau and four-repeat tau mRNAs in individual cholinergic basal forebrain neurons in mild cognitive impairment and Alzheimer's disease. *J. Neurochem.* **96**, 1401–1408.

Ginsberg, S. D., Mufson, E. J., Counts, S. E., Wuu, J., Alldred, M. J., Nixon, R. A. and Che, S. (2010). Regional selectivity of rab5 and rab7 protein upregulation in mild cognitive impairment and Alzheimer's disease. *J. Alzheimer's Dis.* **22**, 631–639.

Glenner, G. G. and Wong, C. W. (1984). Alzheimer's disease: initial report of the purification and

characterization of a novel cerebrovascular amyloid protein. *Biochem. Biophys. Res. Commun.* **120**, 885–90.

Goedert, M. (1993). Tau protein and the neurofibrillary pathology of Alzheimer's disease. *Trends Neurosci.* **16**, 460–5.

Goedert, M. and Jakes, R. (1990). Expression of separate isoforms of human tau protein: correlation with the tau pattern in brain and effects on tubulin polymerization. *EMBO J.* **9**, 4225.

Goedert, M. and Spillantini, M. G. (2017). Propagation of Tau aggregates. *Mol. Brain* **10**, 189–212.

Goedert, M., Spillantini, M. G., Jakes, R., Rutherford, D. and Crowther, R. A. (1989). Multiple isoforms of human microtubule-associated protein tau: sequences and localization in neurofibrillary tangles of Alzheimer's disease. *Neuron* **3**, 519–26.

Goedert, M., Jakes, R., Spillantini, M. G., Hasegawa, M., Smith, M. J. and Crowther, R. A. (1996). Assembly of microtubule-associated protein tau into Alzheimer-like filaments induced by sulphated glycosaminoglycans. *Nature* **383**, 550–553.

Goedert, M., Ghetti, B. and Spillantini, M. G. (2012). Frontotemporal dementia: implications for understanding Alzheimer disease. *Cold Spring Harb. Perspect. Med.* **2**, a006254.

Gómez-Ramos, A., Díaz-Hernández, M., Cuadros, R., Hernández, F. and Avila, J. (2006). Extracellular tau is toxic to neuronal cells. *FEBS Lett.* **580**, 4842–4850.

Gómez-Ramos, A., Díaz-Hernández, M., Rubio, A., Miras-Portugal, M. T. and Avila, J. (2008). Extracellular tau promotes intracellular calcium increase through M1 and M3 muscarinic receptors in neuronal cells. *Mol. Cell. Neurosci.* **37**, 673–681.

Gómez-Ramos, A., Díaz-Hernández, M., Rubio, A., Díaz-Hernández, J. I., Miras-Portugal, M. T. and Avila, J. (2009). Characteristics and consequences of muscarinic receptor activation by tau protein. *Eur. Neuropsychopharmacol.* **19**, 708–717.

Gu, J., Xu, W., Jin, N., Li, L., Zhou, Y., Chu, D., Gong, C. X., Iqbal, K. and Liu, F. (2020). Truncation of Tau selectively facilitates its pathological activities. *J. Biol. Chem.* **295**, 13812.

Guo, J. L. and Lee, V. M. Y. (2011). Seeding of normal tau by pathological tau conformers drives pathogenesis of Alzheimer-like tangles. *J. Biol. Chem.* **286**, 15317–15331.

Hall, M. P., Unch, J., Binkowski, B. F., Valley, M. P., Butler, B. L., Wood, M. G., Otto, P.,

Zimmerman, K., Vidugiris, G., Machleidt, T., et al. (2012). Engineered Luciferase Reporter from a Deep Sea Shrimp Utilizing a Novel Imidazopyrazinone Substrate. *ACS Chem. Biol.* **7**, 1848–1857.

Hall, M. P., Kincaid, V. A., Jost, E. A., Smith, T. P., Hurst, R., Forsyth, S. K., Fitzgerald, C., Ressler, V. T., Zimmermann, K., Lazar, D., et al. (2021). Toward a Point-of-Need Bioluminescence-Based Immunoassay Utilizing a Complete Shelf-Stable Reagent. *Anal. Chem.* **93**, 5177–5184.

Hallinan, G. I., Vargas-Caballero, M., West, J. and Deinhardt, K. (2018). Efficient propagation of misfolded tau between individual neurons occurs in absence of degeneration. *bioRxiv* 372029.

Hallinan, G. I., Vargas-Caballero, M., West, J. and Deinhardt, K. (2019). Tau Misfolding Efficiently Propagates between Individual Intact Hippocampal Neurons. *J. Neurosci.* **39**, 9623–9632.

Hampel, H., Blennow, K., Shaw, L. M., Hoessler, Y. C., Zetterberg, H. and Trojanowski, J. Q. (2010). Total and phosphorylated tau protein as biological markers of Alzheimer's disease. *Exp. Gerontol.* **45**, 30–40.

Hanger, D. P., Byers, H. L., Wray, S., Leung, K.-Y., Saxton, M. J., Seereeram, A., Reynolds, C. H., Ward, M. A. and Anderton, B. H. (2007). Novel phosphorylation sites in tau from Alzheimer brain support a role for casein kinase 1 in disease pathogenesis. *J. Biol. Chem.* **282**, 23645–54.

Hanger, D. P., Anderton, B. H. and Noble, W. (2009). Tau phosphorylation: the therapeutic challenge for neurodegenerative disease. *Trends Mol. Med.* **15**, 112–119.

Harada, A., Oguchi, K., Okabe, S., Kuno, J., Terada, S., Ohshima, T., Sato-Yoshitake, R., Takei, Y., Noda, T. and Hirokawa, N. (1994). Altered microtubule organization in small-calibre axons of mice lacking tau protein. *Nature* **369**, 488–91.

Hasegawa, M., Crowther, R. A., Jakes, R. and Goedert, M. (1997). Alzheimer-like Changes in Microtubule-associated Protein Tau Induced by Sulfated Glycosaminoglycans. *J. Biol. Chem.* **272**, 33118–33124.

Hasegawa, M., Smith, M. J. and Goedert, M. (1998). Tau proteins with FTDP-17 mutations have a reduced ability to promote microtubule assembly. *FEBS Lett.* **437**, 207–210.

Hatch, R. J., Wei, Y., Xia, D. and Götz, J. (2017). Hyperphosphorylated tau causes reduced hippocampal CA1 excitability by relocating the axon initial segment. *Acta Neuropathol.* **133**, 717.

Hill, E., Karikari, T. K., Moffat, K. G., Richardson, M. J. E. and Wall, M. J. (2019). Introduction of Tau Oligomers into Cortical Neurons Alters Action Potential Dynamics and Disrupts Synaptic Transmission and Plasticity. *eNeuro* **6**,.

Hill, E., Wall, M. J., Moffat, K. G. and Karikari, T. K. (2020). Understanding the Pathophysiological Actions of Tau Oligomers: A Critical Review of Current Electrophysiological Approaches. *Front. Mol. Neurosci.* **13**,.

Holloway, P. M., Hallinan, G. I., Hegde, M., Lane, S. I. R., Deinhardt, K. and West, J. (2019). Asymmetric confinement for defining outgrowth directionality. *Lab Chip* **19**, 1484–1489.

Holmes, B. B., DeVos, S. L., Kfoury, N., Li, M., Jacks, R., Yanamandra, K., Ouidja, M. O., Brodsky, F. M., Marasa, J., Bagchi, D. P., et al. (2013). Heparan sulfate proteoglycans mediate internalization and propagation of specific proteopathic seeds. *Proc. Natl. Acad. Sci.* **110**, E3138–E3147.

Holmes, B. B., Furman, J. L., Mahan, T. E., Yamasaki, T. R., Mirbaha, H., Eades, W. C., Belaygorod, L., Cairns, N. J., Holtzman, D. M. and Diamond, M. I. (2014). Proteopathic tau seeding predicts tauopathy in vivo. *Proc. Natl. Acad. Sci. U. S. A.* **111**, E4376-85.

Hoover, B. R., Reed, M. N., Su, J., Penrod, R. D., Kotilinek, L. A., Grant, M. K., Pitstick, R., Carlson, G. A., Lanier, L. M., Yuan, L.-L., et al. (2010). Tau Mislocalization to Dendritic Spines Mediates Synaptic Dysfunction Independently of Neurodegeneration. *Neuron* **68**, 1067–1081.

Horowitz, P. M., Patterson, K. R., Guillozet-Bongaarts, A. L., Reynolds, M. R., Carroll, C. A., Weintraub, S. T., Bennett, D. A., Cryns, V. L., Berry, R. W. and Binder, L. I. (2004). Early N-Terminal Changes and Caspase-6 Cleavage of Tau in Alzheimer's Disease. *J. Neurosci.* **24**, 7895–7902.

Iqbal, K., Liu, F. and Gong, C.-X. (2016). Tau and neurodegenerative disease: the story so far. *Nat. Rev. Neurol.* **12**, 15–27.

Irwin, D. J. (2016). Tauopathies as clinicopathological entities. *Parkinsonism Relat. Disord.* **22**, S29-33.

Ismael, S., Sindi, G., Colvin, R. A. and Lee, D. (2021). Activity-dependent release of phosphorylated human tau from Drosophila neurons in primary culture. *J. Biol. Chem.* **297**, 101108.

Ittner, L. M., Ke, Y. D., Delerue, F., Bi, M., Gladbach, A., van Eersel, J., Wölfing, H., Chieng, B. C., Christie, M. J., Napier, I. A., et al. (2010). Dendritic Function of Tau Mediates Amyloid-β Toxicity in Alzheimer's Disease Mouse Models. *Cell* **142**, 387–397.

Jarvis, S. E. and Zamponi, G. W. (2007). Trafficking and regulation of neuronal voltage-gated calcium channels. *Curr. Opin. Cell Biol.* **19**, 474–482.

Jeganathan, S., Von Bergen, M., Brutlach, H., Steinhoff, H.-J. and Mandelkow, E. (2006). Global Hairpin Folding of Tau in Solution. *Biochemistry* **45**, 2283–93.

Jeganathan, S., von Bergen, M., Mandelkow, E.-M. and Mandelkow, E. (2008). The Natively Unfolded Character of Tau and Its Aggregation to Alzheimer-like Paired Helical Filaments. *Biochemistry* **47**, 10526–10539.

Jicha, G. A., Bowser, R., Kazam, I. G. and Davies, P. (1997). Alz-50 and MC-1, a new monoclonal antibody raised to paired helical filaments, recognize conformational epitopes on recombinant tau. *J. Neurosci. Res.* **48**, 128–32.

Johanna Lee (2019). Advanced Protein Quantification HiBiT Protein Tagging System HiBiT HiBiT. *Promega*.

Kametani, F. and Hasegawa, M. (2018). Reconsideration of Amyloid Hypothesis and Tau Hypothesis in Alzheimer's Disease. *Front. Neurosci.* **12**, 25.

Karch, C., Jeng, A. and Goate, A. (2012). Extracellular Tau Levels Are Influenced by Variability in Tau That Is Associated with Tauopathies. *J. Biol. Chem.* **287**, 42751.

Katsinelos, T., Zeitler, M., Dimou, E., Karakatsani, A., Müller, H. M., Nachman, E., Steringer, J. P., Ruiz de Almodovar, C., Nickel, W. and Jahn, T. R. (2018). Unconventional Secretion Mediates the Trans-cellular Spreading of Tau. *Cell Rep.* **23**, 2039–2055.

Katsinelos, T., McEwan, W. A., Jahn, T. R. and Nickel, W. (2021). Identification of cis-acting determinants mediating the unconventional secretion of tau. *Sci. Reports 2021 111* **11**, 1–19.

Kaufman, S. K., Sanders, D. W., Thomas, T. L., Ruchinskas, A. J., Vaquer-Alicea, J., Sharma, A. M., Miller, T. M. and Diamond, M. I. (2016). Tau Prion Strains Dictate Patterns of Cell Pathology, Progression Rate, and Regional Vulnerability In Vivo. *Neuron* **92**, 796–812.

Kazim, S. F., Seo, J. H., Bianchi, R., Larson, C. S., Sharma, A., Wong, R. K. S., Gorbachev, K. Y. and Pereira, A. C. (2021). Neuronal Network Excitability in Alzheimer's Disease: The Puzzle of Similar versus Divergent Roles of Amyloid β and Tau. *eNeuro* **8**,.

Kfoury, N., Holmes, B. B., Jiang, H., Holtzman, D. M. and Diamond, M. I. (2012). Trans-cellular propagation of Tau aggregation by fibrillar species. *J. Biol. Chem.* **287**, 19440–51.

Kim, W., Lee, S., Jung, C., Ahmed, A., Lee, G. and Hall, G. F. (2010). Interneuronal transfer of human tau between lamprey central neurons in situ. *J. Alzheimer's Dis.* **19**, 647–664.

Kim, J., Gee, Y. and Lee, M. G. (2018). Unconventional protein secretion-new insights into the pathogenesis and therapeutic targets of human diseases. *J. Cell Sci.* **131**, jcs213686.

Kuret, J., Congdon, E. E., Li, G., Yin, H., Yu, X. and Zhong, Q. (2005). Evaluating triggers and enhancers of tau fibrillization. *Microsc. Res. Tech.* **67**, 141–155.

Lasagna-Reeves, C. A., Castillo-Carranza, D. L., Sengupta, U., Clos, A. L., Jackson, G. R. and Kayed, R. (2011). Tau oligomers impair memory and induce synaptic and mitochondrial dysfunction in wild-type mice. *Mol. Neurodegener.* **6**, 39.

Lasagna-Reeves, C. A., Castillo-Carranza, D. L., Sengupta, U., Sarmiento, J., Troncoso, J., Jackson, G. R. and Kayed, R. (2012a). Identification of oligomers at early stages of tau aggregation in Alzheimer's disease. *FASEB J.* **26**, 1946–1959.

Lasagna-Reeves, C. A., Castillo-Carranza, D. L., Sengupta, U., Guerrero-Munoz, M. J., Kiritoshi, T., Neugebauer, V., Jackson, G. R. and Kayed, R. (2012b). Alzheimer brain-derived tau oligomers propagate pathology from endogenous tau. *Sci. Rep.* **2**, 700.

Lasagna-Reeves, C. A., Sengupta, U., Castillo-Carranza, D., Gerson, J. E., Guerrero-Munoz, M., Troncoso, J. C., Jackson, G. R. and Kayed, R. (2014). The formation of tau pore-like structures is prevalent and cell specific: Possible implications for the disease phenotypes. *Acta Neuropathol. Commun.* **2**, 56.

Leterrier, C. (2018). The Axon Initial Segment: An Updated Viewpoint. *J. Neurosci.* **38**, 2135–2145.

Lewis, J. and Dickson, D. W. (2016). Propagation of tau pathology: hypotheses, discoveries, and yet unresolved questions from experimental and human brain studies. *Acta Neuropathol.* **131**, 27–48.

Leyns, C. E. G. and Holtzman, D. M. (2017). Glial contributions to neurodegeneration in tauopathies. *Mol. Neurodegener.* **50**,.

Limorenko, G. and Lashuel, H. A. (2022). Revisiting the grammar of Tau aggregation and pathology formation: how new insights from brain pathology are shaping how we study and

target Tauopathies. *Chem. Soc. Rev.* **51**, 513–565.

Liu, L., Drouet, V., Wu, J. W., Witter, M. P., Small, S. A., Clelland, C. and Duff, K. (2012). Trans-synaptic spread of tau pathology in vivo. *PLoS One* **7**, 1–9.

Lowe, V. J., Wiste, H. J., Senjem, M. L., Weigand, S. D., Therneau, T. M., Boeve, B. F., Josephs, K. A., Fang, P., Pandey, M. K., Murray, M. E., et al. (2018). Widespread brain tau and its association with ageing, Braak stage and Alzheimer's dementia. *Brain* **141**, 271–287.

Magnoni, S., Esparza, T. J., Conte, V., Carbonara, M., Carrabba, G., Holtzman, D. M., Zipfel, G. J., Stocchetti, N. and Brody, D. L. (2012). Tau elevations in the brain extracellular space correlate with reduced amyloid-β levels and predict adverse clinical outcomes after severe traumatic brain injury. *Brain*.

Mandelkow, E., von Bergen, M., Biernat, J. and Mandelkow, E.-M. (2007). Structural Principles of Tau and the Paired Helical Filaments of Alzheimer?s Disease. *Brain Pathol.* **17**, 83–90.

Mandell, J. W. and Banker, G. A. (1996). A spatial gradient of tau protein phosphorylation in nascent axons. *J. Neurosci.* **16**, 5727–40.

Marinković, P., Blumenstock, S., Goltstein, P. M., Korzhova, V., Peters, F., Knebl, A. and Herms, J. (2019). In vivo imaging reveals reduced activity of neuronal circuits in a mouse tauopathy model. *Brain* **142**, 1051–1062.

Martin, L., Latypova, X., Wilson, C. M., Magnaudeix, A., Perrin, M.-L., Yardin, C. and Terro, F. (2013). Tau protein kinases: Involvement in Alzheimer's disease. *Ageing Res. Rev.* **12**, 289–309.

Martini-Stoica, H., Cole, A. L., Swartzlander, D. B., Chen, F., Wan, Y. W., Bajaj, L., Bader, D. A., Lee, V. M. Y., Trojanowski, J. Q., Liu, Z., et al. (2018). TFEB enhances astroglial uptake of extracellular tau species and reduces tau spreading. *J. Exp. Med.*

Matejka, N. and Reindl, J. (2019). Perspectives of cellular communication through tunneling nanotubes in cancer cells and the connection to radiation effects. *Radiat. Oncol.*

McInnes, J., Wierda, K., Snellinx, A., Bounti, L., Wang, Y. C., Stancu, I. C., Apóstolo, N., Gevaert, K., Dewachter, I., Spires-Jones, T. L., et al. (2018). Synaptogyrin-3 Mediates Presynaptic Dysfunction Induced by Tau. *Neuron* **97**, 823-835.e8.

Merezhko, M., Brunello, C. A., Yan, X., Vihinen, H., Jokitalo, E., Uronen, R.-L. and Correspondence, H. J. H. (2018). Secretion of Tau via an Unconventional Non-vesicular

Mechanism. *CellReports* **25**, 2027-2035.e4.

Michel, C. H., Kumar, S., Pinotsi, D., Tunnacliffe, A., St George-Hyslop, P., Mandelkow, E., Mandelkow, E.-M., Kaminski, C. F. and Kaminski Schierle, G. S. (2014). Extracellular monomeric tau protein is sufficient to initiate the spread of tau protein pathology. *J. Biol. Chem.* **289**, 956–67.

Mietelska-Porowska, A., Wasik, U., Goras, M., Filipek, A. and Niewiadomska, G. (2014). Tau protein modifications and interactions: Their role in function and dysfunction. *Int. J. Mol. Sci.*

Mirbaha, H., Holmes, B. B., Sanders, D. W., Bieschke, J. and Diamond, M. I. (2015). Tau Trimers Are the Minimal Propagation Unit Spontaneously Internalized to Seed Intracellular Aggregation. *J. Biol. Chem.* **290**, 14893–14903.

Mirbaha, H., Chen, D., Morazova, O. A., Ruff, K. M., Sharma, A. M., Liu, X., Goodarzi, M., Pappu, R. V., Colby, D. W., Mirzaei, H., et al. (2018). Inert and seed-competent tau monomers suggest structural origins of aggregation. *Elife* **10**, e36584.

Mody, I. (2005). Aspects of the homeostaic plasticity of GABAA receptor-mediated inhibition. *J. Physiol.* **562**, 37.

Mohamed, N. V., Desjardins, A. and Leclerc, N. (2017). Tau secretion is correlated to an increase of Golgi dynamics. *PLoS One* **12**, e0178288.

Morris, M., Maeda, S., Vossel, K. and Mucke, L. (2011). The many faces of tau. *Neuron* **70**, 410–26.

Mudher, A., Colin, M., Dujardin, S., Medina, M., Dewachter, I., Alavi Naini, S. M., Mandelkow, E. M., Mandelkow, E., Buée, L., Goedert, M., et al. (2017). What is the evidence that tau pathology spreads through prion-like propagation? *Acta Neuropathol. Commun.* **5**, 99.

Naini, S. M. A. and Soussi-Yanicostas, N. (2018). Heparan Sulfate as a Therapeutic Target in Tauopathies: Insights From Zebrafish. *Front. Cell Dev. Biol.* **6**,.

Nelson, P. T., Alafuzoff, I., Bigio, E. H., Bouras, C., Braak, H., Cairns, N. J., Castellani, R. J., Crain, B. J., Davies, P., Del Tredici, K., et al. (2012). Correlation of Alzheimer disease neuropathologic changes with cognitive status: a review of the literature. *J. Neuropathol. Exp. Neurol.* **71**, 362–81.

Nobuhara, C. K., DeVos, S. L., Commins, C., Wegmann, S., Moore, B. D., Roe, A. D., Costantino, I.,

Frosch, M. P., Pitstick, R., Carlson, G. A., et al. (2017). Tau Antibody Targeting Pathological Species Blocks Neuronal Uptake and Interneuron Propagation of Tau in Vitro. *Am. J. Pathol.* **187**, 1399–1412.

Oh-hashi, K., Furuta, E., Fujimura, K. and Hirata, Y. (2017). Application of a novel HiBiT peptide tag for monitoring ATF4 protein expression in Neuro2a cells. *Biochem. Biophys. Reports* **12**, 40–45.

Ohmuro-Matsuyama, Y. and Ueda, H. (2019). Protein-Protein Interaction Assays Using Split-NanoLuc. *Bioluminescence*.

Ondrejcak, T., Klyubin, I., Corbett, G. T., Fraser, G., Hong, W., Mably, A. J., Gardener, M., Hammersley, J., Perkinton, M. S., Billinton, A., et al. (2018). Cellular Prion Protein Mediates the Disruption of Hippocampal Synaptic Plasticity by Soluble Tau In Vivo. *J. Neurosci.* **38**, 10595–10606.

Palop, J. J. and Mucke, L. (2009). Epilepsy and Cognitive Impairments in Alzheimer Disease. *Arch. Neurol.* **66**, 435–440.

Patel, N., Ramachandran, S., Azimov, R., Kagan, B. L. and Lal, R. (2015). Ion Channel Formation by Tau Protein: Implications for Alzheimer's Disease and Tauopathies. *Biochemistry* **54**, 7320–7325.

Pérez, M., Valpuesta, J. M., Medina, M., Montejo De Garcini, E. and Avila, J. (1996). Polymerization of tau into filaments in the presence of heparin: the minimal sequence required for tau-tau interaction. *J. Neurochem.* **67**, 1183–1190.

Pérez, M., Medina, M., Hernández, F. and Avila, J. (2018). Secretion of full-length Tau or Tau fragments in cell culture models. Propagation of Tau in vivo and in vitro. *Biomol. Concepts* **9**, 1–11.

Pernègre, C., Duquette, A. and Leclerc, N. (2019). Tau Secretion: Good and Bad for Neurons. *Front. Neurosci.* **13**, 649.

Pickett, E. K., Henstridge, C. M., Allison, E., Pitstick, R., Pooler, A., Wegmann, S., Carlson, G., Hyman, B. T. and Spires-Jones, T. L. (2017). Spread of tau down neural circuits precedes synapse and neuronal loss in the rTgTauEC mouse model of early Alzheimer's disease. *Synapse* **71**, e21965.

Pilliod, J., Desjardins, A., Pernègre, C., Jamann, H., Larochelle, C., Fon, E. A. and Leclerc, N. (2020). Clearance of intracellular tau protein from neuronal cells via VAMP8-induced

secretion. *J. Biol. Chem.*

Pitera, A. P., Asuni, A. A., O'Connor, V. and Deinhardt, K. (2019). Pathogenic tau does not drive activation of the unfolded protein response. *J. Biol. Chem.* **294**, 9679–9688.

Platre, M. P. and Jaillais, Y. (2017). Anionic lipids and the maintenance of membrane electrostatics in eukaryotes. *Plant Signal. Behav.* **12**, e1282022.

Plouffe, V., Mohamed, N. V., Rivest-McGraw, J., Bertrand, J., Lauzon, M. and Leclerc, N. (2012). Hyperphosphorylation and Cleavage at D421 Enhance Tau Secretion. *PLoS One* **7**, e36873.

Polanco, J. C., Scicluna, B. J., Hill, A. F. and Götz, J. (2016). Extracellular Vesicles Isolated from the Brains of rTg4510 Mice Seed Tau Protein Aggregation in a Threshold-dependent Manner. *J. Biol. Chem.* **291**, 12445–12466.

Pooler, A. M., Usardi, A., Evans, C. J., Philpott, K. L., Noble, W. and Hanger, D. P. (2012a). Dynamic association of tau with neuronal membranes is regulated by phosphorylation. *Neurobiol. Aging* **33**, 431.e27-431.e38.

Pooler, A. M., Usardi, A., Evans, C. J., Philpott, K. L., Noble, W. and Hanger, D. P. (2012b). Dynamic association of tau with neuronal membranes is regulated by phosphorylation. *Neurobiol. Aging* **33**, 431.e27-431.e38.

Pooler, A. M., Phillips, E. C., Lau, D. H. W., Noble, W. and Hanger, D. P. (2013). Physiological release of endogenous tau is stimulated by neuronal activity. *EMBO Rep.* **14**, 389–94.

Prusiner, S. B. (1982). Novel proteinaceous infectious particles cause scrapie. *Science* **216**, 136–44.

Rauch, J. N., Chen, J. J., Sorum, A. W., Miller, G. M., Sharf, T., See, S. K., Hsieh-Wilson, L. C., Kampmann, M. and Kosik, K. S. (2018). Tau Internalization is Regulated by 6-O Sulfation on Heparan Sulfate Proteoglycans (HSPGs). *Sci. Rep.* **8**, 1–10.

Rauch, J. N., Luna, G., Guzman, E., Audouard, M., Challis, C., Sibih, Y. E., Leshuk, C., Hernandez, I., Wegmann, S., Hyman, B. T., et al. (2020). LRP1 is a master regulator of tau uptake and spread. *Nature* **580**, 381–385.

Reitz, C. (2012). Alzheimer's disease and the amyloid cascade hypothesis: a critical review. *Int. J. Alzheimers. Dis.* **2012**, 369808.

Rienecker, K. D. A., Poston, R. G. and Saha, R. N. (2020). Merits and Limitations of Studying

Neuronal Depolarization-Dependent Processes Using Elevated External Potassium: *https://doi.org/10.1177/1759091420974807* **12**,.

Robinson, L., Tang, E. and Taylor, J.-P. (2015). Dementia: timely diagnosis and early intervention. *BMJ* **350**, h3029.

Rodríguez-Martín, T., Cuchillo-Ibáñez, I., Noble, W., Nyenya, F., Anderton, B. H. and Hanger, D. P. (2013). Tau phosphorylation affects its axonal transport and degradation. *Neurobiol. Aging* **34**, 2146.

Rodriguez, L., Mohamed, N.-V., Desjardins, A., Lippé, R., Fon, E. A. and Leclerc, N. (2017). Rab7A regulates tau secretion. *J. Neurochem.* **141**, 592–605.

Rodriguez, G. A., Barrett, G. M., Duff, K. E. and Hussaini, S. A. (2020). Chemogenetic attenuation of neuronal activity in the entorhinal cortex reduces Aβ and tau pathology in the hippocampus. *PLoS Biol.* **18**,.

Rouault, A. A. J., Lee, A. A. and Sebag, J. A. (2017). Regions of MRAP2 required for the inhibition of orexin and prokineticin receptor signaling. *Biochim. Biophys. Acta - Mol. Cell Res.* **1864**, 2322–2329.

Rüb, U., Stratmann, K., Heinsen, H., Seidel, K., Bouzrou, M. and Korf, H.-W. (2017). Alzheimer's Disease: Characterization of the Brain Sites of the Initial Tau Cytoskeletal Pathology Will Improve the Success of Novel Immunological Anti-Tau Treatment Approaches. *J. Alzheimer's Dis.* **57**, 683–696.

Saman, S., Kim, W., Raya, M., Visnick, Y., Miro, S., Saman, S., Jackson, B., McKee, A. C., Alvarez, V. E., Lee, N. C. Y., et al. (2012). Exosome-associated Tau Is Secreted in Tauopathy Models and Is Selectively Phosphorylated in Cerebrospinal Fluid in Early Alzheimer Disease. *J. Biol. Chem.* **287**, 3842–3849.

Sanders, D. W., Kaufman, S. K., DeVos, S. L., Sharma, A. M., Mirbaha, H., Li, A., Barker, S. J., Foley, A. C., Thorpe, J. R., Serpell, L. C., et al. (2014). Distinct tau prion strains propagate in cells and mice and define different tauopathies. *Neuron* **82**, 1271–1288.

SantaCruz, K. (2005). Tau Suppression in a Neurodegenerative Mouse Model Improves Memory Function. *Science (80-.).* **309**, 476–481.

Sasaki, M., Anindita, P. D., Phongphaew, W., Carr, M., Kobayashi, S., Orba, Y. and Sawa, H. (2018). Development of a rapid and quantitative method for the analysis of viral entry and release using a NanoLuc luciferase complementation assay. *Virus Res.* **243**, 69–74.

Schöll, M., Lockhart, S. N., Schonhaut, D. R., O'Neil, J. P., Janabi, M., Ossenkoppele, R., Baker, S. L., Vogel, J. W., Faria, J., Schwimmer, H. D., et al. (2016). PET Imaging of Tau Deposition in the Aging Human Brain. *Neuron* **89**, 971–982.

Schultz, M. K., Gentzel, R., Usenovic, M., Gretzula, C., Ware, C., Parmentier-Batteur, S., Schachter, J. B. and Zariwala, H. A. (2018). Pharmacogenetic neuronal stimulation increases human tau pathology and trans-synaptic spread of tau to distal brain regions in mice. *Neurobiol. Dis.* **118**, 161–176.

Schwarz, A. J., Yu, P., Miller, B. B., Shcherbinin, S., Dickson, J., Navitsky, M., Joshi, A. D., Devous, M. D. and Mintun, M. S. (2016). Regional profiles of the candidate tau PET ligand 18F-AV-1451 recapitulate key features of Braak histopathological stages. *Brain* **139**, 1539–50.

Schwinn, M. K., Machleidt, T., Zimmerman, K., Eggers, C. T., Dixon, A. S., Hurst, R., Hall, M. P., Encell, L. P., Binkowski, B. F. and Wood, K. V. (2018). CRISPR-Mediated Tagging of Endogenous Proteins with a Luminescent Peptide. *ACS Chem. Biol.* **13**, 467–474.

Sealey, M. A., Vourkou, E., Cowan, C. M., Bossing, T., Quraishe, S., Grammenoudi, S., Skoulakis, E. M. C. and Mudher, A. (2017). Distinct phenotypes of three-repeat and four-repeat human tau in a transgenic model of tauopathy. *Neurobiol. Dis.* **105**, 74–83.

Sebastián-Serrano, Á., Diego-García, L. De and Díaz-Hernández, M. (2018). The neurotoxic role of extracellular tau protein. *Int. J. Mol. Sci.* **19**, 998.

Shafiei, S. S., Guerrero-Muñoz, M. J. and Castillo-Carranza, D. L. (2017). Tau Oligomers: Cytotoxicity, Propagation, and Mitochondrial Damage. *Front. Aging Neurosci.* **9**, 83.

Sharma, A. M., Thomas, T. L., Woodard, D. R., Kashmer, O. M. and Diamond, M. I. (2018). Tau monomer encodes strains. *Elife* **7**,.

Sigel, E. and Steinmann, M. E. (2012). Structure, Function, and Modulation of GABAA Receptors. *J. Biol. Chem.* **287**, 40224.

Simón, D., García-García, E., Gómez-Ramos, A., Falcón-Pérez, J. M., Díaz-Hernández, M., Hernández, F. and Avila, J. (2012a). Tau Overexpression Results in Its Secretion via Membrane Vesicles. *Neurodegener. Dis.* **10**, 73–75.

Simón, D., García-García, E., Royo, F., Falcón-Pérez, J. M. and Avila, J. (2012b). Proteostasis of tau. Tau overexpression results in its secretion via membrane vesicles. *FEBS Lett.* **586**, 47–54.

Snow, A. D., Mar, H., Nochlin, D., Sekiguchi, R. T., Kimata, K., Koike, Y. and Wight, T. N. (1990). Early accumulation of heparan sulfate in neurons and in the beta-amyloid protein-containing lesions of Alzheimer's disease and Down's syndrome. *Am. J. Pathol.* **137**, 1253–1270.

Stopschinski, B. E., Holmes, B. B., Miller, G. M., Manon, V. A., Vaquer-Alicea, J., Prueitt, W. L., Hsieh-Wilson, L. C. and Diamond, M. I. (2018). Specific glycosaminoglycan chain length and sulfation patterns are required for cell uptake of tau versus -synuclein and -amyloid aggregates. *J. Biol. Chem.*

Sultan, A., Nesslany, F., Violet, M., Bégard, S., Loyens, A., Talahari, S., Mansuroglu, Z., Marzin, D., Sergeant, N., Humez, S., et al. (2011). Nuclear Tau, a Key Player in Neuronal DNA Protection. *J. Biol. Chem.* **286**, 4566.

Takeda, S., Wegmann, S., Cho, H., Devos, S. L., Commins, C., Roe, A. D., Nicholls, S. B., Carlson, G. A., Pitstick, R., Nobuhara, C. K., et al. (2015). Neuronal uptake and propagation of a rare phosphorylated high-molecular-weight tau derived from Alzheimer's disease brain. *Nat. Commun.* **6**, 8490.

Tardivel, M., Bégard, S., Bousset, L., Dujardin, S., Coens, A., Melki, R., Buée, L. and Colin, M. (2016). Tunneling nanotube (TNT)-mediated neuron-to neuron transfer of pathological Tau protein assemblies. *Acta Neuropathol. Commun.* **4**, 117.

Targa Dias Anastacio, H., Matosin, N. and Ooi, L. (2022). Neuronal hyperexcitability in Alzheimer's disease: what are the drivers behind this aberrant phenotype? *Transl. Psychiatry 2022 121* **12**, 1–14.

Taylor, A. M., Rhee, S. W., Tu, C. H., Cribbs, D. H., Cotman, C. W. and Jeon, N. L. (2003). Microfluidic Multicompartment Device for Neuroscience Research †. *Langmuir* **19**, 1551–1556.

Tian, H., Davidowitz, E., Lopez, P., Emadi, S., Moe, J. and Sierks, M. (2013). Trimeric tau is toxic to human neuronal cells at low nanomolar concentrations. *Int. J. Cell Biol.* **2013**, 260787.

Townsend, D., Fullwood, N. J., Yates, E. A. and Middleton, D. A. (2020). Aggregation Kinetics and Filament Structure of a Tau Fragment Are Influenced by the Sulfation Pattern of the Cofactor Heparin. *Biochemistry* **59**, 4003–4014.

Tracy, T. E. and Gan, L. (2018). Tau-mediated synaptic and neuronal dysfunction in neurodegenerative disease. *Curr. Opin. Neurobiol.* **51**, 134–138.

Tracy, T. E., Madero-Pérez, J., Swaney, D. L., Chang, T. S., Moritz, M., Konrad, C., Ward, M. E.,

Stevenson, E., Hüttenhain, R., Kauwe, G., et al. (2022). Tau interactome maps synaptic and mitochondrial processes associated with neurodegeneration. *Cell* **185**, 712-728.e14.

Tuck, B. J., Miller, L. V. C., Katsinelos, T., Smith, A. E., Wilson, E. L., Keeling, S., Cheng, S., Vaysburd, M. J., Knox, C., Tredgett, L., et al. (2022). Cholesterol determines the cytosolic entry and seeded aggregation of tau. *Cell Rep.* **39**, 110776.

Tudorică, V., Bălşeanu, T.-A., Albu, V.-C., Bondari, S., Bumbea, A.-M. and Pîrşcoveanu, M. (2017). Tau protein in neurodegenerative diseases. *Rom J Morphol Embryol* **10**, 1141–1150.

Turrigiano, G. G. and Nelson, S. B. (2000). Hebb and homeostasis in neuronal plasticity. *Curr. Opin. Neurobiol.* **10**, 358–364.

Vandermeeren, M., Borgers, M., Van Kolen, K., Theunis, C., Vasconcelos, B., Bottelbergs, A., Wintmolders, C., Daneels, G., Willems, R., Dockx, K., et al. (2018). Anti-Tau Monoclonal Antibodies Derived from Soluble and Filamentous Tau Show Diverse Functional Properties in vitro and in vivo. *J. Alzheimer's Dis.* **65**, 265–281.

Varkouhi, A. K., Scholte, M., Storm, G. and Haisma, H. J. (2011). Endosomal escape pathways for delivery of biologicals. *J. Control. Release* **151**, 220–228.

Victoria, G. S. and Zurzolo, C. (2017). The spread of prion-like proteins by lysosomes and tunneling nanotubes: Implications for neurodegenerative diseases. *J. Cell Biol.* **216**, 2633–2644.

Vogels, T., Leuzy, A., Cicognola, C., Ashton, N. J., Smolek, T., Novak, M., Blennow, K., Zetterberg, H., Hromadka, T., Zilka, N., et al. (2020). Propagation of Tau Pathology: Integrating Insights From Postmortem and In Vivo Studies. *Biol. Psychiatry* **87**, 808–818.

von Bergen, M., Barghorn, S., Li, L., Marx, A., Biernat, J., Mandelkow, E. M. and Mandelkow, E. (2001). Mutations of tau protein in frontotemporal dementia promote aggregation of paired helical filaments by enhancing local beta-structure. *J. Biol. Chem.* **276**, 48165–74.

Von Bergen, M., Barghorn, S., Biernat, J., Mandelkow, E. M. and Mandelkow, E. (2005). Tau aggregation is driven by a transition from random coil to beta sheet structure. *Biochim. Biophys. Acta - Mol. Basis Dis.* **1739**, 158–166.

Walsh, D. M. and Selkoe, D. J. (2016). A critical appraisal of the pathogenic protein spread hypothesis of neurodegeneration. *Nat. Rev. Neurosci.* **17**, 251–260.

Wang, Y., Martinez-Vicente, M., Krüger, U., Kaushik, S., Wong, E., Mandelkow, E. M., Cuervo, A. M. and Mandelkow, E. (2010). Synergy and antagonism of macroautophagy and chaperone-mediated autophagy in a cell model of pathological tau aggregation. *Autophagy* **6**, 182–183.

Wang, Y., Balaji, V., Kaniyappan, S., Krüger, L., Irsen, S., Tepper, K., Chandupatla, R., Maetzler, W., Schneider, A., Mandelkow, E., et al. (2017). T17. *Mol. Neurodegener.* **12**, 5.

Wang, P., Lo Cascio, F., Gao, J., Kayed, R. and Huang, X. (2018). Binding and neurotoxicity mitigation of toxic tau oligomers by synthetic heparin like oligosaccharides. *Chem. Commun. (Camb).* **54**, 10120–10123.

Wegmann, S., Nicholls, S., Takeda, S., Fan, Z. and Hyman, B. T. (2016). Formation, release, and internalization of stable tau oligomers in cells. *J. Neurochem.* **139**, 1163–1174.

Wegmann, S., Bennett, R. E., Delorme, L., Robbins, A. B., Hu, M., McKenzie, D., Kirk, M. J., Schiantarelli, J., Tunio, N., Amaral, A. C., et al. (2019). Experimental evidence for the age dependence of tau protein spread in the brain. *Sci. Adv.*

Wu, J. W., Herman, M., Liu, L., Simoes, S., Acker, C. M., Figueroa, H., Steinberg, J. I., Margittai, M., Kayed, R., Zurzolo, C., et al. (2013). Small misfolded Tau species are internalized via bulk endocytosis and anterogradely and retrogradely transported in neurons. *J. Biol. Chem.* **288**, 1856–70.

Wu, J. W., Hussaini, S. A., Bastille, I. M., Rodriguez, G. A., Mrejeru, A., Rilett, K., Sanders, D. W., Cook, C., Fu, H., Boonen, R. A. C. M., et al. (2016). Neuronal activity enhances tau propagation and tau pathology in vivo. *Nat. Neurosci.* **19**, 1085–92.

Wu, M., Zhang, M., Yin, X., Chen, K., Hu, Z., Zhou, Q., Cao, X., Chen, Z. and Liu, D. (2021). The role of pathological tau in synaptic dysfunction in Alzheimer's diseases. *Transl. Neurodegener.* **10**,.

Xia, C.-F., Arteaga, J., Chen, G., Gangadharmath, U., Gomez, L. F., Kasi, D., Lam, C., Liang, Q., Liu, C., Mocharla, V. P., et al. (2013). [18F]T807, a novel tau positron emission tomography imaging agent for Alzheimer's disease. *Alzheimer's Dement.* **9**, 666–676.

Xu, Y., Cui, L., Dibello, A., Wang, L., Lee, J., Saidi, L., Lee, J. G. and Ye, Y. (2018). DNAJC5 facilitates USP19-dependent unconventional secretion of misfolded cytosolic proteins. *Cell Discov.* **4**, 1–18.

Xu, Y., Du, S., Marsh, J. A., Horie, K., Sato, C., Ballabio, A., Karch, C. M., Holtzman, D. M. and Zheng, H. (2020). TFEB regulates lysosomal exocytosis of tau and its loss of function

exacerbates tau pathology and spreading. *Mol. Psychiatry*.

Xue, Y., Han, X. H. and Chen, L. (2010). Effects of pharmacological block of GABAA receptors on pallidal neurons in normal and parkinsonian state. *Front. Cell. Neurosci.* **4**, 2.

Yamada, K. (2017). Extracellular tau and its potential role in the propagation of tau pathology. *Front. Neurosci.* **11**, 667.

Yamada, K., Cirrito, J. R., Stewart, F. R., Jiang, H., Finn, M. B., Holmes, B. B., Binder, L. I., Mandelkow, E.-M., Diamond, M. I., Lee, V. M.-Y., et al. (2011). In Vivo Microdialysis Reveals Age-Dependent Decrease of Brain Interstitial Fluid Tau Levels in P301S Human Tau Transgenic Mice. *J. Neurosci.* **31**, 13110–13117.

Yamada, K., Holth, J. K., Liao, F., Stewart, F. R., Mahan, T. E., Jiang, H., Cirrito, J. R., Patel, T. K., Hochgräfe, K., Mandelkow, E. M., et al. (2014). Neuronal activity regulates extracellular tau in vivo. *J. Exp. Med.* **211**, 387–393.

Zehe, C., Engling, A., Wegehingel, S., Schäfer, T. and Nickel, W. (2006). Cell-surface heparan sulfate proteoglycans are essential components of the unconventional export machinery of FGF-2. *Proc. Natl. Acad. Sci. U. S. A.* **103**, 15479–15484.

Zhou, L., McInnes, J., Wierda, K., Holt, M., Herrmann, A. G., Jackson, R. J., Wang, Y. C., Swerts, J., Beyens, J., Miskiewicz, K., et al. (2017). Tau association with synaptic vesicles causes presynaptic dysfunction. *Nat. Commun.* **8**,.